THERMALLY STIMULATED CURRENT STUDIES OF COMPOUND SEMICONDUCTOR THIN FILMS USED FOR PHOTOVOLTAIC APPLICATIONS

A thesis
submitted to
COCHIN UNIVERSITY OF SCIENCE AND TECHNOLOGY
for the award of the degree of
DOCTOR OF PHILOSOPHY

By
N. A. ZEENATH

DEPARTMENT OF PHYSICS
COCHIN UNIVERSITY OF SCIENCE AND TECHNOLOGY
KOCHI - 682 022, INDIA

JULY 1998

CERTIFICATE

Certified that the work presented in this thesis entitled " ***Thermally Stimulated Current studies of compound semiconductor thin films used for photovoltaic applications*** " is based on the bonafide research work done by Smt. N.A.Zeenath under my guidance, at the Department of Physics, Cochin University of Science and Technology and has not been included in any other thesis submitted previously for the award of any degree.

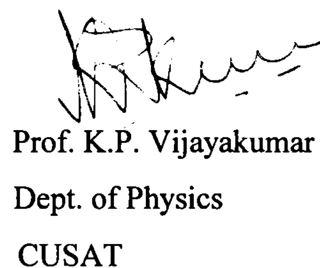

Prof. K.P. Vijayakumar
Dept. of Physics
CUSAT

Kochi-22
July 15, 1998

Contents

Preface i

Chapter 1.
General Introduction to Semiconducting materials

1.1. Introduction 1
1.2 Application of Semiconductors 3
1.3 Charge carriers in Semiconductors 6
1.3.1. Intrinsic Semiconductors 7
1.3.2. Extrinsic Semiconductors 8
1.3.2.a. Impurity levels 8
1.3.2.b. Carrier concentration and Fermi level 10
1.4. Carrier transport in Semiconductors 15
1.4.1 Drift 15
1.4.1.a. Mobility of electrons and holes 16
1.4.1.b. Electrical conductivity 17
1.4.2. Impurity band conduction 18
1.4.2.a. Many body effects 18
1.4.2.b. Effect of randomness in impurity distribution 21
1.4.2.c. Effect of carrier degenerecy 21
1.4.3. Non linear conductivity 21
1.4.4. Diffusion 23
1.5. Excess carriers in Semiconductors 24
1.5.1. Injection of excess carriers 25
1.5.1.a. Injection mechanism 25
1.5.1.b. Low and high level injection 25
1.5.2. Recombination of excess carrier 26
1.5.2.a. Excess carrier life time 27
1.5.3. Mechanism of recombination process 28
1.5.3.a. Direct band to band recombination 28
1.5.3.b. Indirect recombination via deep energy levels in the band gap 29

1.5.3.c. Auger recombination 30
1.5.4. Origin of recombination center 32
1.6. Recombination and trapping 33
1.7. Trapping of minority carriers 36
1.8. Importance of the present work 38
References 43

Chapter 2
Thin Film Preparation Techniques

2.1. Introduction 46
2.2 Physical methods 47
2.2.1. Vacuum evaporation 47
2.2.1.a. Methods of evaporation 49
2.2.2. Sputtering 55
2.2.3. Epitaxial deposition 57
2.2.3.a. Molecular Beam Epitaxy 57
2.2.3.b. Liquid Phase Epitaxy 58
2.2.3.c. Hot Wall Epitaxy 58
2.2.3.d. Metal Organic Chemical Vapour deposition 58
2.2.4. Ion assisted deposition 59
2.2.5. Reactive deposition 59
2.2.6. Ionized cluster beam (ICB) 60
2.3. Chemical methods of film deposition 61
2.3.1. Thermal growth 61
2.3.2. Chemical vapour deposition 62
2.3.3. Electrodeposition 63
2.3.4. Spray Pyrolysis technique 64
2.3.4.a. Growth kinetics 66
2.3.4.b. Chemical aspects 67
2.3.4.c. Characteristic features of spray pyrolysis process 67
2.3.4.d. Properties of spray pyrolysed film 72

2.3.5. Chemical Bath deposition (Solution Growth process) 72

2.3.5.a. Chemical aspects 72

2.3.5.b. Characteristic features of the CBD technique 75

2.3.5.c. Doping 76

2.3.5.d. General properties of CBD films 77

References 78

Chapter 3
Thermally Stimulated Current Measurements Theory and Experiments

3.1. Introduction 83

3.2. Non equilibrium steady state electron statistics for Semiconductors 85

3.2.1. Shockley-Read Statistics 87

3.2.2. Quasi Fermi levels 90

3.2.3. Classification of trapping states based on electron statistics 91

3.2.4. Filling diagram 94

3.2.5. Non equilibrium steady state relaxation 94

3.3. Defect states in Semiconductors 99

3.3.1. Tightly bound (Deep) defect states 99

3.3.2. Weakly bound (Shallow) defect states 99

3.3.3. Intermediately bound defect states 100

3.4. Traps and thermal transport properties 100

3.5. Trap level spectroscopy by thermally stimulated release of trapped carriers

A list of experimental methods 102

3.5.1. Direct methods 102

3.5.2. Indirect methods 103

3.6. Thermally Stimulated Current 105

3.7. Simple trap model 106

3.8. TSC Kinetics 109

3.8.1. TSC due to electron trap 111

3.8.2. TSC due to electron and hole traps 114

3.8.3. TSC due to trap-recombination center pairs 114
3.9. Calculation of activation energy and capture cross section 114
3.10.Experimental details 115
3.10.1. Heating programmes 116
3.10.2. Cryostats and heaters 117
3.10.3. Sample excitation 117
3.10.4. Electrical measurements 118
3.10.5. Details of TSC experiment in the present work 119
3.11. Dark conductivity in Semiconductors 119
References 124

Chapter 4
TSC measurements of CdS thin films

4.1. Introduction 128
4.2. An overview of works on preparation and properties of CdS 128
4.3. Importance of TSC measurements in CdS films 137
4.4. TSC measurements of spray pyrolysed CdS films 137
4.4.1. Experimental details 138
4.4.2. Results and discussion 138
4.5. Dark conductivity measurements of n-and p-type CdS thin films 153
4.6. Analysis of Chemical Bath Deposited CdS thin films 157
4.6.1. Sample preparation 157
4.6.2. Resistance variation with aging and annealing temperature 157
4.6:3. TSC measurements of high resistive CBD CdS thin films 158
4.6.4. Low resistive CBD CdS thin films 162
4.6.4.a. Experimental details 162
4.6.4.b. Results of TSC measurements 163
4.7. Conclusion 176
References 178

Chapter 5
TSC measurements of CBD $CuInSe_2$ thin films

5.1. Introduction 183

5.2. An overview of works on $CuInSe_2$ 184

5.3. Experimental details 190

5.4. Results and discussion 190

5.4.1. TSC measurements 190

5.4.2. Dark conductivity measurements 209

5.5. Conclusion 212

References 213

Chapter 6
Preparation and characterisation of PbS thin films

6.1. Introduction 217

6.2. Review of works on PbS 218

6.3. Sample preparation 222

6.4. Characterisation 223

6.4.1. TSC measurements 224

6.4.2. Dark conductivity measurements 235

6.5. Conclusion 240

References 241

Chapter 7
Preparation and characterisation of FeS_2 thin films

7.1. Introduction 244

7.2. Pyrite crystals 244

7.3. Pyrite thin films 249

7.4. Pyrite as a solar energy material - A comparative study 253

7.5. Preparation and characterisation of spray pyrolysed samples 254

7.5.1. Sample preparation 254

7.5.2. Characterisation 254
7.6 Preparation and characterisation of CBD samples 258
7.6.1. Sample preparation 258
7.6.2. Characterisation of CBD samples 258
7.7. Conclusion 266
References 267

Chapter 8
Summary and Conclusion 270

Preface

Over the last few decades, tremendous progress had been made in the field of solid state physics both in understanding the physics of condensed matter, as well as in developing solid state devices. Of the various branches in solid state physics the most developed branch is semiconductor physics because of its application in microelectronics industry. A large number of new compound semiconductors have been developed for the fabrication of electronic devices over the last few years. Many of these materials exhibit very interesting optoelectronic properties which are yet to be studied in detail.

Semiconductors, by definition, are those materials whose resistivity lies in the range of 10^{-3} to 10^{6} Ω cm. But there are large number of materials with wide ranging electrical and optoelectronic properties. For example we can have materials with conductivity close to that of metals, but their optoelectronic properties will be entirely different from those of metals. Similarly there are wide band gap materials, having properties entirely different from that of insulators. Conduction process in semiconductors is controlled by vacancies, impurities, dislocations, etc. A proper understanding of these levels is essential for the fabrication of electronic device with specific properties.

A number of experimental techniques are available for the electrical characterisation of semiconducting materials. Thermally stimulated current (TSC) measurement is a well-known non isothermal technique for the investigation of trap levels in semiconducting materials. It permits a survey of gap states. Therefore, in the present work, we selected this technique for analysing the semiconducting films of CdS, $CuInSe_2$, PbS and FeS_2 used for photovoltaic application. In addition to this, in the present work, the dark conductivity measurement of these films was also performed.

The thesis is organised in eight chapters that are self contained with separate introduction, conclusion and references. The chapter wise description of the contents of the thesis is given below.

Chapter 1 is a general introduction to semiconductor materials. Starting with elements of semiconductor physics and application of semiconductors, it describes various properties of semiconductor with due importance for electrical properties. It also gives the importance of photovoltaic materials.

Chapter 2 of this thesis describes various techniques used for thin film deposition. Among the different techniques, importance is given to Spray pyrolysis and Chemical bath deposition (CBD) as these chemical methods are used for sample preparation in the present work. Vacuum evaporation is also described as this technique is used for depositing electrode in the present work. Other techniques are only briefly discussed.

Chapter 3 contains the detailed theory of experimental work presented in this thesis. This includes theory of TSC measurements as well as dark conductivity.

In Chapter 4 a review of works on CdS films is given. This chapter has two parts; the first part contains details of preparation and characterisation of spray pyrolysed CdS thin films. TSC measurements on n-type CdS samples revealed that the conductivity of this type of samples is due to mobility of S vacancy as well as due to the charges released from Cd-S vacancy complexes. Effect of annealing on these defect levels was also analysed and found that air annealing results in the removal of vacancy complex and the appearance of another level due to chemisorbed oxygen. But on the other hand vacuum annealing did not affect these defect levels at all. TSC measurements were also performed on the p-type CdS films obtained by doping with copper and this indicated the presence of S vacancy and acceptor level due to the presence of Cu. This results shows that Cu merely diffused into the CdS and no other compound is formed when n-CdS is converted into p-CdS. Variation of irradiation time on TSC spectra of these two types of CdS samples was also studied and these results are linked with calculated cross sections of the defect levels. Different heating rates were used for these samples and results obtained from this study is also discussed. Polarity of different trap levels observed is also determined. Dark conductivity measurements were also taken on n- and p-type CdS samples and results are in good agreement with the TSC results.

In part II of this chapter, results of analysis made on CBD CdS films is described. As prepared CBD CdS samples are high resistive (~10^7 Ω cm) and effect of aging and annealing on sheet resistance of these high resistive samples were studied. TSC measurements of these samples could not reveal any defect level. For the preparation of solar cells of better efficiency, it is felt that a low resistive CdS layer is required at the top surface near to the electrode of the cell. Several attempts were made for converting the CBD films into low resistive one and finally CdS films of resistivity as low as 5 Ω cm could be prepared. This was achieved by treating the CBD CdS films with solutions of $InCl_3$, $CdCl_2$ or $SnCl_4$ etc. TSC measurement of these low resistive CdS samples gave an idea about the defect levels that caused low resistivity. It was found that the carriers from S vacancy, Cd-S vacancy complex, chemisorbed oxygen and chloride ions were the reason for the low resistivity. Calculation of capture cross section shows that the chloride ions contribute much to the low resistive nature of the samples. Effect of annealing on the defect levels was also studied. Discussion of XPS spectra of low resistive CdS film is also included in this chapter.

Chapter 5 describes the analysis made on $CuInSe_2$ (CIS) thin films prepared using CBD technique. CIS based solar cells have shown efficiency > 17% in recent times that is the highest efficiency of a thin film single junction solar cell and this indicates the importance of this material in the field of terrestrial photovoltaic application. Very recently CIS thin films were prepared using CBD techniques for the fabrication of CIS/CdS thin film solar cells in the same laboratory. Naturally the analysis of defect levels in CIS films prepared using this technique is quite essential. From TSC measurements it was detected that there are Se and Cu vacancies in the as prepared CIS samples. On air annealing, Se vacancy disappears and a donor level appears along with the Cu vacancy. On vacuum annealing, nothing is happened to Se vacancy. But instead of Cu vacancy Fe impurity was detected. Probable reason for the origin of Fe impurity is also discussed in this portion.. Effect of variation of light irradiation time and heating rates on the TSC spectra of various CIS samples were discussed in this chapter. Dark conductivity measurements were done on as prepared CIS sample as well as on annealed

samples and results are found to be in good agreement with those obtained from TSC measurements.

PbS is a good semiconductor with low band gap (0.2-0.4 eV). It has been proposed that a solar thermal photovoltaic system employing PbS photocells would be able to achieve 14% efficiency for conversion of solar energy into electrical energy. In Chapter 6 TSC studies on PbS thin films prepared using CBD technique without addition of any oxidant is presented. This chapter also gives a brief review of works on PbS films. From the TSC analysis, it was possible to detect defect level that can act as sensitizing center for photoconductivity in PbS films. Effect of complexing agent on TSC spectra of PbS samples is described in this chapter. Dark conductivity measurements were also made on these samples and results are discussed.

In the last decade, another important semiconductor material namely iron suphide (FeS_2) has received growing attention as a useful material for solar energy application and its first report came in 1984. So far several methods had been employed for its preparation. In the present work attempts were made to prepare FeS_2 films using spray pyrolysis and CBD techniques and the details of these works are included in chapter 7. This chapter also gives a brief review of works on FeS_2 films. At first spray pyrolysis was used for the preparation FeS_2 thin films using air as carrier gas. But XRD analysis indicated that the sample contains iron oxide and FeS phases and not in the FeS_2 form. So attempts were made to prepare these films using CBD technique. XRD analysis of films obtained using this technique showed that the film is amorphous. PIXE spectra showed the presence of Fe and S in the films, but also the presence of Ca impurity from unidentified source. Optical absorption studies were made on these samples and variation of band gap with preparation temperature and annealing temperature is also discussed. TSC measurements did not reveal any defect levels in these samples.

Chapter 8 incorporates the summary and conclusions of the work presented in earlier chapters. Most of the results presented in this thesis have been presented in seminars/symposia and accepted/communicated for publication in journals and details are given here.

List of papers presented/published/communicated in different national seminars/journals

1. Electrical studies on trap levels present in n- and p-type spray pyrolysed CdS thin films
   N.A. Zeenath, K.P. Varkey and K.P. Vijayakumar.
   J. Phys: Condensed Matter. 10(9)(1998)2053
2. Effect of annealing time and temperature on variation of sheet resistance of chemically prepared thick CdS films due to aging
   N.A. Zeenath, P.K. Vidyadharan Pillai and K.P. Vijayakumar.,
   Proc. IV symposium of MRSI, Trivandrum (1993) p 106.
3. Pyrite films for photovoltaic conversion.
   N.A. Zeenath,Gracyamma Joseph and C. Sudha Kartha.,
   Proc. National Solar Energy conf. Trivandrum (1994)
4. Characterisation of CdS films prepared by different techniques using TSC measurements
   N.A. Zeenath, C.Sudha Kartha and K.P. Vijayakumar.,
   Proc. VI MRSI symposium, Kharagpur (1995) Abs. No. 117.
5. Studies on different trap levels present in $CuInSe_2$ thin films prepared using Chemical Bath Deposition
   N.A. Zeenath, P.K. Vidyadhran Pillai, M. Lakshmy, K. Bindu and K.P. Vijayakumar
   Proc. Symposium on Current Status on Solar Energy Material and Systems, Anna University, Chennai (1997) p 36.
6. TSC measurements on chemically deposited $CuInSe_2$ thin films
   N.A. Zeenath, P.K. Vidyadharan Pillai, K. Bindu, M. Lakshmy and K.P. Vijayakumar
   Proc. DAE Solid State Symposium, Cochin University, Kochi (1997) p 178.
7. Studies on low resistive CBD CdS films using TSC and XPS techniques.
   N.A. Zeenath, S.Bini, S.B. Syamala, C.Sudha Kartha, K.P. Vijayakumar and Jun Imai, Dept.of Applied Chemistry and Molecular Science, Iwate University, Japan. Toshihiro Yoshida, Chemical Division,Iwate Industrial Research Institute, Japan. Yasube Kashiwaba, Dept. of Electrical and Electronic Engineering, IwateUniversity, Japan
   Europhysics Letters. (Paper under revision)

8. Study of trap levels by electrical techniques in p-type $CuInSe_2$ thin films prepared using Chemical Bath Deposition
   N.A. Zeenath, P.K. Vidyadharan Pillai, K. Bindu, M. Lakshmy and K.P. Vijayakumar
   Communicated to Physica Status Solidi.
9. TSC measurements of CdS, CuInSe2 and PbS thin films used for photovoltaic Application
   N.A. Zeenath and K.P. Vijayakumar. Accepted in the 5th IUMRS International Conference in Asia, Bangalore, October 13-16, 1998

Chapter 1

General Introduction to Semiconductor materials

1.1. Introduction

The research on semiconductors began almost hundred and fifty years ago. Earlier this type of materials was distinguished from metals and other poor conductors using the property of negative temperature coefficient of resistance - i.e., their resistance generally falls as the temperature is raised, while that of a metal rises. Michael Faraday appears to be the first one to notice this effect, when carrying out experiments on silver sulphide [1,2]. Later it has been found that over a certain range of temperature the resistance of a semiconductor may increase as the temperature is raised, particularly if it contains a fair amount of impurity. At high temperature, however, a point is reached where a rapid decrease in resistance sets in as the temperature is further increased. Again certain metallic films show a negative temperature coefficient of resistance as may also polycrystalline ingots of some metals. Actually these effects are later found to be due to oxide films or actual gaps separating the individual crystals but led to metals like titanium and zirconium once being listed as semiconductors. With these exceptions in mind, however, it is generally true to say that pure semiconductors have a negative temperature coefficient of resistance. They are generally associated with a number of other properties that have been used to distinguish them, which we shall discuss briefly in the following paragraphs.

Except at temperatures not much below their melting point, semiconductors have resistivities considerably higher than good metallic conductors and much less than that of good insulators. A good metallic conductor has a resistivity of the order of 10^{-6} Ω cm at room temperature and an insulator has 10^{12} Ω cm. But semiconductors generally have room temperature resistivities in the range of 10^{-3} to $10^{6}\Omega$ cm.

After Faraday's observation two important advances were made in the field of semiconductor research during 1873 and 1874. The phenomenon of rectification was

observed by F. Braun [3] using substances like lead sulphide and iron pyrite and photoconductivity was observed in selenium by W. Smith [4]. After this, a great deal of work was carried out and a class of substances called semiconductors, with these properties began to emerge. A review of the early work has been done by K. Lark-Horowitz [5], giving a very extensive bibliography containing over 350 references. Similarly another review by A.F. Ioffe [6] gives a good coverage of early Russian works.

The following properties of this type of materials were considered to be very important at that time. i) negative temperature coefficient of resistance ii) resistivity in the range of 10^{-3} to 10^{6} Ω cm iii) generally high thermo-electric power, both positive and negative relative to a given metal iv) rectifying effects are at least non-ohmic behaviour v) sensitivity to light - either producing a photovoltage or change of resistance.

A most important event, as it turned out later, took place in 1879 with the discovery of the Hall effect [7], which dealt with the transverse voltage developed across a conductor carrying a current in a magnetic field. This effect turned out to be the key to understand electrical conduction in semiconductors and in distinguishing them from other poorly conducting substances. A measurement of the Hall voltage enables us to determine directly the number of current carriers per unit volume and whether they are positively or negatively charged. It also enables us readily to distinguish ionic conduction from electronic conduction, a distinction that is very necessary, as the conductivity due to former increases rapidly with temperature, and may lead to a false conclusion.

The first systematic use of Hall effect to study semiconductors appears to be due to K. Baedeker [8] using CuI. Detailed studies of large number of substances were made by J. Konigsberger [9] using the Hall effect. It was found that the number of current carriers in semiconductors are very much less than that in metals but their mobility is somewhat higher. An important result of this work was that the elements like silicon, selenium and tellurium were classified as "semiconductors" and is interesting to note that Ge was also added to this list [10]. Another equally important observation was regarding the sign of the charge carriers. This was sometimes found to be negative as expected for electron but was

also found in many instances to be positive, and even to change from positive to negative as the temperature was raised.

A considerable amount of work on a large variety of substances, thought to be semiconductors was carried out between 1910 and 1930, but not a great deal of fundamental progress was made. In nineteen thirties the stimulus of technological applications again caused an increased interest in these substances. A study of the chemistry of a number of semiconductors led C. Wagner [11] to identify two distinct types of semiconductors - defect and excess semiconductors. Defect semiconductors were those with a metallic content less than that corresponding to stoichiometric composition i.e., oxidised compounds. They generally showed a positive Hall coefficient at low temperature and a positive thermoelectric power. The 'excess' semiconductors were 'reduced' compounds and had an excess of metal. They had generally a negative Hall coefficient at all temperature. For 'defect' semiconductor the Hall coefficient sometimes became negative at high temperatures. These are what we now call respectively p-type (p for positive) and n-type (n for negative) semiconductors.

Much of the uncertainty of the early work on semiconductors arose through a failure to differentiate between effects that arise in the bulk of the material and those which are characteristic of the surface or of the interface between two different materials. Extensive use of compressed powder samples accentuated the surface effects. It was later thought that a negative temperature coefficient of resistance is always a bulk effect but it is now clear that this is not so. Rectification was rightly classified as a surface or interface effect but it is quite interesting to note that a great deal of confusion was there over photovoltaic and photoconductive effects at that time.

1.2. Application of semiconductors

The first important application of semiconductor was to provide rectifiers for low-frequency alternating currents. Such rectifiers, using selenium were made as early as 1886 by C.E. Fritts [12] although they were not used to any extent in power engineering or in electronic equipment till much later. The copper oxide rectifier was introduced by

L.O. Grondahl and P.H. Geiger [13] in 1927 and came to be used extensively as a low power rectifier in battery chargers, wireless sets etc. Even though these devices had limited usage it can be safely stated that these developments led to a great deal of work on both copper oxide and selenium. The photoconductive properties of selenium and copper oxide have been used to provide "exposure meters" for photography and "photo cells" used in the film industry (for transforming the markings on the sound track into electric currents for amplification and reproduction by loudspeakers). Such cells also used in a number of automatic devices such as burglar alarm, train counters etc. By 1904, it was shown that the rectifying properties of semiconductors could be used to provide a detector of the high frequency currents set up in an electric circuit by radiowaves. An interesting controversy arose as to whether the rectification effects were electrical or thermal in origin. This was settled by the extensive work of G.W. Pierce [14] who showed that there could be no doubt that they are electrical.

By 1939, the crystal detectors were replaced by the thermionic valve. With the development of microwave for radar, the crystal detectors came into existence again, since no other device was found to be useful at these extremely high frequencies. Silicon proved to be the best substance for this application. In fact this paved the way for a great deal of fundamental work on silicon at Bell Telephone Laboratories and at Purdue University in USA. Germanium, being the next element to silicon in the same column of the periodic table, was also extensively studied in these laboratories. Since it has much lower melting point and is easier to purify, it was a more suitable substance than silicon for fundamental studies and soon became a well studied semiconductor. As it turned out, its study as a semiconductor was most fortunate since it led to the discovery of transistor action [15]. The detailed study of transistor action and of the controlled injection of current carriers into semiconductors by W. Shockley et al.,[16] led to an enormous increase in research on the properties of Ge and later of Si, as it was realised that the transistor would revolutionize the future development of electronics and would largely replace the vacuum tubes used by electronics industries at that time.

Another group of semiconductors that found important applications is the one known as the infrared photoconductors particularly the sulphide, selenide and telluride of lead. These have been used to make sensitive infrared detectors and great deal of work started in Germany during the years 1940-45. Works and development of infrared detectors has been reviewed by R.A. Smith [17].

The modern successor to the transistor is the integrated circuit (IC) in which many transistors and their associated components such as resistors, capacitors etc., are produced by controlled diffusion of impurities into a small chip of Silicon. This has revolutionized the electronics industry for the second time in two decades and has made possible incredibly complex systems such as the modern electronic digital computer. One other application requires special mention, namely the solid state laser based on the properties of semiconductors. This has provided new advances in spectroscopy and linked with optical fibers it is likely to play a vital part in optical communications. A less complex, but related device, LED is finding widespread use to provide displays for calculators, computers and signaling systems and also have a key role in optical communications.

There are many other important applications of semiconductors that have gained momentum in recent years. For example, the use of Solar cells to provide power for satellite and even their possibilities for wide scale power generation, now being actively examined, are based on the photovoltaic effect in semiconductors. When a semiconductor is exposed to greater than bandgap optical excitation, minority and majority carriers are produced which can be separated using the built in field of a junction or barrier, thereby producing a photo emf and /or generating a photocurrent in an external circuit. This is an attractive device to detect light and efficient means to convert light into electric power. Direct conversion of sunlight into electric power is the most attractive with lowest entropy, without moving parts and requiring almost no maintenance. It has the potential to become the most cost-effective means for global large scale solar energy conversion.

Many of the semiconductors have been studied as materials for non linear optics. It was found that structural modifications involving molecular engineering to produce alternate artificial materials should be attempted to obtain materials with large and fast

optical nonlinearity. Crystal contain periodic arrays of atoms or molecules extending in all the three dimensions. If this is curtailed in one dimension, the electrons of the solids can be confined to the other two dimensions. This is achieved by sandwiching thin ($100A^o$) layers of a semiconductor material between two thick layers of another semiconductor of higher band gap. Such structures are called "quantum wells" and arrays of quantum wells have been found to be excellent candidates for photonics application. Electrons can similarly be confined to one dimension, producing "quantum wires". The next step would be "quantum dots" where the confinement exists in all the three dimensions. A few atoms (10-100) or molecules of a semiconductor formed as a cluster of a few nanometer size and confined by an external potential would make a quantum dot. Molecular Beam Epitaxy and vapour deposition techniques can be used to obtain quantum dots of extremely small sizes. These quantum dots are practical realization of 'particle-in- a box'. The spatial confinement leads to an extension in the momentum space resulting from the basic principle of uncertainty. Electron-hole pairs in semiconductors are known to form quasiparticles called excitons. The typical spatial extension of an exciton in a crystal is called the exciton Bohr radius, typically a few nanometers. If the crystallite size itself falls short of this, interesting effects due to exciton confinement are expected. This is known as the 'strongly confines regime'. Quantum confinement also results in an enhancement in the nonlinear optical response of a semiconductor.

1.3. Charge Carriers in Semiconductors

The band picture of pure semiconductor consists of conduction band (CB) and valence band (VB) separated by a forbidden gap (~1 eV for intrinsic semiconductor). The conductivity of the semiconductors can be greatly varied by adding suitable impurities with low ionization energies (0.01 eV). Many compounds with band gaps higher than 1 eV, when doped, behave like semiconductors. In the following paragraphs, we shall discuss the carrier concentration in a pure semiconductor and then consider the changes due to the addition of impurities, which results in doped or extrinsic semiconductors.

1.3.1. Intrinsic Semiconductors

In intrinsic semiconductors, the charge carriers are thermally generated electron-hole pairs. If n and p denote the electron and hole concentration, then $n = p$ for the intrinsic case. The energy distribution of charge carriers can be obtained using Fermi-Dirac statistics and for electrons having energy E, the probability function may be written as

$$f(E) = \frac{1}{1+\exp(\frac{E-E_F}{kT})} \tag{1.1}$$

where k is the Boltzmann constant, T is the temperature and E_F is the Fermi energy known as the Fermi level.

The number of electron states with energy E and E+dE can be calculated as [18]

$$N(E)dE = \frac{\sqrt{2}}{\pi^2}(\frac{m_e^*}{\hbar^2})^{\frac{3}{2}}(E - Ec)^{\frac{1}{2}}dE \tag{1.2}$$

where m_e^* is the effective mass of the electron and Ec is the energy at the bottom of the CB. The number (n) of electrons or charge carriers can be obtained using equations (1.1) and (1.2) by integrating between Ec and E_{top}(upper most level of CB) respectively, i.e.:

$$n = \int_{Ec}^{Etop=\infty} N(E)\, f(E)\, dE = \frac{\sqrt{2}}{\pi^2}(\frac{m_e^*}{\hbar^2})^{\frac{3}{2}} \int \frac{(E - Ec)^{\frac{1}{2}}}{1 + \exp\frac{E - E_F}{kT}} dE \tag{1.3}$$

For $Ec - E_F >> kT$, the Fermi-Dirac distribution approaches the Boltzmann distribution. One can neglect unity in the denominator. Hence,

$$n = N_c \exp(-\frac{Ec - E_F}{kT}) \tag{1.4}$$

where

$$N_c = 2(\frac{2\pi m_e^* kT}{h^2})^{\frac{3}{2}} \tag{1.5}$$

is the 'effective density of states' in the CB.

Using similar arguments, the number (p) of holes in the VB can be written as

$$p = N_v \exp(-\frac{E_F - Ev}{kT}) \tag{1.6}$$

with N_v, the effective density of states for holes at the top of the VB, given by

$$N_v = 2(\frac{2\pi m_h^* kT}{h^2})^{\frac{3}{2}} \tag{1.7}$$

m_h^* being the effective mass of the hole and Ev is the energy corresponding to the top of the VB.

The Fermi level E_F for intrinsic case can be obtained from equations (1.4) and (1.6)

$$E_F = \frac{Ec + Ev}{2} + \frac{kT}{2} \ln \frac{N_c}{N_v} \tag{1.8}$$

Thus, Fermi level E_F lies midway in the band gap at T=0

Using equations (1.4) and (1.6) we get

$$n.p. = N_c N_v \exp(-\frac{Eg}{kT}) \tag{1.9}$$

where Eg=Ec-Ev is the band gap.

The relationship (1.9) is known as the law of mass action. For intrinsic case

$$n_i = \sqrt{np} = \sqrt{N_c N_v} \exp(\frac{-Eg}{2kT}) = 2(\frac{k}{2\pi\hbar^2})^{\frac{3}{2}} (m_e^* m_h^*)^{\frac{3}{4}} T^{\frac{3}{2}} \exp(-\frac{Eg}{2kT}) \tag{1.10}$$

Equation (1.10) implies that the intrinsic carrier concentration varies with the temperature and band gap. For semiconductors with large Eg, there are practically negligible number of mobile electrons at room temperature. In order to get appreciable conductivity, impurities are added to them. The semiconductor is then called an "extrinsic semiconductor".

1.3.2. Extrinsic semiconductor

1.3.2.a. Impurity levels

Incorporation of impurities or imperfections in a semiconductor introduces localised discrete energy levels within the forbidden band. Its effect can be derived by treating the potential in the vicinity of this impurity as a localised perturbation with the center on the impurity atom itself. If the concentration of the localized perturbation increases (i.e. when the impurity concentration becomes large) the corresponding wave-functions overlap and form an impurity band. Effect of impurities can also be visualised by considering the bond picture. The impurity atom can occupy a substitution lattice site. For example, the addition of a pentavalent impurity to Silicon is equivalent to addition of an extra electron to an otherwise neutral environment and this will introduce a donor level in Si atom. Again addition of trivalent impurity to Si results in the production of acceptor level. The donor levels of low ionisation energies ($E_D \sim 0.05$eV) are termed as 'shallow donor level' and are

located near the CB. Similarly, the shallow acceptor levels are located near the VB as shown in figure 1.1. It may be noted that it is not always possible to predict whether a particular impurity will form a donor or acceptor level. Many elements form more than one donor or acceptor levels [19,20]. Here we have discussed the effect of impurity atoms belonging to the adjacent group (of the periodic table) on the right and left of the elemental semiconductor (the fourth group) which give rise to shallow levels. Suppose doping is done by foreign atom of say VI, VII group on the right side and I and II groups on the left-hand sides. This may give discrete localised levels far removed from the band edges and are known as 'deep levels'. Physically, it signifies that such deep donor and acceptor have rather high ionisation energy (several kT away from the band edges). Such levels are also sketched in figure1.1. labeled as "deep donor (EDD)" and "deep acceptor (EAD)" levels.

In III-V compound semiconductors, group II and VI atoms enter substitutionally replacing group III and V atoms as shallow acceptors and donors respectively. Since the effective mass of electrons and holes differ in III-V compounds, the ionization energies of donor and acceptor levels also differ. Transition metals Fe, Co and Ni have been observed to create deep-lying acceptor state in GaAs [21]. For II-VI semiconducting compounds, group I (e.g. Ag,Cu) and group VII (e.g.Cl) elements would replace II and VI atoms substitutionally to introduce shallow acceptors and donors. Moreover, group III elements (such as In,Ga) replacing group II element in the lattice of II-VI material substitutionally should also introduce shallow donors. For example, in CdS and ZnO crystals, an excess of Cd or Zn respectively act as donors. A non stoichiometric film of CdS rich in Cd is observed to be n-type [22].

In addition to chemical impurities, there are point defects (e.g. vacancies, interstitials), line defects (dislocations), surface defects etc., giving rise to localised levels in the forbidden energy gap. Since these irregularities cause a perturbation in the periodic crystalline field giving rise to energy states in the forbidden energy gap, these gap states are termed as "trapping centers".The electron states near a CB can trap an electron and a hole is trapped in an electron energy state higher but towards the VB edge. The relative positions

are shown in figure 1.2. These gap states are also known as recombination centers facilitating electron-hole recombination by capturing an electron from the CB and subsequently transferring them to the VB, whenever a hole appears near the trap to recombine with the trapped electron

1.3.2.b. Carrier concentration and Fermi level

Consider the case of an n-type semiconductor. Let n and p be respectively the electron and hole concentrations. Further, suppose that the semiconductor is doped with N_D donor atoms and N_A acceptor atoms. The charge neutrality condition can be written as

$$n + N_A^- = p + N_D^+ \quad (1.11)$$

where N_D^+ and N_A^- represent the "ionised" donor and acceptor concentrations (which alone contribute to the mobile carrier concentration) given by [23]

$$N_D^+ = N_D \left[1 - \frac{1}{1 + \frac{1}{g_i} \exp\left(\frac{E_D - E_F}{kT}\right)} \right] \quad (1.12)$$

and

$$N_A^- = N_A \left[1 - \frac{1}{1 + \frac{1}{g_i} \exp\left(\frac{E_A - E_F}{kT}\right)} \right] \quad (1.13)$$

where E_D and E_A are the donor and acceptor level energies and g_i is the degeneracy factor. Using equations (1.13) and (1.6), one can get

$$N_v \exp - \left(\frac{E_F - E_v}{kT}\right) - N_c \exp - \left(\frac{E_c - E_F}{kT}\right) + (N_D^+ - N_A^-) = 0 \quad (1.14)$$

Solving the above equation gives the position of Fermi level

$$E_F = E_{Fi} + kT\sinh^{-1}\left(\frac{N_D^+ - N_A^-}{n_i}\right) \quad (1.15)$$

where E_{Fi} is the intrinsic Fermi level and n_i is the intrinsic carrier concentration.

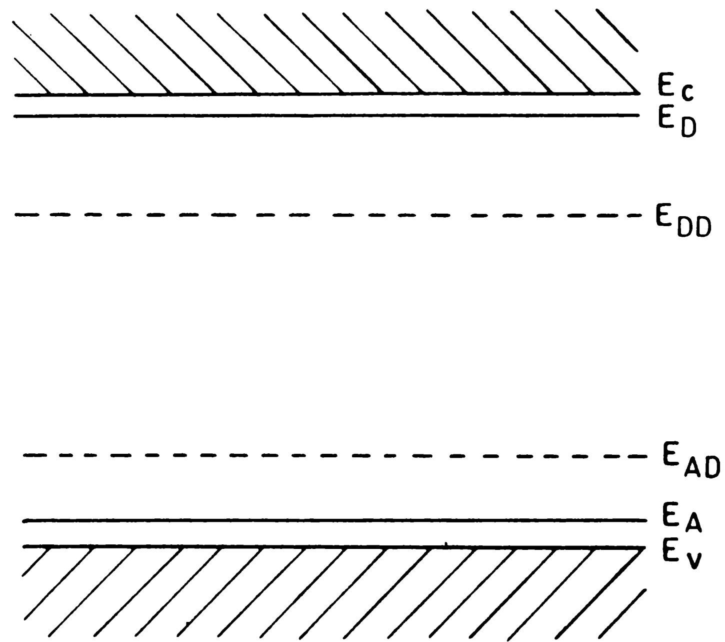

Figure 1.1. Shallow and deep acceptor/donor levels

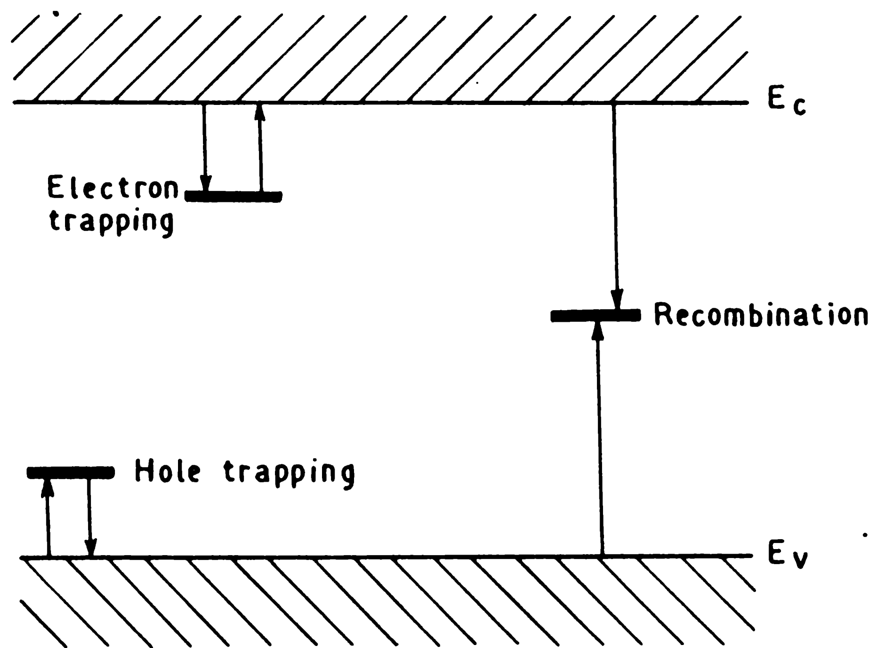

Figure 1.2. Relative position of different types of trapping centers.

Since $\sinh^{-1}x$ is positive for $x > 0$; and negative for $x < 0$, the following may be concluded.

Case1: n-type semiconductor

$E_{Fn} > E_{Fi}$ since $N_D^+ > N_A^-$

Case2: p-type semiconductor

$E_{Fp} < E_{Fi}$ since $N_D^+ < N_A^-$

The relative positions of intrinsic Fermi level (E_{Fi}) and Fermi level for p-type (E_{Fp}) and n-type (E_{Fn}) are shown in figure 1.3.

Case 3: intrinsic or completely compensated extrinsic semiconductor. For intrinsic semiconductors ($N_D^+ = N_A^- = 0$) and for extrinsic semiconductor with complete compensation having equal ionised donor and acceptor atoms ($N_D^+ = N_A^-$)

$$E_F = E_{Fi} \tag{1.16}$$

Case 4.heavily doped semiconductors, $| N_D^+ - N_A^- | >> n_i$. Equations (1.15) simplifies to

$$E_F = E_{Fi} \pm kT\ln\left[\frac{|N_D^+ - N_A^-|}{n_i}\right] \tag{1.17}$$

Since $\sinh^{-1}x \sim \pm \ln |x|$ for large value of x. Here the positive and negative signs respectively represent the case for n- and p-type semiconductors.

If heavy doping of only one type (n- and p-type) is present equation (1.17) simplifies to

$$E_{Fn} \text{ (heavy donor doping)} = E_{Fi} + kT \ln \frac{N_D}{N_c}$$

(1.18)

$$E_{Fp} \text{ (heavy acceptor doping)} = E_{Fi} - kT\ln \frac{N_A}{N_v}$$

The carrier concentration can also be calculated using the charge neutrality condition [equation (1.11)] and the relation for intrinsic semiconductor ($n.p.=n_i^2$) It is given by

$$n = \frac{1}{2}(N_D^+ - N_A^-) + \sqrt{\frac{1}{4}(N_D^+ - N_A^-)^2 + n_i^2}$$

(1.19)

$$p = -\frac{1}{2}(N_D^+ - N_A^-) + \sqrt{\frac{1}{4}(N_D^+ - N_A^-)^2 + n_i^2}$$

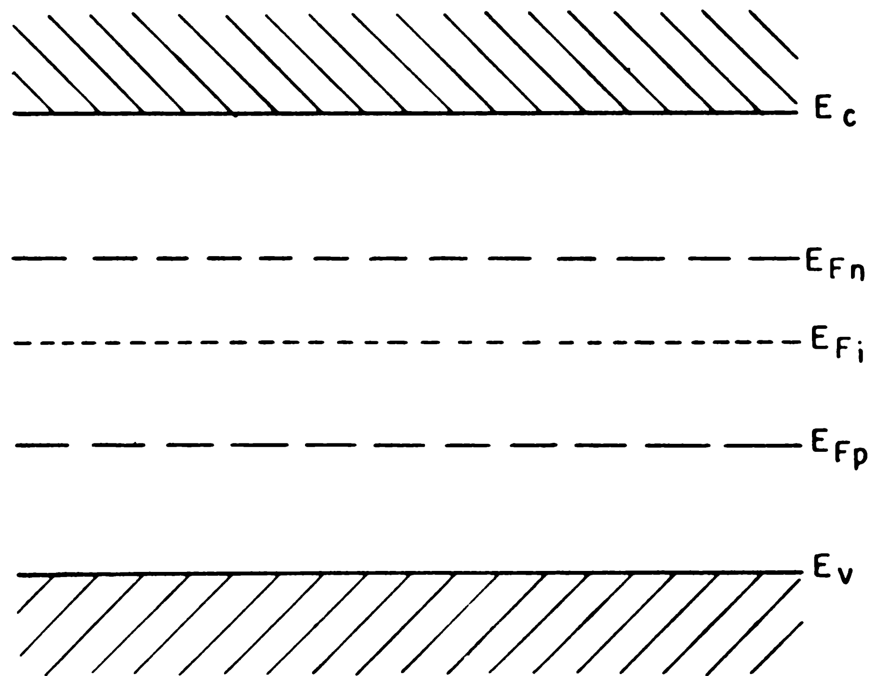

Figure 1.3. Fermi level positions of intrinsic, n-type and p-type semiconductors

which simplify to the following expressions for extrinsic semiconductors with only one type of doping.

$$n = \frac{1}{2}\left[N_D^+ + \sqrt{N_D^{+2} + 4n_i^2}\right] \text{; for n - type case}$$

$$p = \frac{1}{2}\left[N_A^- + \sqrt{N_A^{-2} + 4n_i^2}\right] \text{; for p - type case} \qquad (1.20)$$

1.4. Carrier transport in semiconductors

There are two mechanisms by which current can flow in semiconductors-drift and diffusion. The drift current results from the movement of electrons /holes under the action of an applied electric field and is similar to that in a metal. The diffusive motion of carriers is caused by gradients in carrier concentrations. Concentration gradients can be established by the graded doping of a semiconductor, as well as by the injection of carriers from a suitable source. Besides drift and diffusion, the other basic process is recombination. Taken together with the carrier generation, these processes form the physical basis for all semiconductor devices.

1.4.1. Drift

In an n-type semiconductor with uniform donor concentrations, in the absence of an applied electric field, electrons will undergo a continual random thermal motion interrupted by collisions. The thermal motion leads no net displacement of the electrons over a long enough period of time.

If an electric field is applied to the semiconductor sample, an additional velocity component will be superimposed upon the thermal motion of the carriers. This additional velocity component, the drift velocity, will have a direction opposite to (for electrons) the electric field. Final actual displacement of the electrons is determined by these two components.

The magnitude of the drift velocity at a given time t after a collision will be given by $v(t) = v(0) + at$ where $v(0)$ is the drift velocity immediately upon collision. If we take it as zero, it is equivalent to assuming that the electrons suffer collisions that completely randomize their motion. The magnitude of acceleration is given by $a = qE/m^*$, where m^* is the effective mass of the electrons. If the time interval between collisions is t_{coll}, then the average drift velocity of the electrons will be

$$v_{drift} = (qE/2m^*)t_{coll} = \mu E \quad (1.21)$$

where

$$\mu = v_{drift}/E = q\, t_{coll}/2m^* \quad (1.22)$$

is the mobility of the electrons.

This treatment assumes that the time interval between collisions t_{coll} is independent of the applied electric field. This is a reasonable assumption only so long as the drift velocity is small in comparison to the thermal velocity of carriers (which is about 10^7 cm/sec for Si at room temperature). As the drift velocity becomes comparable to the thermal velocity, its dependence on electric filed will begin to depart from the simple relationship given above. As the electric field increases, drift velocity increases less rapidly. At large enough fields, drift velocity becomes a maximum.

1.4.1.a. Mobility of electrons and holes

The time interval between collisions is determined by the various mechanisms by which the electrons or holes can lose their acquired drift velocity. The probability of a collision taking place in a unit time $1/t_{coll}$ is the sum of the probabilities of collisions due to the various such scattering mechanisms i.e

$$1/t_{coll} = 1/t_{coll,\ impurity} + 1/t_{coll,lattice} \quad (1.23)$$

or

$$1/\mu = 1/\mu_I + \mu_L$$

which correspond to the two most important scattering mechanisms, impurity and lattice scattering.

Impurity scattering is due to the fact that when an electron travels past a fixed charged particle (an ionized acceptor or donor) its path will be deflected by the charge of that fixed particle. The probability of impurity scattering will depend on the total

concentration of ionized impurities (C_T) present in the crystal and μ_I is found to proportional to $T^{3/2}/C_T$. Lattice scattering is due to the thermal vibration of atoms of the crystal lattice which disrupts the periodicity of the lattice and thereby impedes the motion of the electrons μL is proportional to $1/T^{3/2}$.

1.4.1.b. Electrical Conductivity

In the case of a homogeneous semiconductor of length l and cross sectional area A having electron and hole concentration n and p; the electron and hole current densities J_n and J_p are given by

$$J_n = q\, n\, \mu_n\, E$$

$$Jp = q\, p\, \mu_p\, E$$

where E is the electric field experienced by the semiconductor

Total current density $J = J_n + J_p$

$$J = q\, E\, (n\, \mu_n + p\, \mu_p) \qquad (1.24)$$

If V is the voltage applied across the semiconductor and I is the current, the resistance

$$R = V/I = \rho\, l/A = l/\sigma A \qquad (1.25)$$

where ρ is the resistivity and σ is the conductivity

Again $\qquad I/A = |J| = \sigma\, V/l$

But for a uniformly doped bar V/l denotes the electric field, so that

$$J = \sigma\, E \qquad (1.26)$$

From (1.24) and (1.26), one can get

$$\sigma = q\, (n\, \mu_n + p\, \mu_p) = \sigma_n + \sigma_p \qquad (1.27)$$

where σ_n and σ_p denotes the electron hole component of the conductivity respectively.

For an intrinsic semiconductor $n = p = n_i$, so the intrinsic conductivity σI is given by

$$\sigma_i = q\, (\mu_n + \mu_p)\, n_i \qquad (1.28)$$

In the case of extrinsic semiconductor, with equilibrium concentration n_0 and p_0

$$\sigma = q\, (\mu_n\, n_0 + \mu_p\, p_0) \qquad (1.29)$$

In semiconductors both the carrier concentration and mobility are temperature sensitive. Thus the temperature dependence of conductivity is determined by the

temperature dependence of both these quantities. For an intrinsic semiconductor substituting the value of $n_i = k_2 T^{3/2} \exp(-Eg_0/2kT)$ in equation (1.28), we get [24]

$$\sigma_i = q\,(\mu_n + \mu_p)\,k_2 T^{3/2} \exp\,(-Eg_0/2kT) \quad (1.30)$$

where Eg_0 is the value of band gap at 0K and after substituting the temperature dependence of μ_p and μ_n, the equation (1.30) becomes

$$\sigma_i = \text{const.}\ T^{a0} \exp\,(-Eg_0/2kT) \quad (1.31)$$

where a_0 has a value of about -1. In this equation, most of the variation of σ_i is contained in the exponential factor so that a plot of ln σ_i as a function of 1/T gives a straight line whose slope can be used to determine Eg_0.

1.4.2. Impurity band conduction

The ionization energy of shallow donors and acceptors decreases with the increasing concentration of dopants and becomes zero when the impurity concentration reaches a critical value [25] If such a semiconductor is cooled to temperature near 0 K, the conductivity does not drop to zero as in the case of a lightly doped semiconductor but has a finite value. This happens because of impurity band conduction.

When the donor concentration reaches the critical value, it is possible for an electron (or a hole in p-type semiconductor) to move from the ground state of one donor to that of the neighbouring ionized donors by the process of tunneling. In an applied electric field, the magnitude of carriers in one direction becomes energetically favourable compared to the others and the impurity conduction now results with a small activation energy by the "hopping" of the carriers from one impurity site to the another. For nondegenerate materials the distance between neighbouring impurity atoms is large and hopping of carriers becomes highly improbable. In order to describe the energy band structure of a heavily doped semiconductor three additional effects have to be considered.

1.4.2.a. Many Body Effects

Here we must consider many body effects to account for the energies of interaction among the mobile carriers and between carriers and ionized impurities. If we consider the

case of heavily doped n-type semiconductor, many body effects involve ionized donor-electron interaction, electron-electron interaction and electron-hole interaction. These interaction affect the density of quantum states in the conduction and valence band.

i) Donor-electron interaction

We know that in a lightly doped semiconductor, the donor impurity forms an energy level E_D below the CB. The Coulomb screening of donor ions by the majority carrier electrons reduces the impurity ionization energy $E_i = E_C - E_D$. The reduction in the donor ionization energy causes the donor level to move toward the conduction band edge Ec as the donor concentration is gradually increased and ultimately merges into the conduction band. It has been observed that [26] the electron-donor interaction causes only a shift in the donor level toward Ec, but no change occurs in the position of band edges Ec and Ev so that the energy gap Eg remains unchanged.

ii) electron-electron interaction

Electron-electron interaction results in a downward shift in the conduction band edge. This shift is caused by electron exchange energy that evolves from the Pauli's exclusion principle. When the electron concentration in semiconductor becomes sufficiently large, their wave functions begin to overlap. Consequently, the Pauli's exclusion principle becomes operative and electron spread in their momentum in such a way that the overlapping of the individual electron wavefuncion is avoided.

iii) Electron-hole interaction

The majority carriers in a semiconductor screen the minority carriers in the same way as they screen the ionized impurity atoms. In an n-type semiconductor, the electron-hole Coulomb interaction reduces the hole potential energy and causes the VB to move up toward the CB. This upward shift of Ev has been termed the "hole correlation energy" [27]. The hole-hole interaction energy in a heavily doped n-type semiconductor remains negligible because of the very low concentration of holes.

Here we can conclude that the effect of many body interaction on the band structure of a heavily doped semiconductor is to produce a downward shift in Ec and an upward shift in Ev and is illustrated in figure 1.4.

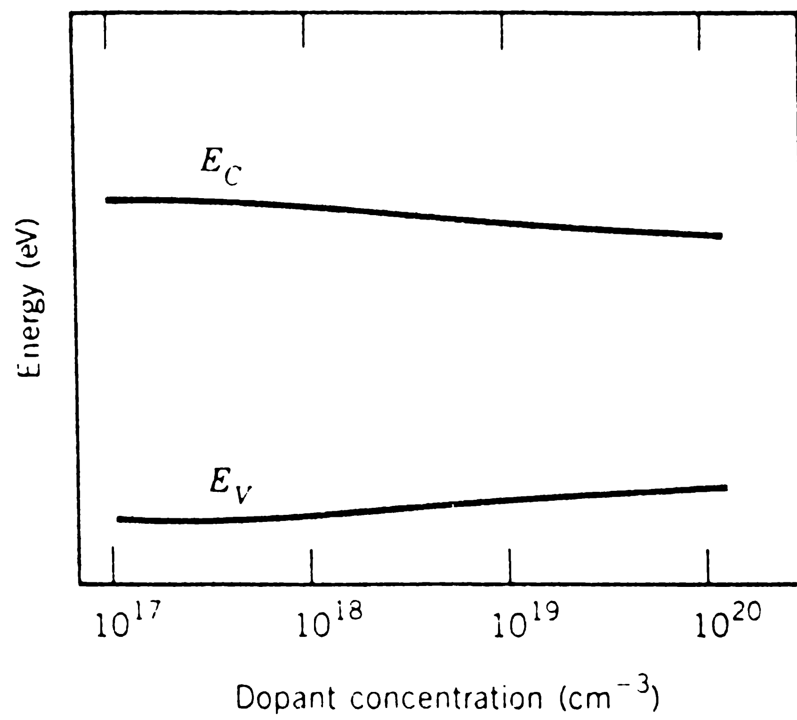

Figure 1.4. Energy band diagram showing the shift of band edges Ec and Ev in a heavily doped semiconductor.

1.4.2.b. Effect of randomness in impurity distribution

The donor and acceptor atoms in a semiconductor have a random distribution and this randomness causes fluctuations in a the local potential. The effect of these fluctuations remains negligible in a lightly doped semiconductor, but in a heavily doped semiconductor they produce a spatially dependent distortion of the quantum density of states. The statistical average of the density of states over the entire crystal, which defines the macroscopic properties of the semiconductor, then shows a tailing of the VB and CB into the energy gap [28]. A high density of randomly distributed dopant impurities further complicates the band structure by creating a band of impurity states. Thus, the discrete donor level in the n-type semiconductor will spread into a band at heavy doping.

1.4.2.c. Effect of carrier degeneracy

In the case of a nondegenerate semiconductor in which the Fermi level lies in the band gap at least 3kT away from the band edges, Maxwell-Boltzmann (MB) statistics are valid and one can get the relation $p_0n_0 = ni^2$. In a heavily doped n-type semiconductor the Fermi level does not remain in the band gap but moves into the CB. A semiconductor in which the Fermi level lies inside either the conduction or the valence band is called a degenerate semiconductor. Such a semiconductor has a large concentration of majority carriers and behaves like a metal . In the degenerate semiconductor we have to use Fermi - Dirac (FD) statistics instead of MB statistics and use of FD statistics reduces the p_0n_0 product below n_i^2. However, the band gap narrowing causes an increase in this product. Thus to incorporate the effect of band gap reduction and the majority carrier degeneracy in a single expression [29], here $p_0n_0 = n_{ie}^2 = K_1^2T^3 \exp(-Eg^{elect}/kT)$ where Eg^{elect} is an effective electrical band gap and has no other significance except that it permits us to express measured p_0n_0 product using the above equation.

1.4.3. Non linear conductivity

In general, the drift velocity $v_d = \mu E$, and it shows that v_d is directly proportional to E and the mobility μ is a constant independent of E. Assuming a strongly n-type semiconductor we observe that

$$J = J_n = \sigma E \tag{1.32}$$

where σ is independent of E since μ is assumed to be constant., This linear relationship between J and E (or between v_d and E) is a statement of Ohm's law. The equation (1.32) is seen to be valid only for low electric fields such that the average drift velocity of carriers is small compared with their random thermal velocity v_{th}. When the electric field becomes large enough to make v_d comparable with v_{th}, Ohms law is no longer valid and the conductivity becomes non-linear.

For a carrier with average drift velocity v_d and charge q, the power generated from the field is qv_dE and if there are no such carriers in a unit volume, the power gained from the field is

$$\text{Power gained/volume} = q\, n_0\, v_d\, E = JE \qquad (1.33)$$

The carriers will reach a steady state at some temperature T_e when all this power is dissipated to the lattice in the form of the emission of phonons. It might be argued that in the steady state the lattice receiving the same power from the carriers as the carriers are receiving from the field. Hence, the lattice temperature should also rise and should ultimately approach the carrier temperature T_e. However this does not happen because the heat capacity of the lattice is enormously large compared to that of electrons and the crystal can lose heat by conduction, convection and radiation. But, when the product J E becomes large, the crystal is also heated up. As long as T_e is only slightly above T, Ohm's law is obeyed and the velocity v_d is proportional to E, making μ a constant. At such value of E electrons and holes are only "warm". As the field is increased gradually, T_e rises continuously and at some value of the field, T_e become significantly higher than T. The carriers now interact more strongly with the lattice, and their average drift velocity falls below the linear projection of its low field value. Consequently, the mobility starts decreasing with the field, and the current voltage characteristic of the semiconductor shows considerable deviation from Ohm's law. The departure from Ohm's law at high electric field can be more readily observed in semiconductors than in metals. The explanation for this is as follows: In metals the electron gas is degenerate, and the average kinetic energy of an electron is on the order of the Fermi energy that is several electron volts and corresponds to a large value of thermal velocity V_{th}. In order to observe the deviation from Ohm's law and to make V_d comparable to V_{th}, the energy gained by an electron from the applied field must

be comparable to its thermal energy. Obtaining this energy in metals requires fantastically large fields at which the metal will melt and evapourate because of joule heating. On the other hand, electron population in a semiconductor is nondegenerate, and the average thermal energy of an electron is only 3kT/2. Hence, a change on the order of kT in the electron energy will cause a perceptible change in its average energy. Changes of this magnitude can be easily achieved by the application of an electric field. It is for these reasons that the nonlinear conductivity could not be observed by early investigators who were mostly concerned with metals. The first observation of nonlinear conductivity was made on Ge in 1951 [30]. Since then, the phenomenon has been observed in all the known semiconductors of importance.

1.4.4. Diffusion

If the concentration of electrons in a semiconductor is not uniform, electrons will diffuse under the influence of the concentration gradient. As in the case of ions, this will lead to an additional contribution to the expression for flux. This contribution is proportional to the concentration gradient and the diffusivity of electrons D_n. The diffusivity of electrons, in turn, is related to the electron mobility by Einstein' relationship

$$D_{n.} = kT\mu_n / q \tag{1.34}$$

the constant kT/q has the dimensions of voltage and is called thermal voltage. Similar considerations apply to the transport of holes. It should be noted that Einstein's relations are true only for non degenerate semiconductors. In the case of degenerate semiconductors, these relations become quite complex [18] and are extremely useful in the discussion of current flow problems in a number of semiconductor devices.

Consider the case of a p-type semiconductor and somehow introduce a few free electrons, the electrons will diffuse through the p-type region away from the region of highest density of electrons. The diffusion process proceeds until equilibrium is reached, that is, until the electron spread about evenly or they have recombined with holes to become bound.

The current density due to electron diffusion is then proportional to the negative of gradient of electron concentration. For a one dimensional model, the diffusion current for electrons [31]

$$J_n = (-q)\, D_n\, (-dn/dx) \tag{1.35}$$

where n is the number of electrons and $D_n = \mu\, kT/q$. For holes the similar equation is

$$Jp = (q)\, D_p\, (-dp/dx) \tag{1.36}$$

Diffusion currents are important in semiconductors but not in metals. The reason is that semiconductor have two types of carriers and also carrier generation is possible in this type of material. A local increase in the concentration of one of the carriers is accompanied by an increase in the other, and the electrical neutrality is maintained even in the presence of a concentration gradient. Metals have only one type of carrier and the self-annihilating large fields set up in the metals resist any effort to create a concentration gradient.

1.5. Excess carriers in Semiconductors

The term "excess carriers" is used for electrons and holes that are in excess of their thermal equilibrium values. Excess carriers can be created in a semiconductor by a variety of processes such as optical excitation, electron bombardment, or injection from a contact. A study of behaviour of excess carriers is important because most of the semiconductor devices operate under nonequilibrium conditions in which electron and hole concentrations are significantly different from their thermal equilibrium values. When excess electrons are introduced in a metal, the process of lattice collisions restores equilibrium. In semiconductor crystals, the processes that restore equilibrium are the diffusion and drift of carriers into or out of the region or the recombination of carriers inside the region. We discussed the drift and diffusion of carriers in the previous sections and recombination of carriers will be discussed in the following sections along with the details of injection of excess carriers.

1.5.1. Injection of excess carriers

1.5.1.a. Injection Mechanisms

The process of optical absorption is an important injection mechanisms. If I(0) is the intensity of the beam incident on a semiconductor material, then the intensity I(d) of the transmitted beam is given by $I(d) = I(0) \exp(-\alpha d)$ where α is the absorption coefficient and has a unit of cm^{-1} if thickness d of the semiconductor is measured in cm. It is seen that when photon energy $h\nu$ is small compared to the band gap Eg, the coefficient α is negligible, and most of the light is transmitted to radiation at these frequencies. The small absorption observed in this region is caused by free electrons that are extracted from lower energy state to higher energy states in a given band. This free carrier absorption obviously does not create electron-hole pairs. As the photon energy increases, α begins to rise rapidly. A photon with energy $h\nu \geq E_g$ is absorbed in the semiconductor because it has enough energy to break the covalent bond and create an electron hole pair. For these frequencies, the crystal becomes opaque to the incident radiation. If a photon has energy considerably in excess of E_g, then an electron excited from the VB to CB will have energy in excess of the average thermal energy. The excited electron now loses energy to the lattice during scattering collisions until its velocity reaches the thermal velocity at that temperature. The process of creating excess carriers by shining light is known as photogeneration. Photogenerated carriers cause an increase in the conductivity of the semiconductor.

Introduction of excess electron-hole pairs in a semiconductor is also known as injection of excess carriers. When excess carriers are injected in a semiconductor, the pn product exceeds n_i^2. An opposite situation is also possible in which $pn < n_i^2$. This happens when the electron and hole concentration are below their thermal equilibrium values. We then talk of extraction of carriers from the semiconductor.

1.5.1.b. Low and High-Level Injection

The carrier injection level is determined by the concentration of excess carriers. When the excess carrier concentration is small compared to the equilibrium majority carrier concentration, it is said to be a low-level injection. If this concentration becomes

comparable to or exceeds the equilibrium majority carrier concentration the injection is called a high-level injection. It has been observed that low level injection is essentially a minority carrier injection because the concentration of majority carriers remains practically unchanged [32]. But in the case of high-level injection, majority carrier concentration will also be changed.

1.5.2. Recombination of excess carrier

It is observed that in a semiconductor in thermal equilibrium the rate of thermal generation G_{th} is balanced by the rate of recombination R. When the semiconductor is illuminated to produce electron-hole pairs by photogeneration at a rate of G_L pairs per unit volume per second, concentration of carriers increases above equilibrium value. Due to increase in concentration, the recombination rate also increases and a steady state is reached when

$$G_{th} + G_L - R = 0 \tag{1.37}$$

Let the excess carriers have been generated by light and the steady state is reached when the light is switched off. At this condition, the excess carriers decay by recombination process and the carrier concentration tends to revert to its equilibrium value. As long as the total concentration n and p are not too large, we can assume that the rate of pair recombination obeys the law

$$R(n,p,T) = \alpha_r (T)\, pn \tag{1.38}$$

where α_r is the constant of proportionality. In dealing with the recombination of excess carriers, the net rate of recombination in excess of the thermal generation rate defined by $U = R - G_{th}$ is important. Thus, when the light is switched off, rate at which the excess carrier decay at a given temperature is given by

$$U = R - G_{th} = \alpha_r (pn - n_i^2) \tag{1.39}$$

Obviously, this is the rate at which the electron and holes in the semiconductor disappear so that this relation can also be written as [28]

$$-\frac{dp}{dt} = -\frac{dn}{dt} = \alpha_r \left[pn - n_i^2\right] \tag{1.40}$$

which is a general relation describing the balance between generation and recombination process. As long as the pn product exceeds n_i^2, the right hand side of equation (1.40) is

positive and both dp/dt and dn/dt decay with time, indicating the recombination of excess carriers. When pn product is decreased below n_i^2, the time derivatives become positive and there is a net generation of carriers.

1.5.2.a. Excess carrier life time

When the light is switched off, besides the recombination in the bulk, electron-hole pairs also recombine at the surface. However, for the sake of simplicity we ignore surface recombination and assure electron-hole concentration to be constant throughout the sample. Writing $p = (p_0 + p_e)$ and $n = (n_o + n_e)$ with n_e and p_e as the number of excess electron and holes, the equation (1.39) becomes

$$U = \alpha_r[(p_0+p_e)(n_0+n_e)-n_i^2]$$

$$= \alpha_r (p_0 n_e + n_o p_e + p_e n_e) \qquad (1.41)$$

which on simplification for n-type semiconductor doped uniformly with N_d donors/cm^3 $n_0 = n_{n0} = N_d$ and $p_0 = p_{n0} = ni^2/N_d$ and since $p_e = n_e$, ignoring $p_e n_e$ in equation (1.41) one can get [33]

$$U = -\frac{dp_n}{dt} = \alpha_r (n_{n0} + p_{n0})\, p_e \qquad (1.42)$$

where $\alpha_r (n_{n0} + p_{n0})$ has the dimension of reciprocal of time and can be written as

$$\tau_p = \frac{1}{\alpha_r (n_{n0} + p_{n0})} \cong \frac{1}{\alpha_r N_d} \qquad (1.43)$$

The constant τ_p is known as the minority carrier lifetime and is a function of temperature, because α_r is temperature dependent.

From equations (1.42) and (1.43) one can get

$$\frac{dp_n}{dt} = -U = -\frac{p_e}{\tau_p} \qquad (1.44)$$

whose solution is $\quad P_e(t) = p_e(0) \exp(-t/\tau_p) \qquad (1.45)$

where $p_e(0)$ is the excess carrier concentration at t = 0 when the light is just switched off. It can be shown that τ_p is the average time that a hole spends before recombining with an electron. The lifetime τ_p is independent of injected carrier concentration as long as the low-level injection condition is maintained .

For a p-type semiconductor similarly we can get

$$n_e(t) = n_e(0) \exp(-t/\tau_n) \tag{1.46}$$

where $\tau_n = 1/\alpha_r N_a$ is the excess electron lifetime. Equation (1.45) and (1.46) describe the decay of excess minority carriers. Since the electrons and holes recombine in pairs, the excess majority carriers decay at the same rate as the excess minority carriers.

1.5.3. Mechanism of Recombination Process

Electron-hole pairs can recombine in a semiconductor in two ways. First method is that an electron can drop directly from the conduction band into an unoccupied state in the valence band. This is known as "band to band recombination". In the second method, an electron initially makes a transition to an energy level lying deep in the band gap, and it subsequently captures a hole from the valence band. This is known as "indirect recombination.

In the process of electron-hole pair recombination, an energy equal to the differences in energy between electron and hole is released. This energy can be emitted as a photon, in which case the recombination is said to be "radiative". Alternatively, the energy can be dissipated to the lattice in the form of phonons. A third possibility is that the energy can be imparted as kinetic energy to a third mobile carrier and this process is called "Auger process". The phonon and Auger recombination are nonradiative.

1.5.3.a. Direct Band-to-Band Recombination

In the case of direct band-to-band recombination, an electron in the conduction band falls into a vacant state in the valence band thus neutralizing an electron-hole pair. Here an electron loses energy of the order of the band gap. In a direct gap semiconductor, the energy is emitted as a photon and the recombination is said to be radiative, In an indirect gap semiconductor, band-to-band transitions involve a large change in electron momentum and the momentum conservation condition requires either emission or absorption of a phonon. Consequently, direct band-to-band recombination had a very low probability in direct gap semiconductor.

In a direct band-to-band recombination, the excess carrier radiative recombination rate Ur and radiative lifetime τ_r are given by [34]

$$U_r = \alpha_r(pn - n_i^2) = \frac{G_{th}}{n_i^2}(pn - n_i^2) \tag{1.47}$$

$$\tau_r = \frac{n_i^2}{G_{th}(n_0 + p_0 + p_e)} \tag{1.48}$$

For a strongly n-type semiconductor having a donor concentration N_d, we have $n_0 \approx N_d$ and $p_0 \approx 0$ and the low-level injection lifetime is obtained by neglecting p_e in equation (1.48)

$$\tau_r \cong \frac{n_i^2}{G_{th}N_d} \tag{1.49}$$

At high level injection p_e is large compared to (p_0+n_0) and

$$\tau_r = \frac{n_i^2}{G_{th}p_e} \tag{1.50}$$

Since G_{th} is more sensitive to temperature variations than n_i^2, the radiative lifetime in equation (1.49) is a slowly decreasing function of temperature.

1.5.3.b. Indirect Recombination via Deep Energy Levels in the Band Gap

Impurity atoms other than donors and acceptors and some types of crystal defects in semiconductor, introduce localized energy levels deep in the band gap away from the band edge. These levels act as stepping stones for electrons between conduction band and valence band, making a substantial enhancement in the recombination process. Depending on its location in the band gap, a deep level can act as an electron or a hole trap or as a recombination center. An electron trap has a high probability of capturing a conduction electron and setting it free after some time. Similar is the case of a hole trap with the only difference that here hole is released into the VB. At a recombination center, the probabilities of electron and hole capture are nearly equal. Thus, an electron capture is followed by a hole capture and this results in the elimination of the electron-hole pair. The potential energy of the pair is lowered in two stages; part of the energy is released when the electron makes a transition from a state in the CB to the deep level center and the rest is released when the

trapped electron recombines with a hole. In general, in both the steps, energy is dissipated in the form of phonons and the recombination is nonradiative.

Many recombination centers have more than one energy level but in most cases only one level dominates the recombination. Four steps that are involved in the recombination of an electron-hole pair through a deep-level center are illustrated in the figure 1.5. Process (i) involves capture of an electron from the CB by the center located at energy Et. Process (ii) is the inverse process of emission of electron from the center into the conduction band and process (iii) represents the capture of a hole from the VB by the center. Finally in process (iv) the center captures an electron from VB leaving behind hole in the band. This is equivalent to the center's emission of a hole into the VB. It should now be clear the if the level is to act as an efficient recombination center, the electron capture (process i) must be followed by the hole capture (process iii) and both these process should have nearly the same probability. If process (i) is followed by the electron emission process (ii), then the center acts as an electron trap. Similarly when process (iii) is immediately followed by (iv), the center acts as a hole trap.

1.5.3.c. Auger recombination

Auger recombination is a three-particle process in which either two electron and a hole or two holes and one electron are involved. This type of recombination is possible for both direct band-to-band and indirect recombination processes with the help of traps.

In band-to-band Auger recombination, there are two types of processes viz., two electrons and one hole process (eeh) and two holes and one electron (ehh) process. In eeh

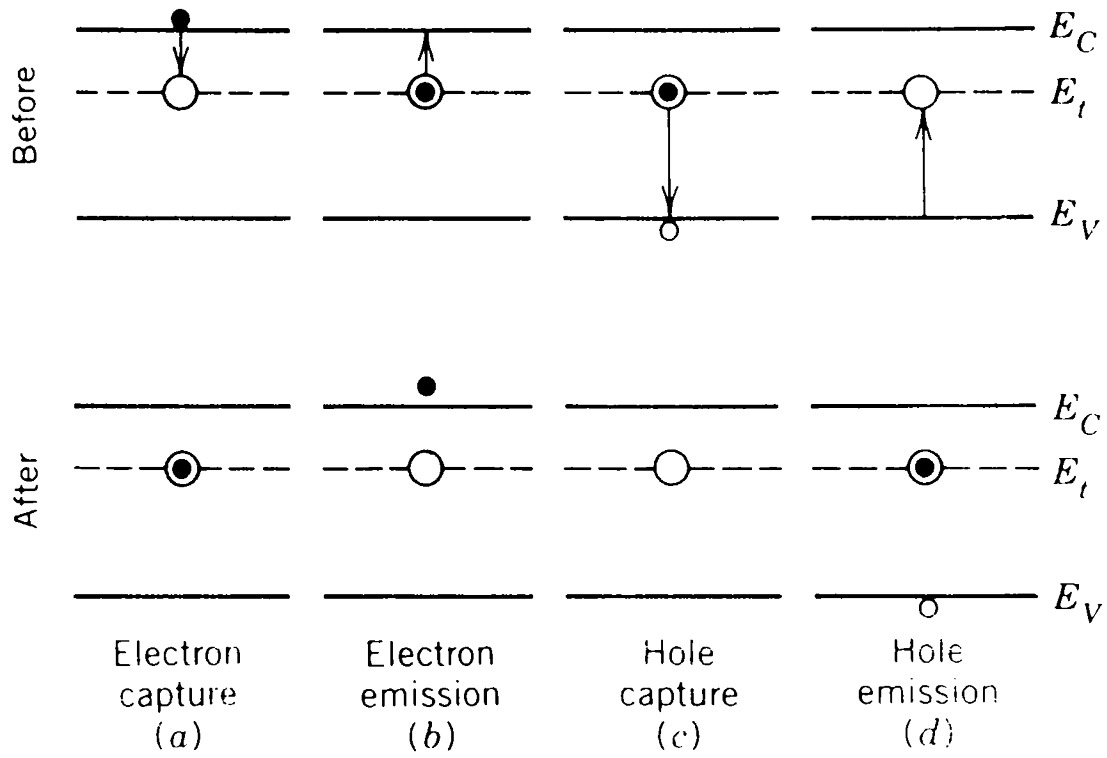

Figure 1.5. Schematic representation of electron-hole pair recombination through the deep level recombination center at thermal equilibrium

process, an electron in the CB makes a transition to an empty state in VB. The energy of electron-hole pair is then transferred to the nearby electron which rises high in the CB. This excited electron now loses its kinetic energy as lattice phonons and returns to thermal equilibrium. In ehh process, the recombining electron imparts its energy to a hole, which transfers the excess energy to a state deep in the VB.

Trap aided Auger processes may become significant at high carrier concentrations and are less understood than the band-to-band Auger process. In one type of trap-aided Auger recombination, a trapped electron makes a transition to the VB by giving its energy to an electron in the CB. This process can become important only in a very heavily doped n-type semiconductor with a high concentration of traps below the Fermi level. In the second process recombination involving two holes and one electron takes place. Here the electron makes a transition to an unoccupied trap level in the bandgap and gives its energy to a hole in the VB.

1.5.4. Origin of Recombination Center

The origin of recombination centers in a semiconductor is related to the presence of impurities, imperfections caused by radiation damage, and unsaturated bonds left near the surface. A brief account of these origins is discussed here. **Impurities** - Impurities can give rise to energy levels near the middle of the band gap and can act as efficient recombination centers. Typical examples are gold and platinum in Silicon and copper in Germanium [30]. **Radiation Damage** - High energy particles such as neutrons, protons electron and γ-rays can displace atom in a semiconductor lattice from their normal positions creating vacancies and interstitial. These vacancies and interstitial can form more complete lattice defects that behave like deep impurities. The minority carrier lifetime in a semiconductor irradiated with high energy particles decreases with increase in the radiation dose. Electron irradiation as a means of excess carrier lifetime control has received considerable attention because it can be performed after device fabrication.The main disadvantageof irradiation is that the radiation induced recombination centers tend to anneal out after a period of time, even when the device is not subjected to high temperature.

Surface States - At the surface of a semiconductor the lattice is abruptly terminated, resulting in unsaturated bonds for the surface atoms. This drastic irregularity introduces a large density of localized energy levels in the forbidden gap. These levels are known as surface states. In contrast to an electron in the bulk that belongs to the entire crystal, a surface electron confines only to an atomic layer. Surface states that have energy levels near the middle of the band gap act as efficient recombination centers.

The density of surface states on a clear surface is of the order of $10^{15}cm^{-2}$, which is about the same as the number of unsaturated bonds. Actual surfaces that are exposed to air are always covered with an oxide layer. Because of the presence of this oxide layer, some of the unsaturated bands gets saturated which causes a reduction in the density of surface states. The typical density of these states on the oxide covered surfaces of silicon and germanium ranges from 10^{11} to 10^{12} states per cm^2. Thermally oxidised silicon surfaces can have densities that are orders of magnitude smaller than these values.

1.6. Recombination and Trapping

Recombination and trapping in semiconductor arise from nonequilibrium distribution of mobile carriers. When non equilibrium concentration of carriers are present one is interested in the rate at which they recombine and thereby approach equilibrium as well as the mechanisms involved. Certain interruptions like trapping events or light emission that may occur before recombination destroys the carriers are also interesting. These phenomena usually are associated with interaction between mobile carriers and crystalline imperfections. Imperfections may be structural or chemical and are the sites of discrete electronic energy level and the methods of measuring these effects are quite sensitive. We discussed the details of recombination mechanism in the previous section and here we give a picture of a recombination center and contrast it with a trapping center. The schematic energy level diagram for recombination centers and trapping centers is shown in figure 1.6. During recombination an electron from the CB may be captured by the center. If this electron is now captured by a hole from the VB, resulting in a mutual annihilation, a

recombination has occurred. However, if the electron is released by the center back to the CB where it originated then the process is a trapping, and the electron was merely trapped for a while, being immobilized temporarily. The arrows on the left indicate that recombination centers can interchange electrons freely with CB or VB. On the right, the arrows indicate that an electron trapping center interchanges electrons only with the CB. In kinetic terms we can describe a recombination center as a localized electronic level in the forbidden gap that has a high probability of exchanging carriers with both bands.

Hall [31] and Shockley and Read [32] have derived the relation between the lifetime of injected carriers and the recombination center properties

$$\tau = \frac{\tau_{p0}(n_0 + n_1) + \tau_{n0}(p_0 + p_1)}{n_0 + p_0} \qquad (1.51)$$

where τ_{n0} and τ_{p0} are constants and

$$n_1 = N_c \exp(E_t - E_c)/kT$$

$$p_1 = N_v \exp(E_v - E_t)/kT \qquad (1.52)$$

E_t being the energy level of the recombination centers. From these definitions it can be seen that $\underline{n_1}$ and $\underline{p_1}$ correspond to equilibrium electron and hole densities when the Fermi level is at E_t.

From equation (1.51) it can be seen that for low resistivity n- and p-type material (n_0 and p_0 very large, respectively) the lifetime τ approaches the values of τ_{p0} and τ_{n0}. These values are related to the cross section for capture of an electron by the empty recombination center, A_n, or to the cross section for capture of a hole by the filled center, A_p, by the expressions [39]

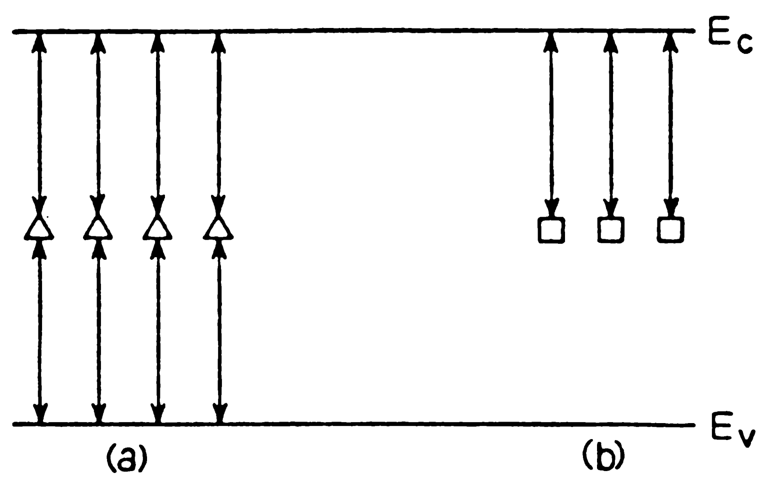

Figure 1.6. Schematic energy level diagram for recombination centers and trapping centers.

$$\tau_{n0} \equiv \frac{1}{N_t \langle vA_n \rangle} \quad \text{and}$$

(1.53)

$$\tau_{p0} \equiv \frac{1}{N_t \langle vA_p \rangle}$$

where N_t is the density of centers, v is the thermal velocity of the electrons or holes, and <vA> is an average of vA over the states of the band. An average is required over the occupied states of the band because in principle both v and A may be functions of the electronic state. In this way when the concentration of recombination centers is known one can calculate the average cross section for capture by the center from the measured values of lifetime.

1.7. Trapping of minority carriers

From kinetic view point a simple trapping of a minority carrier by a trapping center is a special and limited case of the interaction between a minority carrier and a recombination center. The difference between trapping and recombination was seen in figure 1.6. where electron trap is chosen to represent. The arrows representing transitions to both bands from the recombination centers indicate that all electron and hole capture and release rates are important in the recombination process. An electron or hole, after capture, attracts a carrier of the opposite type resulting in mutual annihilation. If either of the rate constants becomes very small compared to the other, a recombination center will become a trapping center. The rate of electron capture will depend upon the rate constant for capture as well as upon the populations of the various levels. The rate constant for capture can be expressed as a product of the cross section for capture A_n times the thermal velocity of electrons, or $A_n v$. The equation for the time rate of change of trapped electrons n_t is [40]

$$\frac{\partial n_t}{dt} = A_n vn (N_t - n_t) - n_t / \tau_g \qquad (1.54)$$

where n is the density of electrons in the CB and N_t the total density of traps which are located at a discrete value of the energy E_t and τg is the mean time for release of a trapped electron.

In order to illustrate the mechanisms involved during trapping, the equation (1.54) will be solved under simplifying conditions such as the concentration of electrons in the CB is assumed to remain constant at its steady state value and the probability of a minority carrier recombining is much greater than the probability of its being captured by a trapping center.The solution of this equation are given by [41]

$$A_n v = \frac{1}{n_l}\left[\frac{1}{\tau_0} - \frac{1}{\tau_g}\right]$$

$$\frac{n_t^{\infty} N_v}{n_l(N_t - n_t^{\infty})} = \exp(Ec - E_t)/kT \tag{1.55}$$

$$N_c A_n v \tau_g = \exp(Ec - E_t)/kT$$

where n_t^{α} is the steady state density of trapped electrons when n_l mobile electrons are maintained by a light source, Ec is the energy at the edge of the CB, Nc is the effective density of states at E_C, and τ_0 is the time constant of electron capture by the traps. When the light is turned on, the mobile electron density increases to n_l in a time of the order of a recombination time. It is maintained at that steady state value until the light is removed. The additional concentrations of electrons and neutralising holes cause the sample conductivity to increase at the same rapid rate to a value $\Delta\sigma_l = q\mu_p n_l(1+b)$ where b is the ratio of electron mobility to hole mobility. The non equilibrium density of electrons increases the net trapping rate and electrons begin to fill the traps. The rate of filling can be changed by adjusting the light intensity and thereby increasing or decreasing n_l. Trapped electrons are immobile and cannot contribute to the conductivity. However, the additional holes required to neutralize the trapped electrons will contribute to the conductivity. When the light is turned off, the concentration of trapped electrons decays from its steady value to its equilibrium value of n_t^0 and the conductivity decreases at the same rate.

1.8. Importance of the present work

The present work concentrate on the study of defect levels in some important compound semiconductor materials used for the fabrication of solar cells. The study on the impact effect of crystal defects on p-n junction devices (designed to be used as devices for light emission, detection and conversion) is of great importance. These devices share a common need for carrier lifetime control and their performance can be degraded by crystal defects. However, light emitting devices are sensitive to defects that reduce the carrier life time by non radiative recombination process, while photodetectors are more affected by defects that shorten the minority-carrier diffusion length. Therefore radiative or nonradiative processes shorten the lifetime and thus reduce the diffusion length and hence the photodiode efficiency.

Certain crystal defects are most relevant to optoelectronic devices

i) Recombination centers present at the exposed surfaces and at heterojunction boundaries

ii) Dislocations and stacking faults incorporated in bulk-grown and epitaxial materials

iii) Dopant precipitates, which may be introduced in the course of doping

iv) Point defects (vacancies, interstitials, contaminants and various atomic complexes) which may be introduced during the growth process.

v) Grain boundaries in polycrystalline materials which introduce recombination centers.

Solar cells have been produced from several semiconductors including Si, GaAs, II-VI compounds such as polycrystalline CdS, I-III-VI_2 compounds such as $CuInSe_2$ etc. The parameters that control the solar cell efficiency are the open circuit voltage (V_{oc}), the short circuit current density (J_{sc}), the fill factor FF (which incorporates the effect of the solar cell's internal resistance) and the spectral distribution of the incident solar power density (P_i). The short circuit current density results from the photogenerated carriers reaching the space charge region that again depends on diffusion length of the carriers. Because the diffusion length varies as the square root of the carrier lifetime, any reduction in the lifetime (other factors remaining constant) decreases cell efficiency. Again carrier recombination at the cell surface reduces the short circuit current density and it plays an important role in reducing the

cell's response to high-energy photons that are absorbed near that surface. In fact, the presence and nature of defects available in solar cell materials are having great impact on the cell performance.

Thermally stimulated Current (TSC) measurements have evolved into a basic tool for the identification and evaluation of trapping and recombination levels due to structural imperfections, impurities and dopants. Various methods of thermally stimulated techniques are available for the characterisation of different materials such as thermoluminescence (TL), Ionic thermal currents (ITC), thermally stimulated currents (TSC), thermally stimulated capacitance (TSCap), thermally stimulated exoemission (TSEE), thermally stimulated depolarization (TSD), thermally stimulated creep (TSCr) and deep level transient spectroscopy (DLTS). The observed phenomena and corresponding materials of various techniques are discussed in chapter 3. Of these, TSC is a well-known non isothermal technique for the investigation of trap levels in semiconducting materials. This is a very sensitive but simple technique. Therefore in the present work, we selected this technique for analysing the semiconducting films of CdS, $CuInSe_2$, PbS and FeS_2. In addition to the results obtained from the TSC measurements, this thesis also discuss the dark conductivity measurements of these films.

CdS polycrystalline films have received intensive study in the past 50 years because of their actual and potential uses in semiconductor devices. The study of defect levels in this materials using different techniques had been reported by various authors [42-50] and are shown in the energy level diagram (figure 1.7) . This figure also gives an idea about the volume of work done on this aspect of the semiconducting material.

$CuInSe_2$ has recently gained prominence as a photovoltaic material in the past decade because of its excellent optical and electrical properties. The literature contains numerous reports on $CuInSe_2$ thin films and a possible exhaustive coverage of the published works is given in the concerned chapter of the thesis. Here again figure 1.8 depicts the energy level diagram indicating various defect levels observed in $CuInSe_2$ [51-57].

Semiconducting materials whose threshold wavelength falls in the IR region are used as infrared detectors and PbS is an important materials for this application. Moreover, PbS photocells were used in solar thermal photovoltaic system for solar energy conversion. Numerous reports indicate the photosensitive characteristics of PbS and a detailed review on this material is included described in chapter 6 of the thesis. In order to study the photosensitive nature of chemically deposited PbS films, TSC measurements were done on these samples.

For more than fifteen years iron pyrite (FeS_2) has been investigated as an important solar cell material because of its extraordinary optical absorption and suitable bandgap. Review of works on FeS_2 are given in chapter 7 and to the best of our knowledge there are no reports giving the details of preparation of FeS_2 thin films using simple CBD technique. Our attempts to prepare this material using CBD and chemical spray pyrolisis are presented in this work along with the characterisation.

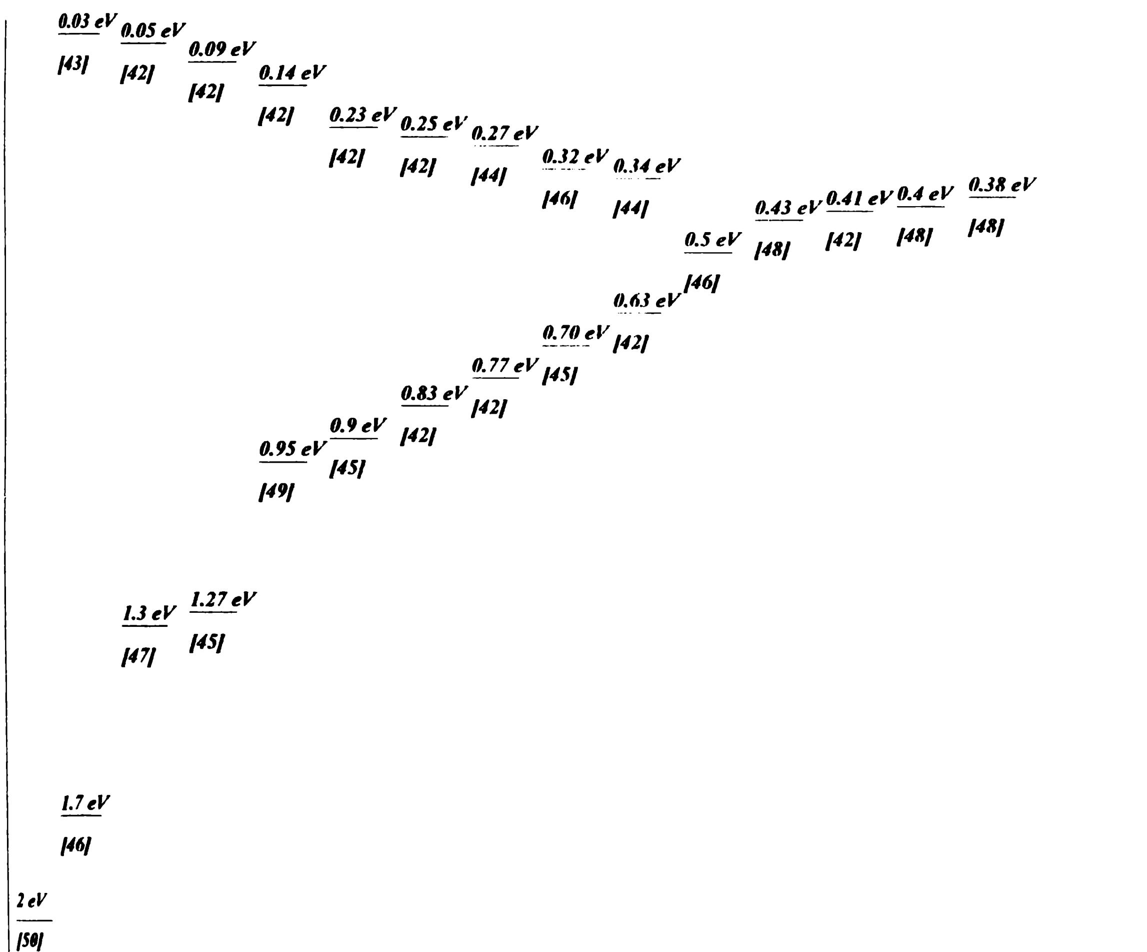

Figure 1.7. Various impurity/defect levels reported in CdS

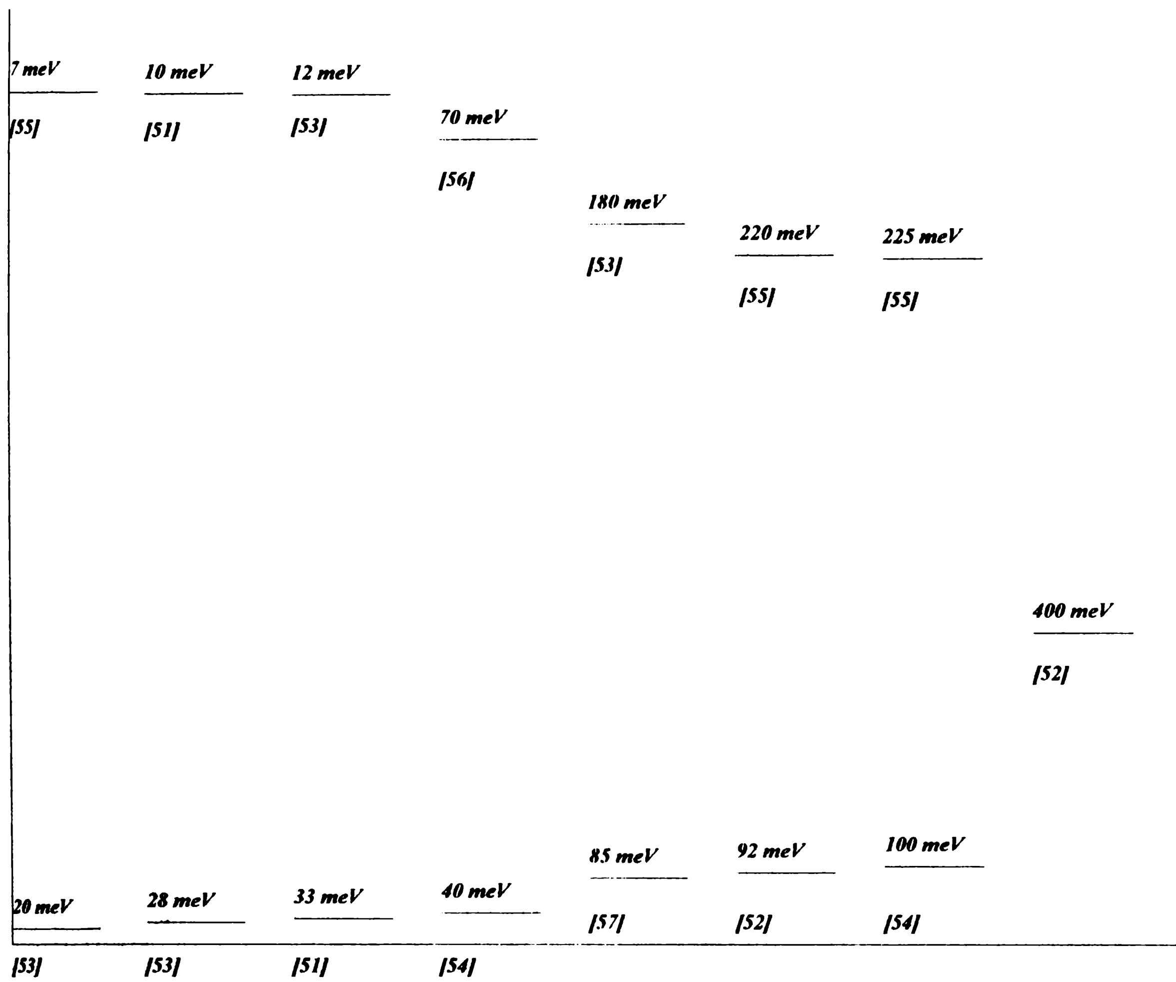

Figure 1.8. Various impurity/defect levels reported in $CuInSe_2$

References

1. Michael Faraday, *Experimental Researches in Electricity, Series IV* (1833) p 433
2. Michael Faraday, *Beibl. Ann.Phys.***31**(1834)25
3. F.Braun, *Ann.Phys.Chem.*, **153**(1874)556
4. W.Smith, *J.Soc.Telegraph Engrs*, **2**(1872)31
5. Lark-Horowitz 'The New Electronic' in *The present state of Physics* (American Assn for the Advancement of Science, Washington, 1954)
6. A.F.Ioffe, *Physics of Semiconductors* (Infosearh 1960)
7. E.H.Hall, *Amer.J.Math.*, **2**(1879)287
8. K.Baedeker, *Phys.Z.* **29**(1909)506
9. L.Konigsberger, *Jb.Radioakt*, **4**(1907)158
10. M.Merrit, *Proc. Nat. Acad.Sci.Wash.*, **11**(1925)743
11. C.Wagner, *Z.Chem.Phys.* **B11**(1930)163,ibid **22**(1933)195
12. C.E.Fritts, *Amer.J.Sci.*, **23**(1883)465
13. L.O.Grondahl, P.H.Geiger, *Trans.Amer.Inst.Elect.Engrs.*,**46**(1927)357
14. G.W.Pierce, *Phys.Rev.*, **25**(1907)31
15. J.Bardeen and W.H. Brattain., *Phys.Rev.*, **74**(1949)1208
16. W.Shockley, G.L. Pearson and J.R. Haynes- *Bell Syst.Tech..J.*, **28**(1949)344
17. R.A.Smith, *Advanc.Phys.*, **2**(1953)321
18. Suresh Chandra, *Photochemical solar cells*, Vol **5**, (New York,1985) p 29
19. S.M.Sze, *Physics of Semiconductor Devices*, (John Wiley, New York,1969)
20. N.B.Hannay, *Semiconductors*, (John Wiley, New York,1959)
21. Suresh Chandra, *Photochemical solar cells*, Vol **5**, (New York, 1985) p 33
22. Suresh Chandra, *Photochemical solar cells*, Vol **5**, (New York, 1985) p 34
23. Suresh Chandra, "Photochemical solar cells", Vol **5**, (New York, 1985) p 35
24. M.S.Tyagi, *Introduction to Semiconductor materials and devices* (John Wiley & Sons 1991)p 112
25. M.S.Tyagi, *Introduction to Semiconductor materials and devices* (John Wiley & Sons 1991)p 114

26. M.S.Tyagi, *Introduction to Semiconductor materials and devices* (John Wiley & Sons 1991)p 93
27. D.S.Lee and J.G. Fossum, *Energy band distortion in highly doped Si*, IEEE Trans. Electron Devices Ed-30, **626** (1983)
28. E.O.Kane, *Solid-State Electron*, **28**(1985)3
29. M.S.Tyagi, *Introduction to Semiconductor materials and devices* (John Wiley & Sons 1991) p 96
30. E.J.Ryder and W. Schokley, *Phy. Rev.*, **81**(1951)139.
31. Michel.M. Cirovic, *Semioconductors Physics, Devices and Circuits*, (Prentics Hall,Inc,New Jersy) p 36
32. M.S.Tyagi, *Introduction to Semiconductor materials and devices* (John Wiley & Sons 1991) p 132
33. M.S.Tyagi, *Introduction to Semiconductor materials and devices* (John Wiley & Sons 1991) p 133
34. M.S.Tyagi, *Introduction to Semiconductor materials and devices* (John Wiley & Sons 1991) p 135
35. M.S.Tyagi, *Introduction to Semiconductor materials and devices* (John Wiley & Sons 1991) p 144
36. M.S.Tyagi, *Introduction to Semiconductor materials and devices* (John Wiley & Sons 1991) p 147
37. R.N.Hall, *Phys.Rev.*, **87**(1952)835
38. W.Shockley and W.T. Read, *Phys.Rev.*,**87**(1952)835
39. N.B.Hannay, *Semiconductors* (Reinfold, New York, 1959) p 486
40. N.B.Hannay, *Semiconductors* (Reinfold, New York, 1959) p 502
41. N.B.Hannay, *Semiconductors* (Reinfold, New York, 1959) p 503
42. J.Woods and K.H. Nicholas, *Brit. J. Appl.Phys.*, **15**(1964)1361
43. R.H.Bube, *J. Chem.Phys.*, **23**(1955)18
44. R.Chandra Sekhar, K.N. Raju, D.Raja Reddy and B.K. Reddy., *J.Phys.D.Appl.Phys.*, **21**(1988)1182
45. H.G.Grimmeis and R.Memming., *J.Appl.Phys.*, **33**(1962)2217

46. J.Wood and D.A. Wright.,Solid State Physics in Electronics and Telecommunication-Proc. International Conf. held in Brussels June 2-7,1958

47. David C Lood, *J.Appl.Phys.*, **45**(1)(1974)492

48. James J Brophy., *Phy. Rev.*, **119**(2)(1960)591

49. D.P.Amalnerkar, M.S.Setty, S.K. Datte and A.P.B. Sinha, *Indian J.Pure and Appl.Phys.*, **22**(1984)662

50. A.G.Valyomana, Sunny Mathew, K.P.Vijayakumar and C.Puryshothaman, *Bulletin of Mat.Sci.*,**16**(1993)55

51. C.Rincon, J.Gonzalez and G. Sanchez Perez., *J.Appl.Phys.*, **54**(11)(1983)6634

52. B.Schumann, C.Georgi, A.Tempel and G.Kuhn., *Thin Solid Film*, **58**(1979)1303

53. T.Irie, S.Endo and S.Kimura, *Jpn.J.Appl.Phys.*, **18**(1979)1303

54. H.Neumann, E. Nowak and G. Kuhn., *Cryst.Res. Technol.*, **16**(1981)1369

55. H.Sobotta, H.Neumann,V.Riede, G.Kuhn, J.Seltmann and D.Oppermann.,*Phys.Status Solidi (a)* **60**(1980)531

56. P.Migliorato, J.L. Shay, H.M. Kasper and S. Wagner., *J.Appl.Phys.*, **46**(1975)1777

57. P.W.Yu, *Solid State Commun.*, **18**(1976)395

Chapter 2
Thin Film Preparation Techniques

2.1. Introduction

Applications of thin films in optics and electronics have made rapid progress in recent years. Consequently, the development of deposition techniques for the preparation of thin films with controlled, reproducible and well defined properties plays an increasingly important role in technological applications. Since the advent of early thermal evaporation technique, a wide variety of deposition methods have been developed for the deposition of thin films.

Thin film properties are strongly dependent on the method of deposition, the substrate materials, the substrate temperature, the rate of deposition, and the background pressure. Specific applications in modern technology demand such film properties as high optical reflection/transmission, hardness, adhesion, nonporosity, high mobility of charge carriers, chemical inertness toward corrosive environments and stability with respect to temperature, stoichiometry and orientation in single crystal film. The application and the properties of a given material determine the most suitable technique for the preparation of thin film of that material.

A thin film deposition process involves 3 steps: i) creation of atomic/molecular/ionic species ii) transport of these species through a medium and iii) the condensation of the species on a substrate. Depending on whether the vapour species has been created by a physical or a chemical process, the methods may be broadly divided into two main groups such as physical methods and chemical methods.

In this chapter, we discuss the different thin film preparation techniques with due emphasis on the techniques employed for the present work.

2.2. Physical Methods

Physical methods involve Vacuum evaporation, Sputtering, Epitaxial deposition, Ion beam and Ion-assisted deposition, Reactive deposition, and Ion cluster beam deposition techniques. In present work, vacuum evaporation technique is used for coating electrodes.

2.2.1. Vacuum Evaporation

Deposition of thin films by evaporation is a convenient technique and is most widely used. One merely has to produce a vacuum environment in which a sufficient amount of heat is given to the evaporant to attain the vapour pressure necessary for evaporation, then the evaporated material is allowed to condense on a substrate kept at a suitable temperature and distance.

Deposition consists of three distinguishable steps i) Transition of the condensed phase (solid or liquid) into the gaseous state ii) Traversal by the vapour of the space between the vapour source and substrate (i.e. transport of vapor from the source to the substrate) iii) Condensation of vapour upon the arrival at the surface (i.e., deposition of these particles on the substrate)

Substrates are made from a wide variety of materials and may be kept at a temperature depending on the film properties required. When evaporation is made in vacuum, the evaporation temperature will be considerably lowered and the formation of oxides and incorporation of impurities in the growing layer will be reduced. The pressure used for normal evaporation work is about 10^{-5} Torr. This also ensures a straight line path for most of the emitted vapour atoms for a substrate-to-source distance of approximately 10^{-5} cm in the vacuum system.

The rate of free evaporation of vapour species m_e from a clean surface of unit area in vacuum is given by the Langmuir expression [1]

$$m_e = 5.83\times10^{-2}\, P_e\, (M/T)^{1/2}\ \text{g cm}^{-2}\ \text{s}^{-1} \qquad (2.1)$$

where T is the temperature, M is the molecular weight of the vapour species and P_e is the equivalent vapour pressure. In terms of the molecules, we may write the evaporation rate as follows

$$N_e = 3.513\times10^{22}\, P_e\,(1/MT)^{1/2}\text{mol.cm}^{-2}\,\text{s}^{-1} \qquad (2.2)$$

However the rate of deposition of the vapour on a substrate depends on the source geometry, the position of the source relative to the substrate and the condensation coefficient.

The substrate is bombarded not only by the particles of the evaporated substrate but also by those of the residual gases. The residual gases in evaporation systems do have a profound influence on the growth and properties of the films. First there is the possibility of collisions between gas molecules and vapour molecules during the transit of the latter from the source to the substrate. The number of collisions depends on the mean free path. The number of atoms N from the total number N_0 traversing a distance l without having a collision is given by [2]

$$N = N_0 \exp(-l/\lambda) \qquad (2.3)$$

where λ is the mean free path in the residual gas. Usually the films are deposited at a pressure of the order of 10^{-5} Torr or less and only a negligible number of collisions between the residual gas and the vapour molecules will take place. As a result, the vapour molecules will exhibit straight line propagation.

Second, the film will be badly contaminated by the residual gases in the vacuum system. Such contamination can arise from gas molecules impinging on the surface of the substrate during deposition. The impinging rate of gas molecules is given by the kinetic theory of gases [2]

$$N_g = 3.515\times10^{22}\, P_g/(M_gT_g)^{1/2}\ \ \text{cm}^{-2}/\text{s} \qquad (2.4)$$

where P_g is the equilibrium gas pressure at temp T_g.

It can be seen that under the conditions of vacuum normally used (10^{-5} Torr) and deposition rate of about 1A°/s, the impingement rate of gas atoms is quite large, which

means that a good amount of gas sorption will occur if the sticking coefficient of the gas atoms is not negligibly small. To obtain films with minimum number of impurities, pressure in the region of ultra high vacuum (10^{-9} Torr) must be used.

2.2.1.a. Methods of Evaporation

The evaporation of materials in a vacuum system requires a container that can support the evaporant as well as supply the heat of evaporation. To avoid contamination of the films deposited, the support material itself must have negligible vapour pressure and should not decompose at the operating temperature. Materials commonly used are refractory metals and oxides. The possibilities of alloying and chemical reactions between the evaporant and support materials must be taken into account while choosing a particular support material. The shape in which the support materials are used depends very much on the evaporant.

The important methods of evaporation are resistive heating, flash evaporation, electron beam evaporation, laser evaporation, arc evaporation and radio frequency heating.

i) Resistive heating

This is the method in which the material to be evaporated is heated by electrical resistance heating. The most commonly used source materials (support materials) are the refractory metals (viz.; tungsten, tantalum and molybdenum) which have high melting point and very low vapour pressure. The structure of these sources is usually wires and foils. Electrical connections are made directly to the source by attaching their ends to heavy copper or stainless steel electrodes. Here the evaporants are fixed directly to the source in the form of wire/powder and upon melting, the evaporant wets the filament. The drop is held by surface tension. Multistrand filaments are also used as source, but they can be used only for metals or congruently evaporating alloys. Moreover once heated, these elements become very fragile and will break if not handled carefully. Oxide coated metal foils are also used as evaporation sources. The power requirements of such sources are much above those of uncoated foils due to the reduced thermal contact between the resistively heated metal and evaporant. Crucibles of quartz, glass, alumina, graphite, beryllia, and zirconia are

used with indirect resistive heating. Even though new and more sophisticated techniques for the preparation of thin films have been developed, electrical resistive heating is still commonly used in laboratory and industry to prepare thin films of elements [3-9], oxides [10-14] and compound semiconductors [15-21].

The main disadvantages of this technique are i) the reaction of the evaporant material with the support crucibles ii) the difficulty in attaining the required temperature for the evaporation of dielectric iii) low rates of evaporation and iv) the dissociation of compounds or alloys upon heating.

ii) Flash evaporation

A common difficulty encountered in the preparation of thin films of multi-component alloys or compounds that tend to distill fractionally (different compounds have different vapour pressure at any given temperature) is that the chemical composition of the film obtained deviates from that of the evaporant. This difficulty is best overcome in 'flash evaporation'. Here the small quantities of the material to be evaporated are dropped in powder form onto a boat hot enough to ensure that evaporation takes place instantaneously. The temperature of the boat should be high enough to evaporate the less volatile material fast. When a particle of the material evaporates, the component with the higher vapour pressure evaporates first, followed by components with lower vapour pressure. In practice, the feed of material is continuous, and there will be several particles in different stages of fractionation on the boat. Moreover, since no material accumulates on the boat during evaporation, the net result of this instantaneous discrete evaporation is that the vapour stream has the same composition as the source material. If the substrate temperature is not high enough to permit reevaporation to take place, stoichiometric compounds or alloy films will be formed. The powdered material can be fed into the heated support using different arrangements (mechanical, electromagnetic, vibrating, rotating etc.) for material feeding.

Flash evaporation techniques have been used to prepare semiconducting thin films of certain compounds from groups III-V [22-24]. Ellis used flash evaporation to prepare

copper sulphide films [25]. Several reports are available on the preparation of semiconducting compounds by flash evaporation [26-29]. Flash evaporation has been very widely used for the preparation of cermet (CERamic plus METal) films that are mixtures of dielectric [30], amorphous chalcogenide films [31] and high Tc superconducting oxide films [32]. Flash evaporation has been used for the preparation of epitaxial layers of $CuInSe_2$ [33]. Later Sridevi and Reddy used a simple flash evaporation technique and prepared thin films of CIS to study the electrical and optical properties [26].

A serious drawback of the flash evaporation technique is the difficulty in preoutgassing the evaporant powder. Degassing the powder can be accomplished to some extend by vacuum storage for 24-36 hours prior to deposition. Otherwise, large quantities of gas may be released during evaporation. Also the expanding gases can cause "spitting" during evaporation.

iii) Electron beam evaporation

In electron beam (EB) evaporation, the vaporization of materials can be accomplished by electron bombardment. Here a stream of electrons is accelerated through fields of typically 5-10 kV and focused onto the surface material for evaporation. The electrons lose their energy very rapidly upon striking the surface and the material melts at the surface and evaporates. That is, the surface is directly heated by impinging electrons in contrast to the conventional heating modes. Because the material in contact with the support crucible remains solid, in effect the molten material is contained in a crucible of itself and the reactions are minimised. Direct heating allows the evaporation of materials from water cooled crucibles, and these are very commonly used in electron beam evaporation. Such water cooled crucibles are necessary for evaporating reactive materials, (especially refractory materials) to avoid almost completely reactions with crucible walls. This allows the preparation of high purity films because crucible materials or their reaction products are practically excluded from evaporation.

By this type of heating, any material can be evaporated, and the rate of deposition varies from fractions of an angstrom per sec. to micrometers per sec. The EB sources have

been found to be versatile and reliable and are used even for materials which can be quite easily and satisfactorily evaporated from an ordinary refractory metal boat.

EB guns can be classified into thermionic and plasma electron categories. In the former type, the electrons are generated thermionically from heated refractory metal filaments, rods or disks. In the latter type the electron beams are extracted from a plasma, confined in a small place. Various EB evaporator devices with axial gun, magnetic focusing and magnetic bending are now readily available commercially to produce thin films for optical, electronic and optoelectronic applications.

EB evaporation has been used for the preparation of thin films of a number of materials: Si [34], $CuInSe_2$ [35], InAs [36], TiO_2 [37], SnO_2 [38] and ITO [39,40].

EB technology is rather expensive and complicated and its use is not justified if (easily controlled) alternative electrical resistance heating is available. This method is of practical importance in certain cases requiring high quality films and in the absence of suitable support materials.

iv) Laser evaporation

In this technique, lasers are used as the thermal source to vaporize the compound materials and preparation of thin films by laser evaporation is a high vacuum technique, where the source of power for evaporation is kept outside the vacuum system. The vaporized material is deposited onto substrate placed in front of the source material inside the vacuum chamber.

This technique offers several advantages

i) Lasers are clean and introduce minimal contamination from the heat source. ii) Film contamination from the support material is reduced because of the surface evaporation characteristics of the beam. iii) With the high power densities obtained by focusing the laser beams, high melting point materials can be vaporized at high deposition rate. iv) Because of the small beam divergence, the laser and the associated equipment could be kept far away,

an attractive feature in radioactive areas. v) Simultaneous or sequential multisource evaporator can be done easily by directing the laser beam with external mirror.

It was Smith and Turner [41] who made a preliminary study using this technique and showed that any materials can be vaporized in vacuum by using directed laser beam as the evaporation power source. They used ruby laser external to the vacuum chamber and a lens focused the radiation from the ruby rod through a window in the bell jar onto the surface of the sample to be evaporated. Most of the films were evaporated from powdered materials placed in small inclined crucibles in the bell jar and deposited onto substrates placed 20 to 50 mm above the crucibles. Lateral motion of the lens allowed the focal spot to fall at desired position on the surface of the material. Smith and Turner could produce optically satisfactory films including Ge, PbTe, and ZnTe [41].

Although some studies using laser as a thermal source have been carried out since this initial report, special attention has been paid only in recent years to this technique. A new ceramic coating technique using a high power CO_2 laser as the heat source was developed by Mineta et.al.[42].

Pulsed laser evaporation can cause rapid heating and cooling of the source material with very high peak temperature, and instant evaporation occurs from very small area of the target. Power is delivered in the form of high power pulses creating flash evaporation conditions, and this leads to the important advantage of congruent evaporation of compound materials. There will be little or no fractionation of its constituents even if they have widely different vapour pressure, and this technique is suitable for the deposition of the thin films of wide range of compounds and alloys. Also the original purity of the source material is maintained, eliminating crucible contamination because the source pellet/target becomes its own crucible. During the evaporation of solid targets, the interaction of a pulsed laser with a solid target can produce high energy particle fluxes (electrons, ions and neutral species), the energies of the particles depending on the material and laser power. This causes surface cleaning due to ion etching and also increases the number of nucleation sites for deposition, enhancing the process of epitaxial growth.

Yang and Cheung prepared SnO_2 film on GaAs and glass substrate using a high power pulsed laser [43]. Laser evaporation had been used to prepare thin films of CdTe, Cd and InSb [44], PbTe and doped PbTe [45], polymers [46], lead chalcogenides[47] and SnO_x [48].

v) Arc evaporation

In this technique, electrodes of the metal to be evaporated are mounted on insulated supports in a vacuum system evacuated to a pressure of 10^{-5}Torr. One of the rod is rotatable and the other is fixed. Using a standard welding generator, the voltage is applied between the electrodes and the rotatable electrode is brought into contact with the fixed rod, held there until a hot spot appeared and then moved away, thus drawing an arc. This results in the rapid deposition of the film of the electrode metals on the substrate plate close to the electrodes.

Arc evaporation was first tried in a conventional vacuum evaporator by Lucas et.al.,[49] to obtain thin films of refractory metal. Films of niobium, tantalum vanadium and stainless steel were obtained using this set up.

Other methods of the preparation of the thin films using vacuum arcs have also been published [50,51], but in the absence of continuous smooth arc discharge, the results are not reproducible.

vi) Radio frequency heating

Radio frequency (RF) heating has been used for vacuum deposition by several investigators [52-54]. By suitable arrangement of RF coils, levitation and evaporation can be achieved, thereby eliminating the possibility of contamination of the film by the support crucible. The evaporant can also be contained in a crucible, which is surrounded by the RF coils.

Preparation of thin film by RF heating is limited because of the coupling needed between the coil and the evaporant and also the difficulty in positioning the coil and the

samples for effective coupling. Also the method requires relatively expensive and bulky RF heating equipment. Again, it is difficult to control the evaporation rate. The method is not commonly used now as a technique for the preparation of thin films.

2.2.2. Sputtering

Bombardment of a surface with high velocity positive ions cause the surface atoms to be ejected. This ejection of atoms from the surface due to bombardment by positive ions is commonly known as (cathode) sputtering. When ejected atoms are made to condense on a substrate, thin film deposition takes place.

Various theories have been put forward to account for the mechanism of cathode sputtering. Several works on the subject of sputtering and sputtering processes of the thin film deposition are available [55-59].

The simplest arrangement for the deposition of thin film by sputtering is the **glow discharge dc sputtering system.** Here the plate of the material to be deposited is connected to a negative dc voltage supply (1-5 kV) and the substrate is mounted on the anode facing the target. A neutral gas such as argon is introduced into the vacuum chamber until the pressure reaches 10^{-1} to 10^{-2}Torr. When electric field is applied, a glow discharge is formed. Here the positive ions strike the target plate, removing from the surface mainly neutral atoms, which eventually condense on the substrate as a thin film.

The operation of a sputtering system calls for a self sustained dc discharge at pressures below 10 mtorr is impossible because there are too few ionizing collisions. The most serious drawback here is contamination of the deposited film by the inert gas used to produce the discharge. This can be minimised if the sputtering is done at low pressure. To increase the ionization and sustain the discharge at this low pressure, additional electrons from a source other than the target must be supplied.

In **triode sputtering** the electrons are provided in the discharge from an independent source. A hot cathode (heated tungsten filament), which emits electrons through thermionic emission, is used to inject electrons into the discharge system. A supported discharge system like this allows operation at much lower pressure (10^{-3} Torr) than that in a conventional glow discharge system. The main limitation lies in the difficulty of producing uniform sputtering from flat targets of large size. Also the supported discharge is difficult to control for reproducible results.

A depositing film is an active getter of impurities, and a sputtering gas, when made to pass over an area of freshly deposited films, cleanses the new film of its impurities. This principle is used in the design of the **getter sputtering system**. The residual gas molecules impinging on an atomically clean metal surface are chemisorbed or form a metal compound and chemical clean up occurs . Rare gases are merely physisorbed and not readily trapped.

For the deposition of insulator films using this technique Davidse and Maissel [60] developed a practical RF sputtering system in which an RF potential is applied to the metal electrode placed behind the dielectric plate target. Here the electrons oscillating in the alternating field have sufficient energies to cause ionizing collisions and to keep the discharge self-sustained. The high voltage at the cathode required in dc sputtering for the generation of secondary electrons is not necessary here to maintain the discharge. Since the electrons have much higher mobility than ions, far more electrons will reach the dielectric target surface during the positive half -cycles, and the target becomes self-biased negatively. The negative dc potential on the dielectric target surface repels electrons from the vicinity of this surface creating a sheath enriched in ions in front of the target. These ions bombard the target, and sputtering is achieved.

Another variant of the sputtering process is **magnetron sputtering,** a magnetically enhanced sputtering technique discovered by Penning [61]. For a simple planar magnetic system, a planar cathode is backed by permanent magnets that provide a torodial field with field lines forming a closed path over the target (cathode) surface. The secondary electrons generated are trapped in cycloidal orbits near the target and prevent self-heating of the

substrate. The confinement of the plasma and the resultant intense plasma allow magnetron sputtering systems to operate at much lower pressures and lower target voltages than are possible for RF diode sputtering. Also here the deposition rates are relatively higher and cover large deposition areas. Low substrate heating allows the use of a variety of applications. Recently, using RF sputtering $CuInSe_2$ films have been prepared [62].

Ion-beam sputtering is another useful film deposition technique affording independent control of the ion beam energy as well as the current density of the bombarding ions. Hence the ion beam generated at an ion source is extracted into a high vacuum chamber and directed at the target material, which is sputtered and deposited on a nearby substrate. The directionality of the beam allows the angle of incidence (target) and angle of deposition (substrate) to be varied. Other advantages over conventional sputtering include the low background pressure and the greater isolation of the substrate from the ion production process.

2.2.3. Epitaxial Deposition.

Oriented growth of one material over another is commonly called epitaxy and epitaxial growth is of particular interest in many semiconductor applications. As a result of nature of deposition process, thin films are invariable fine-grained and have a frozen-in high concentration of structural defects. Solar cell applications require large oriented grains or mosaic monocrystals if single crystal films are not possible. By selecting an appropriate single-crystal substrate, mosaic crystals are epitaxially grown in sizes up to tens of micrometers and small-angle grain boundaries. Epitaxial film deposition may be achieved by a variety of techniques from solution as well as vapour. Commonly used epitaxial deposition techniques are the following.

2.2.3.a. Molecular Beam Epitaxy (MBE)

MBE is a sophisticated and finely controlled epitaxial growth technique [63,64] that is basically an ultra high vacuum evaporation process. Here atomic or molecular beams of the element or constituent elements of the compound are created and directed onto clean, heated single-crystal substrates to form the film. The beam intensities are controlled by the

temperature of the effusion ovens, chosen to provide the necessary flux of the various elements arriving at the surface. In many cases the composition is controlled by the flux ratio, with the fluxes controlled via the source temperature. Fast shutters, introduced between the sources and the substrates, interrupt the beam fluxes, and by controlling the shutters, one can grow layers of precisely controlled characteristics (thickness, dopant profile etc.). Usually an MBE unit contains sophisticated analytical tools like mass spectrometer, low energy electron diffraction (LEED) system etc.

2.2.3.b. Liquid Phase Epitaxy (LPE)

LPE is a thermally controlled technique for the preparation of high purity epitaxial films of semiconductor compounds and alloys. This is a relatively old technique, developed in the 1960s beginning with the work of Nelson [65]. Although the method is simple, in some cases, the thermodynamics of the system makes its use difficult. Other growth techniques are available, but LPE is still used when high quality material is required.. As indicated, however, the morphology is difficult to control and, in addition, the quality of the surface is poor compared to that obtained by MBE.

2.2.3.c. Hot Wall Epitaxy (HWE)

HWE is a vacuum deposition technique in which epitaxial films are grown under conditions as near as possible to thermodynamic equilibrium [66]. This is achieved by having a heated wall between the source and substrate to direct the evaporating molecules onto the substrate. In one system, three resistance heaters are used-one each for the substrate, the wall, and the source. Many variations of this simple hot wall system have been used by different authors to prepare different semiconductor compounds [67,68].

2.2.3.d. Metal-Organic Chemical Vapour Deposition (MOCVD)

MOCVD is a recently developed technique for the growth of thin layers of compound semiconductor materials for the use in optoelectronic and microwave devices. Here various combinations of organometallic compounds and hydrides are used for the growth of the epitaxial layers. Compounds and alloys from Groups III-V and II-VI are commonly prepared by using this technique. GaAs/GaAlAs heterostructures are grown by

MOCVD [69]. One advantage of the MOCVD technique is the ready availability of relatively pure organometallic compounds for most of the elements that are used for the epitaxial growth of the semiconductor compounds. The need for careful construction and system design imposes constraints on the use of MOCVD as an epitaxial growth technique for certain device applications.

2.2.4. Ion Assisted Deposition

Ion-assisted techniques include conventional ion plating [70] and its variants, cathode arc deposition and hot hollow cathode gun evaporation where a significant percentage of the vapour of the source material is ionized. Again there is a concurrent ion bombardment deposition, with a separate ion source irradiating the substrate during deposition in a controlled manner. So also there is a direct ion beam deposition: ion beam consisting of the desired film material are extracted and deposited onto the substrate at low energy.

In **conventional ion plating** the material is evaporated from a resistively heated crucible serving as the anode and the substrate are made the cathode of a diode dc discharge (2-5 kV) normally used in diode sputtering. The variants of ion plating include triode ion plating, hollow cathode discharge ion plating, and magnetron sputter ion plating.

In **cathode arc deposition,** the material is made the cathode in an arc circuit and the material evaporated by the action of vacuum arcs. The arc occurs in regions of few micrometers in size and carries very high current densities.

In all these ion-assisted deposition methods, the properties of the deposited films depend largely on the available energy per condensing atom. The details of this technique have been discussed in two recent review articles [71,72].

2.2.5. Reactive Deposition

Compound thin films (nitrides, oxides, carbides etc.) are prepared by reactive deposition technique entailing the presence of a reactive gas or compound. The material is

converted physically from the condensed phase to the vapour phase by using thermal energy (evaporation) or momentum transfer (sputtering) whereupon a chemical reaction takes place to form the compound film.

In **reactive arc evaporation**, the basic principle is the arc evaporation of the metal in the respective gas. The ionization efficiency in cathode arc deposition processes is as high as 30-50% and this high degree of ionization in the plasma and high energies of the ions increase the reaction efficiency, resulting in the formation of compound films exhibiting enhanced adhesion and density.

In **reactive sputtering,** the sputtered metal from the target reacts with the reactive gas present to form the compound. Sometimes reactive gas is added to make up for a constituent film and this process is also treated as a case of reactive sputtering. Sometimes, a reactive gas reacts with the target during sputtering and a compound is formed on the surface of the target and is called target poisoning. It makes the sputtering rate to drop considerably and effect of target poisoning on sputter deposition depends on the particular metal-reactive gas combination and properties of the compound.

In **reactive ion plating,** a useful development of basic ion plating, the residual atmosphere in the vacuum system contains a reactive gas. Ionization can be improved by the use of various techniques such as hollow discharge and magnetron sputtering.

Reactive ion beam sputter deposition is a modification of the ion beam sputter deposition technique and differs from other reactive deposition methods in that the reactive ion can be introduced in two ways - as ion beams and as a gaseous phase.

2.2.6. Ionized Cluster Beam (ICB)

Ionized cluster beam deposition is a recently developed thin film deposition technique that has been widely used for the preparation of higher quality films of a wide variety of materials [73]. Epitaxial films of many materials on a variety of substrates are obtained at low temperature. The material to be deposited is vaporized and ejected from the

nozzle of a special crucible to expand into high vacuum environment. A supersaturated state is formed by adiabatic expansion. The atoms lose their energy by collision and nucleation starts. The nuclei grow to form clusters having thousand atoms held together by weak interatomic forces. These clusters are ionized by electron bombardment (impact ionization) whereupon they are impinge on it, finally forming the film. The energy of the ionized clusters striking the substrate depends on the potential difference between the substrate and the crucible. Brief reviews of the ICB method of film deposition have been published [74,75].

2.3. Chemical Methods of Film Deposition

Unlike the physical methods of preparation of thin films involving evaporation or ejection of material from a source, chemical methods of thin film deposition entail a definite chemical reaction.

Chemical methods of film deposition in general use simpler equipment and are more economical than physical approaches, although the former methods are complex and difficult to control. Chemical methods involve different types of thin film growth technique such as Thermal growth, Chemical vapour deposition -CVD- (laser chemical vapour deposition, photochemical vapour deposition, plasma enhanced CVD), Electrodeposition, Electroless deposition, Anodic deposition, Spray pyrolysis process and Chemical bath deposition technique (solution growth technique).

In this work, majority of the samples are prepared by spray pyrolysis and chemical bath deposition technique. So these two techniques are treated here in detail while the others are discussed in brief.

2.3.1. Thermal Growth

A large number of films - oxides, carbides, nitrides - can be prepared by heating the metal substrates in the gases of the required type (e.g., in oxygen for O_2). Here the thickness of the film can be increased by increasing the temperature, but the total thickness is limited

since the oxide growth rate generally diminishes with thickness. Since all metals except gold react with O_2 the thermal oxidation is usually carried out by the conventional furnace oxidation and this has been reported for several materials [76-80].

Thermal growth is not a commonly used method, but thermally grown oxides of metals and semiconductors, where the substrate itself provides the metal or semiconductor constituent of the oxide, has been widely investigated. Thermal oxidation of silicon to form SiO_2 have been extensively studied, since SiO_2 has very important applications in silicon technology.

2.3.2. Chemical Vapour Deposition (CVD)

Chemical vapour deposition is an important and popular technique for the preparation of thin films of a wide variety of materials - elements as well as compounds - on various substrates. In this technique, constituents of the vapour phase react to form a solid film on the substrate surface, which is maintained at a suitable temperature. In conventional CVD, the reaction is thermally activated and the reactive gases pass over the heated substrate with a thermal reaction taking place to deposit the film on the substrate. Metal oxides such as Al_2O_3, In_2O_3, CuO etc., have been prepared by this technique [81]. Matsumura has recently reported the application of this technique for the low temperature deposition of silicon nitride [82].

CVD offers many advantages over the other methods of thin film deposition. Using this technique, film with a high degree of purity and good quality with accurately controllable stoichiometric composition and doping levels can be prepared. Because of the good throw power attainable with CVD, coatings of complex shapes are possible. Since many reactions can be accomplished at ambient pressures, the need for expensive high vacuum equipment can be avoided. The higher deposition temperature leads to improved crystal perfection and materials that decompose upon melting or evaporation can be prepared. This process can be adapted to large-scale multisubstrate operation.

However, the technique suffers from several drawbacks namely: i) the thermodynamics and reaction kinetics involved in the deposition process are frequently very complex and poorly understood, ii) usually, higher substrate temperatures are required than in the corresponding physical vapour deposition technique, iii) reactive gases used for the deposition process and the reaction products are, in most cases, highly toxic, explosive, or corrosive, iv) the corrosive vapours may attack the substrate, the deposited film, and the materials of the deposition setup.

Laser Chemical Vapour Deposition (LCVD) is a recently developed CVD technique in which a laser source is used to activate the chemical reaction [83-85]. Here the film growth characteristics will be different from conventional CVD. In photo CVD, the photochemical deposition takes place when high energy photons selectively excite states in the surface-absorbed or gas phase molecules leading to bond rupture and production of free chemical species to form the films or to react to form compound films on the adjacent substrates. It is an attractive technique for the preparation of high quality damage free films for many technological applications [86,87]. Plasma-enhanced CVD is yet another versatile technique for the preparation of variety of materials for micro-electronic, photovoltaic and many other applications [88-90]. Here the plasma is produced by an RF field and it promotes chemical reactions. The average electron energies in the plasma are sufficient to ionize and dissociate most types of gas molecules.

2.3.3. Electrodeposition

Electrodeposition is the process of depositing a substrate by the passage of electric current through the conducting medium (called the electrolyte), producing a chemical change (electrolysis). The system used for electrodeposition consists of an anode and a cathode immersed in a suitable electrolysis. When the electric current is passed, the material is deposited on the cathode. Early works on the electrodeposition have been discussed by Campbell [91] and Lowenheim [92].

The various process parameters that affect the properties of the film grown by electrodeposition are the current density, pH value, bath composition, temperature, electrode

shape and the agitation of the bath. Current density defined as total current divided by the electrode area is one of the most important parameters that determines the overall nature of deposit, particularly the microstructure, efficiency of deposition and the deposition rate. The chemical composition of the bath plays an important role in the deposition process. pH determines the overall conductivity of the electrolyte. The temperature of the bath controls the rate of diffusion of ions and stability of any complexes used. The distribution of current across the electrode and hence the uniformity of the deposited film is affected by the shape of the electrode.

2.3.4. Spray Pyrolysis Technique

The spray pyrolysis technique was described by Chamberlin and Sakarman in 1966 for preparing CdS and certain other sulphide and selenide films [93]. This technique has been developed extensively since then by many workers [94-99].

Spray pyrolysis involves a thermally stimulated chemical species. In this technique an aqueous solution containing soluble salts of the constituent atoms of the compound is sprayed onto a heated substrate in the form of fine droplets by a nozzle sprayer with the help of a carrier gas. Upon reaching the hot surface, these droplets undergo pyrolytic decomposition to form a film on the substrate surface. The hot substrate provides the thermal energy for the decomposition and subsequent recombination. The carrier gas may or may not play an active role in the pyrolytic reaction process (eg.,carrier gas may affect the preparation of SnO_2 films not in the case of CdS)

A schematic block diagram of a typical spray pyrolysis set up is shown in figure 2.1. The spray head and the substrate with heater are kept inside a closed chamber provided with an exhaust fan for removing the gaseous byproducts and other gases. A very fine capillary tube is used for carrying the solution and another tube with comparatively larger diameter is used for carrying the carrier gas. Both the tubes are intercepted at an angle of 80^{0} that gives better results [100] and this avoids the formation of large size droplets in the spray. The carrier gas and the solution are fed into the spray nozzle at predetermined and constant

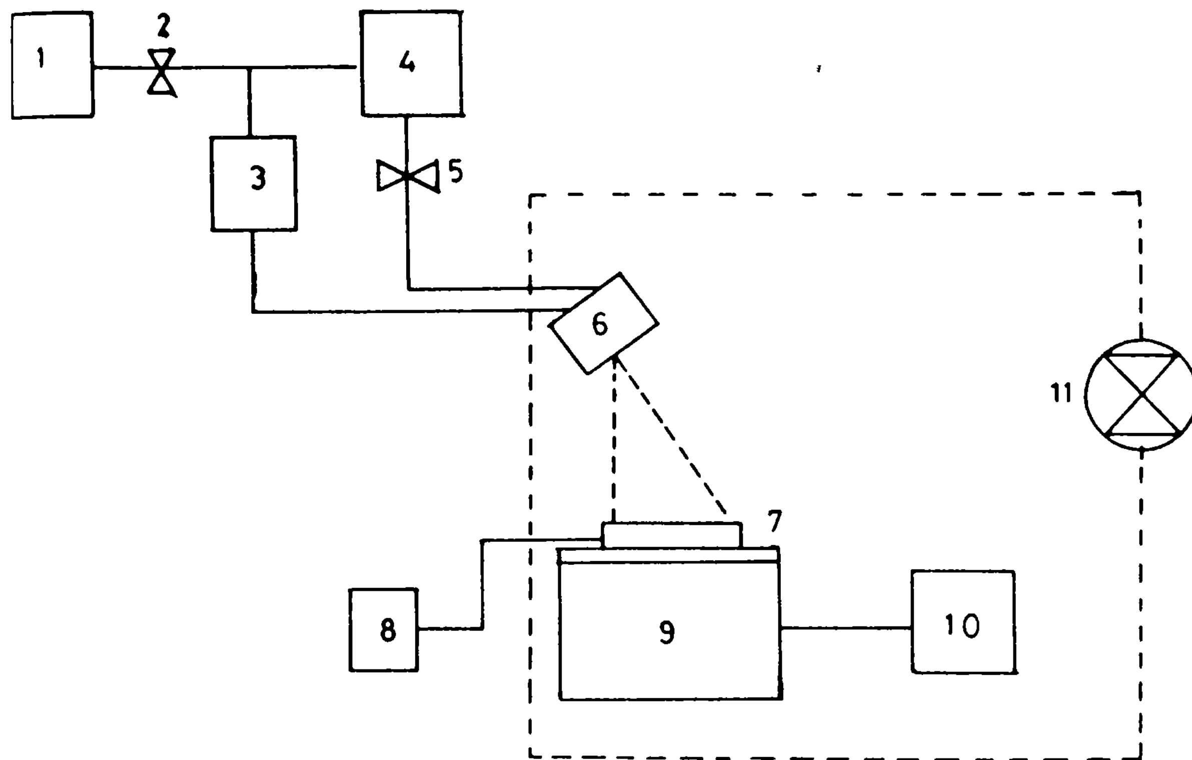

1. Air compressor
2. Gas flow control valve
3. Manometer
4. Solution reservoir
5. Solution flow control valve
6. Spray head
7. Substrate
8. Thermometer
9. Substrate heater
10. Heater control
11 Exhaust fan.

Figure 2.1. Schematic diagram of experimental setup for spray pyrolysis

pressure and flow rates. The substrate temperature is maintained with the help of a feedback circuit that controls the primary and auxiliary heater power supply. The temperature of the substrate holder was measured using a digital thermometer. Large area uniform converge of the substrate is affected by scanning either or both the spray head and the substrate, employing mechanical or electromechanical arrangements. The geometry of the gas and liquid nozzle largely determine the spray pattern, the size distribution of droplets and the spray rate. A wide variety of nozzles have been designed and employed for spraying on stationary and moving substrate.

2.3.4.a. Growth Kinetics

The aerodynamics of the atomization and droplet impact processes had been studied by Lampkin [101]. He could correlate the dynamic features of the spray process with the kinetics of film growth and surface topography. When both the size and momentum of the spray droplets are uniform, optically good quality and smooth films are obtained in the case of CdS. Analysis of surface topography of sprayed CdS films using VASE (Variable Angle Spectroscopic Ellipsometry) [100] indicates that the film prepared at low temperature has high surface roughness and this roughness decreases with increase in substrate temperature. The surface roughness reaches a minimum for films prepared at 280-300^{0}C and thereafter it increases slowly with temperature. This work also revealed that the deposition rate decreases with increase in substrate temperature and as the substrate temperature goes above 300^{0}C the rate of deposition decreases rapidly. At low temperature, growth (deposition) rate is very high leading to the formation of rough films.

The deposition process in spray technique is a resultant of the following steps - 1. spreading of a drop into a disk. 2. pyrolytic reaction between the decomposed reactants . 3. evaporation of the solvent. 4. the repetition of the preceding processes with succeeding droplets. Consequently, the film generally contains disks interspersed into each other. The lateral mobility of the droplets and coalescence and sintering kinetics of the superimposed disks crystallite clusters determine the growth kinetics and microstructural features of the spray pyrolysed films.

The spray pyrolysed films are coherent and pinhole free even at very low (1000°A) thickness, provided the substrate temperature is high enough to cause complete pyrolytic reaction. The microstructure of the film depends very sensitively on several deposition conditions, notably the spray head geometry, carrier gas and liquid flow pattern and rate, droplet velocities, sizes and geometries, nature and temperature of the substrate, the kinetics and thermodynamics of the pyrolytic reaction and temperature profile during the deposition process.

2.3.4.b. Chemical Aspects

The chemicals used for spray pyrolysis have to satisfy the following conditions. 1. On thermal decomposition, the chemicals in solution form must provide the species/complexes that will undergo a thermally activated chemical reaction to yield the desired thin film material and 2. the remainder of the constituents of the chemicals, including the carrier liquid should be volatile at the spray temperature. For a given thin film material, the above conditions can be met by a number of combination of chemicals. However, different deposition parameters are required to obtain comparable quality (structurally) films.

2.3.4.c. Characteristic features of the spray pyrolysis process

i) Growth rate

The chemical and topographical nature and temperature of the substrate, the chemical nature and concentration of the spray solution and its additives and the spray parameters largely determine the growth rate. Film thickness increases nearly linearly with time of spray i.e., with the amount of sprayed solution. The growth rates can be as large as 1000A°/minute for oxide films and 500A° for sulphide films. The figure 2.2 shows the variation of growth rate of CdS films with different preparation temperature after Sunny Mathew [100]. It shows that above 300°C the deposition rate decreases rapidly.

ii) Substrate effects

Generally, the spray pyrolysis process affect the substrate surface. When it is not desirable for the substrate to take part in the pyrolytic reactions, neutral substrates such as glass, quartz, ceramics are used. At lower substrate temperature foggy and diffusely

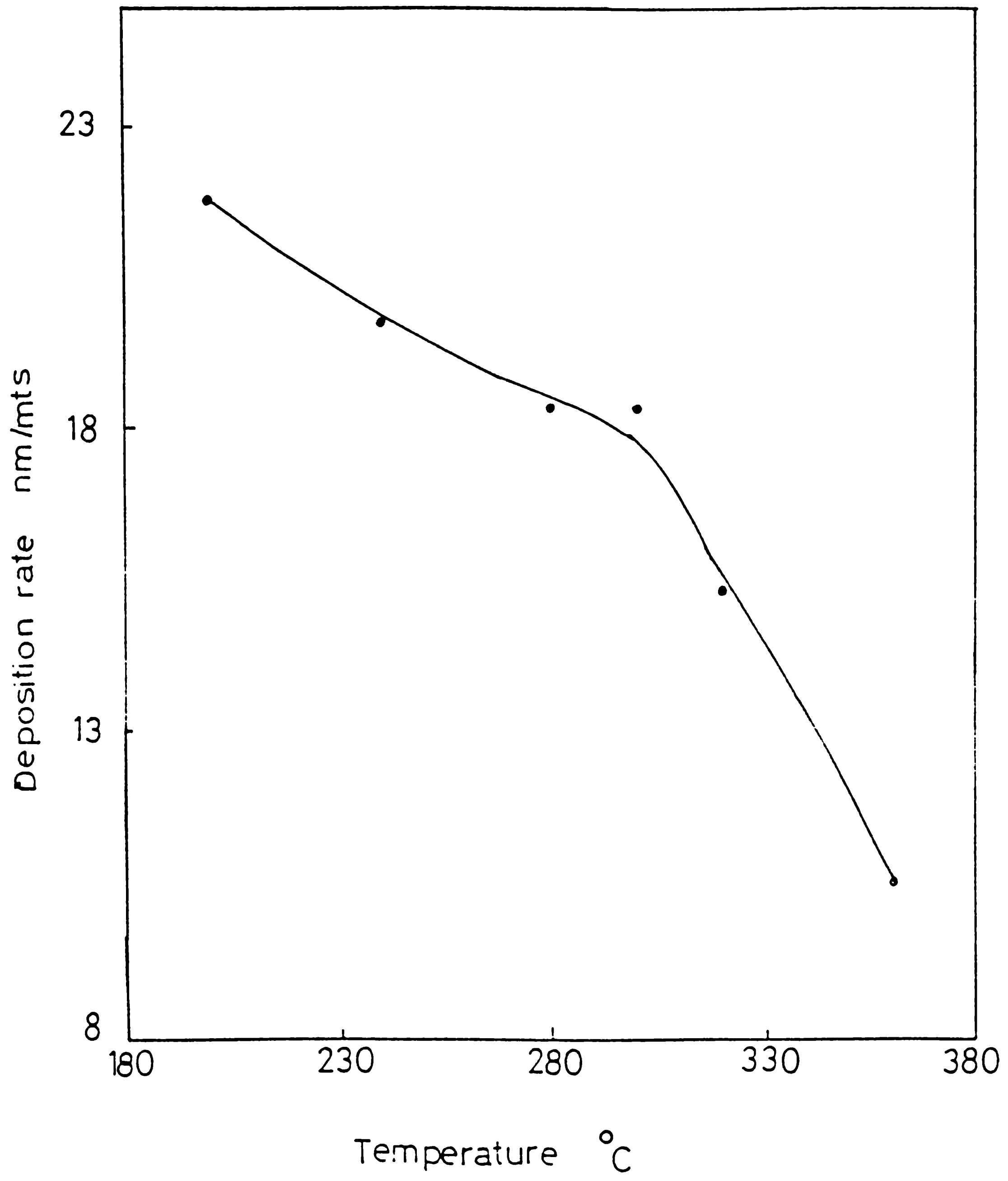

Figure 2.2. Variation of growth rate of CdS films with different preparation temperature

scattering films are obtained. Higher substrate temperature yield thinner, continuous, hard and specularly scattering films. Moreover, at higher temperature, re-evaporation of atomic species may occur, leading to metal-rich deposits.

In the case of CdS films substrate temperature has remarkable significance on its resistivity and crystallinity [100]. Figure 2.3 shows the variation of resistivity of spray pyrolysed CdS films at different substrate temperature. The film has very low resistivity at higher temperature. Figure 2.4 shows the XRD spectra of CdS films prepared at different substrate temperature. The spectra show that the crystalline quality of the films becomes better with increase in preparation temperature.

iii) Film composition

The composition of the film is expected to depend on the kinetics of the spray process and thermodynamics of the pyrolytic process. Stoichiometry of sulphide films does not vary appreciably with the metal-to-sulphur ion ratio in the spray solution for ratios ranging from 1:1 to 1:5, but microstructure of these films is strongly influenced by this ratio [102].

At low enough temperature, if the pyrolytic reactions have not been completed, some byproducts or intermediate compounds will be trapped as impurities in the film. In the case of chloride salts, residual chlorine is often present in films. In the case of CdS film, the chlorine concentration decreases with increasing substrate temperature during pyrolysis.

iv) Multicomponent doping and alloying

Copyrolysis has been successfully utilized by a number of workers [93, 103] to extend the technique to prepare doped and alloyed sulphide and selenide films of Cd, Zn and Pb. Copyrolysis involves choosing appropriate salts and spraying the common solution from one nozzle or by using any multiple nozzles to spray different solutions. Deshotels [104] used different carrier gases to dope CdS films with In and Ga. Copyrolysis has

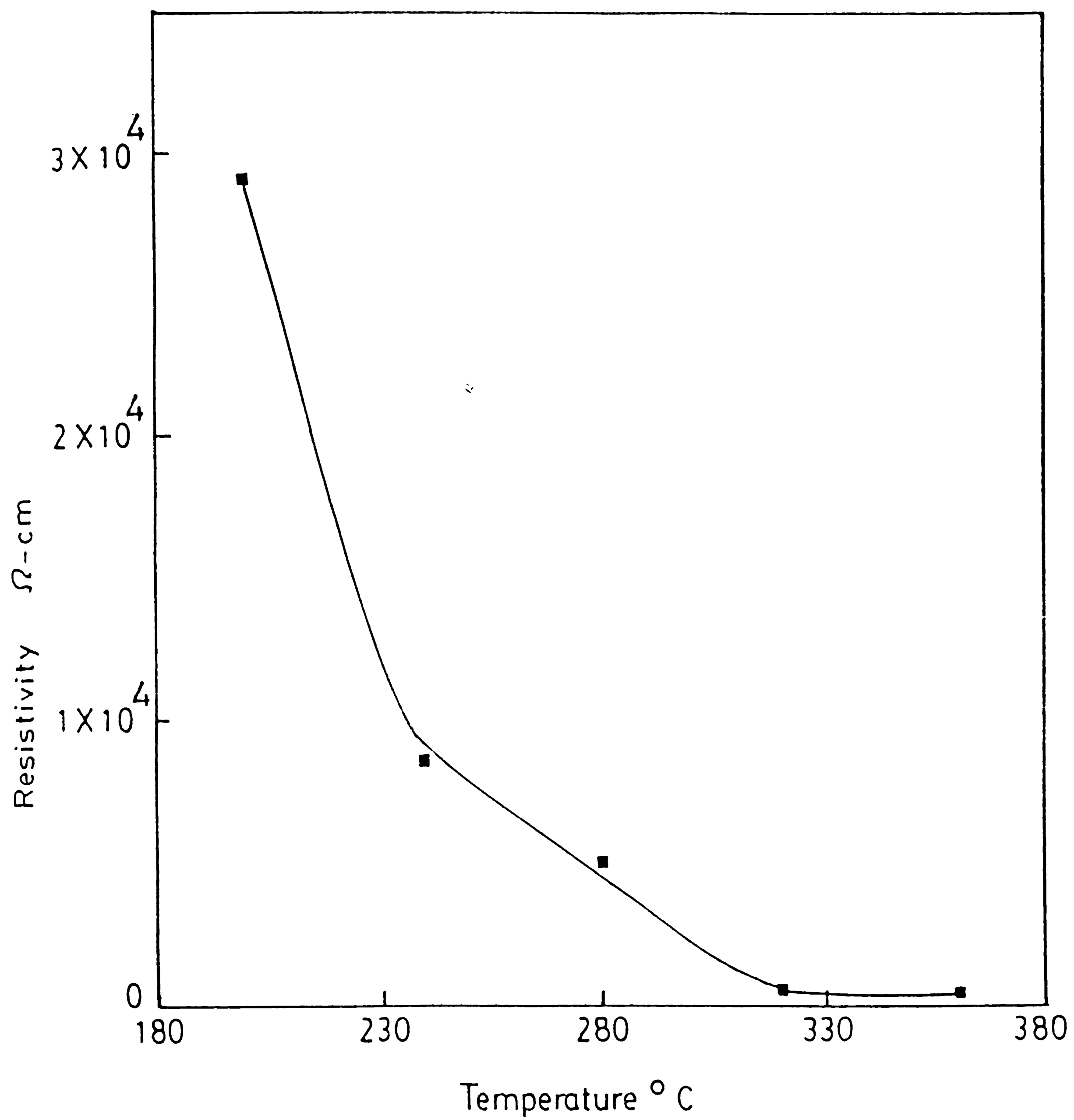

Figure 2.3. Variation of resistivity of spray pyrolysed CdS films at different substrate temperature

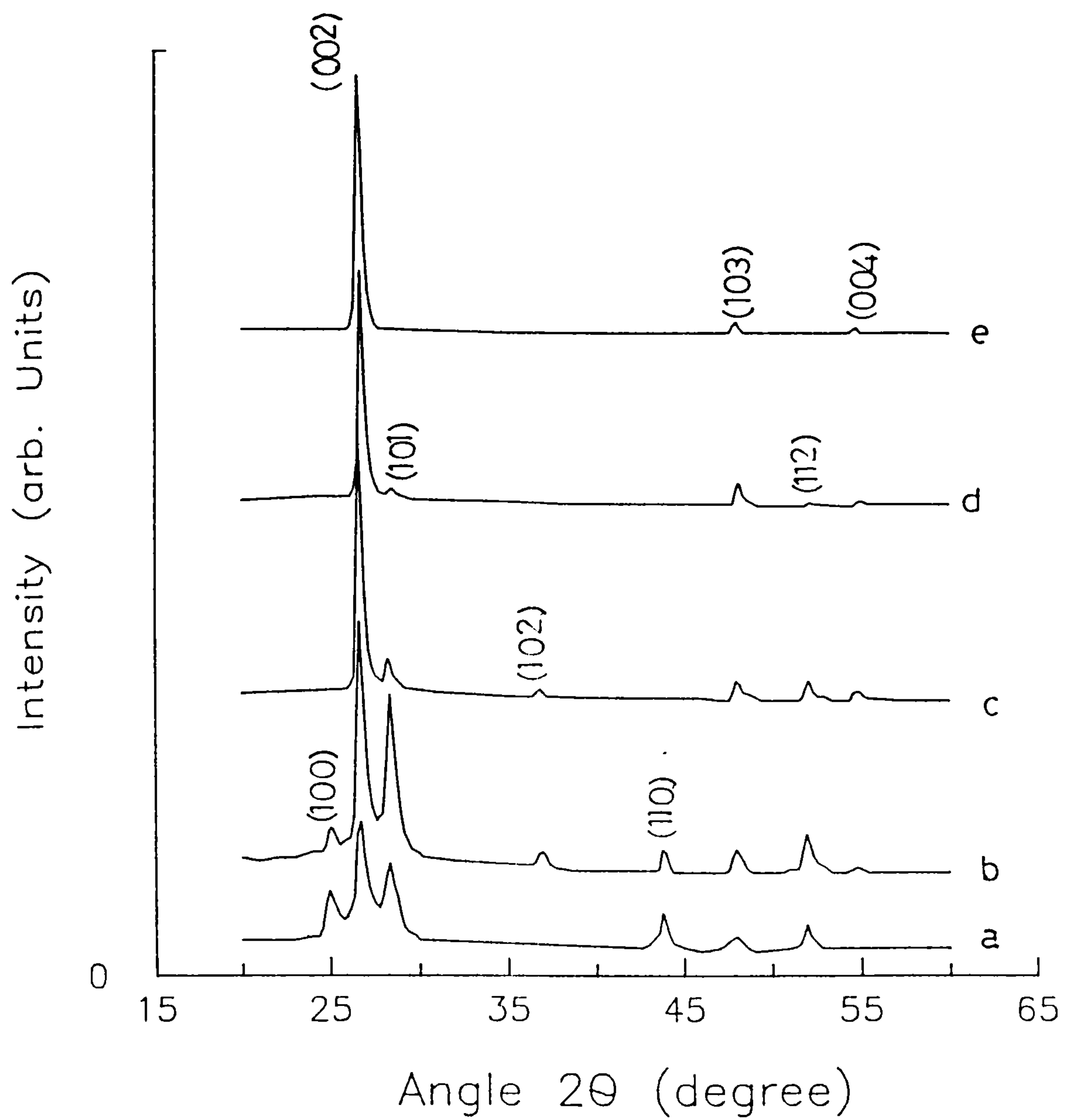

Figure 2.4. XRD spectra of CdS film prepared by spray pyrolysis at different substrate temperatures a) 200°C b) 240°C c) 300°C d) 320°C e) 360°C

been used by some workers [105] to obtain a heterogeneous mixture of oxide and sulphide films. The CdS films are obtained with segregated Al_2O_3 formed at the grain boundaries by cospraying solutions of $CdCl_2$, $AlCl_3$ and thiourea [105].

2.3.4.d. Properties of spray pyrolysed film.

In general, spray deposited films are strongly adherent, mechanically hard, pinhole-free and stable with time and temperature (upto spray temperature). The surface topography of the films is rough with the roughness depending on the spray condition and the substrate temperature [106]. The microstructure ranges from amorphous to micropolycrystalline depending on the droplet mobilities and chemical reactivities of various constituents. Post deposition annealing of films generally affects the oxygen-dominated electrical properties significantly but not the microstructure [107]. At annealing temperature above the spray temperature, or under some reactive environments, recrystallization increases the grain size and may produce some preferential orientation effects [107].

2.3.5. Chemical Bath Deposition (Solution Growth Process)

This technique was first used in 1946 to prepare PbS films for infrared applications [108]. Later this technique was used for the preparation of large area, doped and undoped multicomponent semiconductor films of usual and unusual and metastable structure. It is a solution growth process used for depositing thin films of compound materials. An aqueous solution of a metal complex when mixed with a solution of chalcogen bearing compound, precipitation of chalcogen occurs under certain conditions. When the precipitation is controlled, the compound gets deposited on clean substrates or other nucleating centers present in the solution.

2.3.5.a. Chemical aspects

According to the solubility product principle, in a saturated solution of a weakly soluble compound, the product of the molar concentration of its ions, called the ionic product (IP) is a constant at a given temperature. There is no equilibrium if this relationship is not satisfied. If the ionic product exceed the solubility product (SP), the precipitation occurs. When $IP<SP$, the solid phase will dissolve until the above relation is satisfied.

It is necessary to eliminate spontaneous precipitation in order to form a thin film by a controlled ion-by-ion reaction. This can be achieved by using a fairly stable complex of the metal ions which provides a controlled number of the free ions according to an equilibrium reaction of the type

$$M(A)^{2+} \rightarrow M^{2+} + A$$

the concentration of the free metal ions at a particular temperature is given by

$$[M^{2+}][A]/[M(A)^{2+}] = K_i$$

where K_i is termed as the instability constant of the complex ions. By choosing an appropriate complexing agent, the concentration of the metal ions is controlled by the concentration of the complexing agent and the solution temperature.

If a high concentration of S^{2-} ions exists locally such that the solubility product is exceeded, localized spontaneous precipitation of sulphide can occur. This problem can be overcome by generating chalcogen ions slowly and uniformly throughout the volume of the solution. This is achieved for example, by having thiourea in an alkaline aqueous solution according to the reaction

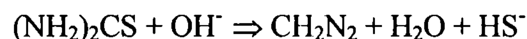

$$(NH_2)_2CS + OH^- \Rightarrow CH_2N_2 + H_2O + HS^-$$

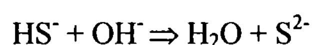

$$HS^- + OH^- \Rightarrow H_2O + S^{2-}$$

The experimental set up to obtain film deposition is shown schematically in the figure 2.5. The substrates are immersed vertically in the reaction bath, which is stirred continuously with a magnetic stirrer. The temperature of the bath is monitored by a contact thermometer that forms a part of a feedback current controlling the heater to maintain a constant temperature. When the IP of the metal and chalcogen ions exceeds the SP of the corresponding chalcogenide, a metal chalocogenide film is formed on the substrate by an ion-by-ion condensation process.

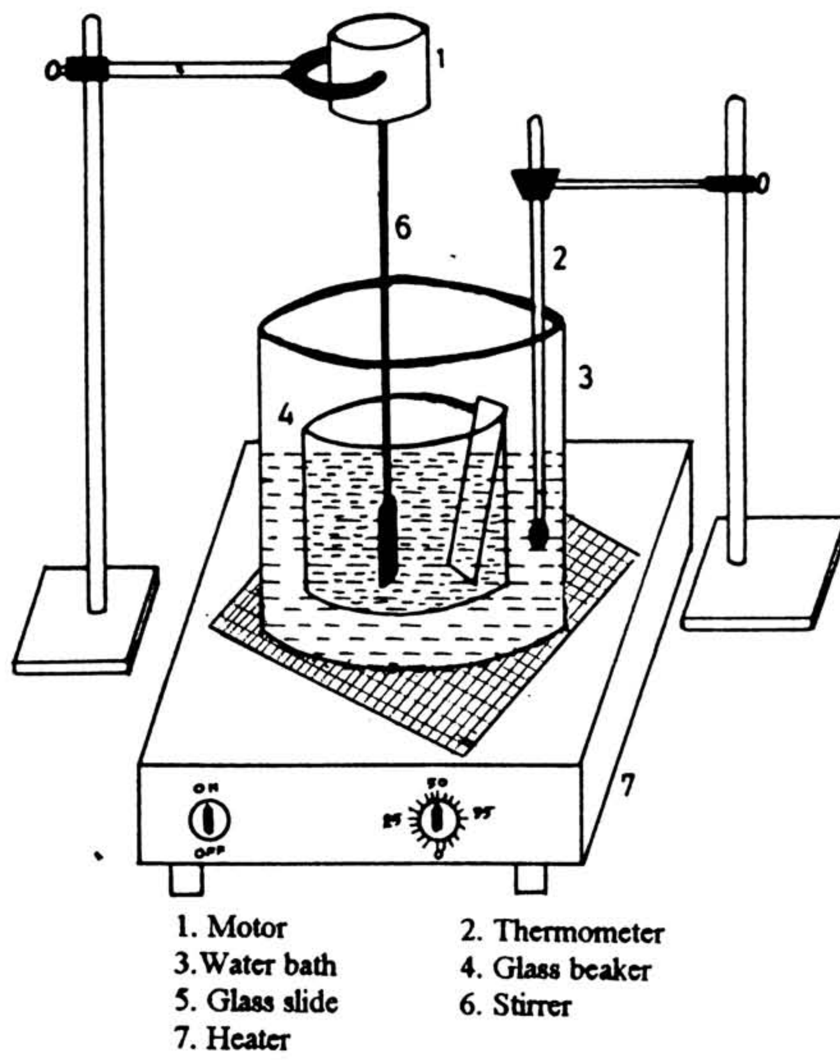

Figure 2.5. Experimental setup used for chemical bath deposition of thin films

2.3.5.b. Characteristic features of the Chemical Bath Deposition technique

The kinetics of growth of a thin film in this process are determined by the ion-by-ion deposition of the chalcogenide on nucleating sites on the immersed surfaces. Initially, the film growth rate is negligible because an incubation period is required for the formation of critical nuclei from a homogeneous system onto a clean surface. Once nucleation occurs, the rate rises rapidly until the rate of deposition equals the rate of dissolution i.e., IP = SP. Consequently the film attains a terminal thickness. On a presensitized substrate surface, no incubation period for nucleation is observed since nucleation centers already exists on the substrate [109]. Also when the substrates are suspended in the container before forming the complex in the solution, film thickness increases in a manner similar to that of sensitized surface, thereby showing that the nuclei for the formation of the film are provided by the solution itself.

i) Nature of the salt

The growth kinetics depends on the salts/compounds used for metal and chalcogenide ions. In general, the rates and terminal thickness are higher for sulphide than for the corresponding selenide films under similar deposition conditions [110]. The deposition rate and terminal thickness initially increase with an increase in the chalcogen ion concentration. At high concentration, however, precipitation becomes more significant, leading to decreased film thickness on the substrate [110].

ii) Complexing agent

The metal (M^{2+}) ion concentration decreases with increasing concentration of the complexing ions. Consequently, the rate of reaction and hence precipitation is reduced leading to a larger terminal thickness of the film. Such a behaviour has been observed for CdSe, CdS and PbSe and ZnS films [111].

In the case of CdS films, the complexing agent has a marked effect. CdS films obtained from $Cd(NH_3)_4^{2+}$ complex have sphalerite, wurtzite or mixed structure, depending on the deposition condition. But films obtained from $Cd(CN)_4^{2-}$ and $Cd(en)_3^{2+}$ complexes have wurtzite structure with c-axis perpendicular to the substrate [111]. Post deposition annealing at temperature greater than $400^{o}C$ for a sufficiently long time leads to appreciable

grain growth. Triethanolamine, ethylene diamine tetra acetic acid, glycine, trisodium citrate are usually used as complexing agents

iii) pH value

The addition of OH^-, i.e., increases in pH, makes the complex more stable, provided the OH^- ions take part in the complex formation. Thus, the free M^{2+} ion concentration is reduced, leading to a decrease in the deposition rate and an increase in the terminal thickness with increasing pH value [109]. If the OH^- ions do not participate in complex formation, film is formed with lower terminal thickness at high pH value.

iv) Substrate effects

Higher deposition rates and terminal thickness are observed for those substrates whose lattices and lattice parameters match well with those of the deposited material [110].

v) Bath/substrate temperature effects.

With increase in the solution temperature, the dissociation of the complex and chalcogen bearing compound increases. The increased concentration of the metal and chalcogen ions, coupled with higher K.E. of the ions results in increased interaction and yields a higher rate of deposition of the metal chalcogenide film. The terminal thickness may increase or decrease with increasing bath temperature depending on the degree of supersaturation. The terminal thickness first increases with increasing supersaturation (owing to increased concentration of ions) and then it decreases at sufficiently high supersaturation at which precipitation dominates. The supersaturation may, however, be controlled by the bath temperature and also by the complexing agent. Using a larger surface area, it is possible to collect more chalcogenide on the surface in the form of film. Moreover, dipping the coated surface again in a fresh solution, results in further deposition of material. Thus thick and multilayer films can be obtained by sequential dippings [112].

2.3.5.c. Doping

Impurities in the starting chemicals can be incorporated into the films only if the impurities form insoluble chalcogenides under the same conditions of deposition and provided their corresponding IP is greater than the SP. Few dopants satisfy these conditions. An important consequence of this fact is that the degree of purity of the starting chemicals is not so important factor in determining the purity of the resulting film if the impurity concentration is low and the corresponding IP<SP.

2.3.5.d. General properties of Chemical Bath Deposited films

Transmission electron microscopy studies of these chemically deposited films have established that the film formation proceeds via nucleation and growth process in a way similar to vapour deposited films [113]. Usually, the films are microcrystalline, with grain sizes typically in the range from 300 to 1000 A^o. The grain size depends on the composition and temperature of the bath and nature of the substrate. The grain size is larger at lower deposition rates, higher bath temperature and for lattice-matched substrates.

When two or more chalcogenides are codeposited, a finer microstructure is obtained, similar to the case of vapour deposited films. The microstructure in multicomponent films is dominated by the size of the various ions and interaction between them.

References

1. I.Langmuir, *Physik*,**2**,14(1913)1273.
2. Joy George in *Preparation of thin films*, MARCEL DEKKER INC 270 MadisonAvenue, New York 110016.
3. M.N.Mahadasi and M.S. AlRobace, *J.Sol. Energy Res* (Iraq),**3**(1986)1.
4. B.P.Rai, *Phy. Stat sol.(a),* **99**(1987)P_k 35.
5. J.George, B.Pradeep and K.S. Joseph, *Phy. Stat sol.(a)*, **100**(1987)513.
6. Siham Mahmond, *J.Mater.Sci.*, **22**(1987)3693.
7. A.Kikuchi, S. Babu and A. Kinbera, *Thin Solid Films*, **164**(1988)153.
8. K.Rajana and S. Mohan, *Thin Solid Films*, **172**(1989)45.
9. F.Volklein, *Thin Solid Films*, **191**(1990)1.
10. D.F.Besnideenhont and R. Prelorius, *Thin Solid Films*, **139**(1986)121.
11. C.Kaito and Y. Saito, *J.Cryst.Growth*, **79**(1986)403.
12. P.Singh and B. Baishya, *Thin Solid Films*, **148**(1987)203.
13. M.A.Jayaraj and C.P.G. Vallabhan, *Thin Solid Films*,**177**(1989)59.
14. F.Lopez and E. Bernabeu, *Thin Solid Films*, **191**(1990)13.
15. K.Suzuki, Y. Ema and T. Hayashi, *J.Appl.Phy.* **60**(1986)4215.
16. M.Isai, T. Kukunaka and M. Ohshita. *J.Mater.Res.(USA)*, **1**(1986)547.
17. S.Chaudhuri, A. Mondal and A.K. Pal, *J.Mater. Sci.Lett.*, **6**(19887)366.
18. V.Damodaradas, N. Soundararajan and M. M. Pattabi, *J. Mater. Sci.*, **22** (1987)3522.
19. R.D.Gould and C.J. Bowler, *Thin Solid Films*, **164**(1988)281.
20. V.J.Rao, D.V. R. Rajan and P.B. Kadan, *Thin Solid Films*, **176**(1989)207.
21. W.Z.Soliman, M.M. El-Nahas and K.M. Mady, *Opt. Pura.Appl.*, **22**(1989)115.
22. J.L.Richards, P.B. Hart and L.M. Gallore. *J.Appl.Phys.*,**34**(1963)348.
23. J.L.Richards in *The Use of Thin Films in Physical Investigations* (J.C. Anderson Ed.), Accademic Press, NewYork, 1996, p.71.
24. E.K.Muller, *J. Appl.Phys.*, **35**(1964)580.
25. E.G.Ellis, *J.Appl.Phys.*, **38**(1967)2906.
26. D.Sridevi and K.V. Reddy, Indian *J.Pure Appl.Phy.*,**24**(1986)392.
27. K.V.Reddy and J.L. Annapurna, *Pramana (Indian)*, **26**(1986)269.

28. B.S.V.Gopalam and K.R.Murali, *Mater.Chem.phys.*,**15**(1986)463.
29. J.L.Annapurna, K.V. Reddy, *Indian J.Pure.Appl.Phy.*, **24**(1986)283.
30. L.B.Braun and D.E. Lood, *Proc.IEEE*, **54**(1966)1521.
31. N.Toghe, K.Kanda and T. Minami, *Thin Solid Films*, **182**(1989)209.
32. M.Ece and R.W. Vook, *Appl.Phy.Lett.*, **54**(1989)2722.
33. B.Schumann, G. Georgi, A. Tempel, G.Kuhn, Nguyen Van Nam, H. Neuman, W. Horig, *Thin Solid Films*, **182**(1989)209.
34. M.P.Sigal,W.R. Graham, and J.J. Santiago-Aviles, *J. Appl.Phys.*, **68**(1990)574.
35. R.Trykozko, R. Bacewicz, J. Filipowicz, *Prog.Cryst.Growth*, **10**(1984)361.
36. G.Burrafato, N.A. Mancine, S. Santagate, S.O. Trofa, A. Torrisi and O. Puglisi, *Thin Solid Films*, **121**(1984)291.
37. H.W.Lehmann and K. Frick, *Appl.Opt.*, **27**(1988)4920.
38. D.Das and R. Banerjee. *Thin Solid Films*, **147**(1987)321.
39. R.Oesterlein and H.J. Krokoszinski, *Thin Solid Films*, **175**(1989)241.
40. H.J.Kroskoszinski and R.Osterlein, *Thin Solid Films*, **187**(1990)179.
41. H.M.Smith and A.F. Turner, *Appl.Opt.*, **4**(1965)147.
42. S.Mineta, N. Yasunga, N. Tarumi, E. Teshigawara, M. Okullomi and M. Ikeda, *Bull.Jpn. Soc.Process.Eng.*, **18**(1984)49.
43. H.T.Yang and J.T. Cheung, *J. Cryst.Growth*, **56**(1982)429.
44. J.J.Dubowski, Proc.SPIE, 668(1986)97.
45. M.Baleva and D. Dekoeva, *J.Mater.Sci.Lett.*,**5**(1986)37.
46. P.Jayarammareddy and M. Sivajuddin, *Bull.Mater.Sci.* **8**(1986)365.
47. M.S.Sendova, *J.Mater.Sci.Lett.*,**6**(1987)285.
48. C.M.Dai, C.S. Su and D.S. Chuu, *Appl.Phy.Lett.*, **57**(1990)1879.
49. M.S.P.Lucas, H.A. Owen, Jr., W.C. Stewart and C.R. Vail, *Rev. Sci. Instrum.*, **32**(1961)203.
50. A.S.Gilmour, Jr., and D.L. Lockwood, *Proc. IEEE*, **60**(1972)997.
51. J.W.Robinson and M.Ham, *IEEE Trans. Plasma Sci.*, PS **3**(1975)222.
52. E.A.Roth, E.A. Margerum amd J.A. Amick, *Rev.Sci.Instrum.*, **33**(1962)686.
53. J.A.Turmer,J.K. Birtwistle and G.R. Hoffman, *J.Sci.Instrum.*, **40**(1963)557.

54. J.Van Andenhove, *Rev.Sci. Instrum.*,**26**(1965)383.
55. K.L.Chopra, *Thin Film Phenomena*, McGraw Hill, NewYork, 1969,p23.
56. L.I.Maissel and R. Glang, Eds.*Handbook of Thin Film Technology*, McGraw Hill, New York, 1970.
57. G.N.Jackson, *Thin Solid Films*, **5**(1970)209.
58. J.L.Vossen, *J. Vac.Sci. Technol.*, **8**(1971)512.
59. R.Behrisch, Ed., *Topics in Applied Physics*, **vol 47**, Sputtering by Particle Bombardment, Springer Vertag, Berlin 1981.
60. P.D.Davidse and L.I. Maissel,, Transactions of the 3rd International Vacuum Congress, Stuttgast 1965, *J.Appl.Phy.*, **37**(1966)574.
61. F.M.Penning, *Physica* (Utrecht) **3**(1930)873; U.S. Patent 2(1939)146,025.
62. Yamanaka, M. Tanda, K. Konagai and K. Takahashi., *Proc. 21st IEEE photovoltaic specialists conf.* (IEEE, NewYork,1990)758.
63. E.H.Parker.E.d., *The Technology and Physics of Molecular Beam Epitaxy*, Plenum Press New York, 1985.
64. W.Knodle *Res. Dev.*, **28**(1986)73.
65. H.Nelson, *RCA Rev.*, **24**(1963)603.
66. J.S.Blakemore, *J. Appl. Phys.*, **53**(1982)k123.
67. C.Geibel, H. Maier and R. Schmitt. *J. Cryst.Growth*, **86**(1988)386.
68. K.Lischka, T.Schmidt, A pesck and H. Sitter, *Appl.Phy.Lett.*, **55**(1989)1220.
69. J.Luff and E.Wudy., *Thin Solid Films*, **175**(1989)213.
70. D.M.Mattox, *Electrochem. Technol.*,**2**(1964)295.
71. N.Savvides, *Thin Solid Films*, **163**(1988)13.
72. H.Oechsuer, *Thin Solid Films*, **175**(1989)119.
73. T.Takagi, *Met.Res. Symp.Proc.*, **27**(1984)501.
74. S.E. Hug, R.A. McMahon and H. Ahmed, *Semi Cond.Sci.Technol*,**5**(1990)771
75. M.Sosnowski and I.Yamada,Neclar Instrum.Methods.*Phys.Rev.***B46**(1990)397
76. S.K.Sharma and S.L. Pandey, *Thin Solid Films*, **62**(1979)209.
77. N.P.Sinha and M. Misra, *Thin Solid Films*, **62**(1979)209.
78. C.D.Fung and J.J. Kopanski, *Appl. Phys. Lett.*, **45**(1984)757.

79. D.Raviendra, Sudeep and J.K. Sharma, *Phys. Stat. Sol. (a)* , **88**(1985)pk83.
80. M.A.Mohammed and D.V. Norgan, *Thin Solid Films*, **176**(1989)45.
81. O.B.Ajai, M.S. Akanni, J.N. Lambi, H.D. Burrows, O.Osasona and B. Podor, *Thin Solid Films*, **138**(1986)91.
82. H.Matsumura, *Jpn.J.Appl.Phys.*, **28**(1989)2157.
83. T.R. Jervis, *J.Appl.Phy.,* **58**(1985)1400.
84. T.H. Baum and C.R. Jones, *Appl.Phys.Lett.*, **47**(1985)538.
85. T.H. Baum, Proc. SPIE Int Soc.Opt.Eng., **1190**(1990)188.
86. R.W. Schwartz, *Mater. Lett.*, **4**(1986)370.
87. D.P. Norton and P.K. Ajmera.,*J. Electron.Mater.*, **19**(1990)367.
88. S.M. Ojha in Physics of Thin Films. Vol.**12**(G.Hass, M.H. Francombe and R.W. Hoffman, Academic Press New York) 1982, p 237.
89. K.Matsushita, T.Sato, Y.Sato, V.Sugiyama, T.Hariu, IEEE Trans.Electron Devices. ED. **31**(1984)1092.
90. A.C. Adams,F.B. Alexander ED,Capio & T.C.Smith,*Solid State Technol.*, **24** (1983)135.
91. D.S.Campbell in Handbook of Thin Film Technology (L.I. Maissel and R. Glang), (Eds), McGraw-Hill, New York, 1970,Ch.5.
92. F.A.Lowenheim, in Thin Film Processes (J.L. Vossen and W. Kern, Eds), Academic Press, New York, 1978, p209.
93. R.R.Chamberlin and J.S. Sakarman, *J. Electrochem. Soc.*, **113**(1966)86.
94. C.S.Wu, R.S. Fiegelson and R.H. Bube, *J.Appl.Phys.*, **43**(1972)756.
95. C.S.Wu, R.H.Bube, *J.Appl.Phys.*,**45**(1977)648.
96. F.Buch, A.L. Fahrenbrch and R.H. Bube, *J. Appl.Phys.*, **48**(1978)1596.
97. M.Saveli, *Proc. Workshop on II-VI solarcells*, Mountpellier (1979)p1-1.
98. A.Banerjee, PremNath, V.D. Vankar, S.R. Das and K.L. Chopra, *Phys.Stat.Sol.(a)*, **46**(1978)723.
99. Chopra, R.C.Kainthla, D.K. Pandya and A.P. Thakoor, Physics of Thin Films, **Vol.12**,Academic Press, New York, 1982.
100. Sunny Mathew, PhD Thesis, Cochin University of Science & Technology, 1994

101.C.M.Lampkin, *Prog.Cry.Growth Characteristics*,**1**(1979)405.

102.Y.Y. Ma and R.H. Bube, *J. Electrochem.Soc.* 124(1977)1430.

103.S.Y.Yin, A.L. Fahrenbruch and R.h. Bube, *J.Appl.Phys.*, **49**(1978)1294.

104.W.J.Deshotels, F. Augustine and A. Carlson, 2nd Quarterly Report, Contract NAS 7-203,Clevite Corp, (1963).

105.A.D.Thakoor, B.R. Mehta, D.K. Pandya and K.L. Chopra, Int. Conf. Metallurgical Coatings San Francisco (1981).

106.Sunny Mathew, P.S.Mukherjee and K.P.Vijayakumar,*Thin Solid Films,***254**(1995)278

107.E.Shanthi, A. Banerjee, V. Dutta and K.L. Chopra, *Thin Solid Films*, **71**(1980)237.

108.R.J.Cashman, *J.Opt.Soc.Am.*, **36**(1946)356.

109.K.L. Chopra, R.C. Kainthla, D.K.Pandya and A.P. Thakoor, Physics of Thin Films, Vol.12. (Academic Press, New York) 1982.

110.I.Kaur, D.K. Pandya and K.L. Chopra, *J. Electrochem.Soc.* **127**(1980)943.

111.R.C. Kainthla, Ph.D. Thesis, Indian Institute of Technology, Delhi (1980).

112.P.K.Vidyadharan Pillai, K.P. Vijayakumar and P.S. Mukherjee, *J..Mater.Sci. Lett.*, **13** (1994)1725.

113.R.C. Kainthla, D.K. Pandya and K.L. Chopra, *J. Electrochem.Soc.*, **127**(1980)77.

Chapter 3
Thermally Stimulated Current Measurements
Theory and Experiment

3.1. Introduction

Much research in Solid State Physics today is devoted to optical and electrical properties of solids because of the remarkable expansion that is taking place in the filed of electronics and optoelectronic devices. Research in this area is aimed at the successful application of existing materials and also for the development of new and improved materials.

Numerous publications indicate a rapid growth of interest among material scientists in determining the relevant properties by means of techniques based on thermal stimulation. The main advantage of this type of technique is that they allow electronic and dielectric relaxation process to be unraveled very quickly. In addition they are convenient and possess high sensitivity and are easy to set up. Thermally stimulated measurements have evolved into a basic tool useful for the identification and evaluation of dielectric loss mechanisms as well as trapping-recombination levels arising from structural imperfections, impurities and dopants.

Thermally stimulated process-TSP find application in research on materials for thin films, microelectronics, power transmission, transducers, energy conversion and electrostatic photography. This is also useful for the analysis of a variety of important devices such as radiation detectors, solar cells, display panels, TV screen luminescent and lasing diodes, field effect transistors, charge coupled devices and switching elements.

Two basic conditions have to be fulfilled for the occurrence of thermally stimulated relaxation (TSR) process; they are i) the system must be removed from the thermodynamic equilibrium and exist in a state which requires the reactants to surmount a free energy

barrier in order to switch back to equilibrium ii) the system must be in contact with a temperature reservoir that provides the thermal energy necessary to activate the relaxation process.

Of interest for the study of thermally activated relaxation from a nonequilibrium steady state situation back to the thermal equilibrium is the ways to remove the system from equilibrium and the phenomena that can be measured or monitored during the relaxation process. Thus the thermally activated relaxation processes are utilized to characterize the reactions taking place. These processes encompass an enormous wealth of biological, chemical and physical phenomena. Theoretical description of this phenomenon is almost entirely based on the so-called absolute rate theory borrowed from chemical reaction kinetics.

The equilibrium of a system may be perturbed by changing the concentration of the reactants, the temperature, pressure, electric or magnetic field (including electromagnetic field) etc. The establishment of a new equilibrium conditions during and after the perturbation may be monitored through the measurement of concentration of the involved species and the results can be utilized for the study of the involved chemical or physical reactions. Since the temperature has a most pronounced effect on the reaction rates, it has to be carefully controlled. Two basic types of relaxation techniques are used. (i) Isothermal relaxation : the perturbation is implemented at a constant temperature that is selected to assure experimentally convenient relaxation times.(ii) Nonisothermal relaxation: the system is perturbed at a sufficiently low temperature to reduce the probability to establish a new statistical equilibrium. Subsequently, the temperature is increased according to a well controlled heating program, thus increasing the reaction rates and the relaxation of the system can be monitored as a function of temperature and time.

The isothermal relaxation technique is most successfully used not only in the study of chemical reactions, but also in electronic reaction kinetics in solids [1-3] and in the technique of deep level transient spectroscopy [4-5]. But nonisothermal relaxation is

employed in the studies of thermally stimulated luminescence, conductivity, exoemission, polarization and depolarization.

Various types of thermally stimulated relaxation process, mode of excitation and observed phenomena are depicted in the table 1.

3.2. Non equilibrium Steady state Electron Statistics for Semiconductors

In this section steady state distribution functions for electrons and holes that arise as a result of an external perturbation of thermal equilibrium are discussed. They provide the initial condition for the thermally stimulated relaxation phenomena of electronic carrier as in thermally stimulated conductivity.

The mathematical treatment of this situation is taken from the work of Shockley and Read [6] for the case of a single trap level and from its extension to arbitrary distribution of traps by Simmon and Taylor [7].

In the following discussion we assume with Simmon and Taylor that an arbitrary distribution N(E) of electron levels exists between the top of the valence band at Ev and the bottom of the conduction band Ec. The state of occupancy determines whether a level act as a hole trap or electron trap. When the level is unoccupied, it is ready to receive a hole and is therefore a hole trap. The charge state of the trap is not considered here, but emphasis is given to cross section for electron or hole capture. Hence a positively charged unoccupied monovalent state is likely to have a large cross section for electron capture.

The purpose of this section is to describe the distribution of electrons and holes over available states during the perturbation and during the subsequent relaxation process. The sequence of the typical TSR experiment starts with a system in thermal equilibrium at temperature T_0, proceeds with the establishment of a nonequilibrium steady state during perturbation (generation of electron - hole pair via photon absorption) at the same

Table 1. Various types of thermally stimulated relaxation process, mode of excitation and observed phenomena

Name	Excitation	Observed Phenomena	Materials
Thermoluminescence TL	Optical or atomic radiation	Light emitted by recombination of detrapped charge carriers	Phosphors
TS conductivity or TS currents - TSC	Optical or atomic radiation	Increase in dark conductivity due to carriers lifted into the CB or VB	Photo - and Semi -conductors
TS-Exoelectron emission-TSEE	Atomic or electron irradiation	Electron emission from the surface of the sample into vacuum.	Insulating or semi insulating layers
Ionic thermal currents-ITC	Electrical	Discharge currents accompanying the disorientation of impurity vacancy dipoles	Ionic crystals
TS Depolarization TSD	Electrical	Discharge current or charge decay induced by dipole disorientation	Dielectric, Semiinsulators Semiconductors
TS Creep TSCr	Mechanical stress	Torsional creep	Polymers
TS Capacitance TS Cap Deep level transient Spectroscopy DLTS	Electrical	Change in capacitance due to release of carriers in a depletion layer	Semiconductors

temperature T_0 and the gradual re-establishment of thermal equilibrium at T_0 or after completion of a heating process at a higher temperature T_1.

The key to the occurrence of thermally stimulated phenomena during this redistribution, is of course, the fact that all real semiconductors possess quantum states in the forbidden gap and that capture and thermal emission transition of holes and electrons take place between the bands and these states. Shockley-Read statistics is the basic statistical approach of such materials as Ge and Si because at present semiconductor technology has advanced to such a degree of sophistication that very pure intrinsic materials can be produced to start with. They can then be back doped with the desired impurity so that the recombination and thermal generation processes are indeed controlled by one or very few different single trapping states. The resulting relative simplicity in the kinetic theory is one of the reasons why the technique of thermally stimulated relaxation has been so immensely successful in these materials.

3.2.1. Shockley-Read Statistics

Consider first a single nondegenerate trap level of density N_t at energy E_t, as a special case of an arbitrary trap distribution. According to Shockley and Read, the capture rate of electrons n_c in the conduction band by the trap is

$$r_\beta = \langle v_n \rangle S_n n_c N_t \, [1 - f(E)] = \beta \, n_c N_t \, [1 - f(E)] \quad (3.1)$$

where $\langle v_n \rangle$ is the average thermal velocity of the electrons, S_n the capture cross section, $f(E)$ the probability the trap level is occupied by an electron and $\beta = \langle v_n \rangle S_n$ is the capture coefficient. In thermal equilibrium,

$$f(E) = \left\{ 1 + \exp[\frac{(E_t - E_F)}{kT}] \right\}^{-1} \quad (3.2)$$

Knowledge of f(E) at any time during the thermally stimulated process together with the knowledge of the respective capture and thermal emission rates completely determines

the statistics of the system under investigation. The rate of thermal release of trapped electrons is r_α and is given by

$$r_\alpha = \alpha N_t f(E), \tag{3.3}$$

where α is the coefficient for thermal emission of electrons from the traps into the conduction band.

Similarly the capture rate for holes from the valence band

$$r_\beta^* = \langle v_p \rangle S_p p N_t f(E)$$

$$= \beta^* p N_t f(E) \tag{3.4}$$

where p is the hole density in the valence band, $< v_p >$ is the average thermal velocity, S_p the capture cross section for holes and β^* the capture coefficient.

The rate of hole emission into the valence band is given by

$$r_\alpha^* = \alpha^* N_t [1-f(E)] \tag{3.5}$$

where α^* is the coefficient for thermal release of holes from the trap into the valence band.

In thermal equilibrium, the net rate of capture and emission of electrons and holes is zero (principle of detailed balance). It is therefore $r_\beta = r_\alpha$ and $r_\beta^* = r_\alpha^*$, which after substituting the value of $n_c = N_c \left\{1 + \exp[\frac{(E_c - E_F)}{kT}]\right\}^{-1}$ and $p = N_v \left\{1 + \exp[\frac{(E_F - E_v)}{kT}]\right\}^{-1}$ yield [8]

$$\alpha = \langle v_n \rangle S_n N_c \exp[-(E_c - E_t)/kT]$$

$$\alpha^* = \langle v_p \rangle S_p N_v \exp[-(E_t - E_v)/kT] \tag{3.6}$$

where N_c is the density of electron states in the CB and N_v the density of hole states in the VB.

Let us now discuss the probability of occupation for a trap in the case of a non equilibrium steady state situation, arising, for example, during the exposure of sample to light quanta of sufficient energy to create electron-hole pairs. When the solid is uniformly illuminated, a steady state is established such that creation of electrons and holes is balanced by capture and thermal release at the respective trapping levels.

For an arbitrary distribution N(E) of non degenerate trapping states per unit energy and volume, this may be expressed as [9]

$$\frac{dn_c}{dt} = G - \int_{E_v}^{E_c} c_n\, N(E)\,[1 - f(E)]\, dE + \int_{E_v}^{E_c} \alpha\, N(E) f(E)\, dE$$
$$\frac{dp}{dt} = G - \int_{E_v}^{E_c} c_p\, N(E)\, f(E)\, dE + \int_{E_v}^{E_c} \alpha^{*}\, N(E)[1 - f(E)]\, dE \qquad (3.7)$$

where $c_n = \langle v_n \rangle S_n n_c$, $c_p = \langle v_p \rangle S_p p$. In this equation the first term G is the net generation rate of electron-hole pairs, second term indicates carrier capture and the third term represents the carrier emission.

In steady state equilibrium $dn_c = dn_p = 0$, and

$$\int_{E_v}^{E_c} N(E)\,[- c_n(1 - f) + \alpha\, f + c_p f - \alpha^{*}(1 - f)]\, dE = 0$$

This is valid for any distribution of trapping states N(E). Therefore the term in the bracket is zero and

$$f(E) = \frac{c_n + \alpha^{*}}{\alpha + \alpha^{*} + c_n + c_p} \qquad (3.8)$$

The probability of occupation in thermal equilibrium is replaced by this new distribution function or occupational function that characterises the nonequilibrium steady state during the ongoing stimulations (perturbation) similar to Fermi Dirac distribution function where the equilibrium Fermi level is replaced by suitable quasi-Fermi level. Also F(E) is independent of the form of stimulation provided the stimulation process does not alter N(E) i.e., no new defect levels are created in the stimulation process.

3.2.2. Quasi Fermi Levels

The use of quasi-Fermi levels for the description of occupation function is quite common in solid state statistics and is based on the assumption that in the nonequilibrium steady state situation the relative populations of electrons over certain available levels are determined by a thermal equilibrium between these levels.

For example, the population of electrons in the CB and in electron traps can be characterised by an occupational function $f = \left\{1 + \exp[-\frac{(E - E_f)}{kT}]\right\}^{-1}$ and a quasi Fermi level E_f such that

$$n_c = N_c \exp[-(E_c-E_f)/kT] \qquad (3.9)$$

Similarly the quasi-Fermi level for holes in the VB is E_p and

$$p = N_v \exp[-(E_p-E_v)/kT] \qquad (3.10)$$

The introduction of quasi-Fermi levels through these occupational distribution functions provide a convenient distribution of the establishment of the non equilibrium steady state during ongoing perturbation and the re-establishment of thermal equilibrium during the thermally stimulated relaxation experiments.

Simmons and Taylor [7] introduced two additional fictitious levels, E_f^n and E_f^p, the quasi Fermi level for trapped electrons and holes respectively which permit one to express the occupational function of traps in a Fermi-Dirac form. This can be done, however, only for a given species of traps such that each species is associated with its own quasi-Fermi levels E_f^n and E_f^p. Naturally, if a large number of different traps are involved, then characterising the statistical properties of these traps via individual quasi-Fermi level is impractical and it becomes more convenient to use equation (3.8) which provides a single occupational function for the system.

In an arbitrary distribution N(E) of traps each set of traps with unique capture cross section, S_n for electrons and S_p for holes will be characterised by its own distribution function and set of values for E_f^n and E_f^p. From equation (3.8) it can be seen that a species

of traps is defined a unique function f(E). Both S_n and S_p may depend on E as well as on T [4,5].

For the development of the quasi Fermi level concept for traps, it is possible to neglect α^* in equation (3.8) at all energies above the equilibrium Fermi level E_F and α at $E < E_F$. Hence

$$f(E) = c_n/(\alpha + c_n + c_p); \qquad \alpha^* << c_n, c_p, \alpha \qquad (3.11)$$

$$f(E) = (c_n + \alpha^*)/(\alpha^* + c_n + c_p); \qquad \alpha << c_n, c_p, \alpha^* \qquad (3.12)$$

These occupational functions may be rewritten in a modified Fermi form in terms of E_f^n and E_f^p [10] as

$$f(E) = \frac{c_n}{c_n + c_p}\left\{1 + \exp\left[\frac{(E_t - E_f^n)}{kT}\right]\right\}^{-1} \qquad (3.13)$$

and

$$1 - f(E) = \frac{c_p}{c_n + c_p}\left\{1 + \exp\left[\frac{(E_f^p - E_t)}{kT}\right]\right\}^{-1} \qquad (3.14)$$

In this form, the occupation functions are now recognised as those for electrons and holes. If we consider, for example, a distribution of traps N(E) belonging to a single species, it is easily seen that the electron states are filled with electrons according to a Boltzmann distribution above E_f^n and occupied to a constant level given by $f(E) = c_n/(c_n + c_p)$ below E_f^n. Similarly, the states are empty (occupied with holes) according to a Boltzmann distribution below E_f^p and filled with holes to a constant level given by $f(E) = c_p/(c_n + c_p)$ above E_f^p. This situation is illustrated in figure 3.1. Under non equilibrium steady state condition $E_f^n > E_f$ and $E_f^p < E_p$. In thermal equilibrium, all quasi Fermi levels coincide with the equilibrium Fermi level E_F.

3.2.3. Classification of trapping states based on electron statistics

Defect states in the forbidden gap may act as electron trap or hole trap depending on their states of occupancy. The introduction of quasi-Fermi levels for trapped electrons E_f^n and hole E_f^p allows the classification of trapping states as shallow or deep traps. The involvement of electron states in the reaction process decreases with increasing energy from

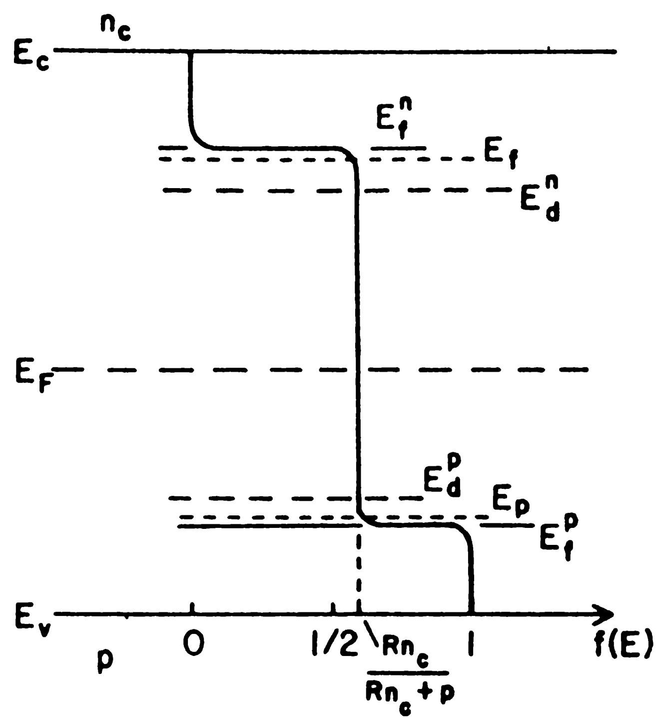

Figure 3.1. A typical occupational function f(E) for an arbitrary distribution of traps

the quasi-Fermi level for trapped electron upto the edge of the CB or with decreasing energy from the quasi-Fermi level for trapped hole down to the top of the VB. Free carriers falling into one of these trapping states will be reemitted with high probability back into the band from which they came from. These states are empty and are termed as shallow traps. Shallow traps are characterized by a very small ionization energy which is of the order of the phonon energies (0.01 eV ~0.04 eV).

Deep traps are those whose ionization energy is many times that of a phonon and consequently, radiationless capture of a free carrier may involve multi-phonon transition. It is to be noted that at elevated temperature (at temperature above several K) shallow trapping states are ionized (empty).

The classification of electronic states within the forbidden gap into traps or recombination centers is very useful in the discussion of all TSR process. Previously we used a generic term 'term' for all states in the gap. However, a clear distinction is possible as to whether, at a given temperature and for a given occupational function, the probability for a carrier to be released from the defect state into one of the two allowed bands is larger than the probability for capture of a free carrier . This is done by introducting demarcation level E_d^n for trapped electrons and E_d^p for trapped holes. According the Rose [1] in a trap distribution N(E), E_d^n is the level at which a the electron has equal probabilities of being thermally released into the CB or of recombining with a free hole. Then one can get using equation (3.4-3.6) for $r_\alpha/r_\beta^* = 1$ and $r_\alpha^*/r_\beta = 1$ and

$$E_d^n = E_v + (E_c - E_p) + kT \ln\left[\frac{< v_p > S_p N_v}{< v_n > S_n N_c}\right] \tag{3.15}$$

$$E_d^p = E_c - (E_f - E_v) + kT \ln\left[\frac{< v_n > S_n N_c}{< v_p > S_p N_v}\right] \tag{3.16}$$

Now it is clear that all states between E_d^n and Ev are recombination centers for electrons and all states between E_d^p and Ec are recombination centers for holes. It can be shown that [4,5] in first approximation, E_d^n is somewhat smaller than the quasi-Fermi level for electrons and

E_d^p somewhat larger than the quasi-Fermi level for free hole. The situation is illustrated in figure 3.2.

3.2.4. Filling Diagram

The purpose of discussing occupational function and of defining a variety of special levels such as quasi-Fermi and demarcation levels is to provide a simple language suitable to efficiently characterise the nonequilibrium steady state situation of a semiconductor during the perturbation of thermal equilibrium. Filling diagrams are simply a plot of f(E) as a function of energy in the energy interval of the band gap and are a convenient means of illustrating not only the initial condition for a thermal relaxation process but may actually be used to indicate the changes of occupational function during the relaxation process itself [11].

Consider f(E) for electrons in the case of some arbitrary trap distribution N(E). The thermal equilibrium is characterised by the fermi level E_F (Figure 3.3) and the nonequilibrium steady state condition during or immediately after uniform illumination of the solid, by one quasi-Fermi level each for trapped electrons and holes. It is assumed that a uniform density N_t of traps (defect states) is present in the solid. Under normal illumination levels (for which the density of free carriers is much smaller than that of trapped carriers) the cross hatched sections below and above E_F are equal in area indicating that as many electrons are trapped above E_F as have been removed from levels below E_F. This is a direct consequence of charge neutrality condition

3.2.5. Non equilibrium steady state relaxation

In this section, we discuss the relaxation of the system after the external perturbation is removed at time t=0.

After removal of the source of external perturbation the system is left in a non equilibrium state the relaxation of which may be considered to occur in two phases i) the excess free carrier decays via recombination with those recombination centers that have the

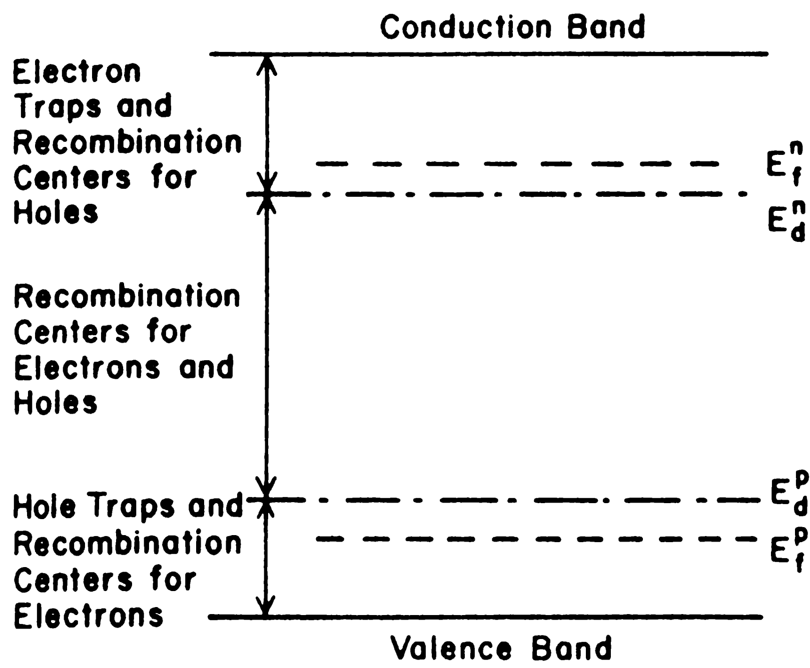

Figure 3.2. Demarcation levels E_d^n and E_d^p of a semiconductor with an arbitrary distribution of traps.

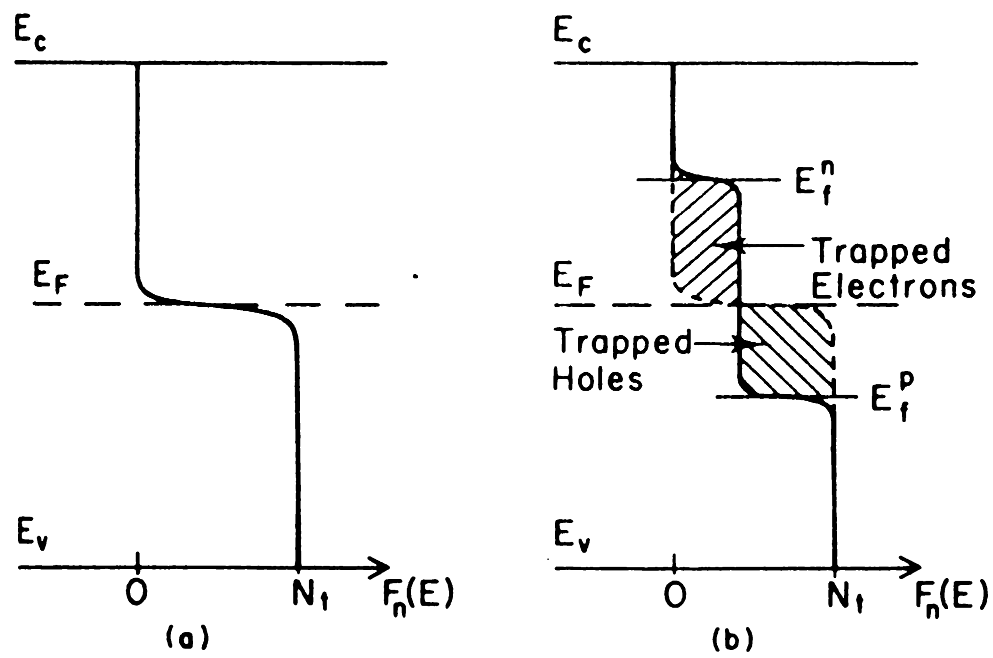

Figure 3.3. Filling diagram $F_n(E) = f(E)N(E)$ of a solid (a) before and (b) after perturbation of the statistical thermodynamic equilibrium.

largest cross section ii) further relaxation toward thermal equilibrium proceeds via thermal release of carriers from the traps into the band and subsequent recombination with recombination centers. The rate limiting step of second phase is the thermal release of trapped carriers. Its probability can be enhanced by increasing the temperature . Precisely that is done in TSR experiments. In this process, the quasi-Fermi levels and demarcation levels move toward the equilibrium Fermi level (Figure 3.4).

In the above case the relaxation kinetics is customarily described by assuming the following terms.

i) band - band transition are relatively unlikely to occur as compared to free carrier recombination with recombination centers.

ii) transitions between trapping states for electrons above E_d^n and for hole below E_d^p are non radiative transitions and involve the emission or absorption of phonons only.

iii) transition between recombination centers and the two bands may be radiative transition involving the emission or absorption of photons

iv) the system, that is the nonequilibrium distribution of electrons and holes over available energy state, is in thermal contact with black body radiation of density Q(E) and phonons of energy density $Q_p(E)$. These densities are the equilibrium densities at the temperature T of the solid so that one can get using equation (3.7)

$$\begin{aligned}\frac{dn_c}{dt} = & -\int_{E_v}^{E_d^n}[a(E) + b(E)\,Q(E)]\,Vn_c\,N(E)\,[1-f(E)]\,dE \\ & + \int_{E_v}^{E_d^n} b(E)\,Q(E)\,V\,N_c\,N(E)\,f(E)\,dE \\ & + \int_{E_d^n}^{E_c} \alpha(E)\,N(E)\,f(E)\,dE - \int_{E_d^n}^{E_c} \beta(E)\,n_c\,N(E)\,[1-f(E)]\,dE\end{aligned} \tag{3.17}$$

The success of Thermally stimulated relaxation technique to obtain information on trapping states in the gap depends critically on whether or not the experiment can be performed under condition that justifies equation (3.17) to be reduced to simple expressions for the kinetic process.

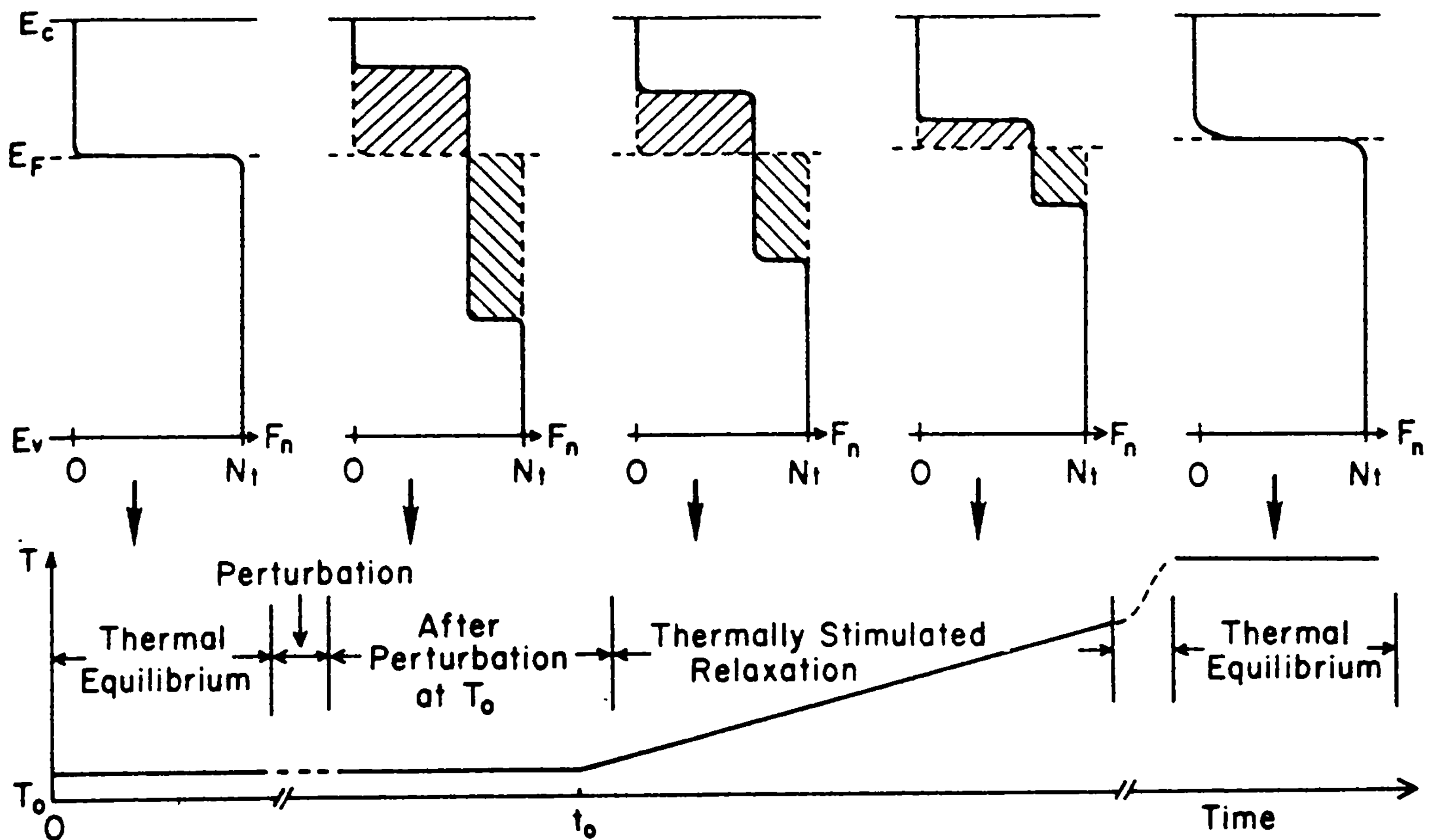

Figure 3.4. Schematic representation of the filling levels $F_n(E)$ for a uniform trap distribution N_t during a typical thermally stimulated relaxation experiment

3.3. Defect states in Semiconductors

Defect levels are localized electronic states in solids due to variety of causes but all leading to a loss of transitional symmetry of the crystal lattice: substitutional or interstitial impurities, vacancies, dislocations as well as termination of the lattice at the surface. Theory of electronic defect states and optical transitions was developed on the basis of the adiabatic approximation. Many-particle system consisting of electrons and nuclei and their mutual interactions is thereby separated into a nuclear part and an electronic part. Coupling between the two is neglected. The resulting many electron Schrodinger equation is further reduced to one electron equation to describe a single representative electron potential V of the perfect lattice which is modified by an additional potential U centered around the location of the point defects [12,13]. This adiabatic theory has reached a high level of sophistication in two limiting cases : deep and shallow defect states.

3.3.1. Tightly Bound (Deep) Defect states

If the wavefunctions of the defect states are localized in the regions where U dominates, the lattice potential may only act as a small perturbation the defect levels are tightly bound and the electronic defect states can be calculated with well-known methods. Successfully treated problems include calculations of the splitting of free atom or ion levels as the impurity is embedded in the matrix of the host crystal and of energy required to remove one or more electrons from the impurity (ionization energy) [14]. The agreement between calculated and observed values of the ionization energy for a number of impurities in semiconductors like Si and Ge is remarkable [15]. Bulk of the knowledge about deep impurities has been obtained from investigations with optical techniques. However, when the recombination is predominantly non radiative or when strong lattice coupling produces broad photon distributions that do not permit a clear identification of involved transitions by optical means, phenomena like TSC and DLTS are used as investigating tools.

3.3.2. Weakly Bound (Shallow) Defect states

Electronic states that are only weakly bound to a defect were characterised by eigenfunctions that extend over a large area of the lattice. In this case, the defect

perturbation U acts as a small perturbation on the periodic lattice potential V and such states are weakly bound defect states. Donor impurities of phosphorous, Arsenic and Antimony in Si and Ge and Aluminium, Gallium and Indium as acceptor impurities are examples. The ionization energies of these impurities are very small (typically 0.01eV in Ge and 0.05 eV in Si). They are conveniently determined by infrared absorption techniques or low temperature Hall measurements [15].

3.3.3. Intermediately Bound Defect states

This defect is considerably localized but the electronic levels are often not just perturbed by the surrounding lattice but grossly distorted. Certain colour centers in wide band gap materials are examples [16,17]. Theoretical study of these defects in ionic insulators is also difficult because of strong polarization effects which produce severe distortion of the ions surrounding the impurity. These distortions are quite different for a defect ground state as compared to excited states. The bulk of the thermoluminescence literature and a considerable fraction of the literature on TSC is concerned with these defect levels in insulators. The study of trap parameters with TSL and TSC techniques in wide band gap materials is, however, limited to those defect levels whose activation energies for the release of trapped carriers do not exceed 1.5 eV. Any larger value will place the glow peak at temperature so high that it becomes difficult to discriminate against the black body background and ionic conductivity.

3.4. Traps and thermal transport properties

Defect levels determine the density of carriers in the transport bands of the extrinsic semiconductors and wide band gap materials. Because of the strong temperature dependence of thermal emission rate and frequently also of non radiative capture rates, the study of thermal transport properties in a range of temperature provides a natural means to obtain information on these trapping parameters. Here thermal transport properties refer only to those related to charge carrier transport in a rather wide sense, but not to thermal

conductivity, impurity diffusion, self diffusion etc., which involve the transport of phonons or atomic species.

In general, various different types of traps and recombination centers may be present and their involvement in the reaction kinetics process will greatly change with temperature. The temperature range in which a specific trap dominates must therefore be identified. This is most conveniently achieved with the aid of nonisothermal temperature scans during which thermally stimulated current or luminescence is monitored. In semiconductors such novel isothermal techniques as deep level transient spectroscopy (DLTS) may be used as well. Of course, the microscopic physical and chemical nature of traps cannot be determined with these methods. At present nonisothermal thermally stimulated relaxation is a very active field of research because of its relative ease with which a TSC or TSL glow spectrum can be measured and the extraordinary sensitivity for detecting traps (perhaps as low as 10^7 /cm^3).

Let us now briefly consider the various steps involved in a TSC experiment. We choose electromagnetic radiation as a means of excitation (perturbation of the statistical thermodynamic equilibrium). The interaction of this radiation with solid leads to a number of electronic phenomena such as production of new defects, generation of both types of carriers as well as filling of trap levels with electrons and holes.

The state of the solid with excess carriers does not represent stable excited state. A fraction of them recombines directly after thermalisation either radiatively or by multiphonon emission. In most materials non radiative transition to defect states in the gap are the dominant mode of decay. The life time of free carriers, $\tau = 1/f \langle v \rangle S$ is determined by the density 'f' of the recombination centers, their thermal velocity $\langle v \rangle$ and the capture cross section S. Electrons captured by states above the electron demarcation level E_d^n and holes captured by states below the hole demarcation level E_d^p may get trapped. The condition for trapping is given when the occupied electron trap has a very small cross section for recombining with a free hole.

After the decay of the excess free carriers due to recombination and trapping transitions, the solid is in the excited state that is characterized by the perturbation of the

statistical equilibrium. The concentration of the remaining free carriers is now determined by the balance between thermal emission of carriers from the traps, retrapping transition and capture by recombination centers.

If the excitation occurred at a low temperature such that the thermal emission rate of carriers from the traps is very small the perturbed equilibrium will exist for a long time and only upon an appropriate increase of sample temperature can the relaxation process proceed at a rate that permits one to monitor it by measuring the conductivity of the sample.

3.5. Trap level spectroscopy by Thermally stimulated release of trapped carriers- A list of experimental methods

All thermally stimulated relaxation reactions discussed so far involve the release of trapped charge carriers into either the CB or VB and their subsequent capture by recombination centers or recapture by other traps. Experimental investigations are undertaken with the goal to determine the characteristics properties of the traps: capture cross section, activation energies, thermal escape rates, nature of traps, concentration of traps and trapped carriers. There are two types of methods namely Direct methods and Indirect methods.

3.5.1. Direct Methods

The reaction rate or thermal escape rate can be monitored directly and thus can be determined by measuring the concentration of trapped carriers as a function of time and/or temperature. This is accomplished by using the material to be studied in a capacitor configuration (e.g., a pn junction) as a schottky barrier or in general as thin film sandwiched between electrodes and by recording the changes in capacitance during the relaxation process. The capacitance change may be measured isothermally at one or several fixed temperature and the experimental techniques employed are known as isothermal capacitance transient (ICAPT) [21-23], deep level transient spectroscopy (DLTS) [24] and double

correlation deep-level transient spectroscopy (DDLT) [25]. These methods differ in their experimental sophistication, convenience in use and sensitivity.

Non isothermal capacitance methods employ thermal scans (heating programs) and are known as thermally stimulated capacitance (TSCAP) [26,27].

3.5.2. Indirect Methods

All the experimental TSR techniques except those described above used in trap level spectroscopy in semiconductors, are indirect methods for the determination of trapping parameters. This involves the measurement of phenomena that are due to charge carriers emitted after thermal stimulation from the traps.

A carrier thermally released from a trap into transport band may be either retrapped by the same species of traps or by a different one and, under the influence of an electric field, may contribute to an externally measurable current or a Hall voltage. It may either be swept out of the region being probed or recombine with a recombination center. Some of the electrons may even overcome the work function barrier and leave the solid together. Traffic of the charge carriers from the traps to the recombination centers or out of the material can be monitored at various stages and thus information on the thermal emission rates can be obtained indirectly.

An indirect method is thermally stimulated capacitor discharge (TSCD) [28,29]. It involves filling the traps at some high temperature (e.g., room temperature) by the application of high fields and subsequent cooling to a lower temperature with the field applied. Thereafter, the field is removed and the sample heated in the usual manner. The current measured during heating consists of two components i) the dielectric relaxation current ii) the current due to carriers thermally released from the trap into the two upper bands. Thus in order to utilize TSCD as a trap-spectroscopic tool, one has to subtract first component from the total current.

Trapping states located in a surface layer of generally less than 50 A^{0} thickness can be probed with the technique of thermally stimulated exoemission (TSEE) technique

[30,31]. During a thermal scan and after perturbation of thermal equilibrium via exposure of the surface to ionizing radiation, low energy electrons are emitted from some insulators, which are supposed to be originating from free electrons in the CB, and their measurement provides indirect information on spectroscopic parameters of traps near the surface [32].

Another technique that is commonly used is thermally stimulated luminescence (TSL) which monitors photons as a function of temperature during the thermal scan. These photons are the result of radiative transitions of free carriers, previously released from traps to recombination centers. TSL have been reported as early as 17th century, but Urbach [33] is generally credited with proposing it as a potentially useful experimental technique for trap level spectroscopy and it is widely used in halides [34], metal oxides [35], sulphides [36],and glasses [37].

During the time of thermally stimulated relaxation process, concentration of free holes and electrons in extrinsic semiconductors is determined by the balance between thermal emission from and the recapture by traps and the capture by recombination centers. In fact, trapping parameters together with the capture rates of carriers, in recombination centers, determine the concentration of free holes and electrons. Measurements of current density $J=e\ (\mu_n n_c\ +p\mu_p)$ will therefore provide trap-spectroscopic information. The experimental techniques employed to perform trap level spectroscopy on this basis is known was isothermal current transient (ICT), thermally stimulated current. (TSC) and thermally stimulated Hall effect.

ITC method consists of measurement of thermally activated release of polarization. It is used for the investigation of the electrical properties of high resistivity solids via the study of thermal relaxation effects. This technique was first introduced and studied in detail by Bucci and Fieschi [38]. It relies upon utilizing the response to an electric field of the dipole moment formed between a point defect and an impurity ion. Here impurity ions and vacancies can be presented as individual defects independent of one another or they may be present as impurity vacancy dipoles. A significant concentration of the paired impurity-vacancy defects can be oriented away from random orientations within a lattice by the

application of a steady electric field. The resulting non random orientation can be immobilised by freezing the sample to a low temperature with the electric field still applied. Upon removing the electric field and warming the specimen at a constant heating rate, the aligned defects relax and oriented back to random positions. In doing so, they produce burst of displacement current that can be monitored as a peak in a detected displacement current. ITC techniques have been applied to the study of many ionic and divalent compounds, semiconductors, polymers and dielectrics [39-44].

In the present work, most of the electrical characterisation of thin film sample was performed using TSC technique and hence this technique is discussed in detail in the following sections.

3.6. Thermally Stimulated Current

First measurements of thermally stimulated current (TSC) alone or simultaneously with TSL was performed by Bube [45,46] Delbecq et al. [47] and Broser et al [48]. Both TSL and TSC are observed in a broad variety of materials e.g. fish, scales, bones, dental enamel, plastics and other organic solids [49], mineral ceramics as well as in amorphous polycrystalline and single crystalline semiconductors and insulators. A TSC spectrum(for historical reasons frequently referred to as glow curves) is a graph of electrical conductivity versus temperature. This usually consists of a number of resolved peaks that may be attributed to different species of traps. Since the escape probability of carriers from trapping sites is proportional to exp ($-E/kT$), the location of a glow peak on the temperature scale provides encoded information on the value of the thermal activation energy. Hence a glow curve represents a spectrum of energies that are required to free carriers from the various species of traps present in the material.

The most simple of reaction kinetics that yields TSC peaks is single trap model and is discussed in section 3.8. The field of TSC developed along two lines. The first one merely made use of the capability of deep traps in certain insulating materials to store charge carriers at or below room temperature for a long time-sometimes thousands of years. Very

successful applications of these phenomena in dosimetry, geology, archaeology etc., were the result. The other approach concentrated on quantitative trap level spectroscopy, employing curve fitting techniques on the basis of the single trap model [50,51] and on efforts to completely understand the detailed features of TSC curves calculated within the frame work of this model [52-54]. The often rather limited success to measure trapping parameters by this approach was not deterrent for ever continuing attempts along this line. A poor fit of experimental and computed glow curves was rarely related to inadequacy of the single trap model but rather to the fact that only approximate solutions of its rate equations were available. Exact solutions of this set of "stiff" differential equations were possible only after the development of powerful numerical computation techniques. The work of Kelly et al in 1971 [53,54] revealed the starting variety of different thermal emission curves that could be obtained from a physically meaningful range of trapping parameters.

It then became evident that it is extremely difficult to correlate theory and experiment by curve fitting alone with any degree of confidence. Any measured and well-resolved glow peak that may be expected to be due to a single type of traps can be fitted with a solution of the single trap parameters. Unfortunately such a fit is not unique, since a number of different model descriptions are conceivable in addition to single trap model. Very little effort has been extended to investigate them [55,56]. In the present state of development TSC give a quick and very sensitive survey of action energy, capture cross section, thermal escape probability and nature of traps.

3.7. Simple trap model

In principle, any defect state in the forbidden gap has a finite cross section for capture of free holes and electrons. Obviously, a trap being Coulomb-attractive for free electrons may be neutral or even repulsive for holes and has a smaller cross section for hole capture as compared to that for electron capture. The capture cross section of a trap is, in a rough approximation, largely determined by its charge state. In the familiar Shockley-Read process [18] the charge Z of a defect center that is effective for hole capture differs from that

effective for electron capture process by unity. A given defect state can be considered attractive or neutral always for one of both types of carriers. If it is singly attractive ($|Z| = 1$) for one type, it will be neutral for the other and if it is doubly ($|Z| = 2$) or triply ($|Z| = 3$) attractive for one, it will be doubly or triply repulsive for the other.

An estimate of capture cross section for Coulomb attractive and repulsive traps on the basis of simple model potentials was made by Rose et al [1] (Figure 3.5. a,b). Assuming that free carriers can be regarded as a diffusing particle having a mean free path for energy loss that is much smaller than the effective capture radius r_c of the traps, probability p(r) for finding it at a distance r from the trap is proportional to the Boltzmann factor $\exp[eV(r)/kT]$ and the area $2\pi r^2$. (V(r) is the defect potential). Calculating the minimum in p(r), the capture cross radius $r_c = e^2/2\varepsilon kT$ is obtained for a Coulomb potential $V(r) = -e^2/\varepsilon r^2$ and the capture cross section ($S = \pi r_c^2$) is seen to be proportional to T^{-2}.

Coulomb attractive defect centers can capture more than one charge carrier and thus turn neutral or even Coulomb repulsive. The latter type of traps is assumed to be surrounded by a potential barrier of height ΔV. Capture of a free carrier requires either a tunneling through or going over this barrier. For example, if $(S_n)_{repul}$ is the cross section for electron capture, it can be obtained by the product of the cross section for a Coulomb attractive trap, S_n and the probability to find the electron at an energy above $e\Delta V$ above $Ec=eV_\infty$ in figure 3.5.c [19] i.e.,

$$(S_n)_{repul} = S_n \frac{\int_{e\Delta V}^{\infty} f(E)N(E)dE}{\int_{Ec}^{\infty} f(E)\, N(E)\, dE} \qquad (3.18)$$

This expression is difficult to evaluate for most distribution function f(E). An estimate of range in which Coulomb-repulsive cross sections are expected to fall may be obtained by assuming the probability to find an electron at $e\Delta V$ is smaller by $\exp[-e\Delta V/kT]$ as compared to finding it at Ec [1]. Thus barrier height of only a few tenths of an electron volt

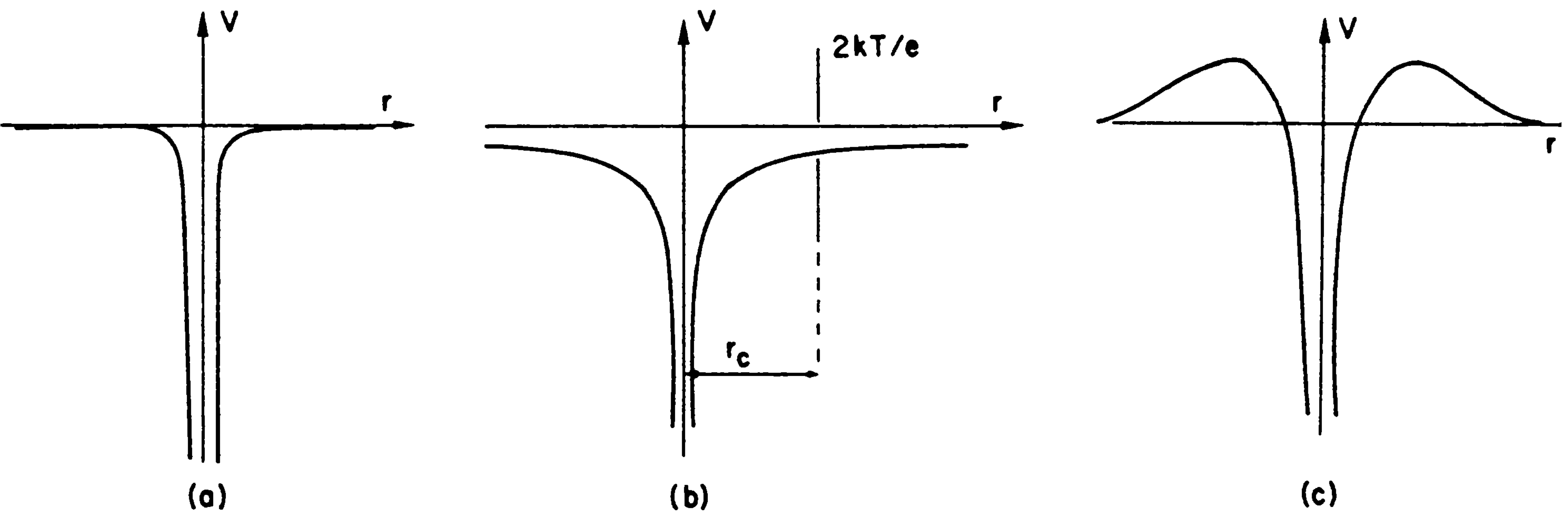

Figure 3.5. Schematic potential distribution of defect levels in semiconductors. (a) Neutral trap (b) Coulomb-attractive trap (c) Coulomb-repulsive trap

may reduce S_n by many orders of magnitude. Further, the cross section for Coulomb repulsive trap centers are expected to be temperature dependent.

For neutral trap centers, an estimate of the capture cross section may be obtained in a similar way as for a Coulomb-attractive center. The Coulomb potential may be replaced by a moderately long range r^{-4} potential [20] that results from the interaction between the charge carrier and the polarization of the trap and the cross sections are expected to be smaller than those for long range r^{-2} potentials because of a reduced capture radius.

3.8. TSC Kinetics

In this section we develop electron kinetic models for thermally stimulated current based on the statistical considerations.

Let us assume an arbitrary distribution N(E) of defect levels in the forbidden gap of the nonmetallic solid and f(E) as the occupation function corresponding to the situation in which free electron and holes are generated and subsequently trapped. This situation is illustrated in figure 3.4 for the special case N(E) = constant. It represents the initial condition at $t = t_0$ Then the equation (3.7) now becomes

$$\frac{dn_c}{dt} = -\int_{E_v}^{E_c} c_n(E)\, N(E)\, [1 - f(E)]\, dE + \int_{E_v}^{E_c} \alpha(E)\, N(E)\, f(E)\, dE$$

$$\frac{dp}{dt} = -\int_{E_v}^{E_c} c_p(E)\, N(E)\, f(E)\, dE + \int_{E_v}^{E_c} \alpha^*(E)\, N(E)\, [1 - f(E)]\, dE \qquad (3.19)$$

where $C_n = \beta n_c$ and $C_p = \beta^* p$, β and β^* being the capture coefficient for electrons and holes and n_c and p, the concentrations of free electrons holes respectively.

Further we assume that at t_o the sample is at a uniform temperature T_0, low enough to prevent thermal emission of both holes and electrons from their respective traps. Increasing the temperature according to a heating program T(t) will increase the thermal

emission coefficient α and α^* according to equation (3.6) and this eventually leads to the redistribution of the trapped carriers over available defect states, until thermodynamic equilibrium is reached again at some higher temperature. Knowledge of N(E), c_n, c_p,α and α^* at $T = T_0$ is in principle sufficient for the complete characterisation of the relaxation kinetics of a given solid. The initial occupational function at T_0 is given by equation (3.8) and its behaviour with temperature during the irreversible scan T(t) is described the equation (3.19). Such solutions have been attempted rarely since no simple method is known to measure f(E,T) directly. Here solutions of equation (3.19) have to be obtained with nonisothermal reaction kinetics. In general, form of kinetics of these equations is mathematically intractable and therefore numerical or approximate solutions can be attempted at best . Again little is gained by this procedure since knowledge of all the rate coefficients and trap distributions is a prerequisite. The rate coefficients for a given solid are unknown and must be determined experimentally. Measurements such as TSC are readily performed but must somehow be interpreted to yield quantitative information on the trapping parameters.

Energy states of the electrons in defect levels i are frequently centered around a narrow energy distribution of $g(E - E_{t,i})$ or are even discrete. In the former case the volume density of the states is given by

$$N_i = \int_{E_v}^{E_c} N(E)\, g(E - E_{t,i})dE \quad \text{with} \quad \int_{E_v}^{E_c} g(E - E_{t,i})dE = 1 \qquad (3.20)$$

Discrete levels have δ function distributions on the energy scales. If there are j different discrete states in the forbidden gap, equation (3.19) can be written in the form

$$\frac{dn_c}{dt} = \sum_{i=1}^{j} \int_{E_v}^{E_c} N(E)\, \delta(E - E_{t,i})\, [(\alpha + n_c \beta_i) f(E) - n_c \beta_i]\, dE$$

$$= \sum_{i=1}^{j} \alpha_i n_i - \beta_i (N_i - n_i) n_c \qquad (3.21)$$

$$\frac{dp}{dt} = \sum_{i=1}^{j} \alpha_i^* (N_i - n_i) - \beta_i^* n_i p$$

Here α_i and α_i * are the "thermal emission coefficient" for electrons and holes respectively while β_i and β_i*, the capture coefficients for electrons and holes, n_i denotes the volume densities of electrons in the state i. Thus depending on the position of state i in the gap (Ni-ni) may be interpreted as the density of trapped holes, empty electron traps or empty recombination centers for electrons.

In order to proceed with model calculation of TSC we must specify, for a given solid which of the levels N_i at E_i are traps or recombination centers-several special cases shall be discussed [51].

i) One or several states N_i are located above the demarcation level E_d^n for electrons and one or several states Ai are located between E_d^p and E_d^n. We assume that shifts of E_d^n and E_d^p during the thermal scan are small enough so that none of the levels changes its nature as trap or recombination levels. After excitation, the levels above E_d^n are partially or completely filled with electrons and the recombination levels are unoccupied so that at t =t_0 all electrons deposited in the traps are missing from the recombination levels (figure 3.6 a,b) - An equivalent case of holes traps below E_d^p can be constructed (figure 3.6. c)

ii) Electron traps N_i above E_d^n are present together with hole traps $N_{h,i}$ below E_d^p (figure 3.6.d). Only one case, namely when there are no additional states present between E_d^p and E_d^n has been treated [57].

iii) The presence of trap-recombination center (or donor-acceptor) pairs constitute a special case. The defect centers are not randomly distributed throughout the solid. Instead donors and acceptors are associated in pairs with varying spatial separation. These configurations are well known from luminescence investigations [12,13,58]. However, they have been discussed only hypothetically conjunction with TSL and TSC [55] and there is no hard evidence available of "pair-type" glow curves. Because of spatially close association of trap and recombination centers, carriers may recombine without being thermally ejected into a transport band (figure 3.6.e)

3.8.1. TSC due to electron trap

This is the case (i) of the above section. Consider a solid that contains only one type of electron traps of volume density N at the discrete level E_t and in addition a set of

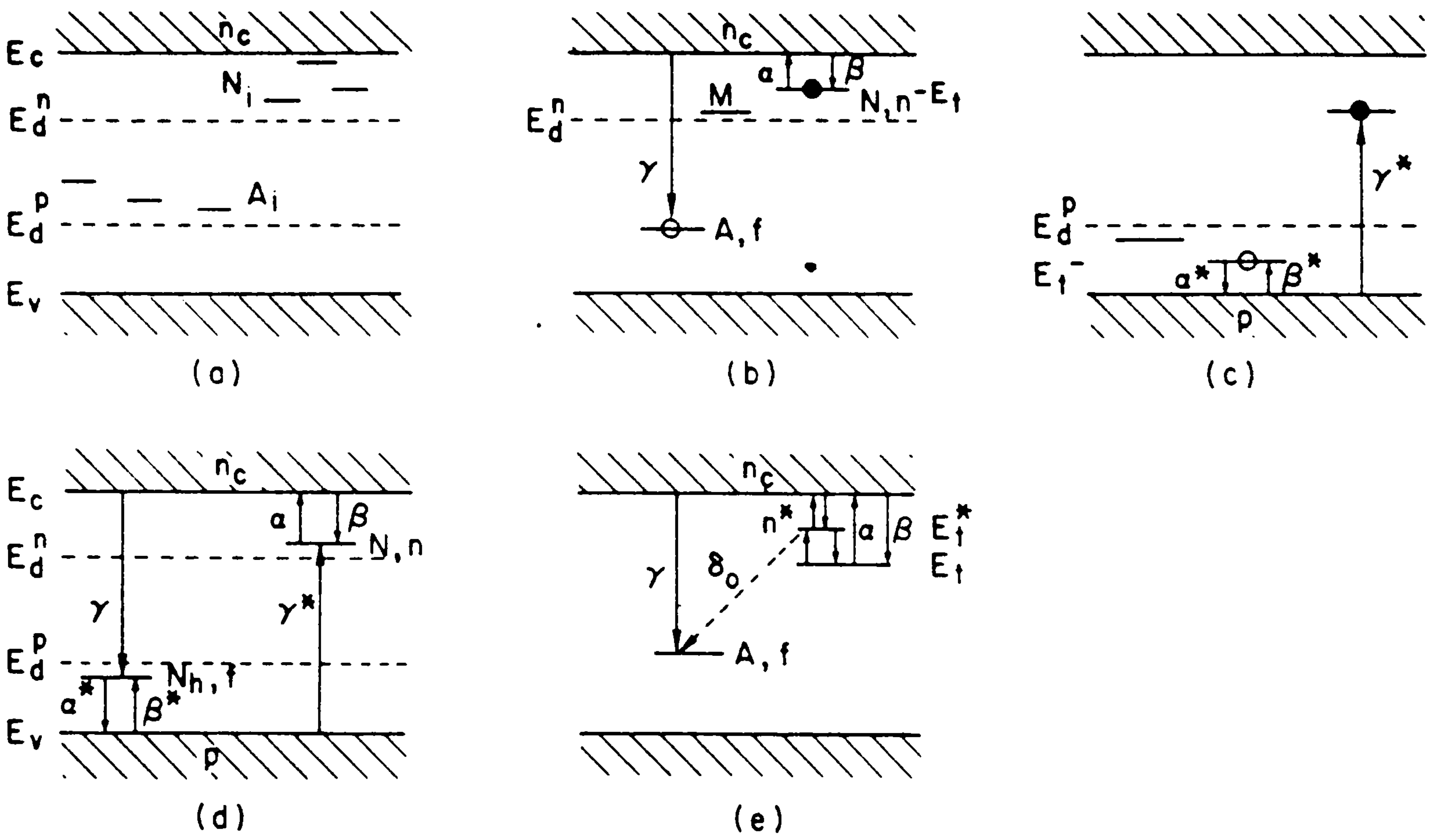

Figure 3.6. Reaction kinetic models involving discrete trap levels and recombination centers

occupied, but otherwise unspecified deeper electron traps of density M (figure 3.6 b). The experiment is performed in a temperature range in which traps N empty but traps M remain 'thermally disconnected' and act only as an untapped reservoir of trapped electrons. The density of recombination centers is unspecified, but a density f of them are empty. At $T=T_0$ a concentration of f_0 empty recombination centers exist due to excitation. Then charge neutrality of the sample requires

$$f=n_c + n + M \tag{3.22}$$

where n_c is the density of free electrons and n that of occupied traps. Equation (3.21) can be simplified to

$$dn_c/dt = \alpha\, n - \beta\, n_c (N-n) - \gamma\, n_c (n_c+n+M) \tag{3.23}$$

Here we denote the capture coefficient for electron traps by $\beta_i = c_n/n_c$ for electron traps by β and that for recombination by γ . The recombination coefficient γ is the sum of γ_r and γ_{nr}, the coefficients for a radiative and non radiative recombination respectively.

Again with equation (3.22), one can get

$$df/dt = dn_c/dt + dn/dt = - \gamma\, n_c (n_c + n + M) \tag{3.24}$$

Numerical solutions of equations (3.23) and (3.24) have been obtained by Braunlich et al [59] and they presented approximate numerical solutions for thermally stimulated current [59,60,61]. Approximate analytic solutions of equations (3.23) and (3.24) are possible only if

$$n_c \ll n \quad \text{and} \quad \frac{dn_c}{dt} \ll \frac{dn}{dt} \tag{3.25}$$

and this yields

$$-\frac{dn}{dt} = \frac{n\,(M+n)\,\alpha}{[(1-R)n + M + RN]} \tag{3.26}$$

and

$$n_c = \frac{\alpha\, n}{\gamma\,[(1-R)n + M + RN]} \tag{3.27}$$

Time dependence of equations (3.26) and (3.27) is replaced by the temperature dependence via the heating program, which is customarily taken to be linear such that $dT=\beta dt$, where β is the heating rate. Occasionally quadratic heating programs ($dT=\alpha T^2 dt$; α =constant) have been employed because they simplify certain integrals which appear in the approximate expressions obtained from equation (3.26) and (3.27) for σ (T).

3.8.2. TSC due to electron and hole traps

Simple "single trap model" is inappropriate whenever electron as well as holes are simultaneously released from their respective traps. Naturally phenomenological rate theory of TSC becomes very complex and usually approximate solutions are considered in which occupied hole traps are only available recombination centers for free electrons and similarly filled electron traps are the only recombination centers for free holes. The conductivity is now given by $\sigma = e(\mu_n n_c + \mu_p p)$.

Simultaneous release of electrons and holes from their respective traps can lead to negative thermally stimulated current as predicted by Braunlich [62] and it is observed in CdTe [63].

3.8.3. TSC due to trap-recombination center pairs

The acceptor-hole pair concept of Williams [64] has proven to be a physically realistic situation in many solids. TSC curves can be obtained for the case that in addition to thermal release into the transport bands, recombination of trapped carriers may also occur simultaneously by thermally activated nonradiative transitions from an excited trap level, The activation energy E_A for those transition is assumed to be smaller that E.

If thermal ejection of carriers from traps occurs exclusively via such transitions within the pair, no TSC curve can be measured and a TSL curve is obtained only when the transition is radiative. Little experimental work has been done on thermally stimulated relaxation of trap recombination center pairs [55].

3.9. Calculation of activation energy and capture cross section

The thermally stimulated current I, due to a single trap of depth E, with negligible retrapping and monomolecular kinetics is given by [65,66]

$$I = I_0 \exp\left[-\frac{E}{kT} - \frac{\nu}{\beta} \int_{T0}^{T} \exp(-\frac{E}{kT})\, dT \right] \qquad (3.28)$$

where T_0 is the initial temperature, ν the attempt-to-escape frequency and β is the heating rate. Hence preexponential factor I_0 is a weak function of temperature and I exhibits a maximum as a function of temperature. As the temperature increases the trapped charge carriers are released and this gives rise to current peaks. Consequently a plot of current versus temperature is called TSC spectrum. If more than one type of trap is present curves obtained from TSC studies may be expected to show several maxima depending upon the activation energy of the traps. The trap depth or the activation energy E of the carriers can be calculated as [65-67]

$$E = \frac{2\,kT_m^{\,2}}{(T_2 - T_1)} \tag{3.29}$$

where $(T_2\text{-}T_1)$ is the width of peak at half maximum value and T_m is the temperature of the peak maximum. Mott and Gurney [68] suggested that capture cross section 'a' of the traps may also be calculated from TSC spectra as

$$a = a_0 \nu \tag{3.30}$$

where $a_0 = 10^{-26}\,cm^2 s$ and

$$\nu = \frac{\beta}{T_m}(\alpha \exp \alpha)$$

and α is defined as $\alpha = \frac{E}{kT_m}$

3.10. Experimental details

The main attraction of TSC as experimental method for the study of defects in semiconductors is its apparent simplicity. The excited sample merely has to be placed onto a heater after attachment of two metallic contacts for voltage biasing connected to a sensitive current meter. Work at low initial temperatures makes it necessary that the experiment to be performed inside a vacuum chamber. As the field evolved, more

complicated heating programs were found to be advantageous in certain situation, but the basic experimental arrangement was never a complex one.

3.10.1. Heating Programs

For most experiments on non-isothermal thermally stimulated relaxation, simple cooling of the sample to the desired initial temperature and a linear increase in temperature after excitation is sufficient to obtain TSC glow curves. Some techniques require more elaborate heating cycles, the details of which depend on the relaxation mechanism under study. Heating programs can also be designed to partially overcome one of the major problems in the measurement of thermally stimulated relaxation, namely the occurrence of unresolved peaks. Several procedures have been devised to this end : the decayed glow curve technique, thermal cleaning and fractional emptying. The first consists of selecting an initial temperature T_0 that is high enough not to fill those traps during excitation that produce the low temperature peak. Thermal cleaning achieves the same result by preheating the sample, excited at T_0 to T_1. Fractional emptying consists of measuring the initial rise of glow peaks during the successive T ramps of gradually increasing upper temperature limits. A histogram of the slopes, obtained from semi logarithmic plot of glow curve intensity vs 1/T reveals the spectrum of the activation energies involved in the otherwise unresolved glow peaks [69].

The rates β in a linear heating program $dT=\beta dt$ should be carefully considered. In general, a compromise between fast heating (to improve the signal to noise ratio) and uniform heating of the sample is chosen. Bonfiglio [70] showed that the temperature difference between the back (heated) and front surface of a flat sample for a given heating rate β may be estimated from $\Delta T = qd^2c\varepsilon/k$, where c is the specific heat, k the thermal conductivity, ε the sample density and d is its thickness. Temperature gradients across the sample may lead to hysteresis effects during fractional emptying experiments. Heating with photon beams [71] or "hot anvil" systems [72] are used to achieve extreme rates.

3.10.2. Cryostats and heaters

Standard optical metal or metal-glass cryostats are commonly used in low temperature studies of TSC after installation of a heater system. Less expensive facilities for liquid N_2 temperature had been designed [71] and closed cycle cryotips may be employed as well.

The heaters commonly consist of a resistive wire or a co-axial heating cable with an insulated heating wire inside a flexible metal tubing. These are usually powered by dc supplies or special electronic control units [73]. Optical heating using light pipes has been explored also [74].

Transparent windows are required whenever the sample is excited by optical means. The window material is chosen according to the transparency requirements: glass (0.33-2μm) quartz (0.18μm to visible), LiF (0.11μm to infrared), thin films of poly ethylene, mylar, beryllium or aluminium (X- and γ-rays).

3.10.3. Sample Excitation

The statistical equilibrium of the sample can be perturbed in many ways. TSC can be produced after mechanical deformation, however, ionizing radiation or carrier injection are used most often.

For excitation in the visible range of the electromagnetic spectrum lasers or incandescent and gas discharge lamps together with filters or monochromators have been used. The excitation of the sample may involve band- band transition with subsequent trapping of the carriers or lead to internal conversion of localized defects [75]. Such secondary effects as optical quenching or sample heating during exposure to radiation should be minimized or controlled. Strongly absorbed light in conjunction with an appropriate bias voltage leads to photoinjection of carriers [76]. High energy radiation does, of course, not only fill the traps but produce new defects in most samples (radiation damage) [77].

3.10.4. Electrical measurements

TSC experiments are customarily analysed assuming the sample behaves "ohmic", that is the contacts do not introduce an inhomogeneity in the distribution of electric field or carrier density and a uniform bulk density of the carriers extends through the entire sample. Contact barriers are neglected. Henisch and Popeseu [78,79] analysed carrier and field distribution under isothermal and stationary conditions and found that, in the limiting case of zero current flow, a convenient measure of the field inhomogeneity near the contacts is given by the Debye length

$$L_D = \left(\frac{\varepsilon\, kT}{2e^2\, n_c}\right)^{1/2} \qquad (3.31)$$

It turns out that L_D is rather small for life time semiconductors (where carrier life time is large) and that it can be appreciable in comparison to the sample length in relaxation semiconductors (where carrier lifetime is small).

Stationary current flow (carrier injection from the contacts into the sample) results in more complex field and carrier distribution along the sample, which depends largely on the injection or current composition ratio. The measurement of carrier density via TSC experiments is not a simple matter and inhomogeneities in both the carrier and the electric field distribution along the sample may seriously affect the validity of the results obtained. Traditional TSC theory yields expression for conductivity as σ (T) = $e(n_c\mu_n + p\mu_n)$, but in experiments we measure current and not the conductivity. Inhomogeneities are always associated with diffusion currents as well, a fact that is usually neglected in the theory of TSC. Experiments should always be carried out in such a way as to minimize injection effects.

Contact materials and configuration used in TSC experiments vary widely and depend on the particular application. Metal electrodes can be attached to the sample by evaporation, ultrasonic soldering (e.g., indium, or indium-gallium alloys and gold) or by application of conductive pastes.

Biasing the sample is in general a simple matter. Stable dc power supplies, floating or with one grounded outlet, or dry cell batteries are convenient to use because the currents through the sample are in general extremely small and require use of pico ammeter or electrometer. Lock in amplifier can be considered whenever the signal can be modulated.

3.10.5. Details of TSC experiment in the present work

Schematic diagram of experimental set up used for TSC measurement in the present work is shown in figure 3.7 while figure 3.8 shows the various parts of the conductivity cell. Top of the cell was closed vacuum tight using a circular metal plate from which a liquid nitrogen cooled cold finger was introduced into the cell. At the end of the cold finger a film holder was connected by welding. The holder is provided with a heater in order to vary the temperature of the sample. All insulations of the holder was made using the teflon. Chromel-Alumel thermocouple was used for temperature measurement. Sample with two electrodes (indium/ silver of area $0.5cm^2$, thickness $3000A^o$)coated keeping a distance of 1 cm between them on the top surface was loaded on the sample holder. The pressure inside the cell was kept at 10^{-2} Torr. Sample was cooled to liquid nitrogen temperature (100K). As the next step, sample was excited using a Tungsten-Halogen lamp (Oriel 6394, 25 Watt). The time of excitation was varied in the range 1-10 minutes for different samples. After the excitation, sample was heated at a constant rate (0.05K/sec) using a steady dc power supply. Current was measured using an electrometer (ECIL - EA815) varying the sample temperature from 100K to 500K. During this time a dc field of 6V/cm was applied on to the thin film sample along the film plane.

3.11. Dark conductivity in Semiconductors

The detailed theory of the electrical conductivity in semiconductor is given in Chapter 1. Lattice defects profoundly affect the electrical behaviour under certain conditions of defect concentration and temperature. Acceptor and donor impurity atoms also account for the extrinsic semiconducting properties. The basic idea of conductivity in a semiconductor is that electrons occupying donor levels (or holes occupying acceptor levels) may contribute to the electrical conductivity other than the usual process of thermal excitation followed by band conduction.

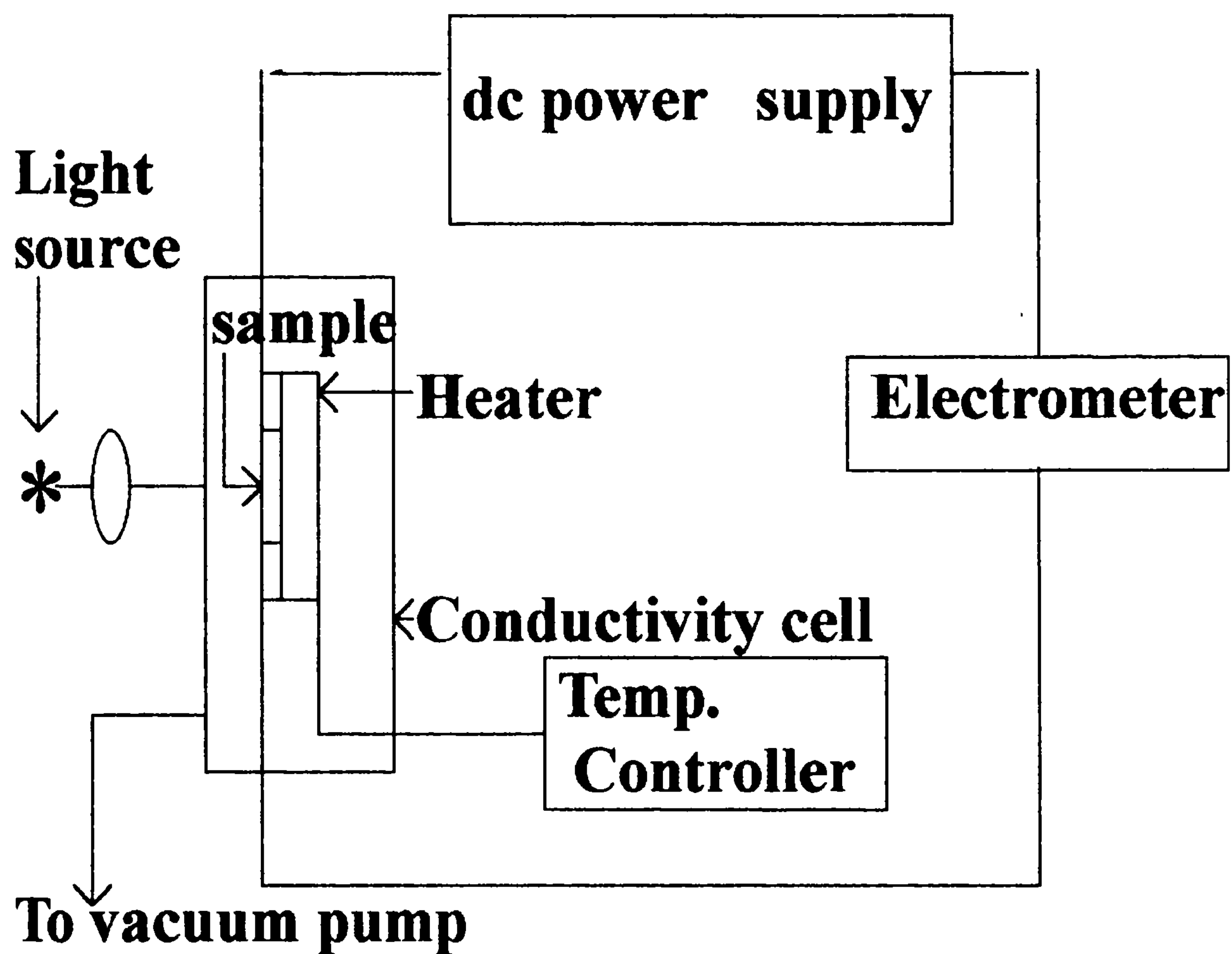

Figure 3.7. Schematic diagram of experimental set up for TSC measurement

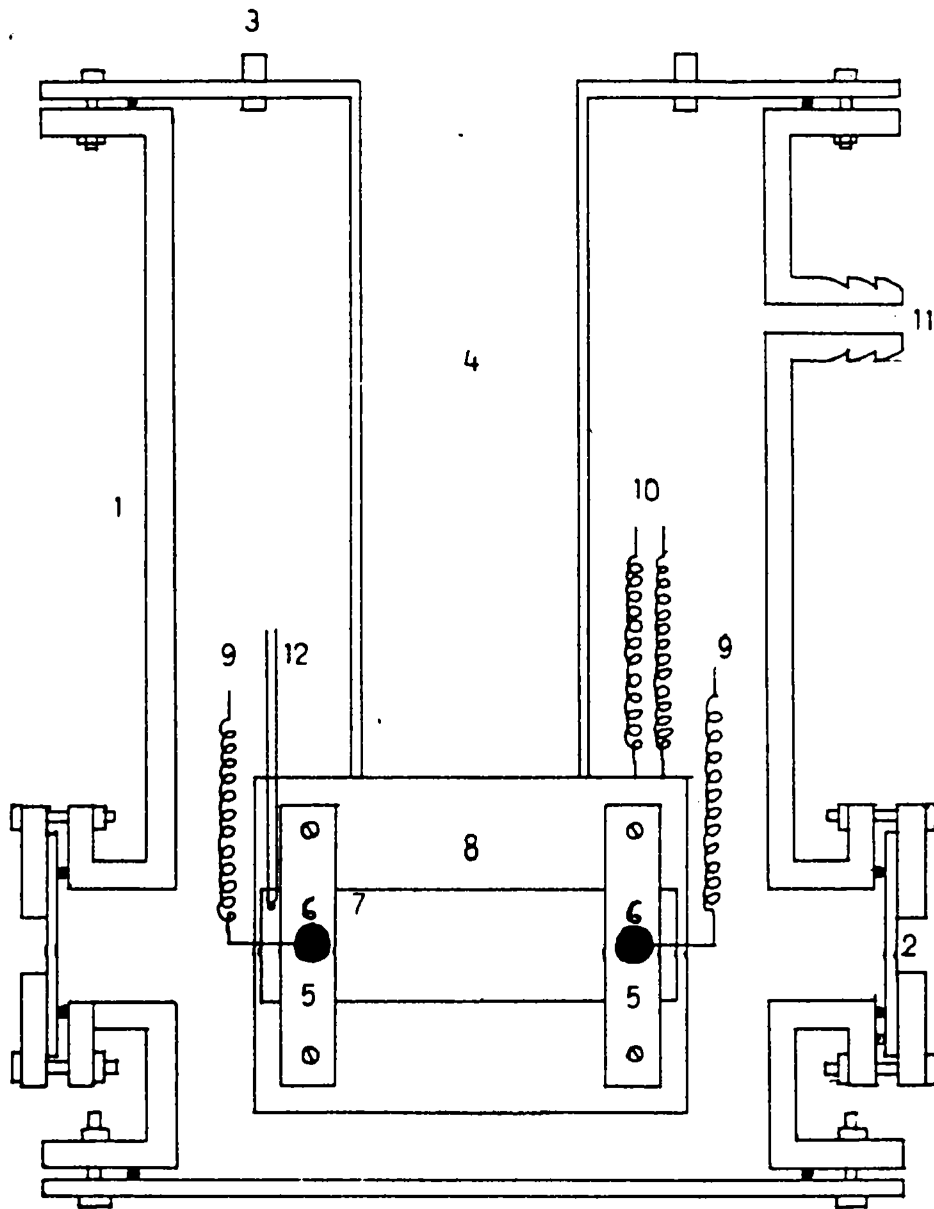

1. Metal cylinder
3. B.N.C.
5. Teflon blocks
7. Substrate with film
9. Electrode-BNC inter-connections
11. Pumping ports

2. Glass window
4. LN_2 chamber
6. Electrode
8. Heater/Substrate holder
10. Electrical connections to the heater
12. Thermocouple

Figure 3.8. Various parts of the conductivity cell

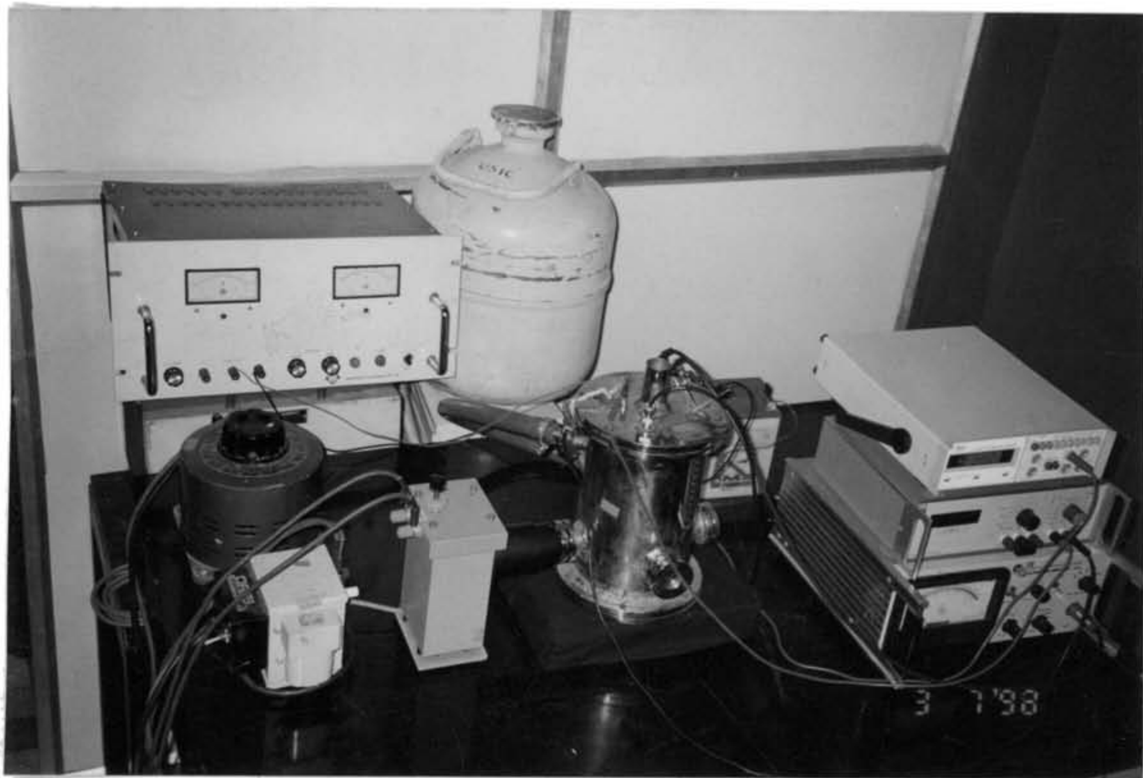

Experimental set up for TSC studies

The conduction mechanism can be determined by measuring the variation of current in a semiconductor with temperature. The conductivity of a semiconductor depends on two factors i) The number of charge carriers per unit volume ii) the mobility of the carriers through the substance under an applied electric field. As the temperature is increased from absolute zero, the electrons in the defect levels get excited to CB (or to the VB in the case of holes) and contribute to the conduction. This process will continue until the defect levels are exhausted. The increase in conductivity with temperature holds in the near intrinsic region when number of carriers increases with temperature more rapidly than the decrease in mobility [79].

The exponential variation of dark conductivity for intrinsic semiconductor with temperature is given by [80]

$$\sigma = \sigma_0 \exp [-E/2kT] \tag{3.32}$$

where σ_0 is a constant, k is Boltzmann constant, T is temperature and E is the band gap.

For extrinsic semiconductor, the variation is given by

$$\sigma = \sigma_0 \exp [-E/kT] \tag{3.33}$$

Hence the exponential increase in conductivity is related to activation energy needed for thermal motion of the charge carrier.

The equation (3.33) can be modified as

$$\log \sigma = \log \sigma_0 - E/kT$$

The plot of log σ versus 1000/T is called Arrhenius plot. From the slope of the graph the activation energy can be calculated using the equation $E = 10^3 mk$ where m is the slope of the graph and k is Boltzmann constant. When the sample contains different defect levels the Arrhenius plot will have different slopes, giving different activation energies corresponding to the various defect levels. The slope of intrinsic region of the curve gives activation energy required for an electron to go from VB to CB that gives the band gap of the materials. Thus dark conductivity measurement techniques provide an important tool for the determination of activation energy and hence this study also can yield the information regarding the defect levels.

In the present work we used the same experimental set up used for TSC measurement for the dark conductivity measurement. For dark conductivity measurement, the thickness of the sample was measured using gravimetric method. It was mounted in the conductivity cell and was then cooled to the liquid nitrogen temperature (100K). Conductivity of the sample was calculated for different temperature values (in the range 100K to 500K) by measuring the current through the sample under a dc field of 6V/cm.

References

1. A.Rose, *Concepts in photoconductivity and Allied problems* (Inter Science, New York, 1963)
2. R.H.Bube, *Photoconductivity of Solids* (Wiley, New York, 1960)
3. R.H.Bube, *Electronic properties of crystalline solids* (Academic Press, New York, London,1974)
4. C.H.Henry, V.D. Lang, *Phys. Rev.B.*, **15**(1977)989
5. R.Passler, *Phys. Status Solidi (b)* **85** (1978)203
6. W.Shockley, W.T. Read, *Jr.Phys.Rev.*, **87**(1952)835
7. J.G.Simmons, G.W. Taylor, *Phys.Rev.*, **B4**(1971)502
8. P.Braunlich, *Thermally Stimulated Relaxation in Solids* (Springer-Verlag Berlin Heidelberg, New York, 1979) p 8
9. I.Broser, R.Broser-Warminsky, *Ann.Phys.*, 6F,**16**(1955)361 *Br.J.Appl.Phys.Suppl.*, **4**(1955)90
10. P.Braunlich, *Thermally Stimulated Relaxation in Solids* (Springer-Verlag Berlin Heidelberg, New York, 1979) p15
11. J.G.Simmons, G.W. Taylor, *Phys.Rev.*, **B5**(1971)1619
12. F.Bassani, G. Pastori Parravicini, *Electronic states and Optical transitions in Solids*, Science of the Solid state, **Vol.8**, (Paragon Press, Oxford, 1975)
13. F.E.Williams, *Luminescence of Inorganic Solids*, (Academic Press, New York, 1966) pp 2
14. C.J.Ballhausen, *Introduction to Ligand Field Theory* (Mc Grew-Hill, New York, 1962)
15. A.G.Milnes, *Deep Impurities in Semiconductors*, (Wiley, New York, 1973)
16. W.D.Compton, J.H. Schulman, *Colour centers in Solids*, (Pergamon Press, New York, 1968)
17. P.D.Townsend, J.C. Kelly, *Colour centers and Imperfections in Insulator and Semiconductors* (Chatto and Windus Brigaton, London, 1973)
18. W.Shockley and W.T. Read, *Jr.Phys.Rev.*, 87(1952)835
19. A.Barrand, Ph.D Thesis, National Technical Information Service, Springfield, Virginia (1967)

20. E.F.Smith, P.T. Landsberg, *J.Phys.Chem.Solids*, **27**(1966)1727
21. R.Williams, *J.Appl.Phys.*, **37**(1966)3411
22. Y.Furukawa, Y.Ishibashi, *Jpn.J.Appl.Phys.*, **5**(1966)837
23. L.D.Yau, C.T. Sah, *Appl.Phys.Lett.*, **21**(1972)157
24. D.V.Lang, *J.Appl.Phys.*, **45**(1974)3014,3023
25. H.Leferre, M.Schulz, IEEE Trans., ED-7,973(1977)
26. C.T.Sah, L. Forbes, L.L. Rosier, A.F. Tasch, *Jr.Solid-State Electron*, **13**(1970)759
27. C.T.Sah, J.W. Walker, *Appl.Phys.Lett.*, **22**(1973)384
28. H.A.Mar, J.G. simmons, Phys.Rev.B. 8(1973)3865. *Appl.Phys.Lett.*, **25**(1974)503
29. B.T.kolomiets, V.M. Lyubin, *Phys.Status Solidi (a)*, **17**(1973)11
30. H.Nassenstein: *Z. Naturforsch*, **10 a** (1955)944
31. V.Bichevin, H. Kaambre, *Phys.Status Solidi (a)* 4, K 235(1971)
32. P.Braunlich, *Thermally Stimulated Relaxation in Solids* (Springer-Verlag Berlin Heidelberg, New York, 1979) p 25
33. F.Urbach Wien Berichte (II,A) **139 C**(1930)363
34. H.J.Kos, S. Mieke, *Phys. Status Solidi (a)*, **50**(1978) K165
35. P.Iacconi, D.Lapraz, R.Caruba, *Phys.Status.Solidi (a)*, **50**(1978)275
36. S.Vaidya, P.S. Diwan, J.D. Ranade, *Ind.J.Pure and Appl.Phys.*, **16**(1978)486
37. A.Doil, *Jpn.J.Appl.Phys.*, **17**(1978)279
38. C.Bucci and R. Fieschi, *Phys.Rev.Lett.*, **12**(1964)16
39. N.Beltrami, R.Capelletti and R. Fieschi, *Phys.Lett.*, **10**(1964)279
40. G.P.Jr. Williams and D.Mullis, *Phys.Stat.Sol. (a)*, **28**(1975)539
41. A.M.Hor and P.W.M. Jacob, *J.Electrochem.Soc.*, **125**(1978)430
42. J.Wagner and S. Mascarenhas, *Phys.Rev.B.*, **6**(1972)4867
43. T.Tanaka, S. Hiralayashi and K. Shilayama, *J.Appl.Phys.*, **49**(1978)784
44. U.Syamaprasad, Ph.D Thesis, Cochin University of Science and Technology, 1981
45. R.H.Bube, *Phys.Rev.*, **83**(1951)393, **99**(1955)1105, **101**(1956)1668, **106**(1957)703
46. R.H.Bube, *J.Chem.Phys.*, **23**(1955)18
47. C.J.Delbecq, P.Pringsheim, P.H. Yaser., *Z.Phys*, **138**(1954)266
48. I.Broser, R. Broser-Warminsky, *Brit.J.App.Phys.Suppl.*, **4**(1955)90

49. F.Pliquett, M.K. Solneev, *Experimentellen and Theoretischen Biophysik*, **Vol 22** (Georg Thieme, Leipzig, 1978)
50. R.Chen, *J.Mat.Science.*, **11**(1976)1521
51. P.Kivits, H.J.L. Hagebeuk, *J.Luminescence*, (1971)1
52. I.J.Saunders, *J.Phys.C.*, **2**(1969)2181
53. P.Kelly, P. Braunlich, *Phys Rev.B.* **1**(1970)1587
54. P.Kelly, M. Laubitz, P.Braunlich, *Phys Rev.B.*, **4**(1971)1960
55. P.Braunlich, *Z.Phys*, **177**(1964)320
56. P.Kivits, *J. Luminescence*, **16**(1978)119
57. P.Braunlich, *Ann.Phys.* (Leipzig) 7F, **12**(1963)262
58. B.I.Stepanov, V.P. Gribkovskii, *Theory of Luminescence* (Iliffe Books, London, 1968)
59. P.Braunlich, P. Kelly, *Phys.Rev.B.*, **1**(1970)1596
60. P.Braunlich, *Ann.Phys.Chem.Sol.*, **12**(1960)265
61. P.Braunlich, *J.Appl.Phys.*, **38**(1967)2516
62. P.Braunlich, *J.Appl.Phys.*, **39**(1968)2953
63. V.P.Zayachkivskii, P.P. Bleisyuk, A.V. Savitskii, *Fiz Tekh Poluprovadu*, **12**(1978)970
64. F.E.Williams, *J.Phys.Chem.Sol.*, **12**(1960)265
65. A.G.Milnes, *Deep Impurities in Semiconductors*, (Wiley New York, 1973) p 226
66. T.Datta, R. Noufi and S.K. Deb, *J.Appl.Phys.*, **59**(5)(1986)1548
67. A.G.Valyomana, Ph.D Thesis, Cochin Uty. of Sci. and Technol.,1992
68. N.F.Mott and R.W. Gurney, *Electronic Processes in Ionic crystals*, 2nd ed (Oxford University, New York, 1940) p 108
69. H.Gobrecht, D. Hoffmann, *J.Phys.Chem.Sol.*, **27**(1966)509
70. G.Bonfiglioli, *Thermoluminescence in Geological materials* (Academic Press, New York, 1968)
71. G.C.Smith, *Phys.*, **148**(1966)816
72. D.Grogan, J.P. Ashmore, G.Bradley, J.G. Scott, Proc.5th Intern.Symp. on Exoelectron emission & Dosimetry, Germany, 1976
73. A.Taylor, *Phys.Status Solidi*, **37**(1970)401
74. E.B.Podgorasak, P.R. Moran. *Phys.Rev.B.*, **8**(1973)3405

75. P.R.Moran. D.E. Fields, *J.Appl.Phys.*, **45**(1974)3266

76. L.Langouet, C.R.A.S. **B 268**(1969)418

77. C.Lehmann, *Interaction of Radiation with Solids and Elementary Defect Production* (Northhold, Amsterdam, 1977)

78. C.Popescu, H.K. Henisch, *Phys.Rev.B.* **11**(1975)1563

79. H.K.Henisch, C. Popescu, *Nature* **257**(1975)363

80. R.A.Smith, *Semiconductors*, (Academic Publishers, Calcutta, 1989) p 121

Chapter 4

TSC measurements of CdS thin films

4.1. Introduction

II-VI compound semiconductors have played an important role in the early research on photovoltaic effects because of their direct band gap from near UV to far infrared. For direct band gap semiconductors, the band to band absorption rises steeply, normally being greater than 10^4 cm^{-1} for photon energies above the band gap energy. This results in an absorption length of ~1µm. Extensive work had been done in the area of solar cells fabricated using these semiconductors along with Copper Indium Selenide, Indium Phosphide and other semiconductors.

Cadmium Sulphide (CdS) is one of the most prominent members of this class of semiconductors with a direct band gap of 2.4 eV. As-prepared CdS is normally n-type with a typical carrier concentration in the range of 10^{16}-10^{18} cm^{-3} [1,2] and has a mobility of 300cm^2/V/sec [3]. It is frequently used as a window layer in a variety of thin film solar cells and variety of techniques had been employed for its preparation. Most of these works have been reviewed in the following section and effort is also made to have a review work on the properties of CdS films, that are important in the relevant field of application.

4.2. An overview of works on preparation and properties of CdS

Works on CdS crystal had been reported as early as 1954. Reynolds et al first observed the photovoltaic effect in CdS crystals with various metal electrodes [4]. Later R.H. Bube reported [5] the measurements of photoconductivity and crystal imperfections in CdS crystals. All conducting crystals showed only a very slight dependence of photoconductivity on temperature with a maximum near 100°C and all insulating crystals showed a much greater variation of photoconductivity with temperature. Bube again reported [6] the speed of response of photoconductivity for high intensity excitation in CdS.

The minimum response time observed for the samples tested was 250 μsec (rise time) and 300 μsec (decay time).

Later photochemical effects in CdS crystals were reported by Woods et al [7]. Here Cd rich crystals showed a trap level at 0.25 eV and sulphur rich crystals showed three trap levels at 0.41, 0.83 and 0.63 eV below the CB. Trap levels in Cd-rich crystals disappeared when irradiated with white light at room temperature whereas levels in sulphur rich crystals disappeared after heat treatment at 100°C. These effects were found to be reversible and a tentative explanation for this was given in terms of associated defects. Photo induced chemisorption on insulating CdS crystals was also reported during the same period [8]. David C Look reported [9] high temperature annealing in electron irradiated CdS crystals. The study of annealing kinetics revealed an activation energy of about 1.3 eV and this was attributed to sulphur vacancy motion. Tell et al reported [10] the Raman effect in CdS crystals and they determined the frequency and symmetry character of the fundamentals. X-ray photoelectron spectra of CdS crystal were reported by Marychurch et al [11] and from temperature dependence studies of the Cd:S ratio they observed that heating in ultra high vacuum leaves the surface sulphur rich.

Origin of photovoltaic effect in vapour deposited CdS layer was reported in 1962 by Grimmeiss et al *[12]. Later another group reported [3] the crystallinity and electronic* properties of evapourated CdS films. According to this work, the electron mobility was having strong dependence on the reorientation of the crystallites, but is only slightly affected by their size. The reported value of mobility for photogenerated carrier was 300 $cm^2/V/sec$. Determination of optical constants (n and k) of evapourated CdS films was reported by Khawaja et al [13]. In 1976, Simov et al developed [14] the method of surface photovoltage spectroscopy to study the surface properties of evapourated CdS films. The spectrum obtained in their work indicated the presence of donor-like surface states in CdS films. The photoangular effect for polycrystalline CdS films obtained by vacuum evapouration was investigated by Porada et al [15]. The dependence of photoelectric voltage on the angle of incidence and wavelength of light was also reported in this work. Low resistive and high mobility thin films of CdS were grown using vacuum evapouration by Dawar et al [16].

X-ray diffraction studies showed that these films are well oriented with a preferential growth of crystallites in the (002) plane and observed conductivity was in the range of 0.088 Ω^{-1} cm^{-1} - 1.34 Ω^{-1} cm^{-1}. Later the same group reported [17] the effect of laser irradiation on structural and electrical properties of CdS thin films deposited by resistive heating technique. XRD studies showed that the crystallinity of these films was improved on irradiation with a pulsed laser and it was also reported that Hall coefficient and mobility were increased with increase of energy density as well as the number of laser pulses.

Effect of low temperature annealing (100-250°C) on the thickness of the evapourated CdS films was investigated using absorption spectrophotometry [18]. It was observed that optical absorption in the CdS film deposited on mica substrate decreases with increase in the annealing temperature. A decrease in film thickness of about 5 % was also reported with increasing annealing temperature. In 1993, Shi Yul Kim et al published a paper [19] on structural, electrical and optical properties of In doped CdS films prepared using vacuum evapouration. The crystalline orientation of these films changed from the (002) plane to the (110) plane as the In concentration increased. Also the grain size became smaller and the facets on the grains diminished. The resistivity of CdS films decreased with increase in In concentration and then increased with further increase in In concentration due to the variation of the carrier concentration and Hall mobility. The lowest resistivity value was 5×10^{-3} Ω cm at an In concentration of 3×10^{20} cm^{-3}. The optical band gap increased from 2.42 eV for undoped films to 2.6 eV for the CdS films with an In concentration of 3×10^{20} cm^{-3}. The optimum In concentration for the window layer of $CdS/CuInSe_2$ solar cells was obtained as $3 \times 10^{20} cm^{-3}$. A morphological and structural study of evapourated film was presented by Ashour et al [20]. They found that films exhibit wurtzite structure and films with maximum grain size with minimum residual strains were obtained at deposition temperature 150°C.

In 1975, Shay et al [21] reported the production of CdS thin films using MBE technique. Following this, electrolyte deposition technique was developed [22] to prepare CdS thin films. Later CdS thin films doped with In had been grown by ionized deposition on glass and their properties were reported [23]. Resistivity of CdS:In films depends on

substrate temperature; a minimum resistivity of $6.4 \times 10^{-3}\ \Omega$ cm was obtained at a substrate temperature of 200°C. Transmittance of the films increases from less than 5% to 60% by ionization at a substrate temperature of 60°C. Crystallographic characterisation of these films had also been investigated in this work. Air-annealed pellets of photoconducting CdS were also reported in the same period by Amalnerkar et al [24]. They made chemical identification of the surface impurity phases on these photoconducting CdS pellets. CdS thin films prepared using Sputtering [25-27], CVD [28], CSVT [29,30], Screen printing [31,32], Anodization [33] and Electrophoresis [34] were also reported.

R.R.Chemberlin and J.R. Sakarmann developed spray pyrolysis technique for the first time to prepare CdS thin films [35]. Preparation of CdS thin films using this technique and their properties were later reported by Yale Y Ma et al [36]. Another group published a paper [37] on electrical and photoconducting properties of spray pyrolysed CdS films. Values of activation energy calculated for the plots of dark resistivity as a function of temperature were 0.03 eV and 0.65-0.95 eV for various samples. These values were attributed to donor chloride ions and to complexes of associated Cd and sulphur vacancies in nearest neighbour sites respectively. The mechanism of photoconductivity in polycrystalline spray pyrolysed CdS thin films had been studied using Hall effect as well as dark and photo conductivity measurements [38]. A structural approach to the analysis of electronic properties of sprayed CdS films was reported by H.L.Kwok [39]. He examined the effects of different film structures on electronic and photovoltaic properties using physical lumped models. The influence of annealing temperature on photoconductivity of spray pyrolysed films was reported [40] in 1993. The important observation in that work was that annealing of these films at 373 K resulted in maximum photoconductivity. Again photoconductivity at all wavelengths was found to decrease with increase of annealing temperature and became a minimum at 473 K. Optical constants of spray pyrolysed CdS films were calculated using variable angle spectroscopic ellipsometry by Sunny Mathew et al [41]. This work showed that the real part (n) and imaginary part (k) of the complex refractive index of spray pyrolysed CdS films differ from those of vacuum coated films and this was explained by assuming spray coated film to be having two layer structure. The surface layer has optical properties different from those of bottom film due to the surface

irregularities. Later the same group reported [42] optical and surface properties of these films. In that paper variation in the real and imaginary parts of the refractive index with substrate temperature was studied and found that these values increase with increase in substrate temperature.

Preparation of CdS films using Chemical Bath Deposition process was described by Pavaskar et al in 1977 [43]. The improvements on the electrical resistivity of CBD CdS films were reported later [44]. It was reported that the dark resistivity of these samples decreased by two orders as they were annealed using cw Ar+ laser. Under laser irradiation, evapouration of Cd ions on the surface of the sample takes place and a Cd annealing atmosphere was created. This Cd atmosphere annealing process could be responsible for the formation of S^{2-} vacancies by the Schottky mechanism and this phenomenon is responsible for the decrease in electrical resistivity. The phenomenon of oxygen chemisorption in highly photosensitive thick films of CdS was studied [45] indirectly by measuring the dark current as a function of (i) the temperature during the oxygen adsorption-desorption cycles and (ii) time of exposure to air. They observed an extrinsic surface state induced by strongly chemisorbed oxygen at 0.9 eV below the bottom of the CB. Effects of annealing the CBD CdS in air were investigated using XPS and XRD techniques and these films were found to be having cubic structure [46]. Air annealing at 300°C for 30 minutes results in a CdO film predominantly consisting of CdO and $CdSO_4$ -like species.

In 1987, the photocurrent response in chemically deposited CdS thin films and a critical discussion of the very high photoconductivity in those films had been presented by P.K.Nair et al [47]. They reported high photosensitivity ($\sigma_p/\sigma_d > 10^9$), photoconductivity (~ 10 Ω^{-1} cm^{-1}) CBD films with a very long photoconductivity decay time (13 hours per decade). Later the same group reported [48] the solar assisted chemical deposition of highly photosensitive CdS thin films with optical transmission in the 70-80% range for wavelength above the band gap absorption. Optoelectronic characterisation of CBD CdS film was also reported by them [49]. The photocurrent decay time of these films was depending on the

bath temperature and the duration of storage. It ranged from a few seconds to 10^4 seconds per decade.

Hiroshi UDA et al published a paper [50] on the structural and electrical properties of CdS films prepared using CBD technique. The dark conductivity ($>10^4\ \Omega^{-1}\ cm^{-1}$ in the case of as-deposited films) was decreased by about three orders of magnitude (to about 10 $\Omega^{-1}\ cm^{-1}$) upon annealing in N_2 atmosphere at 300-500°C for 20 minutes and this was caused by an increase in electron concentration. Effect of post deposition treatments on morphology, structure and opto-electronic properties of CBD CdS films was reported [51]. The band gap shift in these films was studied using photoacoustic spectroscopy [52]. This experiment gave a clear picture of the band gap shift due to annealing at different temperatures. The shift increased upto a critical annealing temperature at which a structural transformation occurs from cubic to hexagonal. O de Melo et al [53] reported that CdS films prepared using CBD technique can be converted into low resistive one by annealing in S_2 and H_2+In atmosphere and they obtained low resistivity of 11Ω cm at an optimum annealing temperature of 350°C.

Thermal annealing studies of CBD CdS thin films were reported by Hernandez et al in 1994 [54]. They studied the optical and electrical properties of the film before and after annealing at different temperatures and found that the absorption edge shifts towards the higher wavelengths in CdS films. This was attributed to the structural transformation from cubic to hexagonal phase. Jayakrishnan et al had reported [55] the study of structural changes and physical properties of CdS thin films after multiple dip coating and thermal annealing using XRD, SEM, and electrical characterisation. Rapid thermal annealing at 5×10^{-2} Torr resulted in the reduction in resistivity of films from $10^6\ \Omega$ cm to 0.16 Ω cm, whereas slow annealing for 30 minutes at the same vacuum resulted in a resistivity of $10^5\ \Omega$ cm. The observed reduction in resistivity was attributed to the oxygen desorption. Kolhe et al. investigated [56] air annealing of dip coated CdS films using XPS.

Tomas et al studied [57] the influence of thermal annealing in different atmosphere on the band gap shift and resistivity of CBD CdS films. Annealing in hydrogen atmosphere

reduced the resistivity of the films from 10^7 Ω cm in the as-deposited state to 0.15Ω cm by passivating the chemisorbed oxygen at the grain boundaries. In 1995, Yu et al characterised [58] the CBD CdS films and they confirmed the presence of quantum size effects based on the blue shift in the optical band gap of the film. The films were found to be hexagonal with a preferred orientation. Kale et al [59] have carried out extensive characterisation of chemically deposited CdS films. Depending upon conditions of the deposition, CBD CdS films showed a blue shift as high as 0.35 eV in the optical band gap. It was found that as the deposition temperature decreases from 358 K to 273 K, the band gap increases for 2.4 to 2.7 eV.

Recently in 1997, the bath parameters for the preparation of CBD CdS thin films of good adhesion and uniformity were standardised by K.L.Narayanan et al [60]. The reduction in resistivity of these samples during air annealing was attributed to the conversion of substantial fraction of the film into CdO phase. Structural transformation caused by heat treatment of dip coated CdS films was also reported by them [61]. However, these authors could not observe a reduction in resistivity of this type of CdS films from "rapid thermal annealing" as reported by Jayakrishnan et al [55].

Ion implantation studies in CdS is an important field of research from much earlier time. In 1968, the effect of implantation of phosphorous ions in CdS crystals was reported [62]. Lattice disorder produced by ion implantation of CdS crystals with Bi+, Kr+, Ar+ and Ne+ had been studied using RBS/channeling and TEM techniques [63]. Ratna Sagar et al studied [64] the amorphisation of CdS thin films due to argon ion irradiation in dense plasma focus. The structural characterisation of CdS single crystal platelets after Bi ion implantation with the help of TEM was reported [65]. According to this work, the ion implanted CdS did not exhibit gross degradation of the Wurtzite structure to amorphous zones. Tell et al [66] implanted Bi and Cu ions into CdS and studied various properties including optical absorption photoluminescence and photovoltage. Annealing behaviour of the insulating layer in ion implanted CdS was investigated by Masafumi Yakaguchi [67] where it was observed that ion implanted CdS diodes show increase in resistivity and became photosensitive after annealing above 673 K. Chester reported[68] conductivity

changes in CdS after irradiation with Co and Cs gamma rays at room temperature. Kitagawa et al studied [69] defect recovery in CdS crystals irradiated with 10 MeV electron at 77K and observed at least three stages of recovery between 80 and 410 K. Effects of low temperature annealing on the defects created by 200 keV electrons in CdS was also reported [70]. Recently Raman scattering and optical absorption studies of Ar+ implanted CdS thin films have been reported by K.L.Narayanan et al [71]. Post implantation annealing of CBD CdS films showed a more stable hexagonal phase, while the as-prepared sample showed the presence of both cubic and hexagonal phases. Effect of irradiation induced disorder on the optical absorption spectra of CdS thin films were also reported [72] by the same group. They also used positron annihilation technique to analyse the effect of ion implantation in CdS [73].

It was generally believed that the formation of p-type CdS is very difficult because of self-compensated effects due to sulphur vacancies [74]. A few authors had reported [75,76] attempts to form p-type CdS crystals by compensation of donors with copper acceptors. Preparation of p-type CdS films had been reported [77] for the first time by Grimmeiss et al in 1962. They employed vapour deposition of Cu compounds on predeposited CdS films followed by adequate annealing for the diffusion of Cu into the CdS films. Later p-type CdS crystalline films sputtered in presence of phosphine were reported by Lichtensteiger et al [78]. Various researchers [79,80,81] have tried to dope impurities by ion implantation technique to form p-type CdS. Keitoku et al [82] reported the conversion to p-type CdS films prepared by laser ablation method. They doped Cu atoms into CdS thin films and found that type conversion is possible at doping level of 5 atomic percent copper content.

In 1992 conversion of evapourated n-type CdS into p-type was reported by Kashiwaba et al [83]. In that work CdS wAs-deposited on a Cu films at about 475 K facilitating the diffusion of copper. The resistivity of the films increased with increase in Cu doping but decreased for values of Cu/Cd atomic ratio over 0.5%. It was proposed that the Cu compensate the donor due to sulphur vacancies and the conductivity type was converted to p-type. I-V characteristics of p-CdS/n-CdS film structure showed rectification.

4.3. Importance of TSC measurements in CdS films

CdS is used as a window material in conjunction with highly absorbing materials like CdTe [90,91] Cu_2S [92], InP [93] and $CuInSe_2$ [94]. Loferski suggested that [95] CdS is an effective window material for use in tandem solar cells whose theoretical efficiency can be very large. Moreover, it is reported that [96] one of the reasons for low efficiency of $CuInSe_2$/CdS thin film solar cells prepared using CBD is due to the high series resistance of the device that mostly arises from the high resistance of the window CdS layer. Resistance of the CdS layer depends mainly on defect levels present/stoichiometry in the material. TSC measurement is an effective tool for studying the defect levels in semiconducting samples.

Several workers have reported TSC data on CdS like single crystals [97-99] and only a few data are available on the TSC measurements of CdS films in the literature. High temperature TSC in sprayed CdS films were reported by Chandra Sekhar et al [89]. The effect of oxygen desorption process in CBD CdS thin films was studied using TSC technique by Vigil et al [100].

As mentioned earlier, several techniques had been employed for the preparation of CdS thin films. Among these, spray pyrolysis and CBD techniques are widely used for the low cost production of large area solar cells and these two techniques are used for sample preparation in the present work also. In the following section, we present the results of TSC studies on spray pyrolysed as well as CBD CdS thin films, both in As-deposited and in annealed conditions.

4.4. TSC measurements of spray pyrolysed CdS films

As stated earlier (in section 4.2), normally the as-prepared CdS films were n-type and the conductivity is determined by the quantity of excess Cd^{++} or vacancy of S^{--} present in the film. But recently there is an interest in preparing p-type CdS and section 4.2 gives a

brief review of work in this direction also. This section of the thesis describes the results of TSC studies on such samples prepared in our lab. Through this study we could get a clear picture of the energy levels available in p-type CdS.

4.4.1. Experimental details

The conversion of n-type CdS into p-type is achieved through thermal diffusion of copper and the details of this technique are reported elsewhere [87,88]. For TSC measurements, vacuum evapourated thick indium contacts were given to the sample at a distance of 1 cm. The two contacts were on the top surface of thin film sample. After giving the contacts, the sample was mounted in metallic vacuum cell in the experimental set up for TSC measurement and the details of the experimental set up are given in chapter 3. The sample was first frozen to 100 K which is low enough to make the probability of thermal release of carriers negligible and was then exposed to an optical excitation for a fixed time. Time of excitation was selected after number of trial experiments as 5 and 10 minutes. After the excitation, sample was heated (at the rate of 0.05K/sec) from 100 K to 500 K, and the current was measured under the dc field of 6V/cm using an electrometer.

4.4.2. Results and Discussion

Figure 4.1 shows the TSC spectra of as-prepared n-type CdS film. Under 5 minutes light excitation, the spectra depicted only one peak (460 K) whose activation energy was calculated (using equation 3.29) to be 1.2 eV (Table 1). TSC spectra of same type of sample gave one more peak of activation energy 0.4 eV (340 K) under the light excitation of 10 minutes. It was reported earlier that 1.2 eV level is due to mobility of sulphur vacancies [9,101]. The value of activation energy 0.4 eV obtained under 10 minutes light excitation corresponds to the activation energy of charge carriers released from the complex of cadmium and sulphur vacancies localized in nearest neighbouring sites. These traps are expected to be present in CdS crystals also [7]. Values of capture cross section of these defect levels were calculated using the equation (3.30) and are given in table 1. From the table it is clear that 0.4 eV level has got smaller capture cross section ($10^{23}cm^2$) than that of 1.2 eV trap level ($10^{-16}cm^2$). Due to the very low cross section it is very diificult to fill the

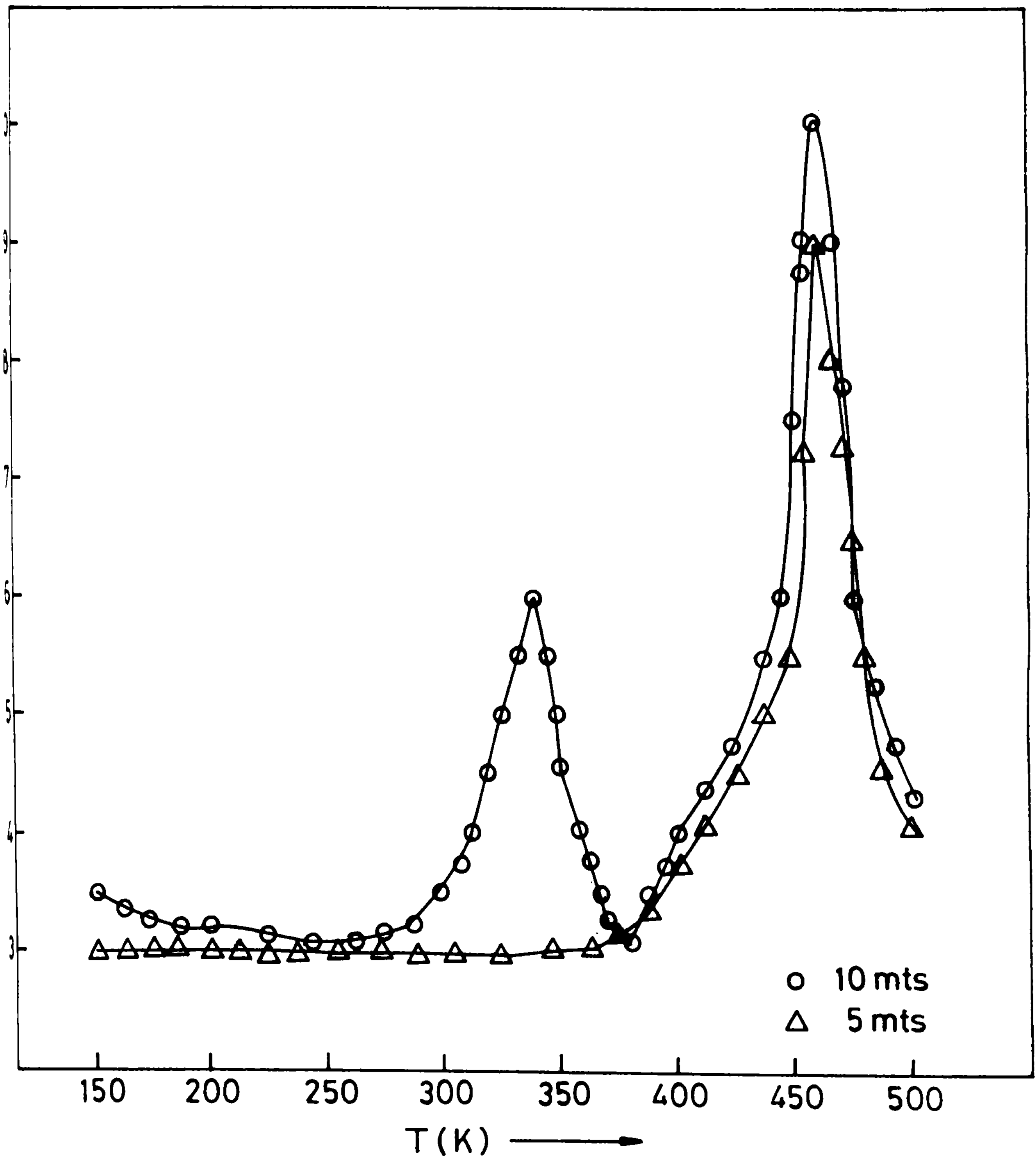

Figure 4.1. TSC spectra of as-prepared n-type CdS thin film under different excitation time

Table 1. The values of activation energies and capture cross sections of n & p-type CdS samples obtained from TSC measurements.

Sample type	Activation energy (eV) for different light excitation time		Capture Cross section (cm^2) for different light excitation time	
	5 min.	10 min.	5 min.	10 min.
n-type CdS	1) 1.21±0.01	1) 1.21±0.01 2) 0.40±0.01	1) 5.2×10^{-16}	1) 5.2×10^{-16} 2) 1.04×10^{-23}
p-type CdS	1) 1.21±0.01 2) 0.73	1) 1.22 2) 0.74	1) 5.2×10^{-16} 2) 6.9×10^{-16}	1) 7.1×10^{-16} 2) 1.9×10^{-16}

level with a carrier and this may be the possible reason that the 0.4 eV trap level is not detectable under the light excitation time of 5 minutes.

TSC spectra of n-CdS annealed in air (100-300°C for 1 hour) are shown in figure 4.2-4.4 and calculated value of activation energies and capture cross sections are given in table 2. Here also under 5 minutes light excitation we could detect a trap level of activation energy 1.2 eV (450 K) corresponding to sulphur vacancy motion in all samples irrespective of annealing temperatures. Under 10 minutes excitation, these air annealed samples revealed one more peak of activation energy ~0.9 eV (335 K) and of smaller cross section ($10^{-23}cm^2$). This smaller value of cross section is responsible for longer exposure time for the detection of this peak. It was reported earlier that 0.9 eV is due to chemisorbed oxygen [102] and this effect was also reported by Mark in CdS crystals [8]. In these samples, since there is no trap level of complexes of Cd and S vacancies, we strongly believe that this level corresponding to 0.9 eV in our sample may be due to the chemisorption of oxygen at these vacancy states. This happened as a result of annealing in air.

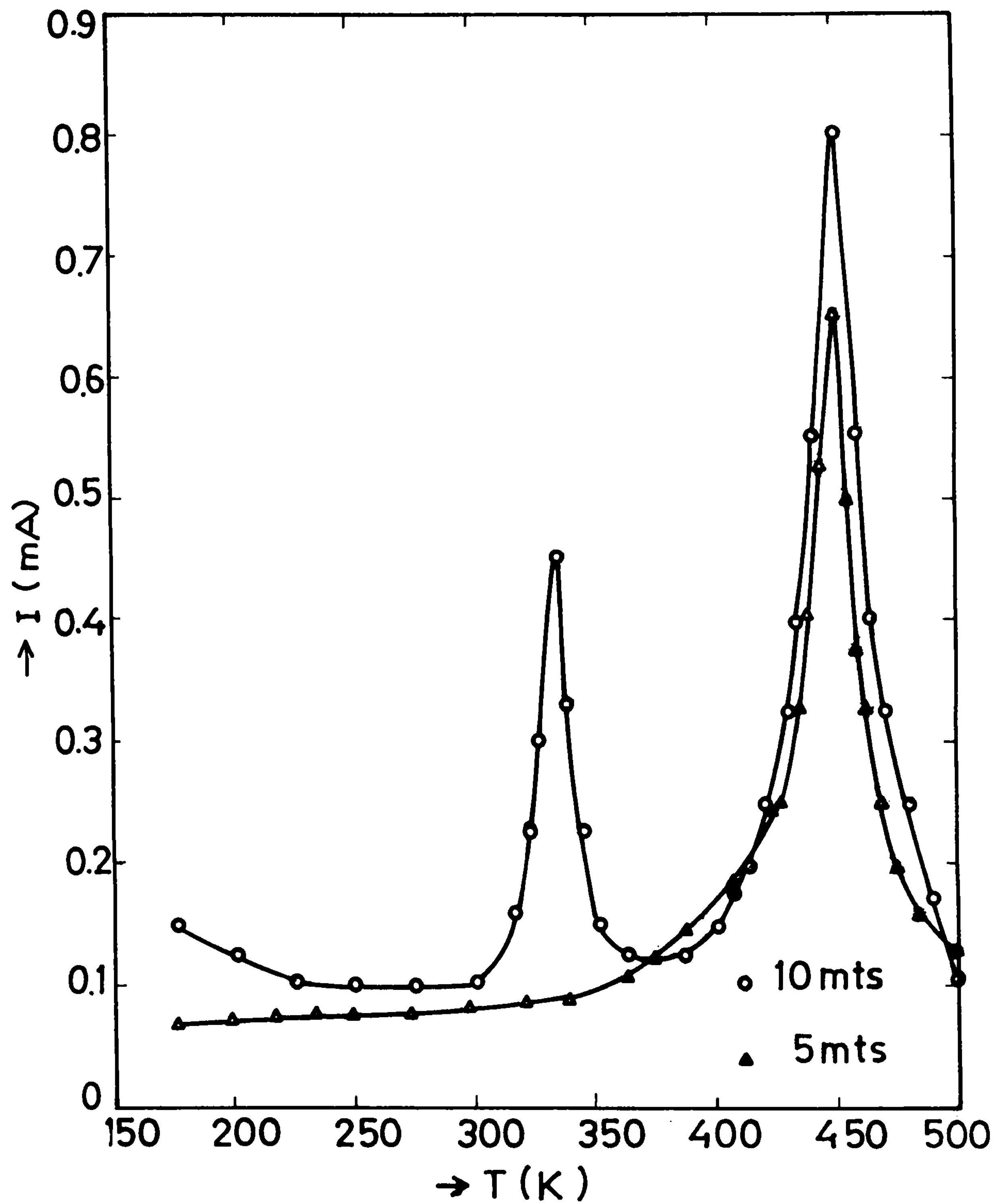

Figure. 4.2. TSC spectra of n-type CdS thin film annealed in air (at 100°C for 1 hour) under different excitation time

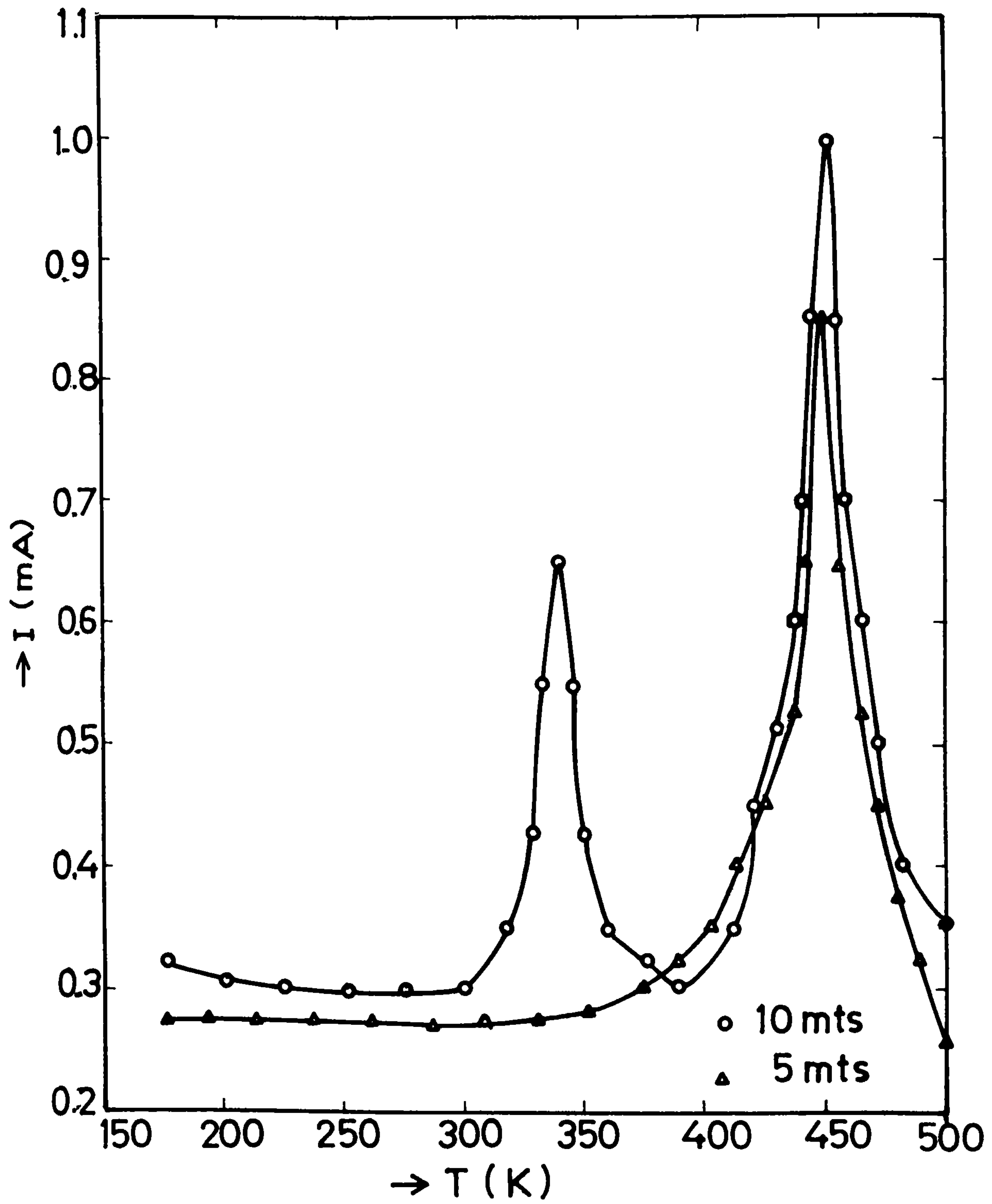

Figure 4.3. TSC spectra of n-type CdS thin film annealed in air (at 200°C for 1 hour) under different excitation time

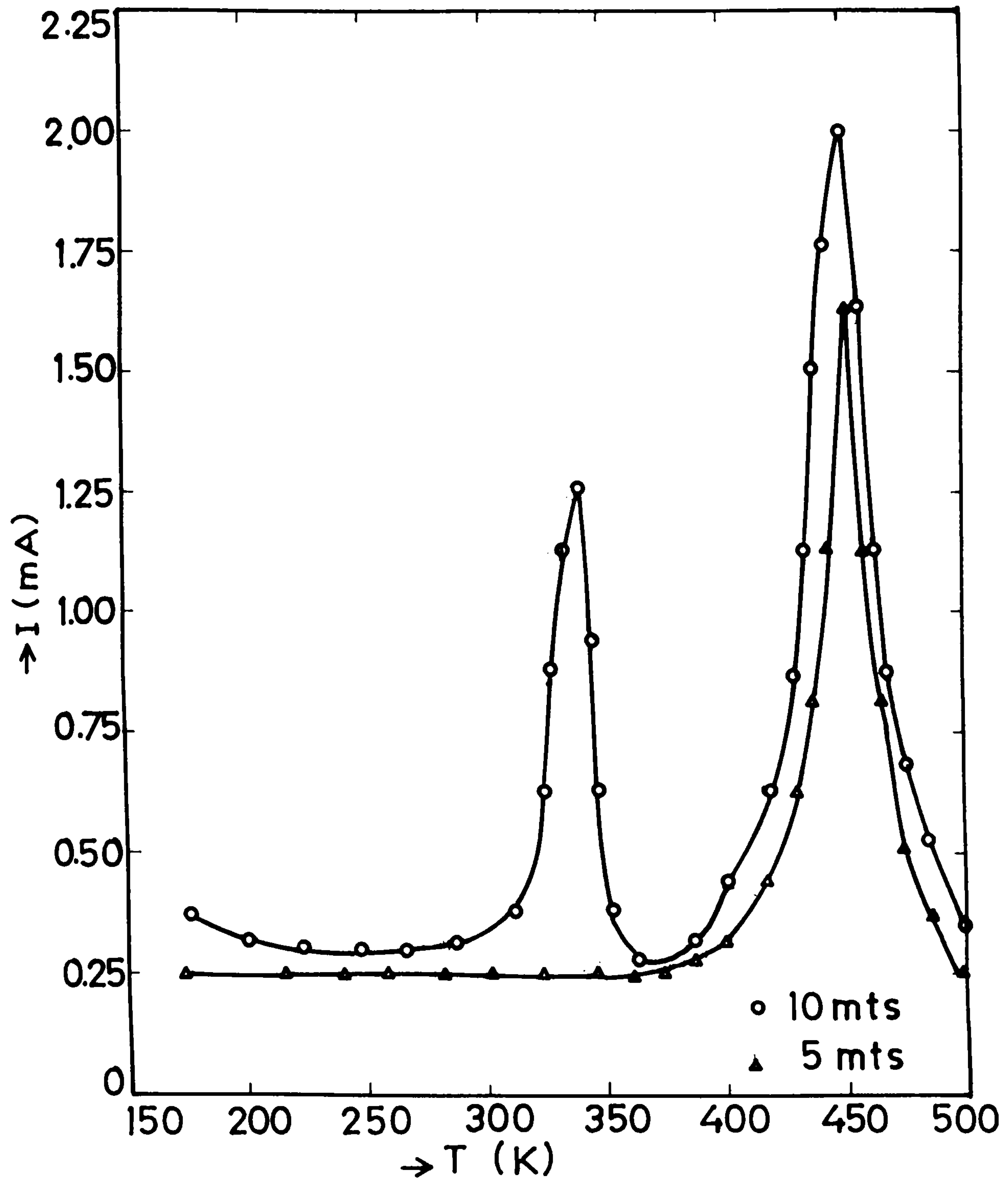

Figure 4.4. TSC spectra of n-type CdS thin film annealed in air (at 300°C for 1 hour) under different excitation time.

Table 2. The values of activation energies and capture cross sections of air annealed n-type CdS films obtained from TSC measurements.

n-type CdS films air annealed at different temperature	Activation energy (eV) for different light excitation time		Capture cross section (cm^2) for different light excitation time	
	5 min.	10 min.	5 min.	10 min.
100°C	1) 1.27	1) 1.27 2) 0.90	1) 78×10^{-16}	1) 78×10^{-16} 2) 2.64×10^{-18}
200°C	1) 1.27	1) 1.27 2) 0.91	1) 78×10^{-16}	1) 78×10^{-16} 2)7.48×10^{-18}
300°C	1) 1.27	1) 1.27 2) 0.92	1) 78×10^{-16}	1) 78×10^{-16} 2) 21.1×10^{-18}

TSC spectra of vacuum annealed n-CdS at 100-300°C for 1 hour are shown in figures 4.5-4.7 and calculated values of activation energy and capture cross sections are shown in table 3. Under 5 minutes light excitation, irrespective of annealing temperature, these samples show only one peak of activation energy 1.2 eV that again indicate mobility of S vacancy. Under 10 minutes light excitation, all these samples give one more peak of small cross section and corresponding activation energy was calculated to be 0.4 eV. This shows the presence of complexes of sulphur and cadmium vacancies in the neighbouring sites. Thus TSC measurements indicate that on vacuum annealing in the range of 100-300°C, nothing has happened to the defect levels in as-prepared n-CdS.

TSC spectra of p-type CdS is shown in figure 4.8. Interestingly, two peaks (460 K & 290 K) are observed in this case irrespective of the duration of light excitation. The activation energies and capture cross sections of these peaks were calculated and are shown in table 1. It is to be noted that the defect levels corresponding to these two peaks are having same order of capture cross section and are observed even under an excitation time

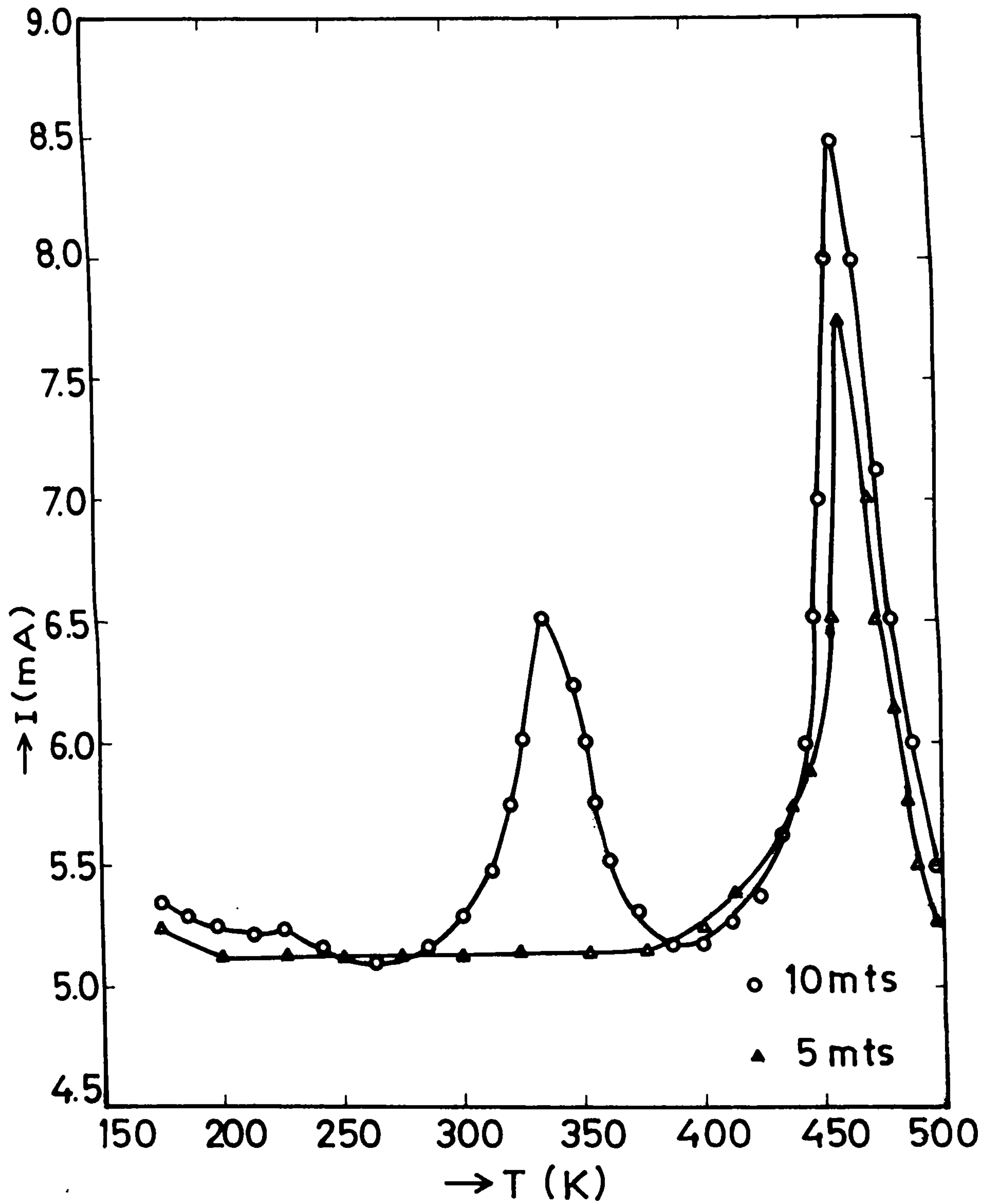

Figure 4.5. TSC spectra of n-type CdS thin film annealed in vacuum (at 100°C for 1 hour) under different excitation time.

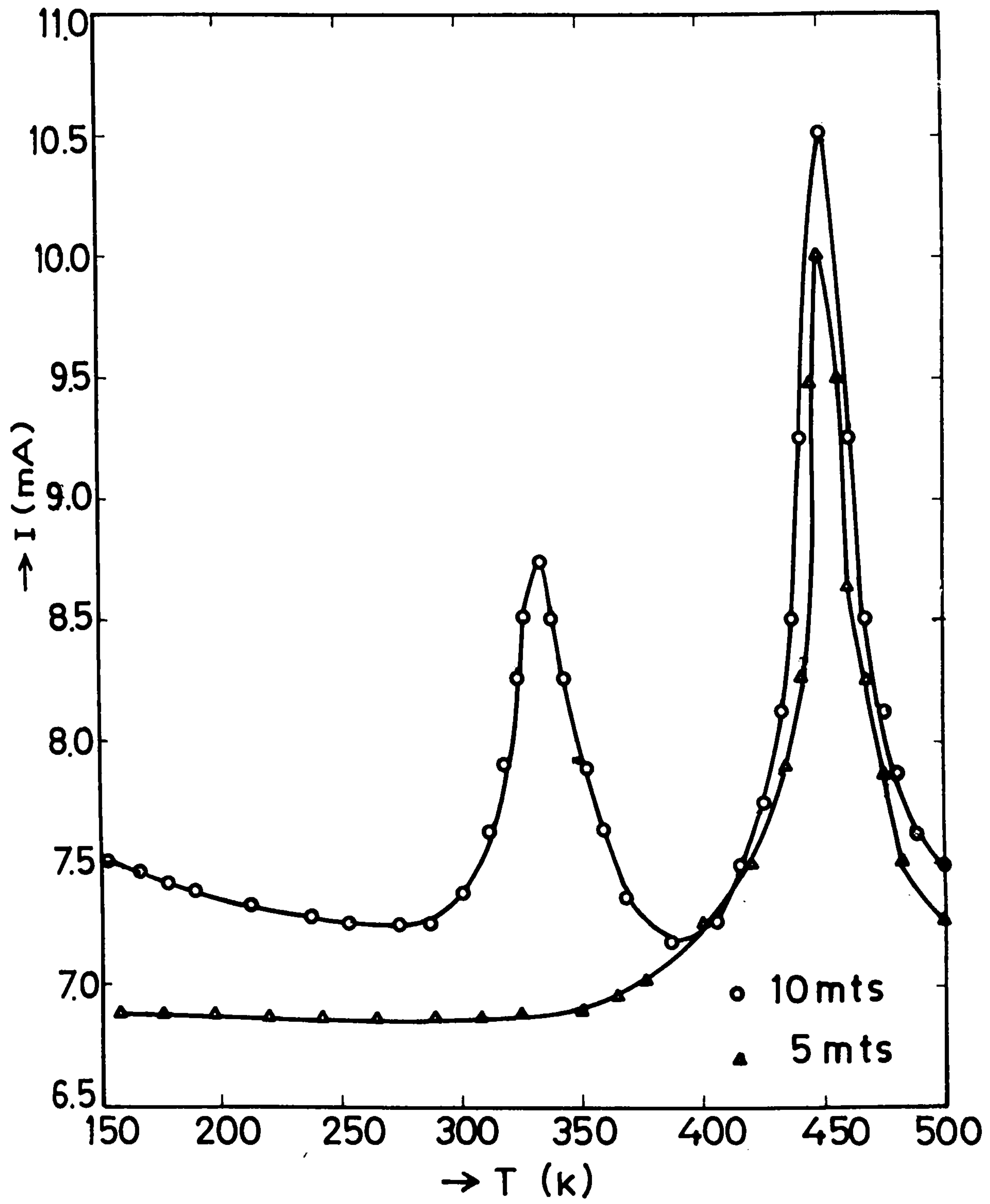

Figure 4.6.TSC spectra of n-type CdS thin film annealed in vacuum (at 200°C for 1 hour) under different excitation time

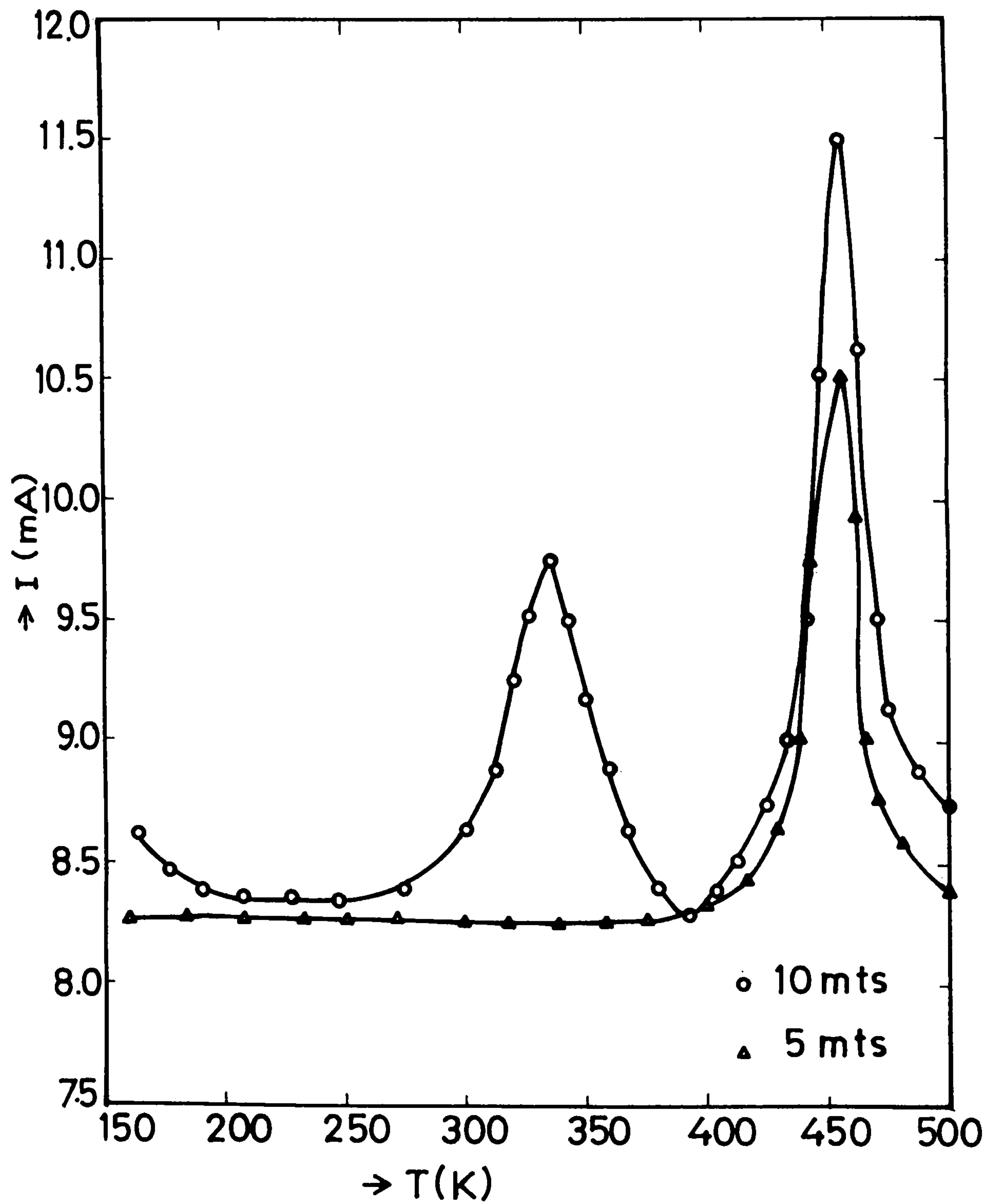

Figure 4.7. TSC spectra of n-type CdS thin film annealed in vacuum (at 300°C for 1 hour) for different excitation time.

Table 3. The values of activation energies and capture cross sections of vacuum annealed n-type CdS films obtained from TSC measurements.

n-type CdS films vacuum annealed at different temperature	Activation energy (eV) for different light excitation time		Capture Cross section (cm^2) for different light excitation time	
	5 min.	10 min.	5 min.	10 min.
100°C	1) 1.21±0.01	1) 1.21±0.01 2) 0.41	1) 3.48×10^{-16}	1) 3.48×10^{-16} 2) 2.51×10^{-23}
200°C	1) 1.24±0.01	1) 1.24±0.01 2) 0.41	1) 10.0×10^{-16}	1) 10.0×10^{-16} 2) 2.5×10^{-23}
300°C	1)1.23±0.01	1) 1.23±0.01 2) 0.41	1) 9.8×10^{-16}	1) 9.8×10^{-16} 2) 2.5×10^{-23}

of 5 minutes (It is interesting to note that for n-type samples only one peak is observed under 5 minutes light excitation). The activation energies of these two peaks of p-type sample were calculated to 1.2 eV (mobility of S vacancy) and 0.72-0.75 eV. Since p-type sample is Cu doped, we expect a trap level of Cu impurity in this sample and we found that 0.77 eV is an acceptor level of Cu impurity [83]. It was reported [83] earlier that resistivity of Cu doped CdS sample first increases with increasing Cu concentration and shows an unmeasurably high value at about 0.5 at % of Cu. However, it shows a drastic decrease with further increase of Cu content upto about 25 at % of Cu. It was also reported that Cu atoms substituted for Cd sites acts as acceptors and according to Y. Kashiwaba et al, the increase of electrical resistivity to unmeasurably high value by Cu doping is due to the compensation of donors which are probably due to sulphur vacancies [83]. They also suggest that the remarkable decrease of electrical resistivity above 0.5 at % of Cu is due to the increase of active Cu atoms substituted for Cd sites and this give rise to a p-type conductivity to the sample. In the present work, we could detect Cu impurity as such in

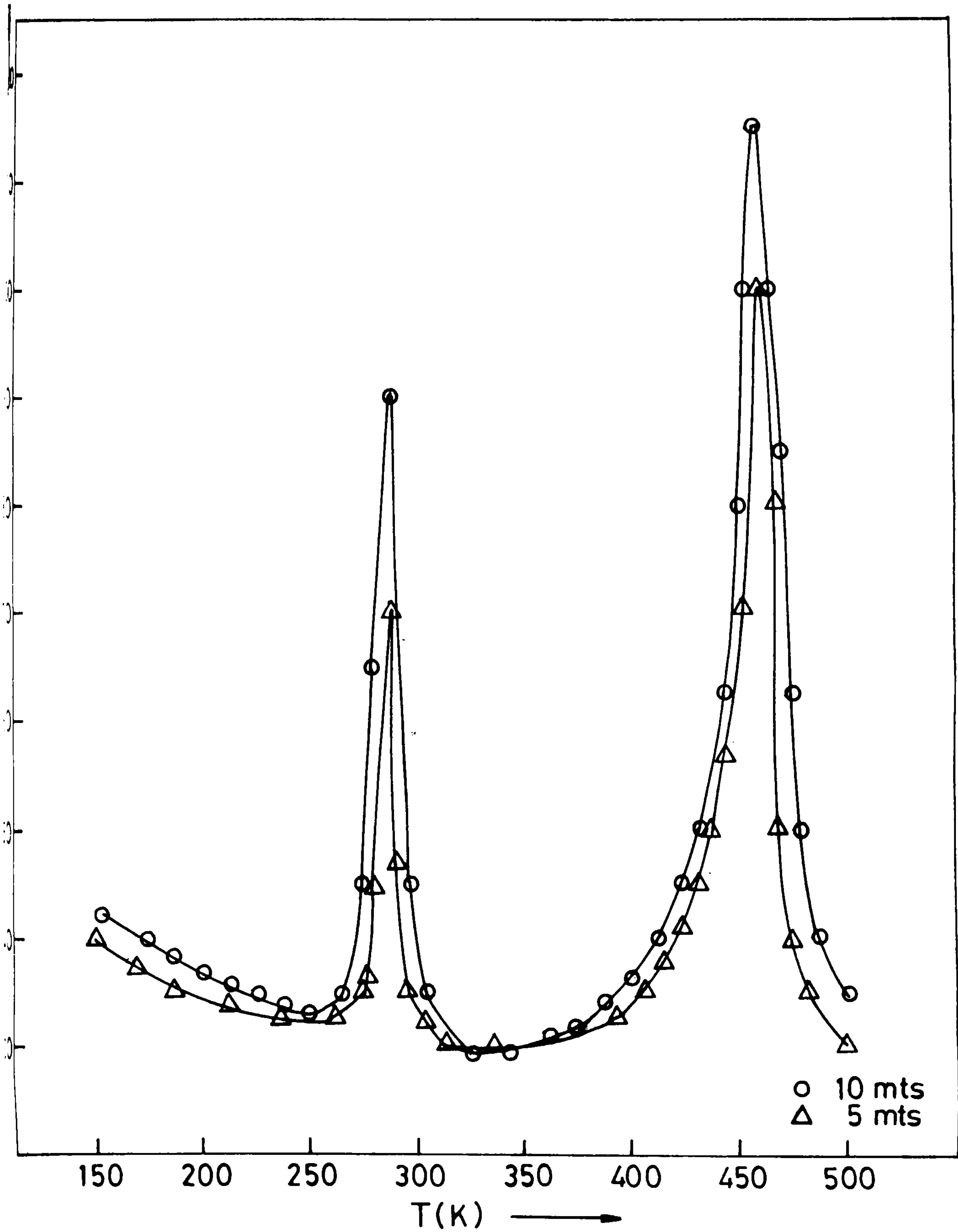

Figure 4.8. TSC spectra of p-type CdS thin film under different excitation time

the p-type sample and there is no trace of complexes of Cd and S vacancies even after 10 minutes light excitation. One can hence conclude that it may be the Cu impurity on Cd sites that gives the p-type conductivity to spray pyrolysed CdS films.

It was also reported that [83,86,87] as a result of Cu doping, no other compound such as Cu_xS is formed and Cu diffused almost completely into the CdS. Our result is also in good agreement with this, since we are not getting any other peak except Cu impurity and mobility of S vacancy in p-type CdS.

To determine nature of traps formed in n and p-type sprayed CdS samples TSC measurements were performed at constant heating rate, by changing the polarity of bias voltage applied to the irradiating surface. For this type of measurement film was-prepared on SnO_2 coated glass substrates and one electrode coated on the top surface of the film and the other on the SnO_2 surface so that it is having contact to bottom surface of the film. Figure 4.9. shows the electrode structure for this measurement. At first the positive terminal of the biasing voltage cell was connected to the electrode on the sample and irradiation is given to this surface. After the completion of TSC experiment, the polarity of biasing voltage given to the electrode on the sample was changed to negative and TSC experiment was repeated. When the surfaces were irradiated, two types of carriers were formed in this domain and were separated by the bias voltage. Then different types of charge distribution would result according to the trapping center [103].

Figure 4.10. shows the TSC curves for as-prepared n-CdS sample with positive bias and negative bias applied to irradiating surfaces. From the spectra it is clear that I_{max} is higher for the case of positive bias voltage for the peak of activation energy 0.4 eV and hence the hole carrier is dominant and it is a hole trap. However, from its cross section value it is known that this is a 'weak' trap. But for the second peak corresponding to 1.2 eV, I_{max} is higher for the case of negative bias voltage and hence this defect is an electron trap.

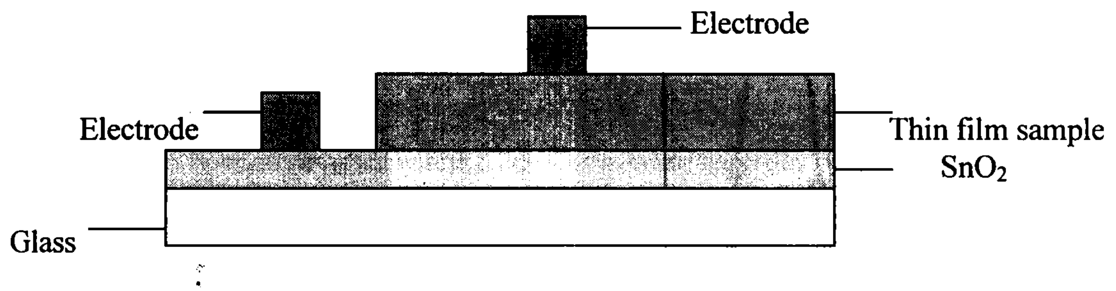

Figure 4.9. Electrode structure for finding nature of traps observed in TSC studies.

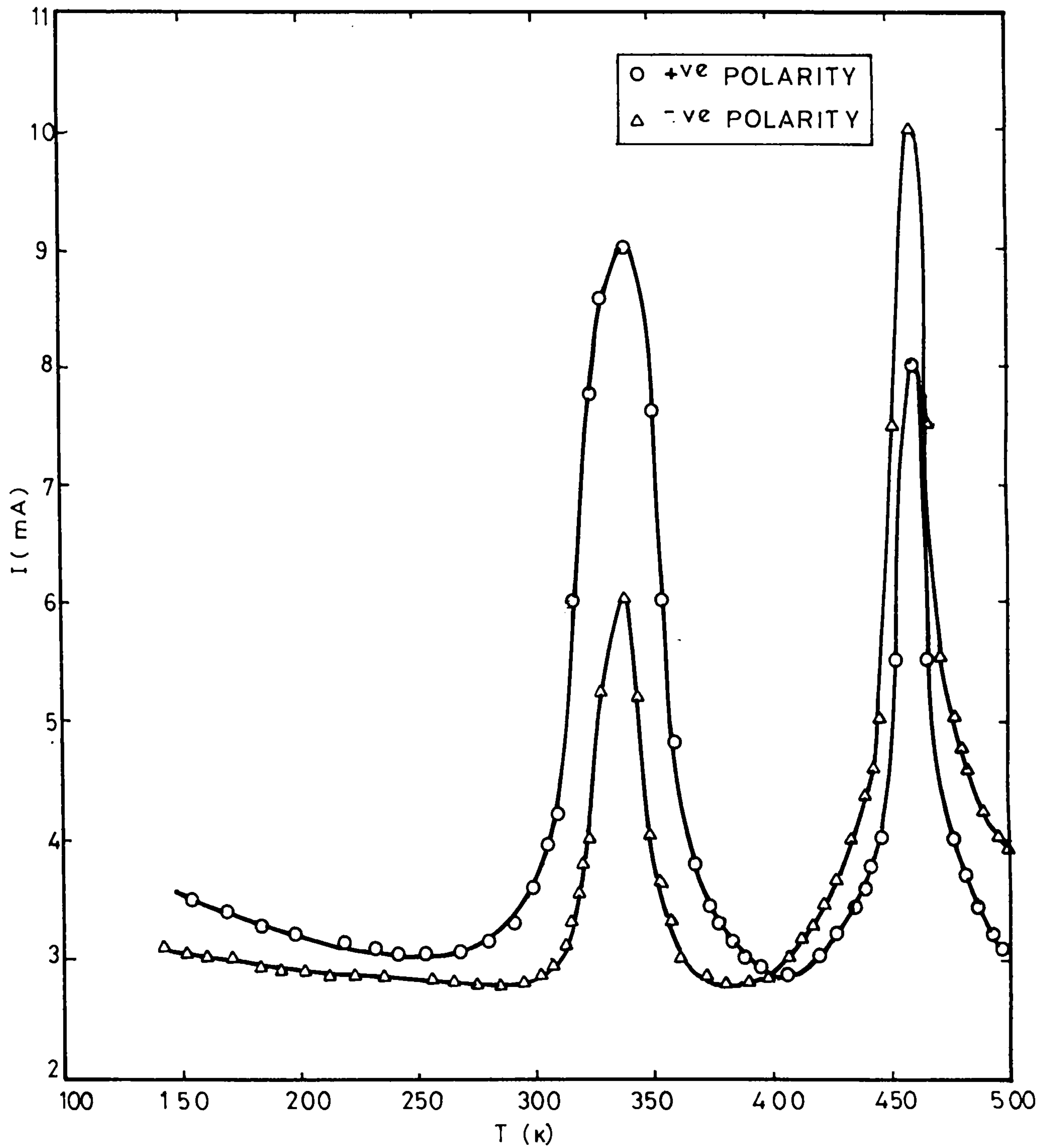

Figure 4.10. TSC spectra of n-type CdS thin film under 10 minutes excitation with positive and negative polarity applied to the irradiating surface.

TSC spectra of p-type CdS sample with positive and negative bias voltage applied to the irradiating surface are shown in figure 4.11. From this, it is very clear that peak of activation energy 1.2 eV corresponds to electron trap while peak due to Cu impurity (0.72-0.75 eV) corresponds to a hole trap.

4.5. Dark conductivity measurements of n and p-type CdS thin films

For the dark conductivity measurements vacuum evapourated indium contacts were given on the top surface of the samples keeping a distance of 1 cm between the electrodes. The sample was then mounted in the metallic cell and pressure during the measurement was kept at 10^{-2} Torr. Measurements were carried out after applying a steady voltage of 6V across the electrodes. In this case also the resulting current was measured using an electrometer when sample temperature was varied from 100 K to 500 K. Conductivity of the sample was calculated for different temperature and a graph of log σ versus $10^3/T$ was plotted in all the cases. (Details of the experimental set up are given in chapter 3).

Arrhenius plot of vacuum annealed (300°C) n-CdS and as-prepared p-CdS are shown in figure 4.12. and 4.13. respectively. The plot of vacuum annealed n-CdS showed only one peak that corresponds to an activation energy of 1.2 eV and this indicates the mobility of sulphur vacancy in this sample as obtained from TSC measurements. Here we did not get the presence of a trap level corresponding to complex of cadmium and sulphur vacancies. This may be due to the very low value of capture cross section (as indicated in TSC measurement also). Moreover, the Cd-S vacancy complex was found to be a hole trap and in the case of dark conductivity measurements on an n-type CdS, there is no chance of minority carrier (hole) generation. Interestingly Arrhenius plot of p-CdS gives two slopes and activation energies are calculated to be 1.2 eV and 0.75 eV indicating the presence of sulphur vacancy and Cu impurity. Thus it can be seen that dark conductivity measurements very well supports the results obtained from TSC measurements.

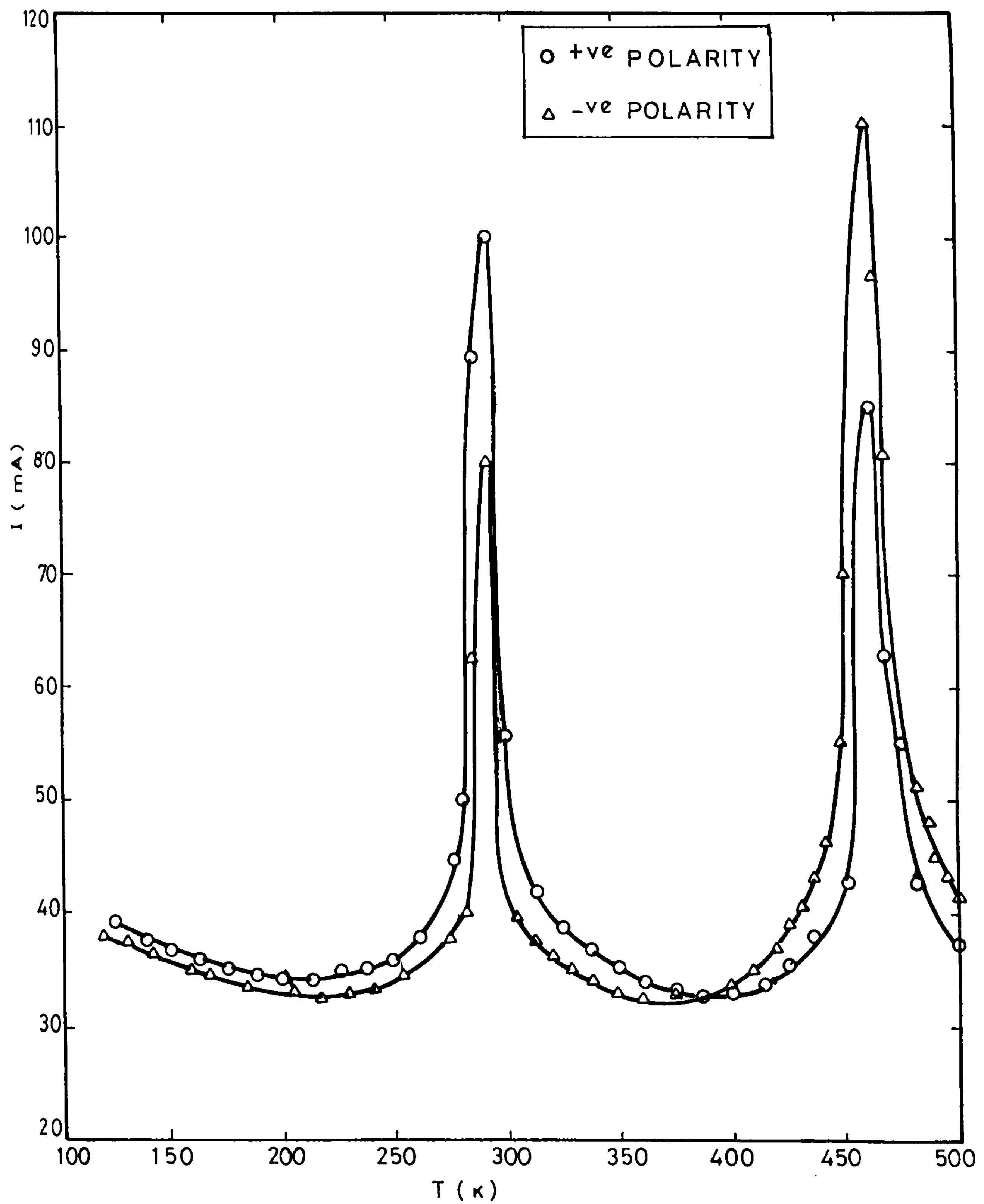

Figure 4.11. TSC spectra of p-type CdS thin film under 10 minutes excitation with positive and negative polarity applied to the irradiating surface.

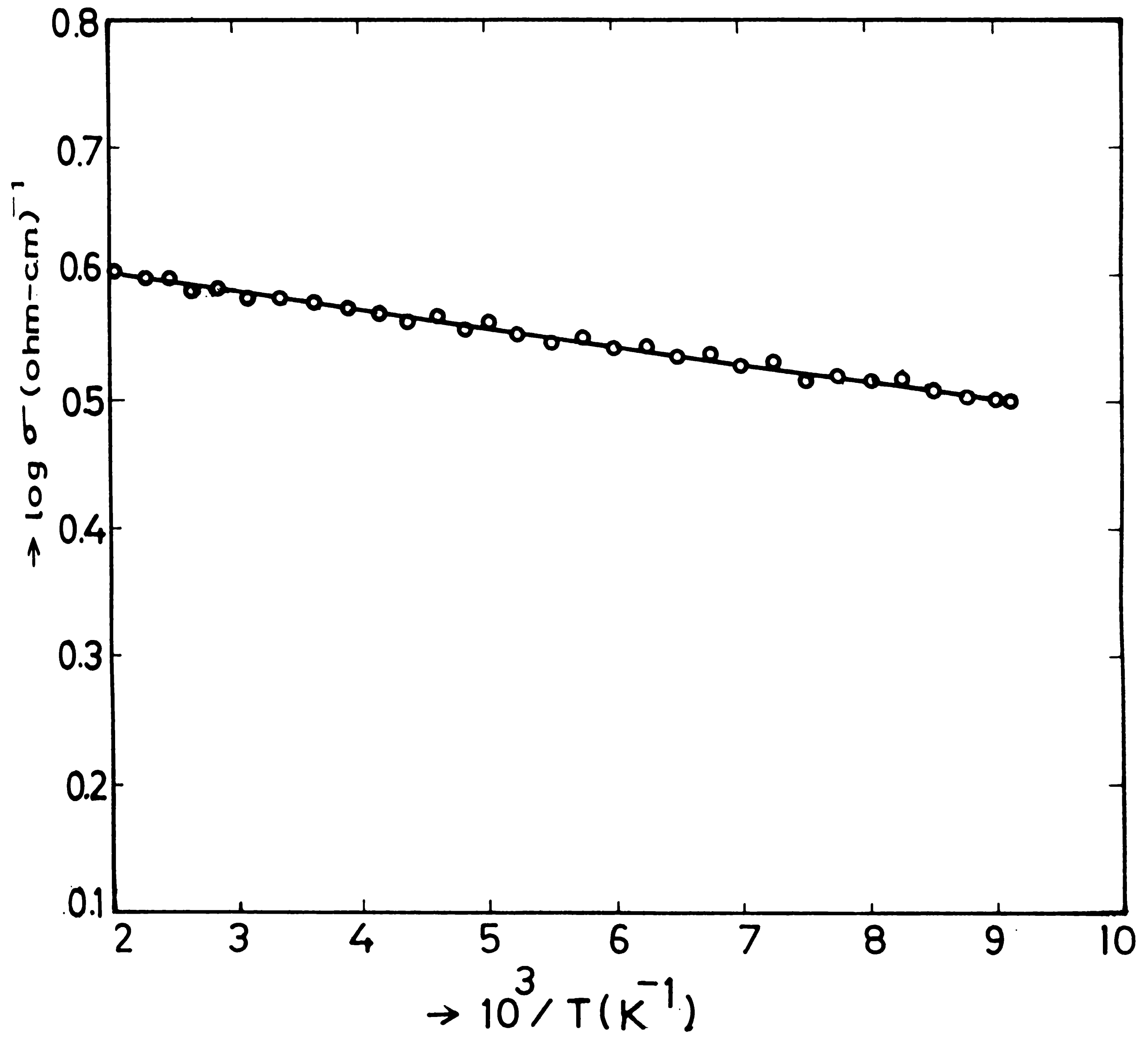

Figure 4.12. Arrhenius plot of n-type CdS thin film annealed in vacuum (300°C)

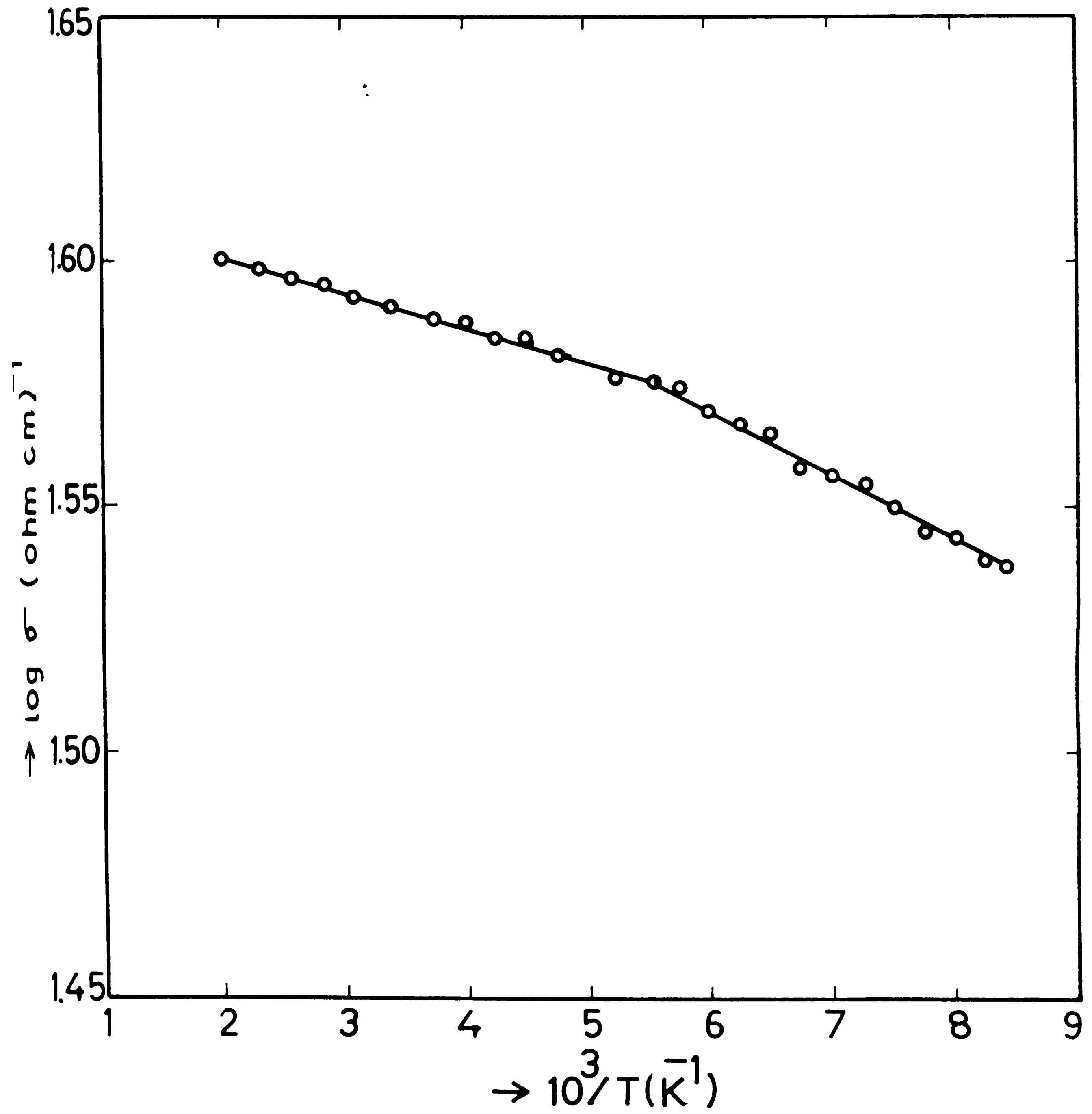

Figure 4.13. Arrhenius plot of p-type CdS thin film

4.6. Analysis of Chemical Bath Deposited (CBD) CdS thin films

Recently there is a revival of interest in dip coated CdS thin films with its use as a high resistance buffer layer in the commercial production of CIS/CdS/ZnO solar cells and modules [104,105]. This may be due to the fact that the dip-coated CdS films are found to be having very good crystallinity. In the present section, we discuss the preparation, resistance variation and TSC measurements of this type of CdS thin films.

4.6.1 Sample Preparation

The CBD technique for the deposition of CdS was based on the slow release of Cd^{++} ions and S^{--} ions in aqueous alkaline bath and their reaction resulting in the deposition of the compound on the substrate. For complexing Cd^{++} ions, different complexing agents had been used by different groups. In the present work, Triethanolamine [TEA] as the complexing agent and CdS thin films are formed as per the following reaction [106]

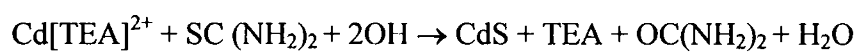

$$Cd[TEA]^{2+} + SC(NH_2)_2 + 2OH \rightarrow CdS + TEA + OC(NH_2)_2 + H_2O$$

In this work CdS films were prepared from a reaction mixture containing solutions of $CdCl_2$ and thiourea. These solutions (one molar concentration) were taken in the ratio (by volume) 1:1. TEA was added to $CdCl_2$ solution to get the complex molecule while ammonia solution was added to adjust the pH value at 10. The solution was taken in a beaker that was kept in a water bath at a temperature of 80°C. Ultrasonically cleaned glass slides placed vertically in the beaker served as the substrate for deposition. Films of thickness 1μm could be prepared from this deposition mixture in a deposition time of 1 hour. These films could also be deposited over SnO_2 surface when the SnO_2 layer acts as the lower electrode.

4.6.2. Resistance variation with aging and annealing temperature

As-prepared samples showed sheet resistance of $10^{11}\Omega/\square$ and resistivity of the order of 10^7 Ω cm. In order to study the effect of annealing on the resistivity, the samples were annealed at different temperature from 100-350°C. On annealing sheet resistance of the

samples was found to be decreasing. These annealed samples were again used for studying the variation of sheet resistance due to aging. For this, measurements were taken for 12 days noting the resistivity values at the interval of 24 hours. Figure 4.14. shows the variation of sheet resistance of the samples (annealed at different temperature)due to aging. Inset in this figure depicts the variation of sheet resistance of the sample annealed at 250°C. It is very clear that the samples annealed at 250°C has got the least value for sheet resistance. It is also clear from the graph that sheet resistance of samples annealed at different temperature goes on increasing with time with an exception of the sample annealed at 250°C K. For this sample also sheet resistance increases for the first few days, and then remains almost a constant.

In order to study the effect of annealing time, the samples were annealed for different time from 1 to 4 hours at 250°C and resistivity was measured at the interval of 24 hours for 12 days and figure 4.15. shows the result of this observation. It is clear that sample annealed for 3 hours has got least resistance and its resistance becomes more or less constant, after keeping for few days. But sheet resistance of other samples annealed for 1,2, and 4 hours goes on increasing with days. From this study of variation of sheet resistance of CBD CdS films, we conclude that it is possible to reduce the resistivity of CBD CdS samples if they are annealed at 250°C for 3 hours. The least value of resistivity obtained in this case is $\sim 10^5\ \Omega$ cm. It is to be mentioned here that the least resistivity obtained for these films, is not suitable for solar cell application where it is necessary to be in the range 10-100 Ω cm.

4.6.3. TSC measurements of high resistive CBD CdS thin films

We conducted the TSC measurements of the highly resistive samples, in As-deposited as well as in annealed conditions. Figure 4.16. gives the TSC spectra of CBD CdS film annealed at 250°C for 3 hours. The spectra depict no peaks at all, which indicate that this sample possess no defect states/levels detectable in TSC measurement. All high resistive CBD CdS samples also showed the same behaviour in TSC measurements. Hence we believe that one of the reasons for the high resistivity of these sample is the absence of defect/impurity levels in the forbidden band gap which help the easy production of carriers.

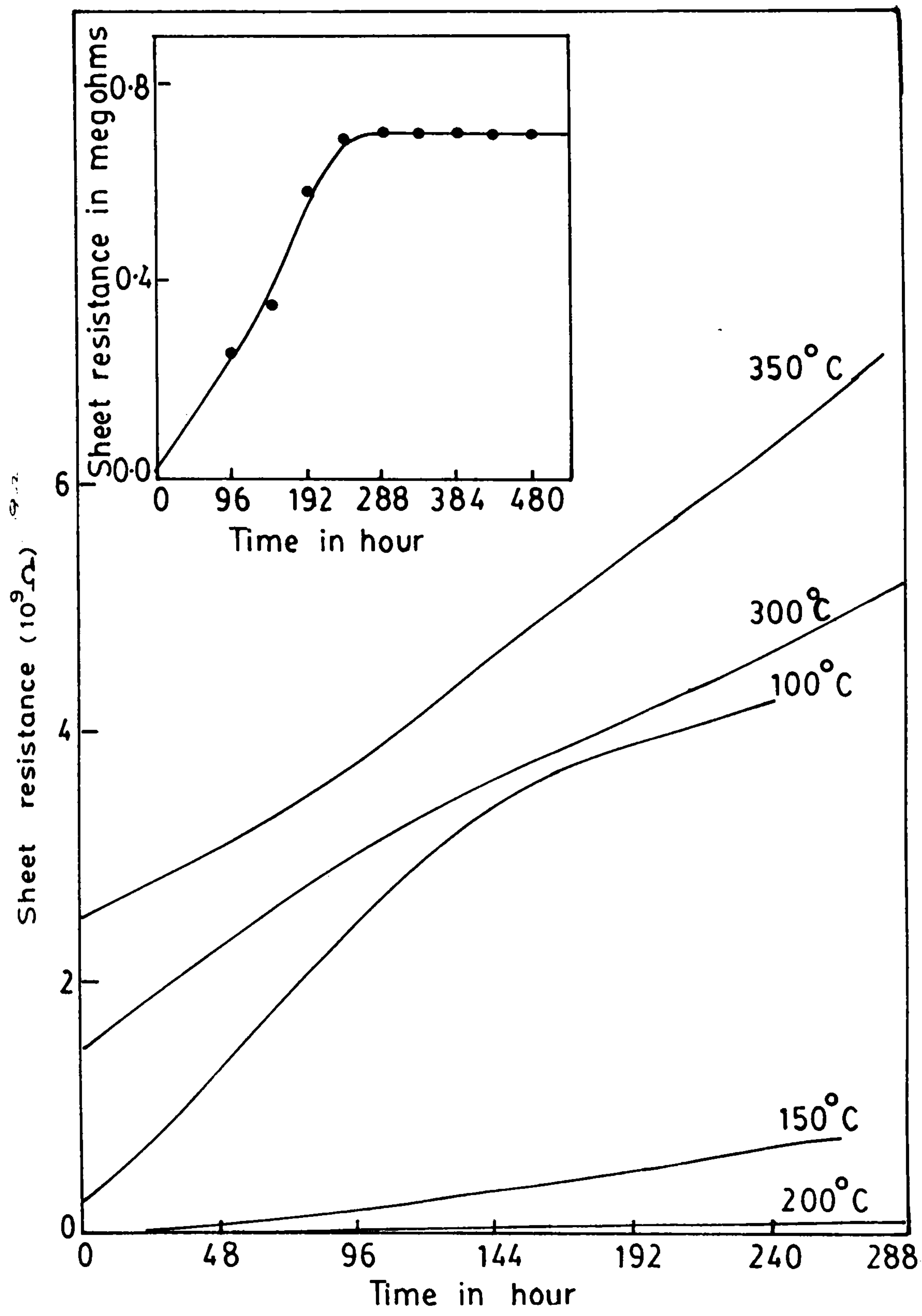

Figure 4.14. Sheet resistance variation of CBD CdS thin film (annealed at diff.temperature) due to aging. Inset shows the variation for the sample annealed at 250°C.

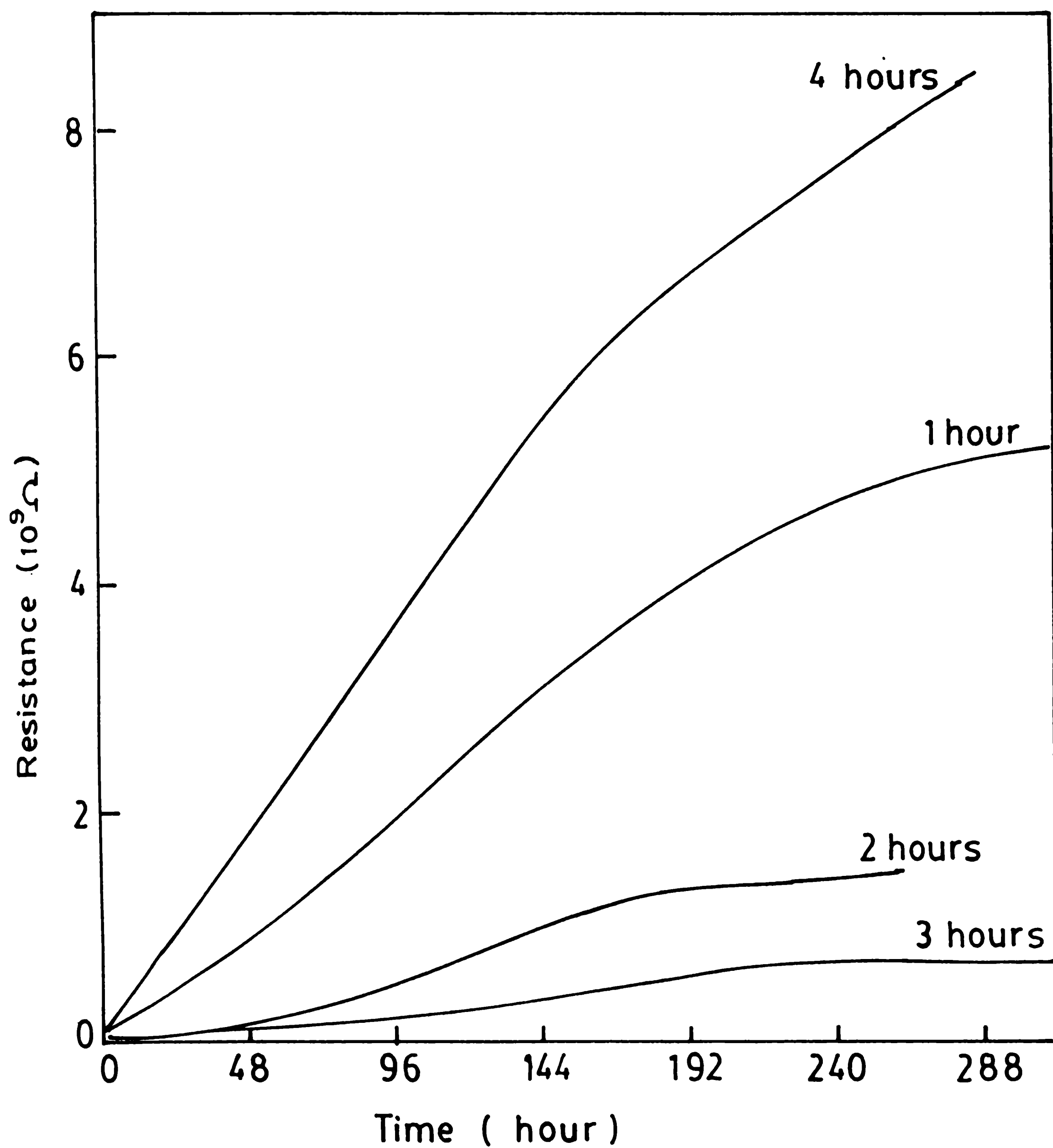

Figure 4.15. Sheet resistance variation of CBD CdS thin film annealed (at 250°C) for different timings due to aging.

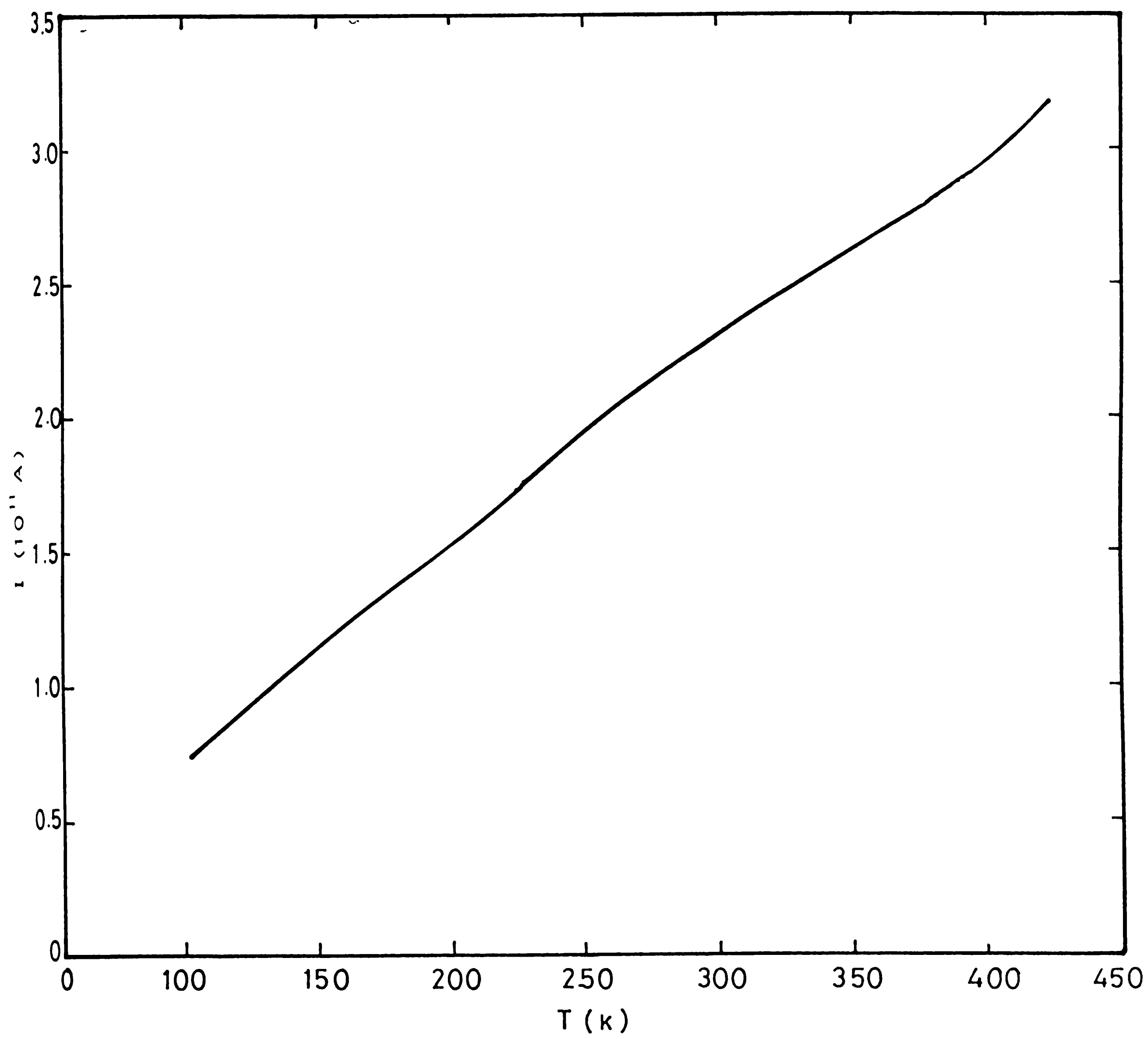

Figure 4.16. TSC spectra of high resistive CBD CdS thin film

This may be mainly due to the fact that CBD process is very slow and hence these samples may be having very low concentration of defects/impurities. But annealing may be resulting in the increase of the grain size of the samples causing an increase in diffusion length of carriers. This may be the reason for the slight reduction in resistivity.

4.6.4. Low resistive CBD CdS thin films

Even though high resistive CdS film is desirable near the junction of a solar cell in which CdS is used as the window layer, a low resistive CdS layer is required at the top surface (near the top electrode) for high efficiency solar cells. In our laboratory $CuInSe_2$/CdS solar cells could be fabricated completely by the CBD technique [96]. The efficiency of which was found to be 3.1%. The low efficiency of the device may be due to the high series resistance of the cells and this is caused mainly by the high resistance of the CdS layer near the top electrode.

The production of low resistive CBD CdS films had been reported by many groups [50,53,107,108,109]. One of the reports [53] is by O.De Melo et al in which CdS samples were first annealed in S_2 atmosphere at 250°C and after that in H_2+In atmosphere at different temperatures from 300-400°C. They obtained least resistivity of 11 Ωcm at an optimum annealing temperature of 350°C.

4.6.4.a. Experimental details

In the present work, we could successfully prepare low resistive CdS films by a process developed in our lab earlier and use these samples to detect the trap levels that caused the low resistive nature of the films. The details of preparation of this type of films have been reported elsewhere [110,111]. Here the high resistivity CBD CdS films (10^7 Ω cm) were treated chemically so as to dope these with chloride/metal ions, which can act as donors. For this samples were treated with solutions of $CdCl_2$, $InCl_3$ and $SnCl_4$. It was observed that resistivity decreased to very low value (5 Ω cm), but it was not clear whether the metal ion or the chloride ion was acting as the donor.

Table 4 shows the values of resistivity of various samples. From this table, it is obvious that by treating CBD CdS films with $CdCl_2$, $InCl_3$ and $SnCl_4$ solutions, one can get low resistive CdS films. Of these, $InCl_3$ gave lowest resistivity. On annealing in air, there was slight increase in resistivity. But even then, the values are very low compared to the as-prepared films. However on vacuum annealing resistivity values increase considerably and becomes almost equal to that of as-prepared CBD CdS films.

4.6.4.b Results of TSC Measurements

TSC spectra of the low resistive (unannealed-treated with three different solutions) samples are shown in figure 4.17- 4.19. The spectra show three distinct peaks. The activation energy values corresponding to these peaks were calculated to be 0.4 eV(375 K), 0.1 eV (275 K) and 0.03 eV (150 K) (Table 5). Of these, the peaks at 275 K (0.1 eV) and 150 K (0.03 eV) correspond to individual sulphur vacancies [112] and chloride ions respectively [113]. The 0.4 eV center usually occur along with 0.83 eV center and are often found in both sulphurrich and Cd rich crystals [5]. These traps are complexes of associated Cd and S vacancies in nearest neighbouring sites. But in the present study only the center at 0.4 eV was observed.

The XPS analysis of the CdS sample treated with $CdCl_2$ has clearly shown the presence of chlorine. There is drastic decrease of the concentration of the sulphurand a slight decrease of Cd concentration on the surfaces of the samples . The XPS spectrum is shown in figure 4.20. Thus it is evident that the decrease in resistivity observed in our study is due to the presence of defect level corresponding to S^{--} vacancy (0.1 eV), Cd-S vacancy complexes (0.4 eV) and impurity level corresponding to chloride ions (0.03 eV).

Table 4. Resistivity values of different CBD CdS films treated with $InCl_3$,$CdCl_2$ and $SnCl_4$ in as-prepared and in annealed (air and vacuum) condition.

Sample type		Resistivity Ω cm
CBD CdS films without post dipping		10^7
CBD CdS dipped in $InCl_3$ solution	As-prepared	5
	Air annealed	11
	Vacuum annealed	6×10^7
CBD CdS dipped in $CdCl_2$ solution	As-prepared	50
	Air annealed	80
	Vacuum annealed	20×10^7
CBD CdS dipped in $SnCl_4$ solution	As-prepared	100
	Air annealed	170
	Vacuum annealed	100×10^7

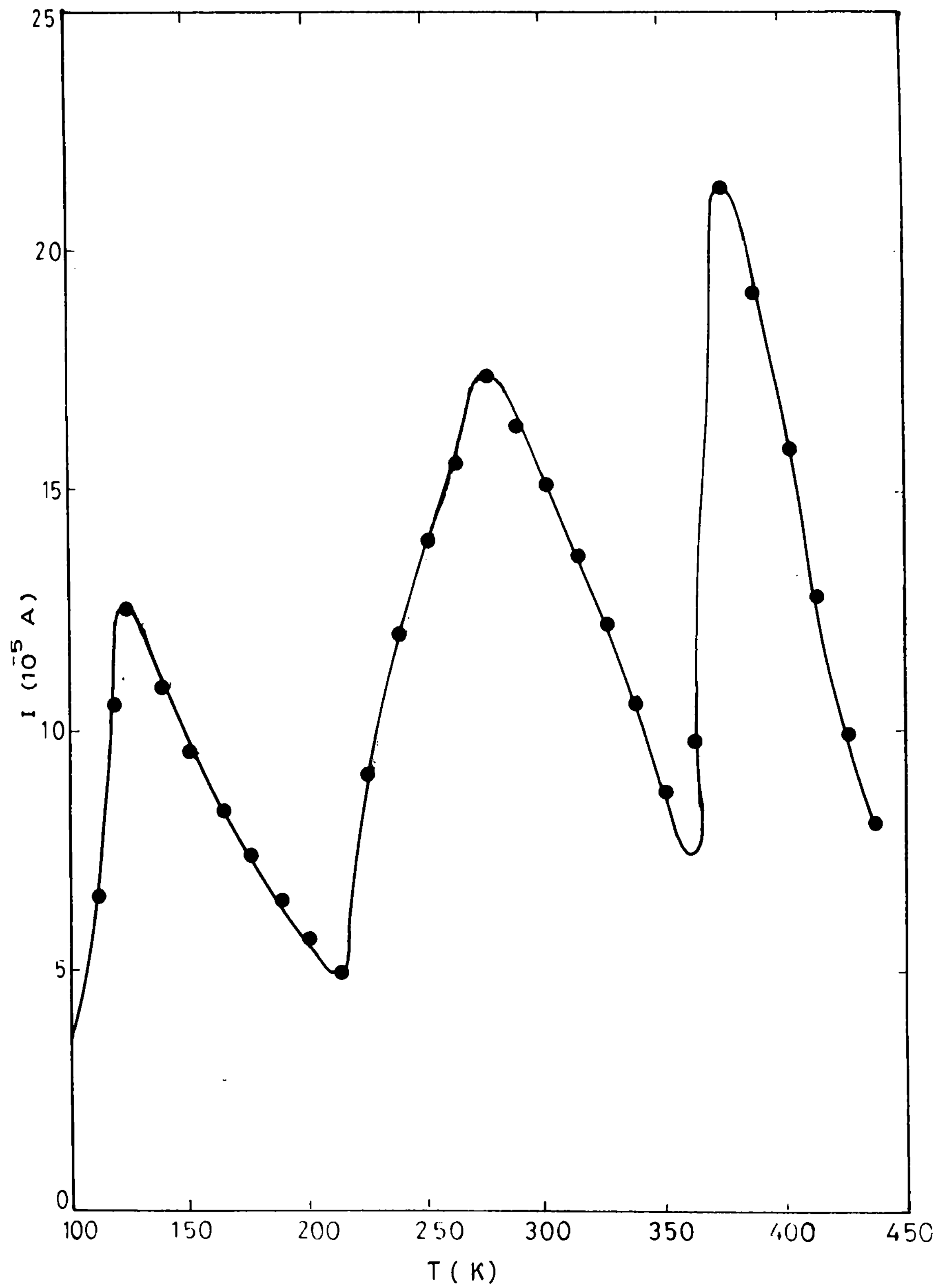

Figure 4.17. TSC spectra of low resistive CBD CdS thin film treated with $InCl_3$ solution

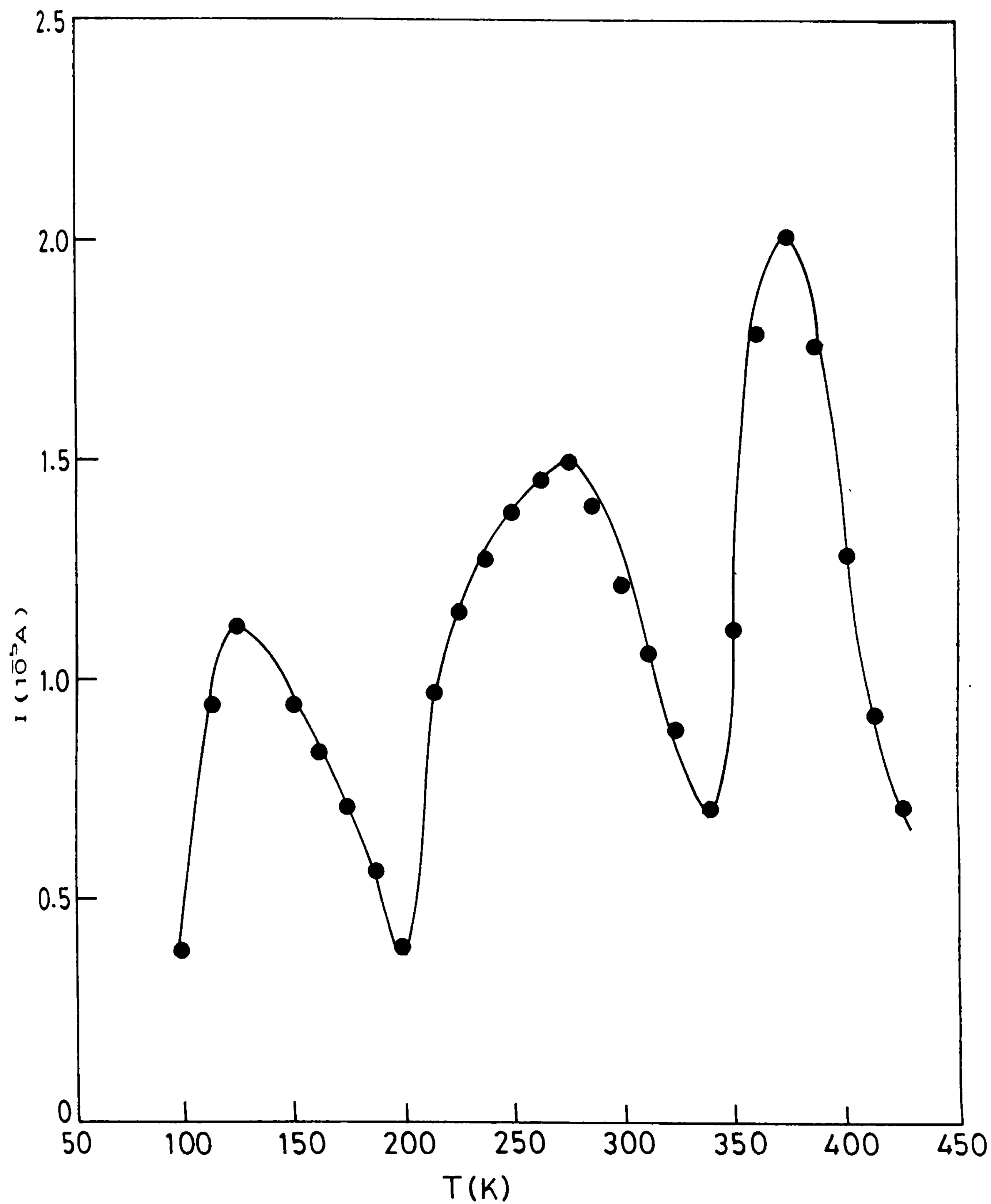

Figure 4.18. TSC spectra of low resistive CBD CdS thin film treated with $CdCl_2$ solution

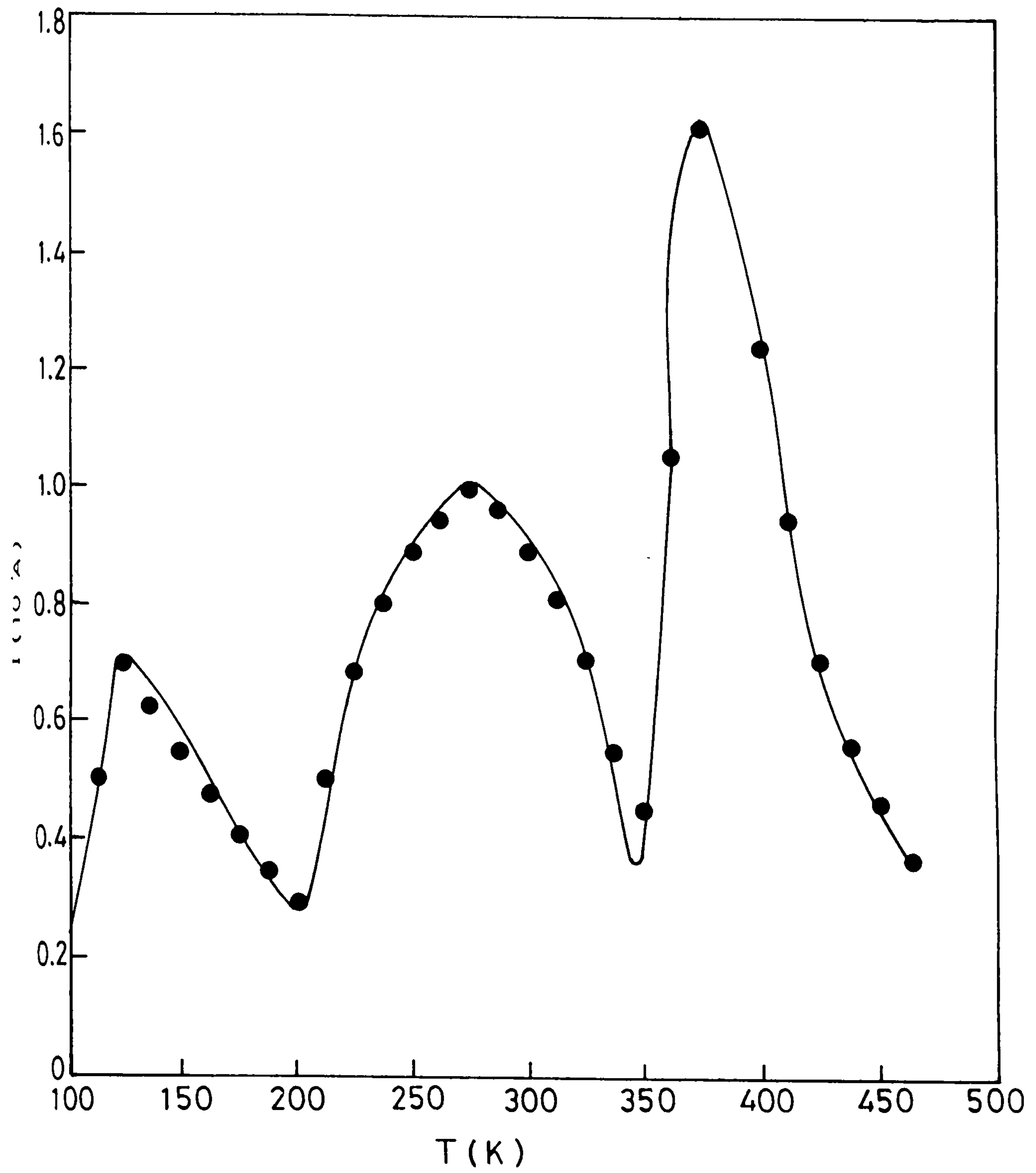

Figure 4.19. TSC spectra of low resistive CBD CdS thin film treated with $SnCl_4$ solution

Table 5. Shows values of activation energies and capture cross sections of various traps obtained from TSC spectra.

CBD CdS films		Activation energy eV	Capture cross section 10^{-26} cm^2
Dipped in	As-prepared	1) 0.40 2) 0.10 3) 0.03	1) 0.003 2) 0.05 3) 0.18
$InCl_3$ soln.	Air annealed	1) 0.92 2) 0.1	1) 0.004 2) 0.05
Dipped in	As-prepared	1) 0.40 2) 0.10 3) 0.03	1) 0.003 2) 0.05 3) 0.21
$CdCl_2$ soln.	Air annealed	1) 0.92 2) 0.1	1) 0.004 2) 0.05
Dipped in	As-prepared	1) 0.40 2) 0.10 3) 0.03	1) 0.003 2) 0.05 3) 0.021
$SnCl_4$ soln.	Air annealed	1) 0.92 2) 0.1	1) 0.004 2) 0.05

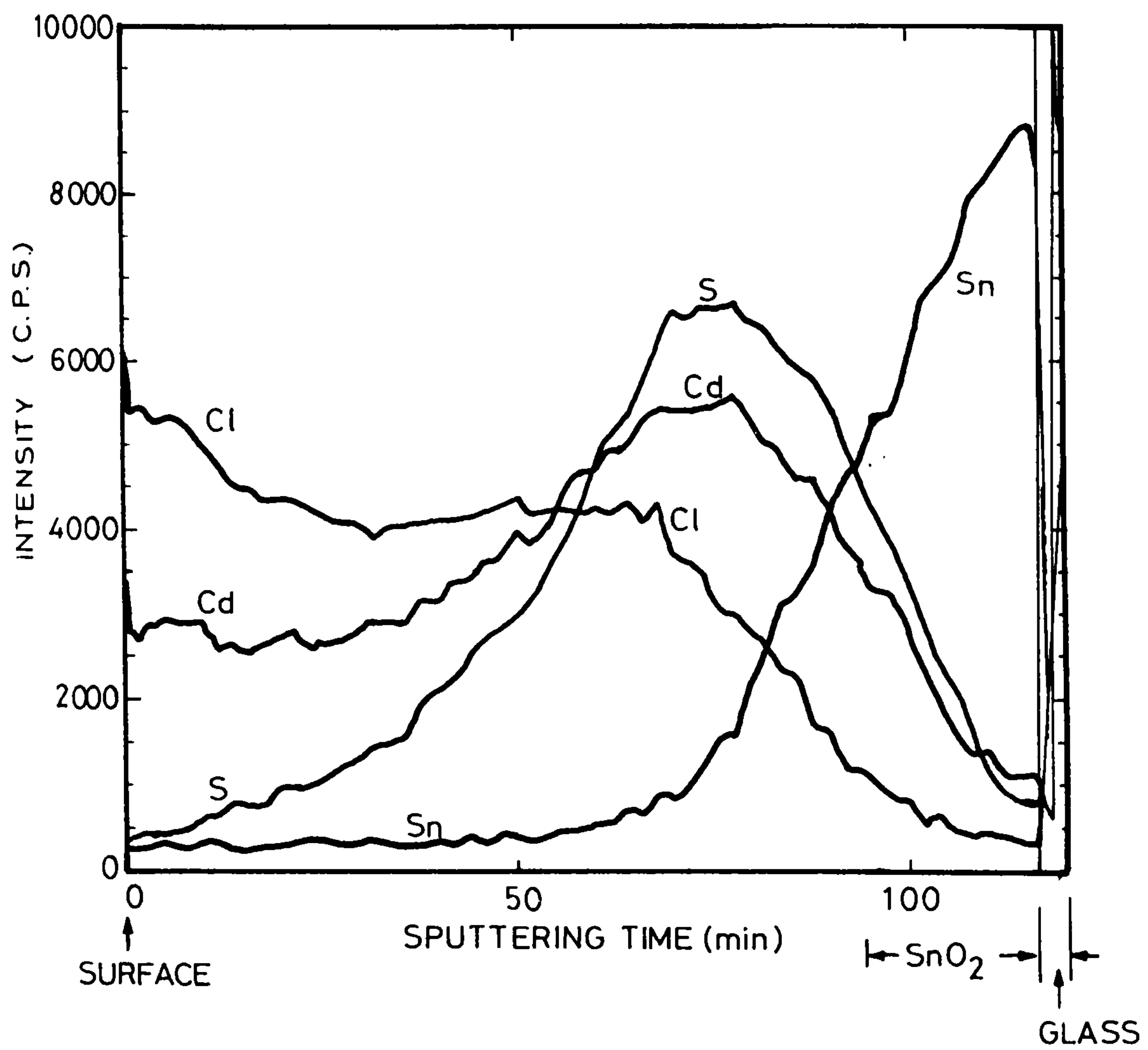

Figure 4.20. XPS spectra of low resistive CBD CdS thin film treated with $CdCl_2$ solution

Values of capture cross section for these levels were calculated and are shown in table 5. The capture cross section is found to be larger for the trap due to chloride ions ($\sim 10^{-28} cm^2$) than the other level ($\sim 10^{-29}$ cm^2) and this indicates that carriers can be easily captured by this center. Capture cross section of the same order was reported in the case of sprayed CdS [89]. The activation energy of this trap is only 0.03 eV and hence major contribution for the increase in conductivity of post treated CdS films may be due to the presence of this center.

The resistance was lowered much more in the case of samples dipped in $CdCl_2$ and $InCl_3$ solution than in $SnCl_4$ solution. Even though the number of chloride ions is more in $SnCl_4$ this solution is found to be more corrosive and hence much of the film got dissolved in $SnCl_4$ solution.

To find the nature of trap levels observed in low resistive samples, TSC measurement was conducted with positive and negative bias voltage applied to the irradiating surface. The spectra are shown in figure 4.21. From this it is clear that level due to chloride ion (0.03 eV) is an electron trap and the other two levels (independent S vacancy-0.1 eV and Cd-S complex vacancy -0.4 eV) are hole traps.

TSC spectra of samples annealed in air are shown in figure 4.22-4.24 Here instead of three peaks, spectra depict two peaks of activation energy 0.1 eV (275 K) and 0.92 eV (400 K) which are attributed to independent S vacancies and chemisorbed oxygen [8,113,114]. Only these two defect levels contribute for the conductivity of air annealed samples. Thus from TSC measurement we could find that the chloride ion of low resistive CdS films and complexes of Cd and S vacancies disappear on air annealing. Instead there arises an impurity level due to the presence of chemisorbed oxygen.

We conducted TSC measurements on vacuum annealed samples and typical TSC spectra are shown in figure 4.25. These samples do not have any defect levels that can be detected using TSC measurements as evident from the spectra (no peak is observed). Probably, this may be the reason for the high resistivity obtained for the vacuum annealed samples.

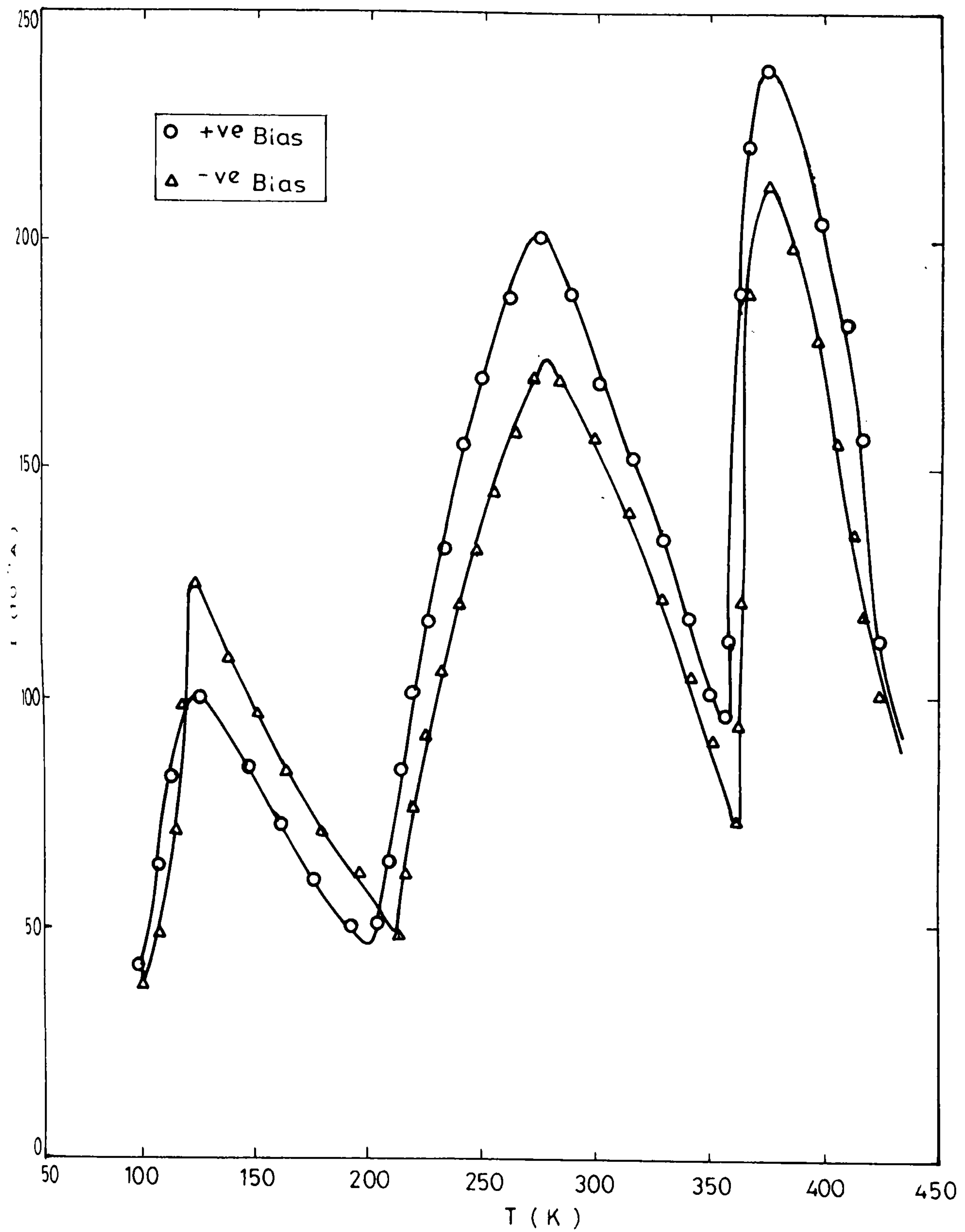

Figure 4.21. TSC spectra of low resistive CBD CdS thin film (treated with $InCl_3$ solution) with positive and negative bias voltage applied to the irradiating surface.

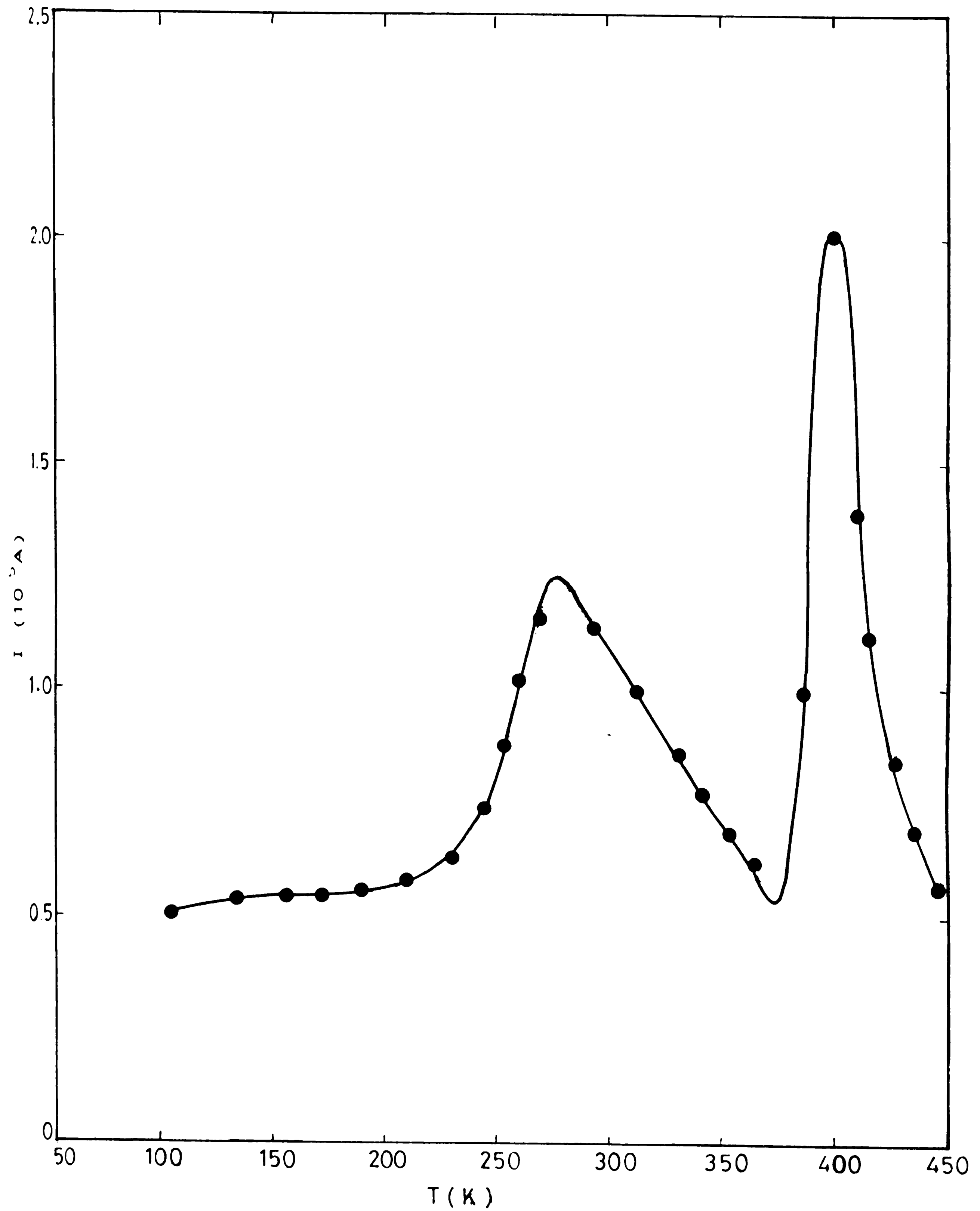

Figure 4.22. TSC spectra of CBD CdS thin film treated with $InCl_3$ solution and annealed in air.

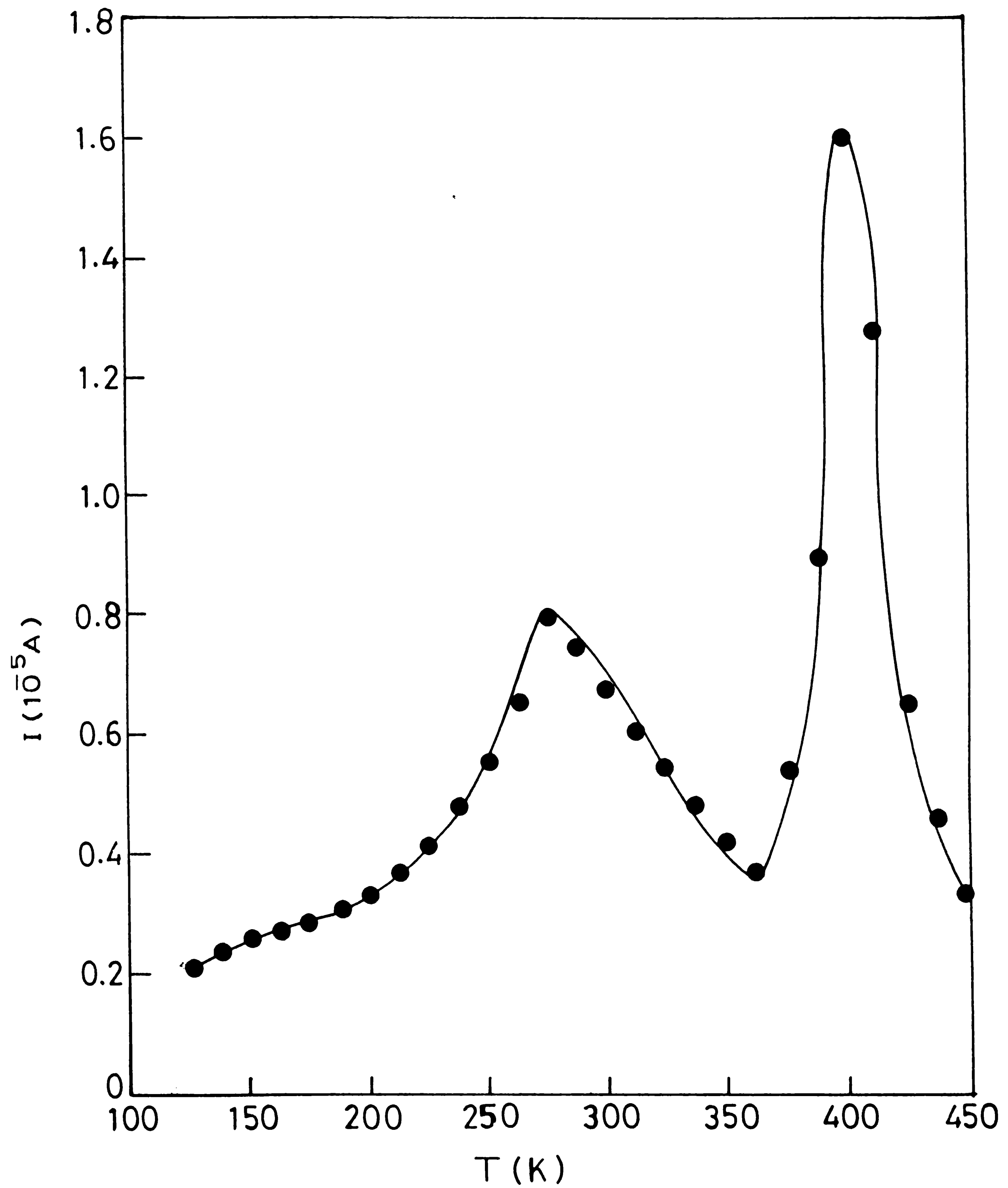

Figure 4.23. TSC spectra of CBD CdS thin film treated with $CdCl_2$ solution and annealed in air.

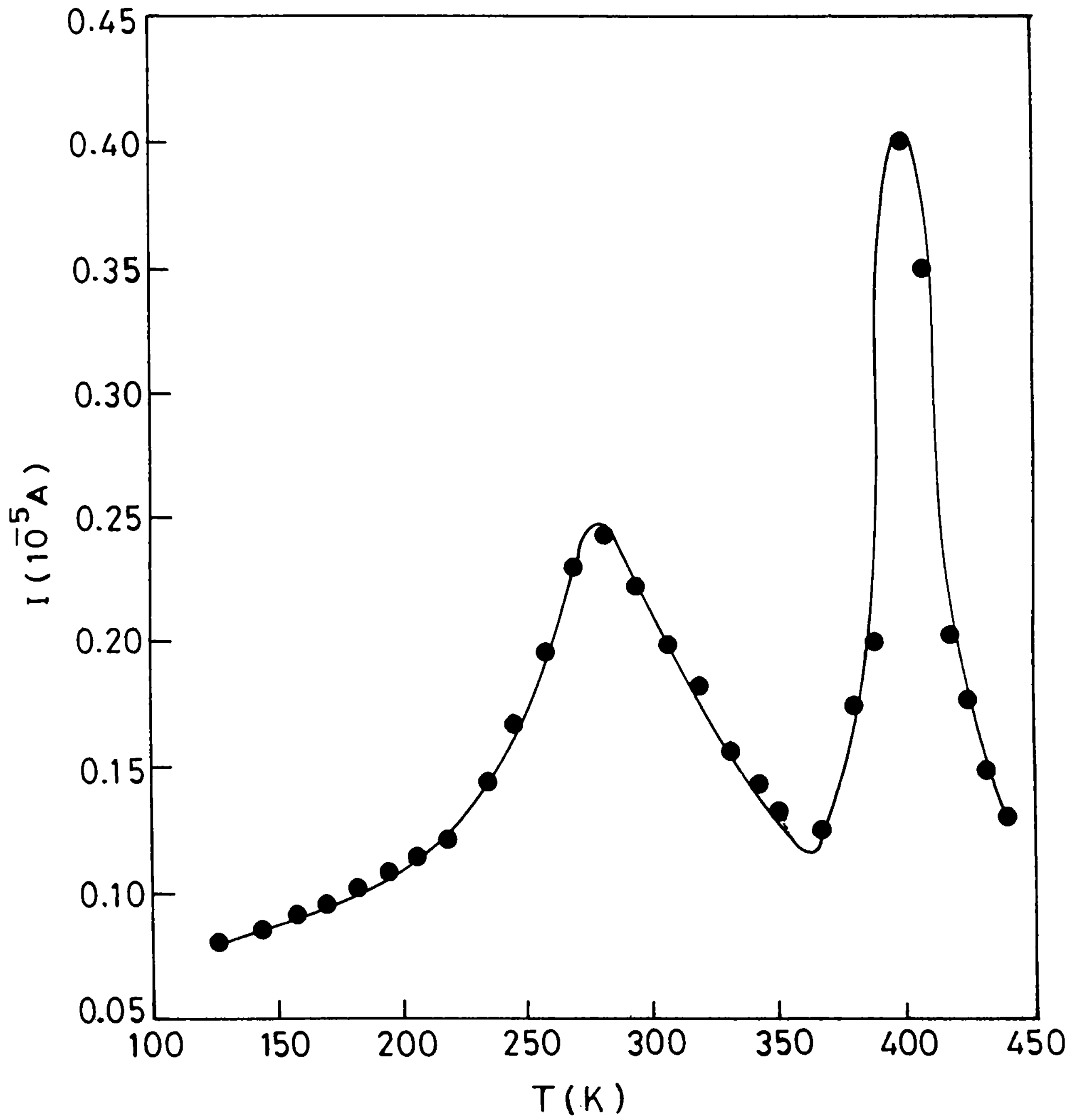

Figure 4.24. TSC spectra of CBD CdS thin film treated with $SnCl_4$ solution and annealed in air.

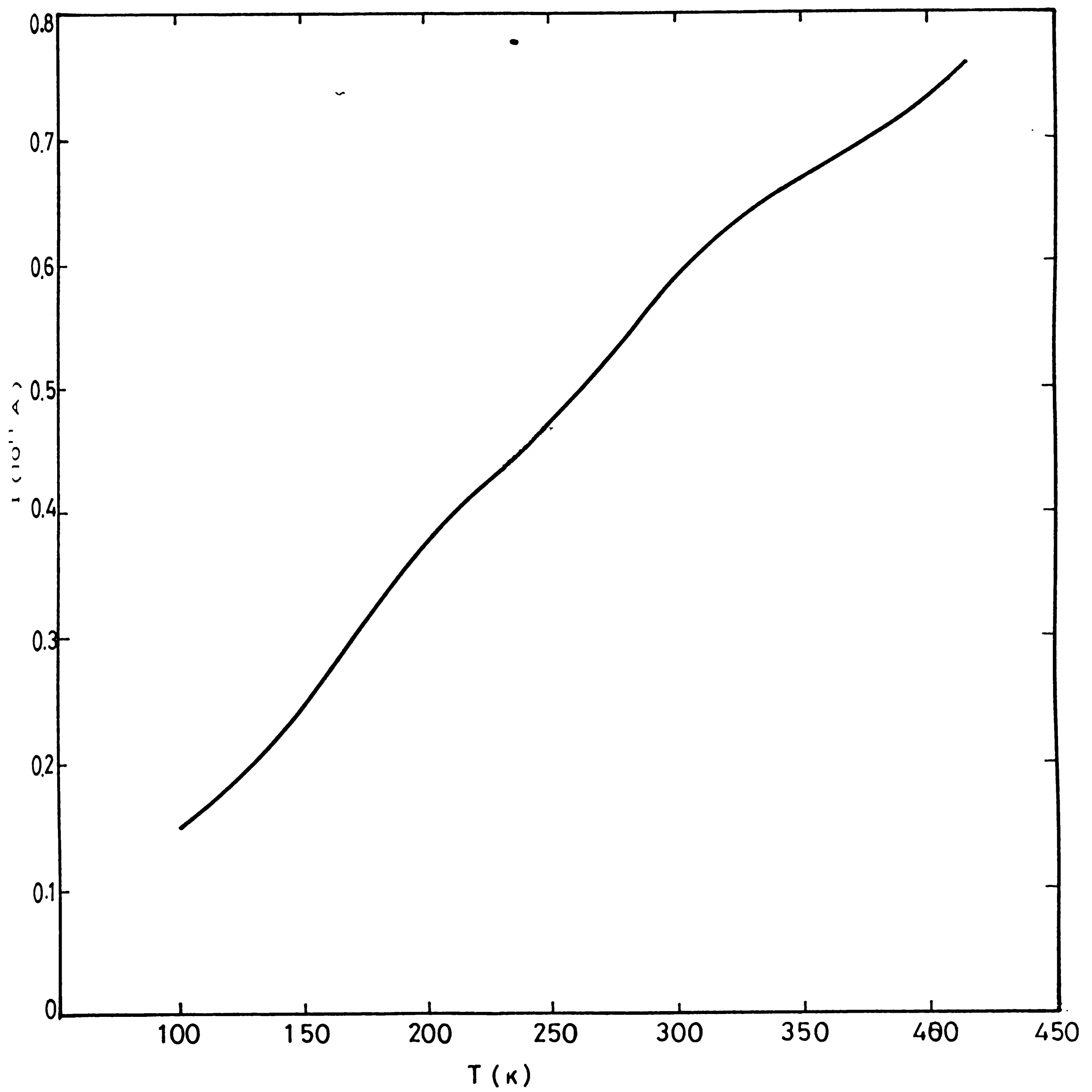

Figure 4.25. TSC spectra of CBD CdS thin film treated with $InCl_3$ solution and annealed in vacuum.

4.7. Conclusion

We conducted TSC measurements on n-and p-type spray pyrolysed CdS thin films in order to study the activation energies of trap levels present in the samples. From TSC measurements we found out mobility of sulphurvacancy as prominent defect in as-prepared and in annealed (both in air and vacuum) n-type CdS samples. But in addition to this S vacancy, as-prepared and vacuum annealed n-CdS samples showed an additional level of complexes of Cd and S vacancies of smaller cross section, which we could detect only under an excitation time of 10 minutes. In the case of air annealed n-CdS samples, even with 10 minutes light excitation, we did not get the presence of complexes of Cd and S vacancies. Instead of that we could get a trap level of chemisorbed oxygen. TSC measurements of p-type CdS give two distinct trap levels, namely S vacancy and Cu impurity, both in the case of 5 minutes and 10 minutes light excitation. A possible explanation is also discussed here and we found that it is the Cu impurity on Cd-S vacancy site that gave p-type conductivity to the CdS films. Nature of different trap levels existing in these samples is also determined. We have also made a study on existing trap levels by dark conductivity measurements in n and p-type CdS samples and these results are found to be in good support of the results obtained from TSC measurements.

As-prepared CBD CdS films are high resistive ($10^7\Omega$ cm) and the variation of sheet resistance with aging and annealing is also included in this study. It is found that CBD CdS films of resistivity 10^5 Ω cm could be obtained after air annealing at 250°C for 3 hours. This chapter also discusses a simple technique of producing low resistive CdS films in which high resistive CdS films were subjected to a post dipping in various solutions of $CdCl_2$, $InCl_3$ and $SnCl_4$. It is also found that the samples dipped in $InCl_3$ showed least resistivity (5 Ω cm) and effect of annealing on the resistivity values of these samples was studied. On annealing in air, resistivity of these samples increased slightly but on the other hand annealing in vacuum resulted in making the sample high resistive again. TSC measurements of high resistive CBD CdS films revealed that the samples contain no defect levels detectable in these measurements. But the low resistive CBD CdS samples indicate the presence of Cd-S vacancy complex, independent S vacancy and chloride ions. Annealing

in air removes the Cd-S vacancy complex, but these samples possess S vacancy and chemisorbed oxygen. TSC measurements of vacuum annealed low resistive CBD CdS films indicate no defect levels and this explains the high resistive nature of these samples.

References

1. L.L.Kazmerski, F.R.White, M.S.Ayyagiri, Y.J.Juang and R.P.Patterson, *J.Vac.Sci.Technol.*, **14**(1977)65
2. C.Wu and R.H.Bube, *J.Appl.Phys.*, **45**(1974)648
3. J.Dressner and f.V.Shallcross, *J.Appl.Phys.*, **34**(8)(1963)2390
4. D.C.Reynolds, G.Leiss, L.L.Antes and R.E.Marburger, *Phys.Rev.*, **96**(1954)533
5. R.H.Bube, *J.Chem.Phys.*, **23**(1)(1955)18
6. R.H.Bube, *J.Appl.Phys.*, **27**(10)(1956)1237
7. J.Woods and D.A.Bright, Proc.of international conf., Brusseles, June 2-7 (1958) p880
8. Peter Mark, *J.Phys.Chem.*Solids, **25**(1964)911
9. David C Look, *J.Appl.Phys.*, **45**(1)(1974)492
10. B.Tell, T.C.Damen and S.P.S.Porto, *Phys.Rev.*, **144**(2)(1966)771
11. M.Marychurch and G.C.Morris, *Surface Science*, **154**(1985)L251
12. H.G.Grimmeis and R.Memming, *Communications*, (1962)3596
13. E.Khawaja and S.G.Tomlin, *J.Phys.D.Appl.Phys.*, **8**(1975)581
14. S.Simov, M.Kalitzova, E.Nikolova and I.Babtov, *Surface Science*, **59**(1976)115
15. Z.Porada and E.Schabowska-Osiowska, *Thin Solid Films*, **175**(1989)249
16. A.L.Dawar, P.K.Shishodia, Gayatri Chauhan, Anil Kumar, and P.C.Mathur, *Thin Solid Films*,**201**(1991)L1
17. A.L.Dawar, P.K.Shishodia, Gayatri Chauhan, Anil Kumar and P.C.Mathur, *J.Appl.Phys.*, **67**(1990)6214
18. A.K.Chaterjee and S.C.Datt, Indian *J.of Pure and Appl.Phys.*, **31**(1993)453
19. Shi Yul Kim, dong Seop Kim, Byung Tae Ahn and Ho Bin Im, *Thin Solid Films*, **229**(1993)227
20. A.Ashour, R.D.Gould and A.A.Ramadan, *Phys.Status Solidi (a)*, **125**(1991)541
21. J.L.Shay, S.Wagner, K.Bachman, E.Buchler and H.M.Kasper, Proc.11th Photovoltaic specialist Conf., Phoenix AZ 1975, IEEE (New York, 1975) p 503
22. R.Krupa and A.Wrzesinska, *Acta Phys.Pol.*, **A53**(1978)675
23. Akio Kuroyanagi and Toshikazu Suda, *Thin Solid Films*, **176** (1989)247
24. D.P.Amalnerkar, S.R.Sainkar and S.Badrinarayanan, *J.Mater.Sci.Lett.*, **8**(1989)862

25. S.Durand, *Thin Solid Films*, **44**(1977)43

26. A.Piel and H.Murray, *Thin Solid films*, **44**(1977)65

27. R.Hill, *Solid-State and Electron Dev.*, **2**(1978)S49

28. M.Arienzo and J.J.Loferski, Proc. 2nd EC Photovoltaic Solar Energy conf., (Berlin, 1979) p 361

29. K.Mitchell, A.L.Fahrenbruch and R.H.Bube, *J.Vac.Sci.Technol.*, **12**(1975)909

30. A.Yoshikawa and Y.Sakai, *J.Appl.Phys.*, **45**(1974)3521

31. N.Croitoru and S.Jakobson, *Thin Solid Films*, **56**(1979)L5

32. Z.Porada and E.Schabowska, *Thin Solid films*, **66**(1980)L55

33. J.Vedel, M.Soubeyrand and E.Castel, *J.Electrochem.Soc.*, **124**(1977)177

34. E.W.Williams, K.Jones,A.J.Griffiths, D.J.Roughley, J.M.Bell, J.H.Steven, M.J.Huson, M.Rhodes and T.Costich, Proc.2nd EC Photovoltaic Solar Energy conf. (Berlin, 1979) p874

35. R.R.Chamberlin and J.S.Sakarman, *J.Electrochem.Soc.*, **113**(1966)86

36. Yale Y Ma and R.H.Bube, *J.Electrochem.Soc.*, **124**(9)(1977)1430

37. B.K.Gupta, O.P.Agnihotri and Ahmar Raza, *Thin Solid Films*, **48**(1978)153

38. J.W.Orton, B.J.Goldsmith, J.A.Chapman and M.J.Powell, *J.Appl.Phys.*, **53**(3)(1982)1602

39. H.L.Kwok, *J.Phys.D.Appl.Phys.*, **13**(1980)1911

40. A.G.Valyomana, Sunny Mathew, K.P.Vijayakumar and C.Purushothaman, *Bull.Mater.Sci.*, **16**(1)(1993)55

41. Sunny Mathew and K.P.Vijayakumar, *Bull.Mater.Sci.*, **17**(3)(1994)235

42. Sunny Mathew, P.S.Mukerjee and K.P.Vijayakumar, *Thin Solid Films*, **254**(1995)278

43. N.A.pavaskar, C.A.Menezes and A.P.B.Sinha, *J.Electrochem.Soc.*, **124**(1977)743

44. G.Martinez and J.L.Martinez, *Appl.Phys.Lett.*, **40**(12)(1982)1031

45. D.P.Amalnerkar, M.S.Setty, S.K.Date and A.P.B.Sinha, *Indian J.of Pure and Appl.Phys.*, **22**(1984)662

46. Shailaja Kolhe, S.K.Kulkarni, A.S.Nigavekar and S.K.Sharma, *Solar Energy Materials*, **10**(1984)47

47. P.K.Nair,M.T.S.Nair and J.Campos, *Solar Energy Materials*, **15**(1987)441

48. P.K.Nair, M.T.S.Nair, J.Campos and L.E.Sansores, *Solar Cells*, **22**(1987)211

49. P.K.Nair, J.Campos and M.T.S.Nair, *Semicond.Sci.Technol.*, **3**(1988)134

50. Hiroshi UDA, Seiji Ikegami and Hajimu sonomura, *Jpn.J.Appl.Phys.*, **29**(1)(1990)30

51. P.J.Sebastian, J.Campos and P.K.Nair, *Thin Solid Films*, **227**(1993)190

52. O.Zelaya-Angel, J.J.Alvarado-Gil, R.Lozada-Morales, H.Vargas and A.Ferreira da Silva, *Appl.Phys.Lett.*, **64**(3)(1994)291

53. O.de Melo, L.Hernandez, O.Zelaya-Angel, R.Lozada-Morales and M.Becerril and E.Vasco, *Appl.Phys.Lett*, **65**(10)(1994)1278

54. L.Hernandez, O.de Melo. O.Zelaya-Angel and R.Lozada-Morales, *J. Electrochem. Soc.*, **141** (1994)3238

55. R.Jayakrishnan, S.R.Kumar and R.K.Pandey, *Semicond.Sci.Technol.*, **9**(1994)97

56. S.Kolhe, S.K.Kulkarni and A.S.Nigavekar, *Solar Energy Materials*, **10**(1984)47

57. S.A.Tomas, O.Vigil, J.J.Alvarado-Gil, R.Lozada-Morales, O.Zelaya-Angel, H.Vargas and A.Ferreira da Silva, *J.Appl.Phys.*, **78**(1995)2204

58. I I Yu, Tetsuhiko Isobe and mamoru Senna, *Materials Research Bulletin*, **30**(1995)975

59. S.S.Kale, U.S.Jadhar and C.D.Lokhande, *Ind.J.of Pure and Appl.Phys.*, **34**(1996)324

60. K.L.Narayanan, K.P.Vijayakumar, K.G.M.Nair and G.V.N.Rao, *Bull.Mater.Sci.*, **20** (3)(1997)287

61. K.L.Narayanan, K.P.Vijayakumar, K.G.M. Nair, N.S.Thampi and K.Krishnan, *J.Mat.Sci.*, **32**(1997)4837

62. W.W.Anderson and J.T.Mitchell, *Appl.Phys.Letts.*, **12**(10)(1968)334

63. W.R.Parikh, D.A.Thompson and G.J.C. Carpender, *Radiation effects*, **98**(1986)289

64. Ratna Sagar and M.P.Srivastava, *Phys.Lett.A*, **183**(1993)209

65. P.K.Govind and F.J.Fraikor, *J.Appl.Phys.*, **42**(1971)2476

66. B.Tell and W.M.Gibson, *J.Appl.Phys.*, **40**(1969)5320

67. Masafumi Yamaguchi, *Jpn.J.Appl.Phys.*, **15**(1976)723

68. R.O.Chester, *J.Appl.Phys.*, **38**(1967)1745

69. M.Kitagawa and T.Yoshida, *Appl.Phys.Lett.*, **18**(1971)41

70. M.Kitagawa and F.J.Bryant, *Radiation effects*, **33**(1977)181

71. K.L.Narayanan, K.P.Vijayakumar, K.G.M.Nair, B.Sundarakkannan, G.V.N.Rao and R.Kesavamoorthy, *Nucl.Instr.Meth.Phys.Res.*,**B132**(1997)61

72. K.L.Narayanan, K.P.Vijayakumar, K.G.M.Nair and N.S.Thampi, *Physics Status Soilidi (b)*, **240**(1997)8

73. G.Venugopal Rao, G.Amarendra, B.Viswanathan, K.L.Narayanan and K.G.M.Nair, Solid State Physics (India) **Vol 39**C (1996)219

74. A.L.Fahrenbruch and R.H.Bube, Fundamental of *Solar Cells* (Academic Press, London,1983) p 425

75. D.C.Reynolds, L.C.Greene, R.G.Wheeler and R.S.Hogan, *Bull.Am.Phys.Soc.*, **1**(1956)111

76. J.Woods and J.A.Champion, *J.Electron and Control*, **3**(1960)243

77. H.G.Grimmeiss and R.Memming, *J.Appl.Phys.*, **33**(1962)3596

78. M.Lichtensteiger, I.Lagnado and H.C.Gatos, *Appl.Phys.Letters*, **15**(12)(1969)418

79. E.R.Pollard and J.L.Hartke, *Bull.Am.Phys.Soc.*, **14**(1969)115

80. Y.Shiraki, T.Shimada and K.F.Komatsubara, *J.Appl.Phys.*, **43**(1972)710

81. F.Chernow, G.Ruse and L.Wahim, *Appl.Phys.Lett.*, **12**(1968)339

82. S.Keitoku, H.Ezumi, H.Osono and M.Ohta., *Jpn.J.Appl.Phys.*, **34**(1995)138

83. Y.Kashiwaba, I Kanno and T.Ikeda, *Jpn.J.Appl.Phys.*,**31**(1992)1170

84. Y.Kahiwaba, A.Tada and I.Ikeda, *Jpn.J.Appl.Phys.*, **33**(1994)L1613

85. P.J.Sebastian, *Appl.Phys.Lett.*, **62**(1993)2956

86. Sunny Mathew,P.S.Mukherjee and K.P.Vijayakumar, *Jpn.J.Appl.Phys.*,**34**(1995) 4940

87. K.P.Varkey and K.P.Vijayakumar, *Jpn.J.appl.Phys.*, **36**(1997)L394

88. K.P.Varkey, K.P.Vijayakumar, Jun Imai, Toshihiro Yoshida and Y.Kashiwaba, *Bull.Mater.Sci.*, **20**(8)(1997)1085

89. R.Chandra Sekhar, K.N.Raju, D.Raja Reddy and B.K.Reddy, *J.Phys.D:Appl.Phys.*, **21**(1988)1182

90. T.L.Chu, S.S.Chu, J.Britt, C.Ferekides, C.Wang, C.Q.Wu and H.S.Ullal, *IEEE Electron Device Lett*, **43**(1992)303

91. J.Britt and C.Ferekides, *Appl.Phys.Lett.*, **62**(1993)2851

92. S.R.Das, P.Nath, A.Banerjee, K.L. Chopra, *Solid State Commun.*, **21**(1977)49

93. L.M.Fraas and Y.Ma, *J.Cryst.Growth*, **39**(1977)92

94. Kenneth Zwibel, Harin S Ullal and Bolko G VonRoedern, 25th IEEE Photovoltaic specialist conf. (Washigton DC,1996) p 159

95. J.J.Loferski, Proc.16th IEEE Photovoltaic specialist conf., (San Diego, 1982) p312

96. P.K.Vidyadharan Pillai, K.P.Vijayakumar, *Solar Energy Materials and Solar Cells*, **57**(1998)47

97. H.B.Im, H.E.Mathews and R.H.Bube, *J.Appl.Phys.*, **41**(1970)2581

98. E.Tscholl, *Philips Res.Rep.Suppl.*, **6**(1968)

99. Reddy D Raja, B.K.Reddy and P.J.Reddy, *J.Phys.D.Appl.Phys.*, **16**(1983)645

100.O.Vigil, E.Vasco and O.Zelaya-Angel, *Mater.Lett.*, **29**(1996)1

101.A.G.Valyomana, K.P.Vijayakumar and C.Purushothaman, *J. Mater. Sci. Lett.*, **9**(1990) 1025

102.A.G.Valyomana, Ph D Thesis, Cochin University of Science and Technology, 1992.

103.T.W.Kang, C.Tong, J.Y.Leem, T.W.Kim, *J.Appl.Phys.*, **69**(5)(1991)3115

104.Lars Stott and Jonas Hedstrom, *Appl.Phys.Lett.*, **6**(1993)597

105.Takayuki Negami, Mikihiko Nishitani, Mitusuke Ikeda, Takahirowada, *Solar Energy Materials and Solar Cells*, **35**(1994)215

106.A.Mandal, T.K.Chaudhuri and P.Pramanik, *Solar Energy Materials*, **7**(1983)431

107.Ito, kazuao,Shiraishi and Kanehiro, *Solar Energy Materials and Solar Cells*, **35**(1-4)(1994)179

108.M.T.S.Nair, P.K.Nair,R.A.Zugaro,E.A.Meyers, *J.Appl.Phys.*,**75**(3)(1994)1557

109.Kim, Shi Yul, dong Seop, Ahn, Byung Tae, IM, Ho Bin, *J.Mater.Sci.Mater.Electron*, **4**(2)(1993)178

110.P.K.Vidyadharan Pillai, Ph D. Thesis, Cochin Uty of Sci.and Technol., 1997.

111.N.A.Zeenath, S.Bini, S.B.Syamala, C.Sudha Kartha, K.P.Vijayakumar, Jun Imai, Toshihiro Yoshida and Yasube kashiwaba, *Europhysics Letters*- (paper under revision)

112.J.Wood and K.H.Nicholas, *Brit.J.Appl.Phys.*, **15**(1964)1361

113.P.Mark, *J.Phys and Chem Solids.*, (GB) **26**(1965)959, **26**(1965)1767

114.D.P.Amalnerkar, M.S.Setty, S.K.Date and A.P.B.Sinha, *Indian J of Pure and Appl.Phys.*, **22**(1984)662

Chapter 5
TSC Measurement of CBD $CuInSe_2$ thin films

5.1. Introduction

In recent years the number of papers published in I-III-VI_2 compound semiconductors has increased considerably. Much effort has been devoted to gain a better understanding of the electronic, electrical and optical properties of these compounds, since some of these material have potential for practical applications in the fabrication of devices [1,2] for instance, in non-linear optics, light emitting diodes, optical detectors and solar cells. This class of ternary semiconductors crystallise in chalcopyrite structure and are ternary analogues of the binary II-VI compounds (ZnS, ZnSe, CdS etc.). They cover a wide-gap range (1.0-2.5 eV) and all of them have very small lattice mismatch with CdS, which is a wide band gap semiconductor, very much used in heterojunction solar cells, as an n-type window. Moreover, most of them can be made either n- or p-type conducting. Hence chalcopyrites are very important in the field of photovoltaics.

$CuInSe_2$ (CIS) whose binary analogue is $Cd_{0.5}\,Zn_{0.5}$ Se, is one member of this family of compounds that was originally studied by Hahn et al [3]. It crystallises in chalcopyrite structure with lattice parameters a=5.785 A^o and c/a=2 at room temperature [4]. CIS has a direct band gap between 0.94 and 1.06 eV [5,6] depending upon the growth and annealing conditions. In contrast to II-VI binary analogue, it can be made either n-or p-type [7,8]. The band structure, large absorption coefficient ($>1\times10^5$ cm^{-1}) and possibility of making n or p-type conducting make this material a strong candidate for photovoltaic application. In 1975, Shay et al [9] have reported 12% efficient solar cell involving CdS epitaxially grown on single crystals CIS. Recently CIS based thin film solar cells have shown 17.7% efficiency [10] which is the highest efficiency of a thin film single junction solar cell and this indicates the importance of this material in the field of terrestrial photovoltaic applications.

The three requirements of a photovoltaic cell for large scale terrestrial use are high efficiency, good stability and low cost. The CdS/CIS thin film cell, which is at present under intensive investigation, can fulfil the first two requirements. The cost of the cell is determined, to a major extent, by the method of preparation of the semiconductor layers. Recently the low cost production of CIS thin films using CBD technique has been reported by Vidyadharan Pillai et al [11] from our laboratory itself. Later they could fabricate CIS/CdS thin film solar cells [12] using CBD technique, but with low value (3.1%) of efficiency. One of the factors affecting the efficiency of thin film solar cells is the electrical properties of the film which in turn depends mainly on the presence of different trap levels. The electrical properties of I-III-VI_2 compounds are believed to be dominated by the presence of intrinsic defects such as Cu, In, Se vacancies and interstitials [7]. A better knowledge of the properties of intrinsic and extrinsic impurities /defects in CIS is necessary in order to improve the efficiency of CIS based solar cells. This chapter describes the TSC measurements of the chemical bath deposited CIS thin films and dark conductivity measurements. The first part of the chapter presents a review of work done in CIS semiconductor material and is followed by the description of present work.

5.2. An overview of works on $CuInSe_2$

Electrical properties and luminescence spectra of CIS (melt-grown) single crystals were reported as early as in 1975 [7]. Later Phil Won Yu reported [13] the behaviour of the low temperature emission spectra of melt grown p-type and Cd implanted n-type CIS with changes in temperature and exciton intensity. In 1978, the optical properties of flash evaporated CIS thin films were studied in the photon energy range from 1 to 3 eV by Horig et al [14].

Studies on epitaxial layers of CIS on GaAs substrates were reported in 1978 by Schumann et al [15]. Films produced at $T_{sub} \leq 720$ K were found to be n-type and those formed at higher temperature were p-type. Two different acceptor levels with ionisation energies 92 meV and 400 meV were found in those samples. In 1979, electrical and optical properties of thin p-type films prepared by vacuum evaporation from the chalcopyrite CIS

had been reported by A.F. Fray [16]. Growth of CIS thin films using molecular beam epitaxy had been reported by Grindle et al [17]. They also fabricated CIS/CdS heterojunction that exhibited a maximum solar conversion efficiency of ~ 5%.

Later in 1982, Clayton et al reported [18] the production of CIS thin films using spray pyrolysis. They suggested optimum spray conditions by thermodynamical calculation using a free energy minimisation computer program applied to Cu-In-Se system. Heat treatments of these films were performed in order to produce conductivities and crystal structures for photovoltaic applications and are discussed in detail. Following this, 11% conversion efficiency and excellent stability with a Cd(Zn)S/CIS structure had been reported [19]. Analysis of CIS crystals using luminescence study had been reported by Rincon et al [20] in 1983. They obtained an absorption edge at (1.023 ± 0.003)eV, a donor state at (10 ± 2) meV and an acceptor state at (33 ± 2)meV. Deposition of CIS films using coevaporation of Cu, In and Se and their electrical and crystalline properties were reported by Varela et al [21,22]. Following this work, totally sprayed thin film solar cells of CIS/Cd(Zn)S with efficiency of about 3% was reported by Polla Raja Ram et al [23]. Later the phenomenon of photoluminescence and photoconductivity of CIS single crystals were reported by Lange et al [24].

In the year 1986, wonderful progress was made in the field of CIS thin films and CIS based solar cells and numerous publications are available during this period. A detailed study of transport properties of CIS crystal had been reported by S.M. Wasim [25]. In that work possible origins for different donor and acceptor levels derived from electrical and optical measurements were suggested. From thermal conductivity measurements, the presence of Fe as Fe_{In}^{3+} in some CIS samples was also confirmed. Electrodeposition of CIS thin films was reported by Gary Hodes et al [26]. They also reported morphological, compositional and photoelectrochemical behaviour of these layers. Almost at the same time, Isomura et al published a paper [27] on dc sputtering and vacuum evaporation of CIS films from synthesised bulk materials. Later electrical and optical properties of CIS thin films were reported by Sridevi et al [28] and these films were p-type having an acceptor level due to Cu vacancy of activation energy 100 meV.

Photo electrical properties of CIS thin films prepared using flash evaporation and electron beam evaporation were reported by Trykozko et al [29]. This paper presents a comparison of the photoconductivity and absorption measurements leading to the conclusion that the quantum efficiency is constant over the energy range investigated. Fabrication process of CIS/CdS cells using physical vapour deposition along with a detailed description of the deposition system used to grow CIS films had been reported by Birkmire et al [30]. They could prepare high efficiency (11.1%) solar cells over a broad range of processing conditions with excellent thermal stability. Later role of oxygen in CIS thin films and CdS/CIS devices was reported by Noufi et al [31]. This work showed that treating the device in a solution of chemical oxidant has the same effect as that due to annealing in air. Again results of oxidation can be reversed by treating the device in a solution of reducing agent. This paper also gave some methods by which we can use the oxygen in this material to improve the electrical properties and there by the performance of CdS/CIS device. Later CIS based thin film tandem solar cells had been reported by Meakin et al [32]. TSC measurements in p-type CIS films prepared using coevaporation of the elements had been reported by Datta et al [33]. They found that annealing in air appears to passivate TSC activity and they could detect three defect levels at 35, 45 and 100 meV in those samples.

In 1987, Martil et al published a paper [34] on CIS thin films prepared using RF sputtering in Ar/H_2 atmosphere. They could prepare chalcopyrite polycrystalline CIS thin films of grain size 1μ m, having optical band gap 1.01 eV and resistivity in the range from 10^{-1} to 10^{-3} Ω cm. CdS induced homojunction formation in crystalline p-type CIS was reported by Matson et al [35]. In that work it was suspected that the deposition of CdS onto single crystal (p-type) CIS at $200^{o}C$ resulted in a CIS homojunction rather than the expected heterojunction. All materials like CdS, Cd, Au and Mo deposited have resulted in p-type conversion and experimental evidence for conversion was presented along with possible origin of defects. People were also concerned with health and safety condition required in the research and large scale production of CIS based solar cells. There is publication [36] in this direction also.

There had been some interest in the preparation of p-type CIS thin films for photovoltaic application using Chemical Bath Deposition technique. Garg et al reported [37] the deposition of stoichiometric (1:1:2) films using this technique. These films had a band gap of 1.15 eV, absorption coefficient $\sim 10^5$ cm^{-1} and a p-type resistivity of 10^3 Ω cm. Study of deep levels using Deep Level Transient Spectroscopy (DLTS) in CIS films and fabrication of CdS/CIS solar cells had been reported in 1989 by Christoforou et al [38]. They could detect a hole trap of concentration 5×10^{-4} cm^{-3} located 0.7 eV above VB edge and an electron trap of concentration 5×10^{13} cm^{-3} located 0.35 eV below the CB edge. By the end of 1988, CIS solar cells of efficiency 14.1% had been reported [39] in which they used the structure ZnO/thin CdS/CIS/Mo glass.

Effect of annealing on the optoelectronic properties of $Cu_{0.9}$ In_1 Se_2 films was reported by Sharma et al [40] and they found that annealing in In vapour or in vacuum changes p-type CIS into n-type that is possibly caused by the increase in Se vacancies. Enhanced grain growth in polycrystalline CIS films using "rapid thermal processing" was observed in 1990 by Albin et al [41]. Later cathodic electrodeposition of CIS thin films was reported by Guillen et al [42] and XRD analysis showed the formation of CIS films of chalcopyrite structure at temperature higher than 350°C.

Fabrication of CIS based photoelectrochemical cells was reported by J.W. Chu et al [43] and annealing effects on individual loss mechanism in these cells were reported by Sasala et al [44]. Large area CIS based cell modules were demonstrated by Mitchell et al [45] and an efficiency of 14.1% could be achieved on 940 cm^2 modules. The preparation and properties of selenized CIS thin films were reported by Kim et al [46]. These films that have mole ratios larger than 0.28 had a chalcopyrite phase and those having lower ratios were with a sphalerite phase. Films containing Cu_xSe phase had a Cu-rich phase while those without Cu_xSe had an In-rich phase. Later the photoluminescence study of CIS thin films was reported by Tanda et al [47].

The steady state and transient photoconductivity measurements on CIS films prepared using solution growth technique had been performed as a function of temperature and illumination intensities by Manorlal et al [48]. They found that photoconductivity increases exponentially with increasing temperature and photocurrent obeys a power law $I_{ph} \alpha F^{\gamma}$, where γ has value close to 0.5 and F is the light intensity level. By the end of 1993, fabrication of CIS solar cells on flexible foil substrates was reported by Bulent et al [49]. Flexible devices of Mo/CIS/CdS/ZnO heterojunction were fabricated on Mo foils with conversion efficiency of above 8 % in this work.

In 1994, surface-sensitive UV photoelectron yield spectroscopy was employed to study electron acceptor levels at the surface of chalcopyrite structure Cu-In-Se thin films by Shigemi Kohiki et al [50]. Shallow acceptor levels ascribable to defects Cu_{In} and V_{cu} were observed for near -stoichiometric and In-rich films. Another method developed for growing low cost and large area CIS thin films was close-spaced vapour transport in a vertical closed tube [51]. Nearly stoichiometric films were grown at temperature as low as 350°C with deposition rate of 0.5μm/min and grain size of the order of 1μm. Supersaturate type CIS solar cells were fabricated by preparation of CIS films on CdS films. These films had large grains and this work was reported by Takayuki Negami et al [52]. The best cell performance obtained was V_{oc}=0.357V, J_{SC} = 32.2mA/cm^2 FF= 0.582 in 0.075cm^2 area and with η =6.71 %. Room temperature deposition of CIS thin films using simple CBD technique was reported by Vidyadharan Pillai et al [11] during the same period. They obtained p-type films of band gap 1.3 eV (unannealed), 1.01 (vacuum annealed) and having absorption coefficient 1.8×10^5 cm^{-1}.

Recently, solid-liquid reaction mechanism in the formation of high quality CIS by the Stacked Elemental Layer (SEL) technique was developed by Adurodija et al [53]. The nature of the deposited single layer of Cu, In and Se and the reactions involved in the binary compounds Cu-Se, In-Se and Cu-In after annealing at different temperature was used to provide evidence for the formation of CIS from the ternary compound Cu-In-Se using XRD, EDX, and SEM. The formation of CIS thin films by selenization employing CVTG (chemical vapour transport by gas) of electroless deposited Cu-In alloy was also reported

during this period by Sebastian et al [54]. Growth of CIS films on glass and SnO_2 thin films using a close spaced vapour transport in closed tube using diode was reported in 1996 by Masse et al [55]. Samples were analysed using X-ray and SEM. They showed that films grown on SnO_2 surface can have very strong (100) or (001) preferred orientation probably induced by the substrate and not by the experimental condition.

In 1996, flexible and light weight CIS solar cells on polyimide substrates had been developed by Bosol et al [56] and high efficiency graded band gap thin film polycrystalline $Cu(InGa)Se_2$ based solar cells were reported by Miguel A Contreras et al [57]. In the second work, several devices with total area conversion efficiency above 16% (the highest measuring 16.8% under standard reporting condition) were developed. Achievement of a 17.2% device efficiency fabricated for operation under concentration (22 sun) was also reported in that work. All high efficiency devices reported were made from compositional graded absorbers.

Very recently in 1997, electrical conductivity of flash evaporated CIS films were reported [58]. The p and n-type films deposited at substrate temperature of 373 and 423K indicate impurity conduction at temperature lower than 290 K. A $T^{-1/4}$ dependence of conductivity was observed for the film due to variable-range hopping of carriers. Effects of annealing on CIS films grown by MBE [59], structural and optical properties of electrodeposited CIS layer [60] and electrical properties of Na incorporated $Cu[In_{1-x}Ga_x]Se_5$ thin films [61] were reported in the same year. Improved compositional flexibility of $Cu(InGa)Se_2$ based thin film solar cells by sodium control technique [62], improved performance of $Cu(InGa)Se_2$ thin films solar cells using evaporated Cd free buffer layers [63], fabrication of graded band-gap $Cu(InGe)Se_2$ thin film mini modules with a $Zn(O,S,OH)_x$ buffer layer [64], improved $Cu(InGa)(S,Se_2)$ thin film solar cells by surface sulfurization [65] and examination of blocking current voltage behaviour through defect chalcopyrite layer in $ZnO/CdS/Cu(InGa)Se_2/Mo$ solar cells [66] were also reported in 1997. More publications on Raman spectra of sprayed CIS films [67], effect of crystal symmetry on electronic properties of CIS and related compounds [68] are available during the same

period. Later in 1998, Vidyadharan Pillai et al reported low cost CIS/CdS thin film solar cells of efficiency 3.1 % fully prepared using CBD technique [12].

5.3. Experimental Details

Thin films of CIS were prepared using CBD technique from a deposition mixture at 25°C containing aqueous solutions of ions of copper, indium and selenium which is maintained at pH of ~ 6.5. More details of the preparation are described elsewhere [11,12]. Samples were annealed in air and vacuum (10^{-2} Torr) in the temperature range from 423 K to 473 K for 1 hour. Silver paint contacts were given to the sample and its ohmic nature was verified.

We conducted TSC measurements of as-prepared CIS samples as well as annealed samples using the experimental set up discussed in chapter 3. Here the duration of optical irradiation time was varied from 1-4 minutes.

For dark conductivity measurements, thickness of the sample was measured using gravimetric method. Films of thickness 250 nm were used in these experiments The details of the experimental set up used for dark conductivity measurements were also described in chapter 3. Conductivity of the sample was measured at different temperatures in the range 100 K to 500 K. These measurements were also carried out for both as-prepared and annealed samples.

5.4. Results and Discussion

5.4.1. TSC Measurements

TSC spectra of as-deposited CIS samples under 1, 2 and 4 minutes light excitation is shown in figure 5.1. With 1 and 2 minutes light excitation, the TSC spectra exhibited only one peak whose activation energy was calculated to be 70 meV (Table 1). But the spectra of same type of sample showed one more peak of activation energy 40 meV on increasing the light excitation time to 4 minutes. Since the sample was not doped, the defect observed

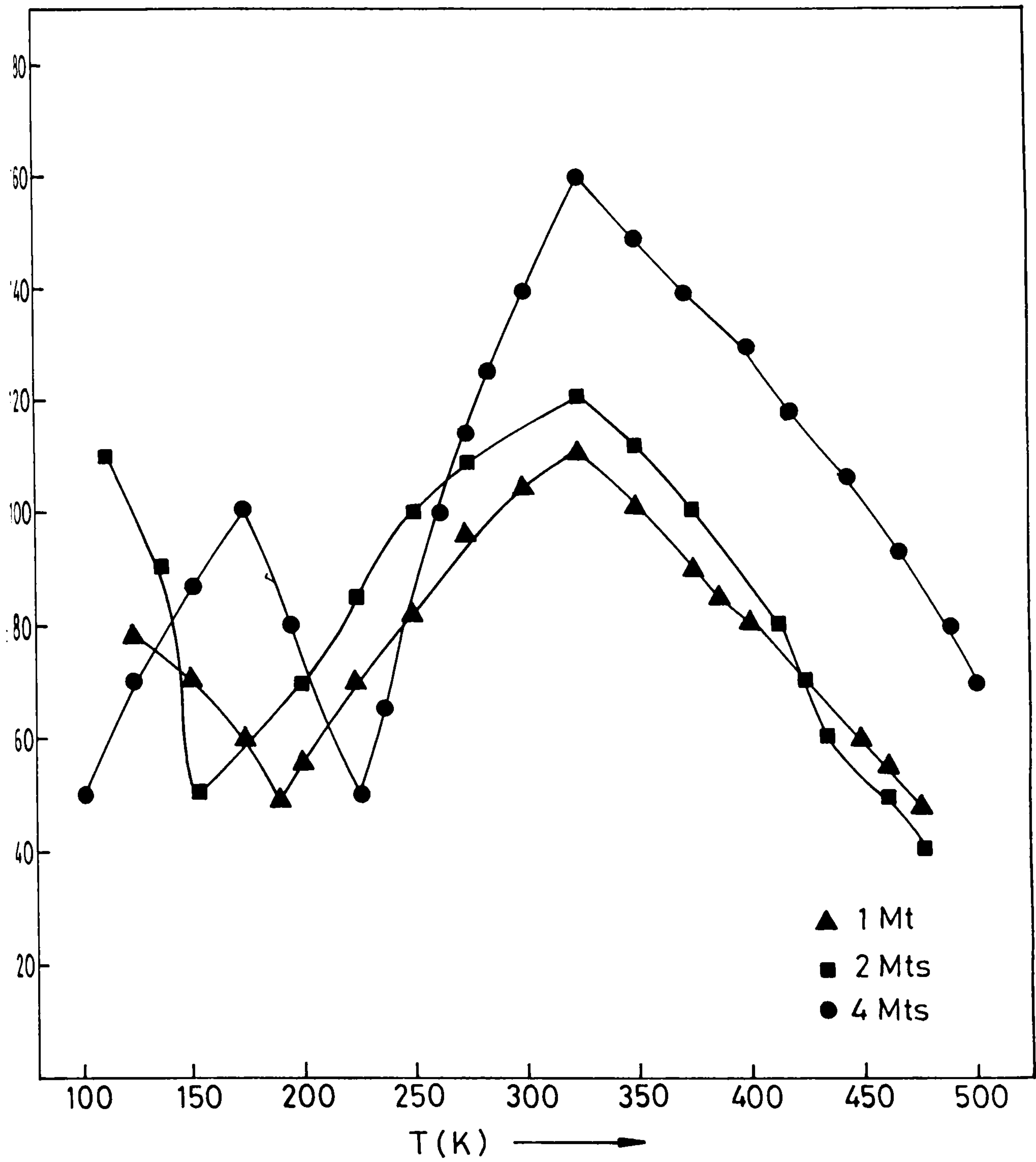

Figure.5.1.TSC spectra of as-deposited CBD CIS samples under different excitation time

Table 1.Values of activation energy of various trap levels in $CuInSe_2$ thin film samples obtained from TSC measurement

Sample type		Activation energy (meV) for different light excitation time 1mt.	2 mts.	4 mts
Unannealed		70.08±0.52	70.08±0.81	1) 70.08±0.54 2) 40.63±0.58
Air annealed at	150°C	220.8±1.38	219.8±1.35	1) 220.7±1.48 2) 40.63±0.58
	175°C	220.8±1.38	220.8±1.38	1) 220.8±1.38 2) 85.28±1.01
	200°C	220.8±1.38	220.6±1.38	1) 220.8±1.38 2) 85.18±1.07
Vacuum annealed at	150°C	70.89±0.55	70.62±0.54	1) 70.89±0.55 2) 400.2±4.85
	175°C	70.02±0.60	70.89±0.55	1) 70.89±0.55 2) 400.43±4.56
	200°C	70.62±0.54	70.02±0.6	1) 70.89±0.55 2) 400.23±2.94

must be intrinsic. It was reported earlier that the donor level of 70 meV was probably due to selenium vacancy [47,69]. Selenium is volatile and vacancies occur during the deposition process itself. The level having activation energy of 40 meV had been reported to be an acceptor level [12] and was attributed to Cu vacancy by Migliorato [7]. Presence of acceptor and donor levels due to Cu and Se vacancies respectively had been suggested by Yu [13] also. It had been suggested that copper vacancies were easily formed in CIS because copper could participate weakly in the covalent bonding [70]. From photoluminescence study also, an acceptor level of 40 meV was identified and attributed to Cu vacancy by M. Tanda et al

[47]. The values of capture cross section of these trap levels are given in table 2. From the table it is very clear that the cross section of acceptor level is very small compared to that of donor level. Probably this may be the reason why the level corresponding to Cu vacancy (acceptor level) becomes "visible" only after the irradiation for 4 minutes.

Table 2. Values of capture cross sections of various trap levels in $CuInSe_2$ thin film samples obtained from TSC measurement.

Sample type		Capture Cross Section (10^{-26} cm^2) for different Light excitation time		
		1 mt.	2 mts.	4 mts.
Unannealed		4.62×10^{-3}	4.68×10^{-3}	1) 4.62×10^{-3} 2) 0.10×10^{-3}
Air annealed at	150°C	0.481	0.402	1) 0.475 2) 0.011
	175°C	0.481	0.481	1) 0.481 2) 0.142
	200°C	0.481	0.475	1) 0.481 2) 0.160
Vacuum annealed at	150°C	4.81×10^{-3}	4.68×10^{-3}	1) 4.81×10^{-3} 2) 3.28×10^{-3}
	175°C	4.62×10^{-3}	4.81×10^{-3}	1) 4.81×10^{-3} 2) 3.80×10^{-3}
	200°C	4.68×10^{-3}	4.68×10^{-3}	1) 4.81×10^{-3} 2) 3.26×10^{-3}

TSC spectra of CIS samples annealed in air at different temperature (at 150, 175 and 200°C) are depicted in figure 5.2-5.4. With 1 and 2 minutes light excitation TSC spectra of all samples show only one peak (irrespective of annealing temperature) corresponding to a level having activation energy 220 meV. It was reported that this level corresponds to donor level and no clear reason for its existence was given [71-72]. But here the Se vacancy, which existed in as-deposited sample, disappeared on air annealing and donor level of 220 meV appears. Under this circumstances, we conclude that the 220 meV donor level may be due to the adsorption of oxygen during air annealing in the Se vacancy of as-deposited samples. With 4 minutes excitation time, these samples gave one more peak of smaller capture cross section compared to that of previous one and this again corresponds to Cu vacancy. In the case of sample annealed at 150°C, the corresponding activation energy is 40 meV (Cu vacancy) while in the samples annealed at 175°C and 200°C it is found to be 85 meV. It was reported by M.Tanda et al [47] that the level corresponding to 85 meV was also due to Cu vacancy. Hence it is concluded that air annealed samples have Cu vacancy with smaller capture cross section as in the case of as-deposited samples.

Figures 5.5 - 5.7 show the TSC spectra of CIS samples annealed in vacuum (10^{-2} Torr) at different temperature (423-473 K). As in the case of air annealed samples. These samples also showed one peak irrespective of annealing temperature under 1 and 2 minutes light excitation. Activation energy of this trap level was found to be 70 meV, which is the donor level of Se vacancy similar to the case of as-deposited samples. After 4 minutes light excitation, these samples showed an additional peak of smaller capture cross section having trap depth of 400 meV. A similar acceptor level was detected by S.M. Wasim [25] in CIS from thermal conductivity measurements and this was attributed to be due to Fe impurity. Many other authors [15,72,73] detected Fe impurity in CIS samples. The existence of Fe impurity in CIS as a contamination in Cu was observed from electron paramagnetic resonance [74,75] also. In the present investigation, we prepared the CIS samples using CBD from a reaction bath containing aqueous solutions of salts of copper, indium and selenium as mentioned earlier. Fe impurity can come from (most probably)

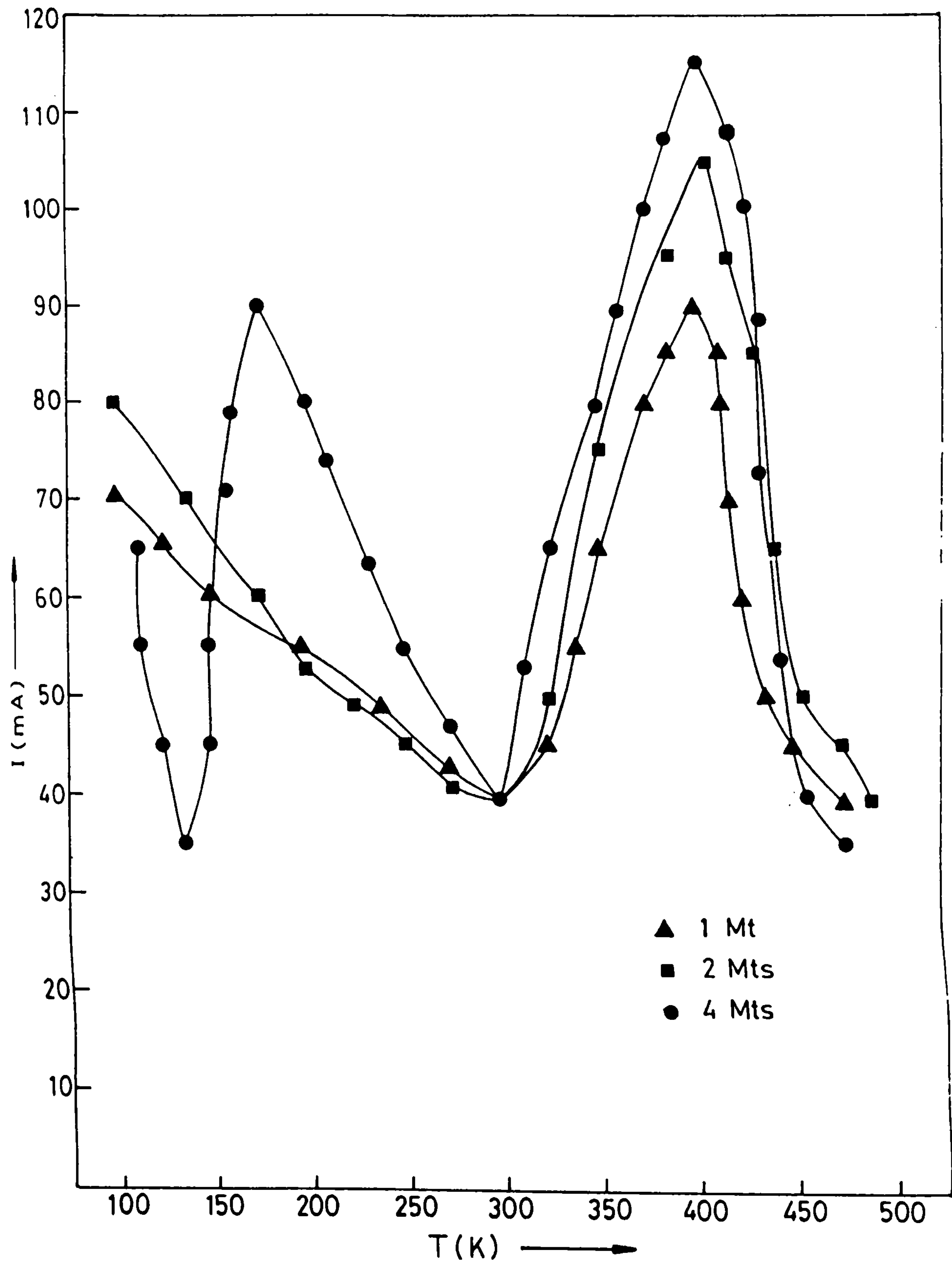

Figure 5.2 TSC spectra of CBD CIS film annealed in air at 150°C for different excitation time

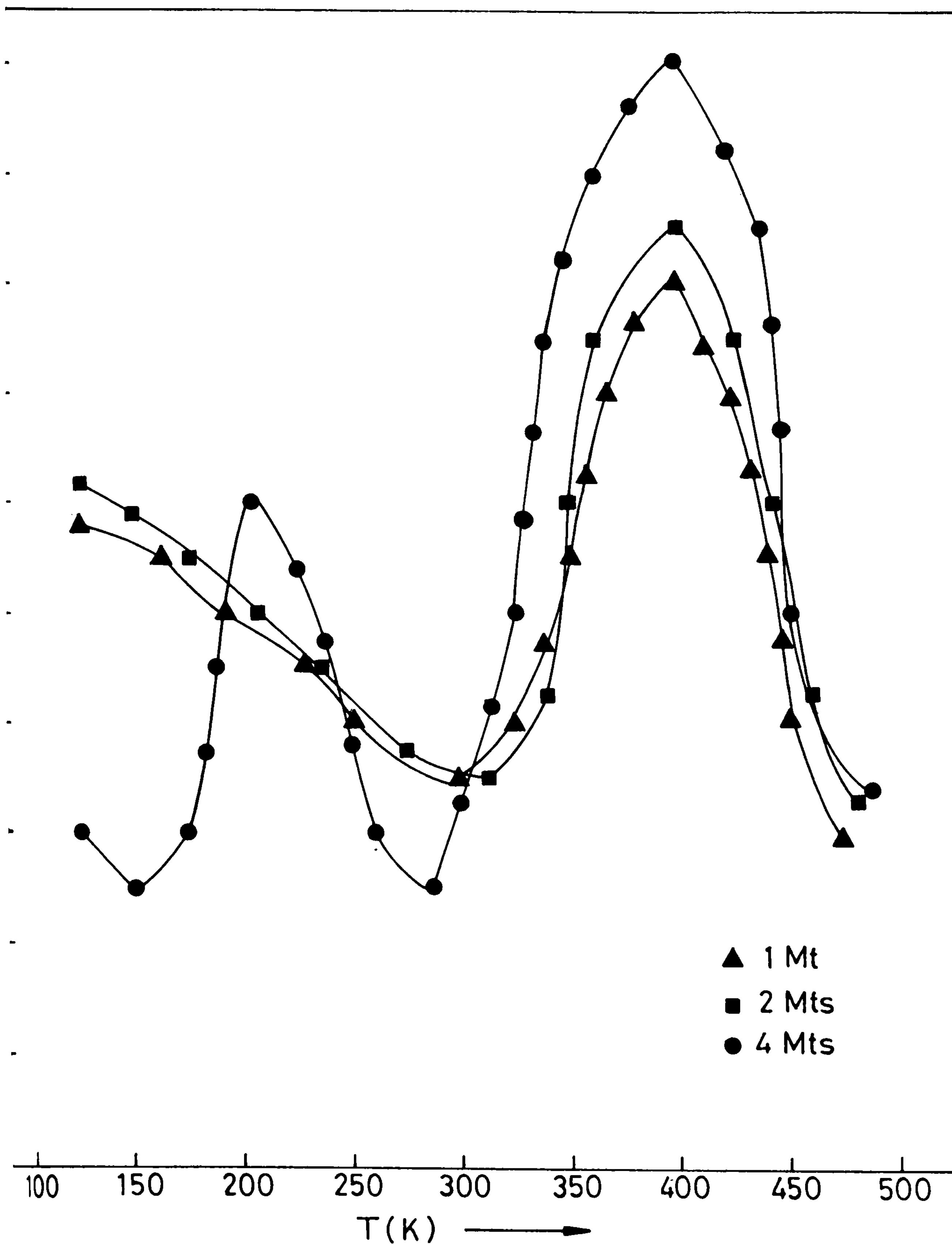

Figure 5.3. TSC spectra of CBD CIS film annealed in air at 175°C for different excitation time

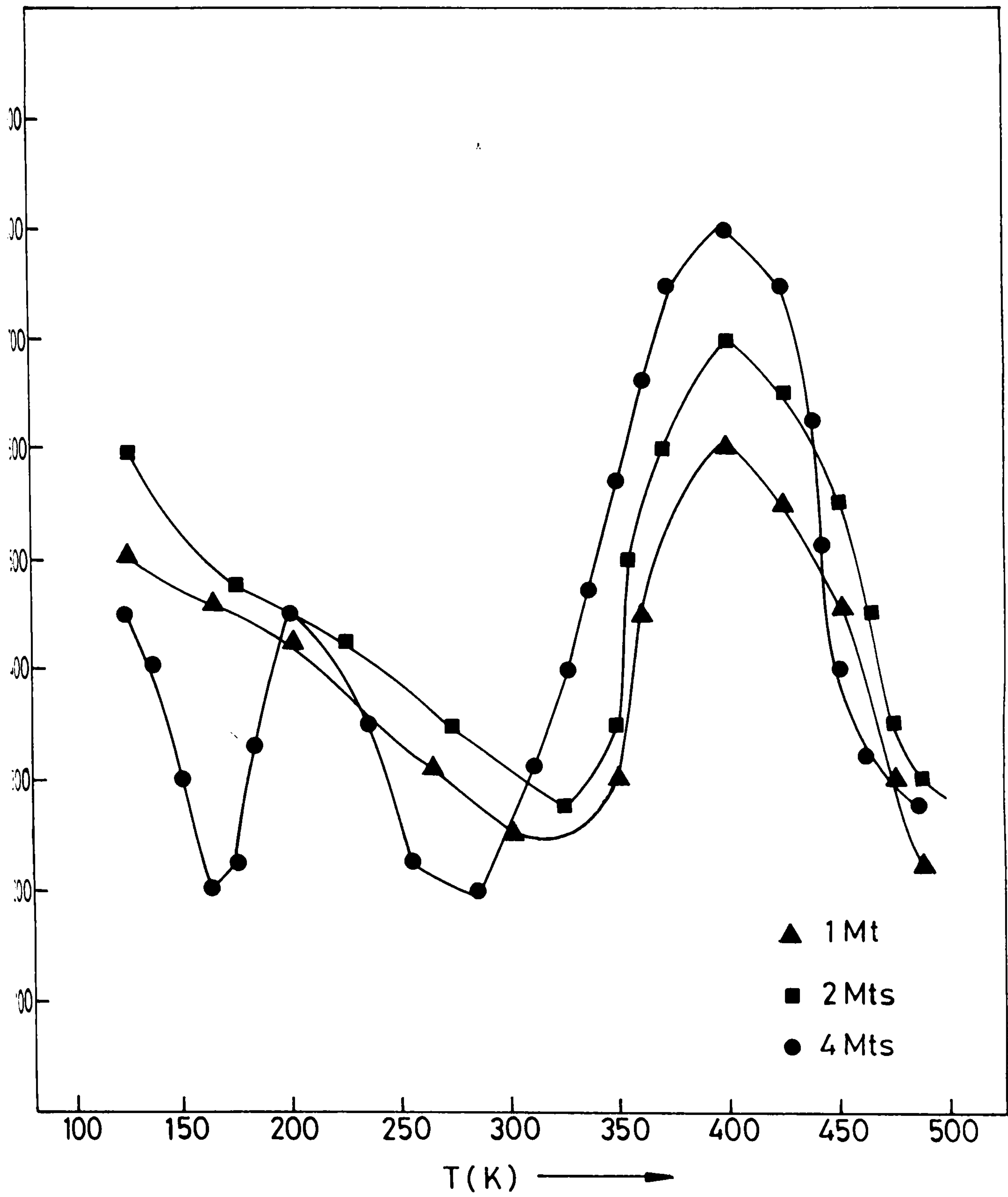

Figure.5.4. TSC spectra of CBD CIS film annealed in air at 200°C for different excitation time

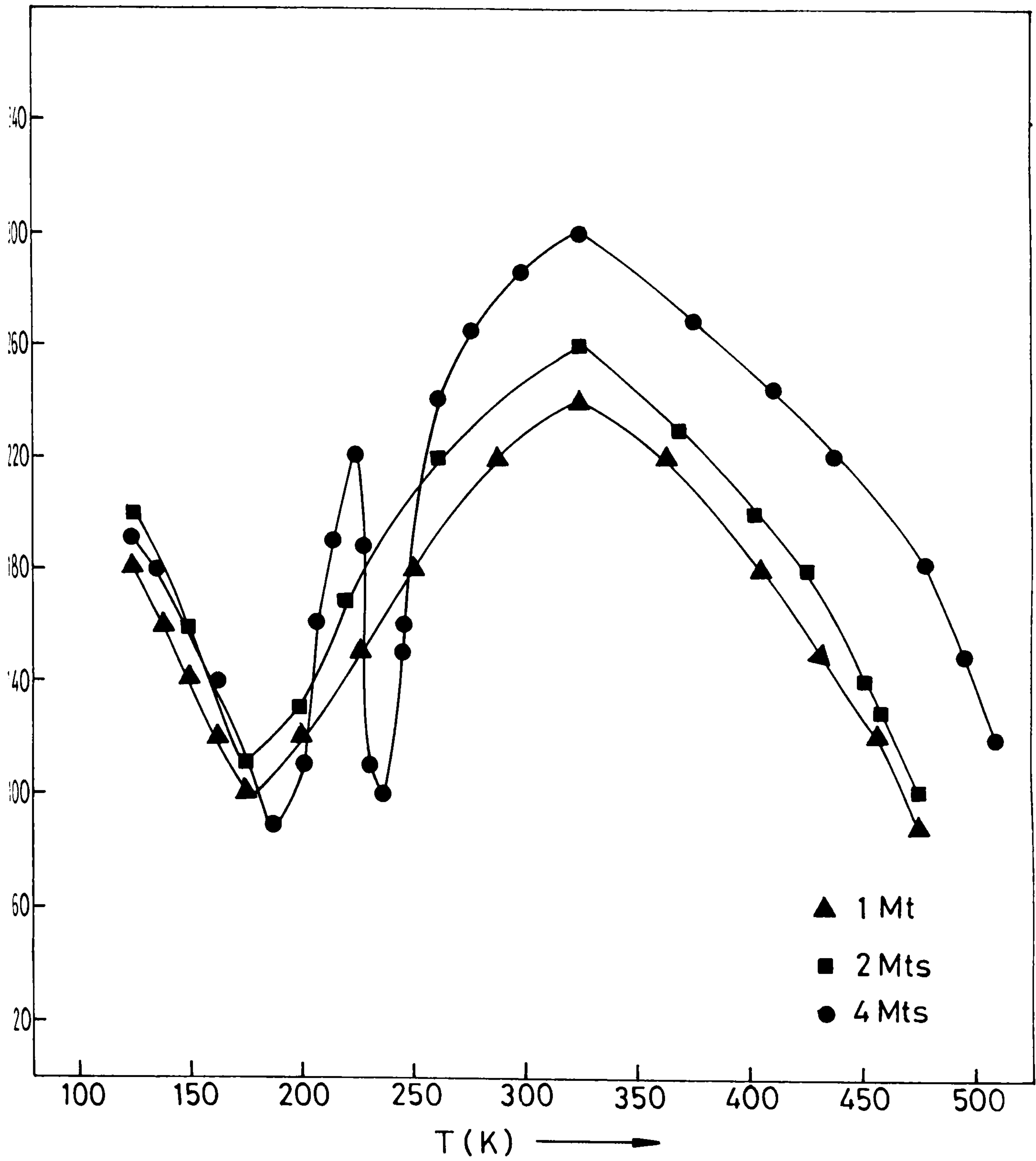

Figure.5.5. TSC spectra of CBD CIS film annealed in vacuum at 150°C for different excitation time

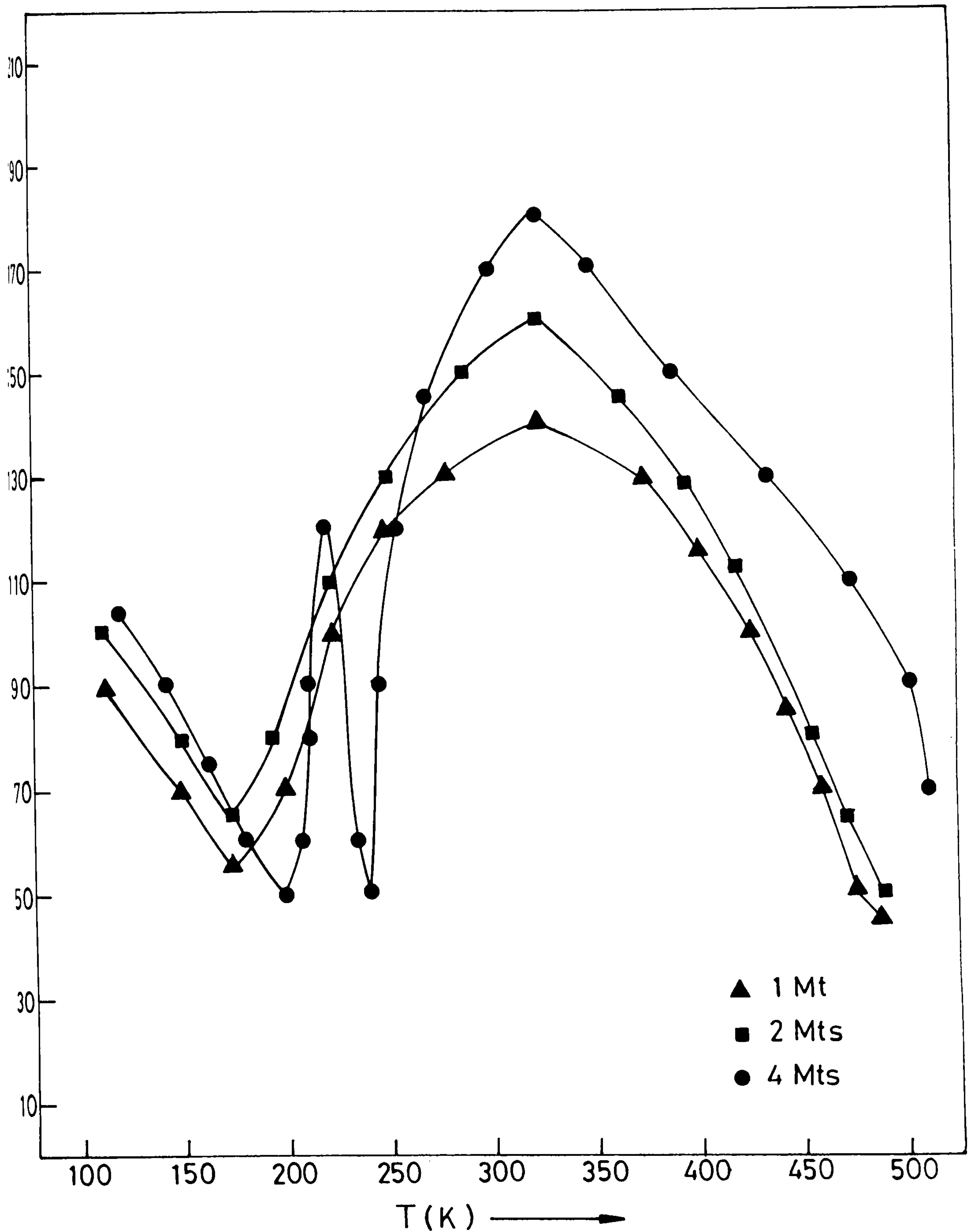

Figure.5.6 TSC spectra of CBD CIS film annealed in vacuum at 175°C for different excitation time

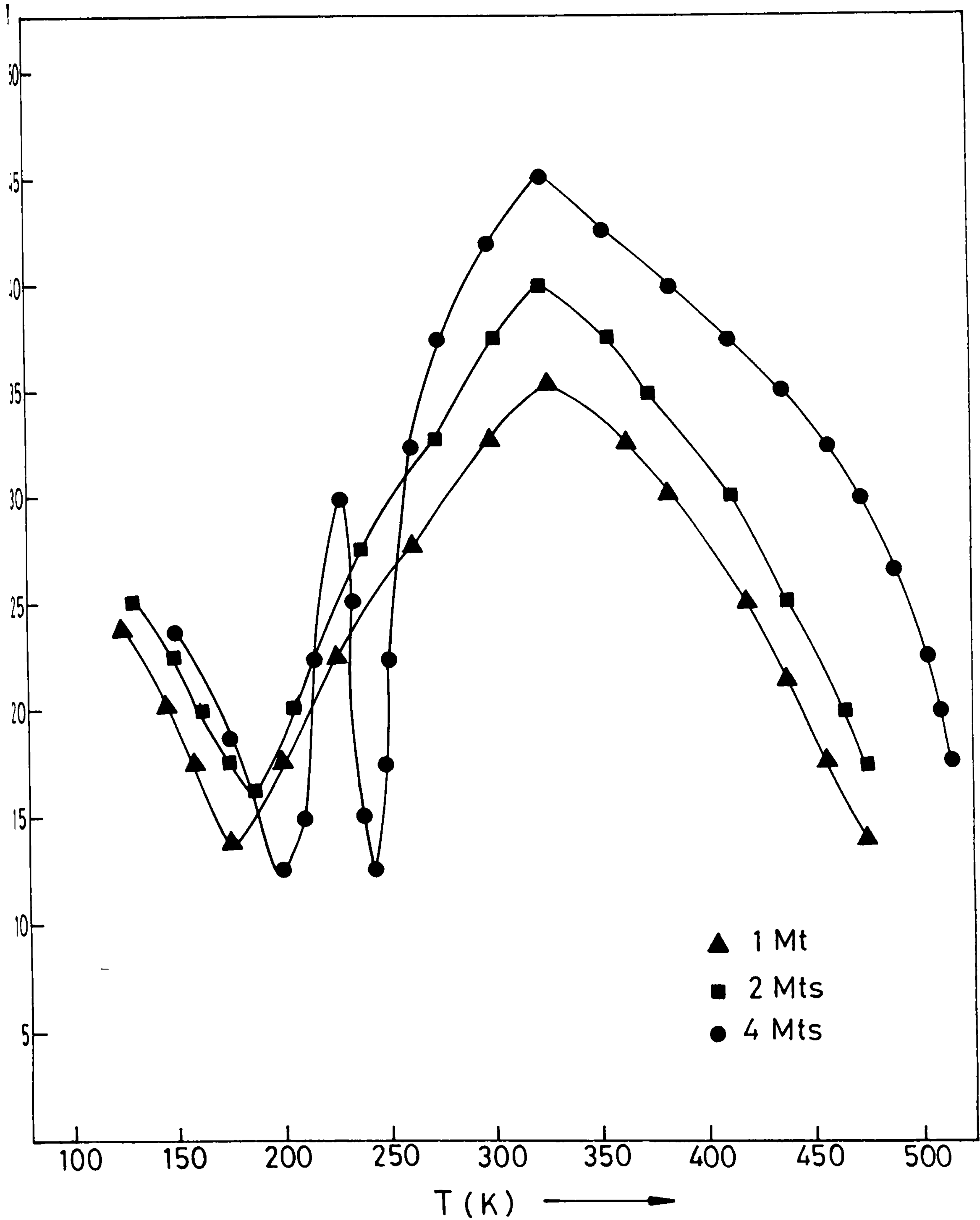

Figure.5.7. TSC spectra of CBD CIS film annealed in vacuum at 200°C for different excitation time

the copper salt. When Fe is present in the reaction mixture with a pH ~7, $Fe(OH)_3$ may be formed which decomposes and deposits as γ-FeO along with CIS film. When this film is annealed in air Fe_2O_3 may be formed and this will not give any TSC peak. But when the sample is annealed in vacuum FeO may be transformed into FeSe and SeO_2. FeSe is unstable and will be associated with other molecules or defects. This may give rise to a TSC peak. The peak due to Fe impurity in vacuum annealed samples may be explained in this way.

In order to study the effect of heating rate on the TSC spectra of CIS samples, we conducted TSC measurements of air- annealed samples for different heating rate. Figure5.8. shows the TSC spectra of air annealed sample for three different heating rate [β_1=0.05K/s, β_2=0.1K/s, β_3=0.15K/s] under 4 minutes light excitation. We note here that the current increases as the heating rate increases, and all peaks shifts to higher temperature as the heating rate increases. We have seen that the TSC equation for current (equation 3.28)

$$I = I_0 \exp\left[- \frac{E}{kT} - \frac{\nu}{\beta} \int_{T0}^{T} \exp\left(- \frac{E}{kT}\right) dT \right]$$

whereβ is the heating rate. Since

$$\left[\frac{dI}{dT}\right]_{T=Tm} = 0$$

the above equation becomes

$$\ln\left(\frac{T_m^{\ 2}}{\beta}\right) = \frac{E}{k}\frac{1}{T_m} + \ln\left(\frac{E}{k\nu}\right)$$

This is in the form of a straight line equation. A plot of $\ln\left(\frac{T_m^{\ 2}}{\beta}\right)$ versus (1000/T) for different β corresponding to one peak (donor level) in air annealed CIS samples is shown in figure 5.9. Similar plot corresponding to acceptor level is shown in figure 5.10. From the slopes of the graphs the activation energy corresponding to each trap is calculated as 104.3 meV(acceptor level) and 224.25 meV(donor level). This 104.3 eV was found to be due to Cu vacancy [28] and these values are found to be in agreement with the values obtained from previous measurements.

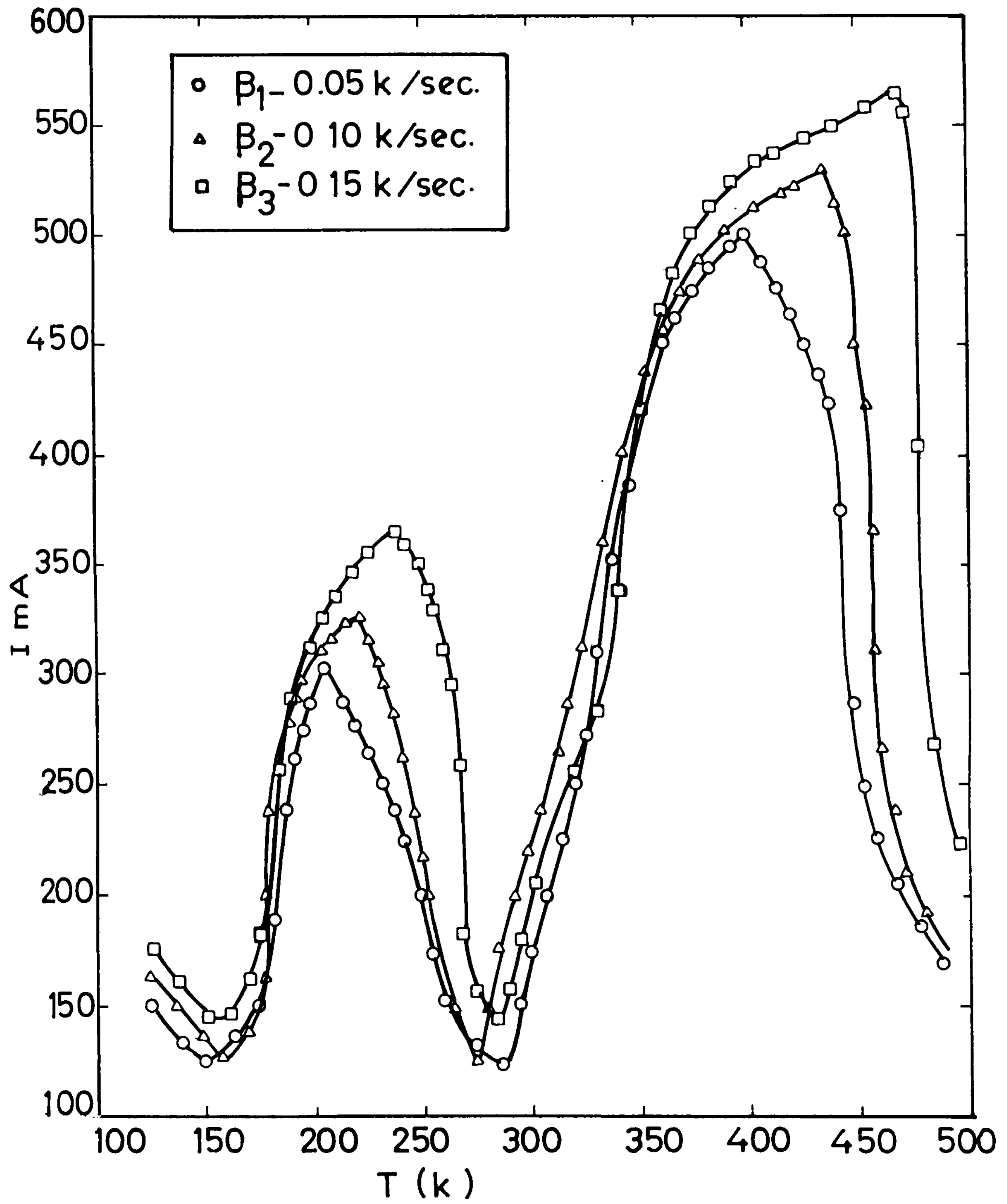

Figure 5.8. TSC spectra of CBD CIS film annealed in air for different heating rate

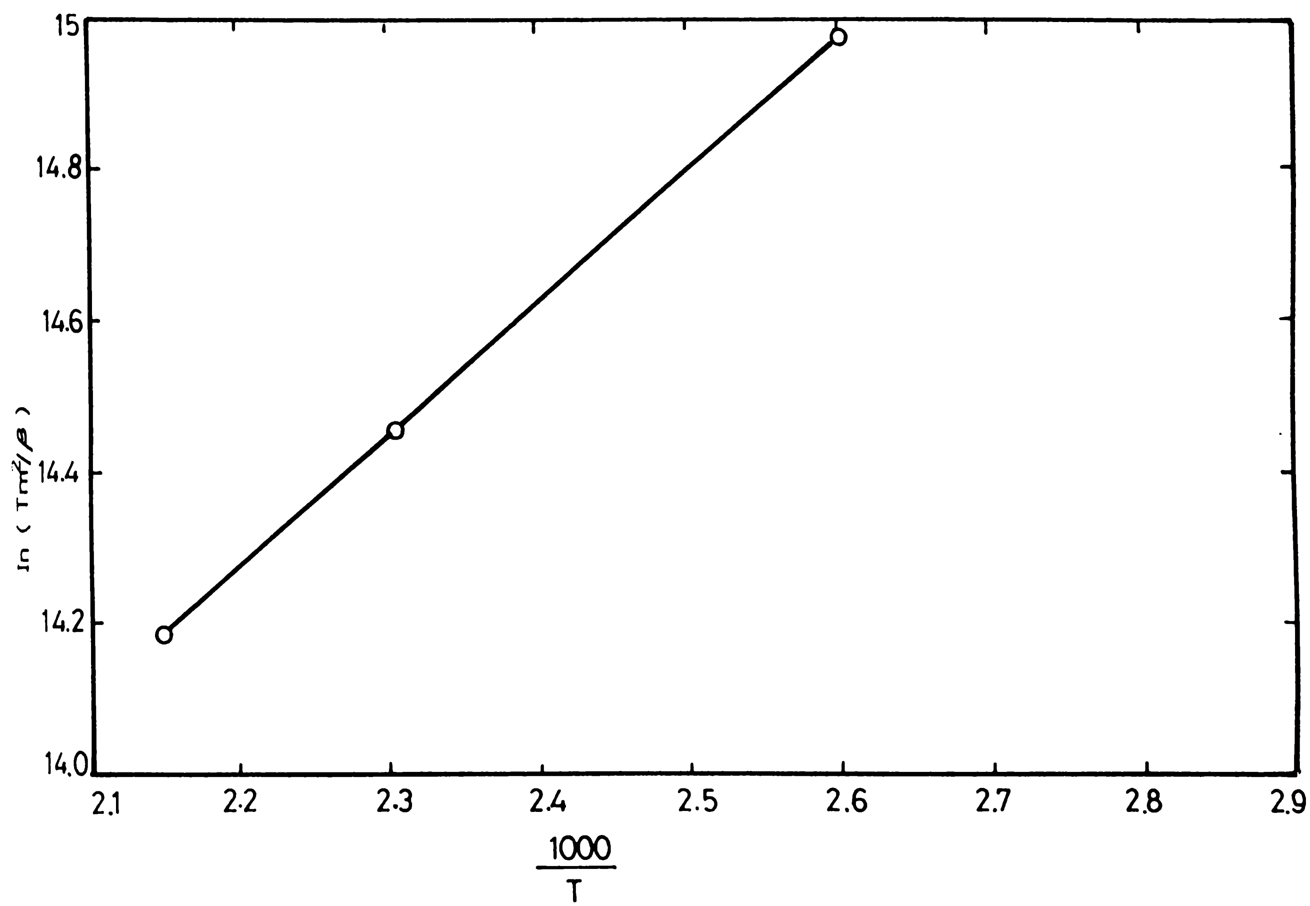

Figure 5.9. Plot of $\ln\left(\frac{T_m^{\ 2}}{\beta}\right)$ as a function of (1000/T) corresponding to donor level

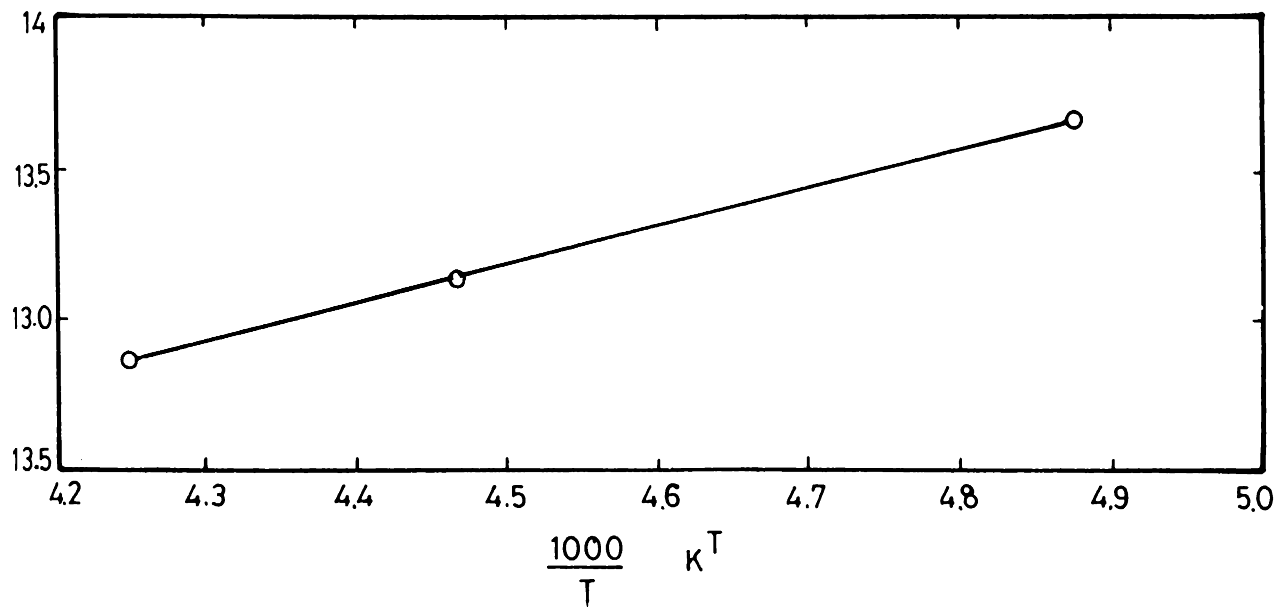

Figure.5.10. Plot of $\ln\left(\frac{T_m^2}{\beta}\right)$ as a function of (1000/T) corresponding to acceptor level

To determine type of traps formed in CBD CIS samples TSC measurements were performed, at constant rising rate, by changing the polarity of bias voltage applied to the irradiating surface. Figure 5.11. shows the TSC curves for as-deposited CIS samples with positive and negative bias applied to irradiating surface. From the spectra it is clear that I_{max} is higher for the case of positive bias voltage and hence the hole carrier is dominant here in the trap due to Cu vacancy (40 meV). But for the second peak corresponding to Se vacancy, I_{max} is higher for the case of negative bias voltage and hence this defect is an electron trap. TSC spectra of CIS samples annealed in air and vacuum with positive and negative bias voltage applied to the irradiating surface are shown in figure 5.12 and 5.13 respectively. Nature of different traps in CIS samples as obtained from this analysis is shown in table 3.

Table 3. Nature of different traps in CBD CIS samples

CIS sample type	Observed trap levels	
	Activation energy (meV)	Nature of traps
As-deposited	1) 70 2) 40	1) electron trap 2) hole trap
Annealed in air	1) 220 2) 85	1) electron trap 2) hole trap
Annealed in vacuum	1) 70 2) 400	1) electron trap 2) hole trap

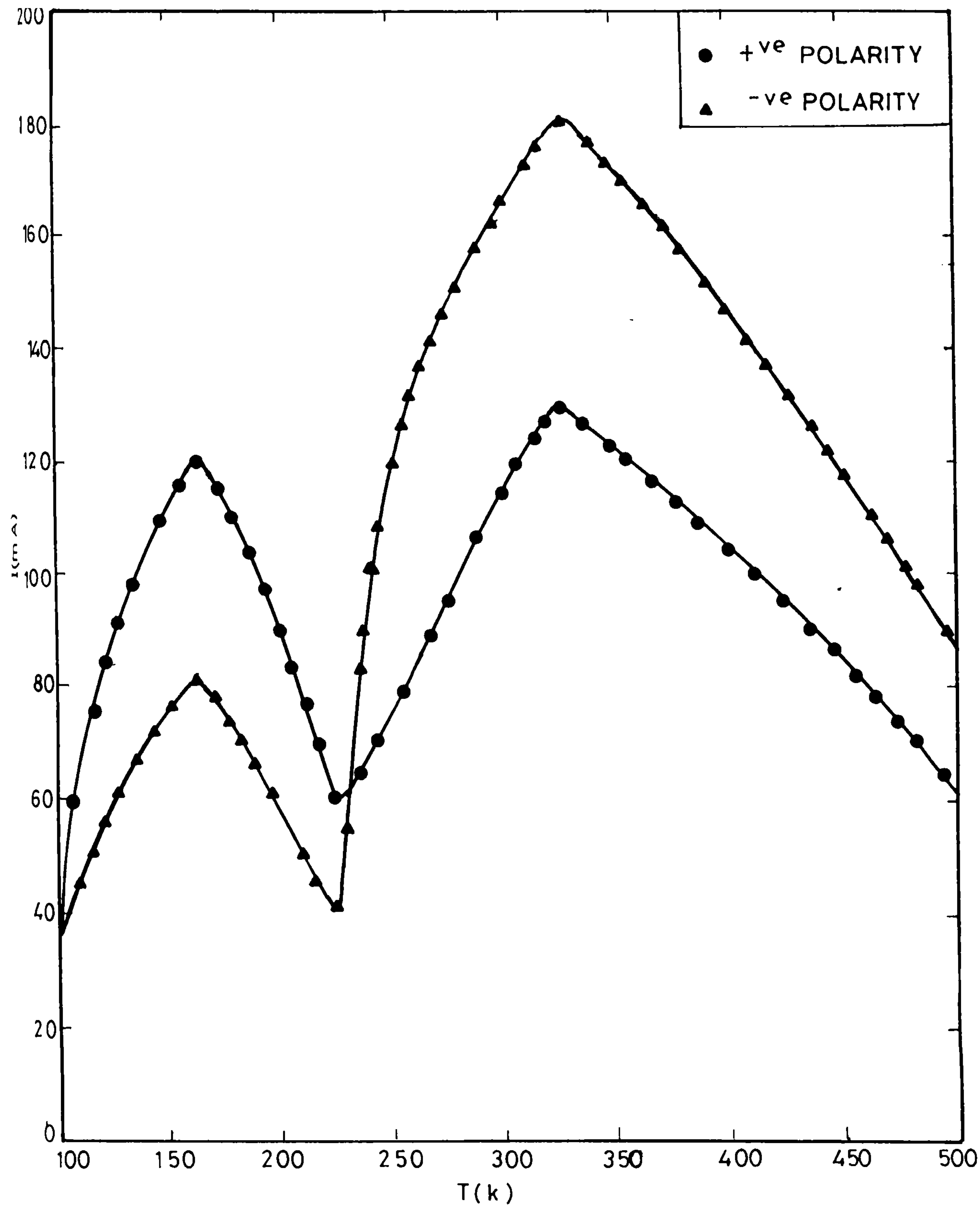

Figure 5.11 TSC spectra of as-deposited CBD CIS film with positive and negative polarity applied to irradiating surface

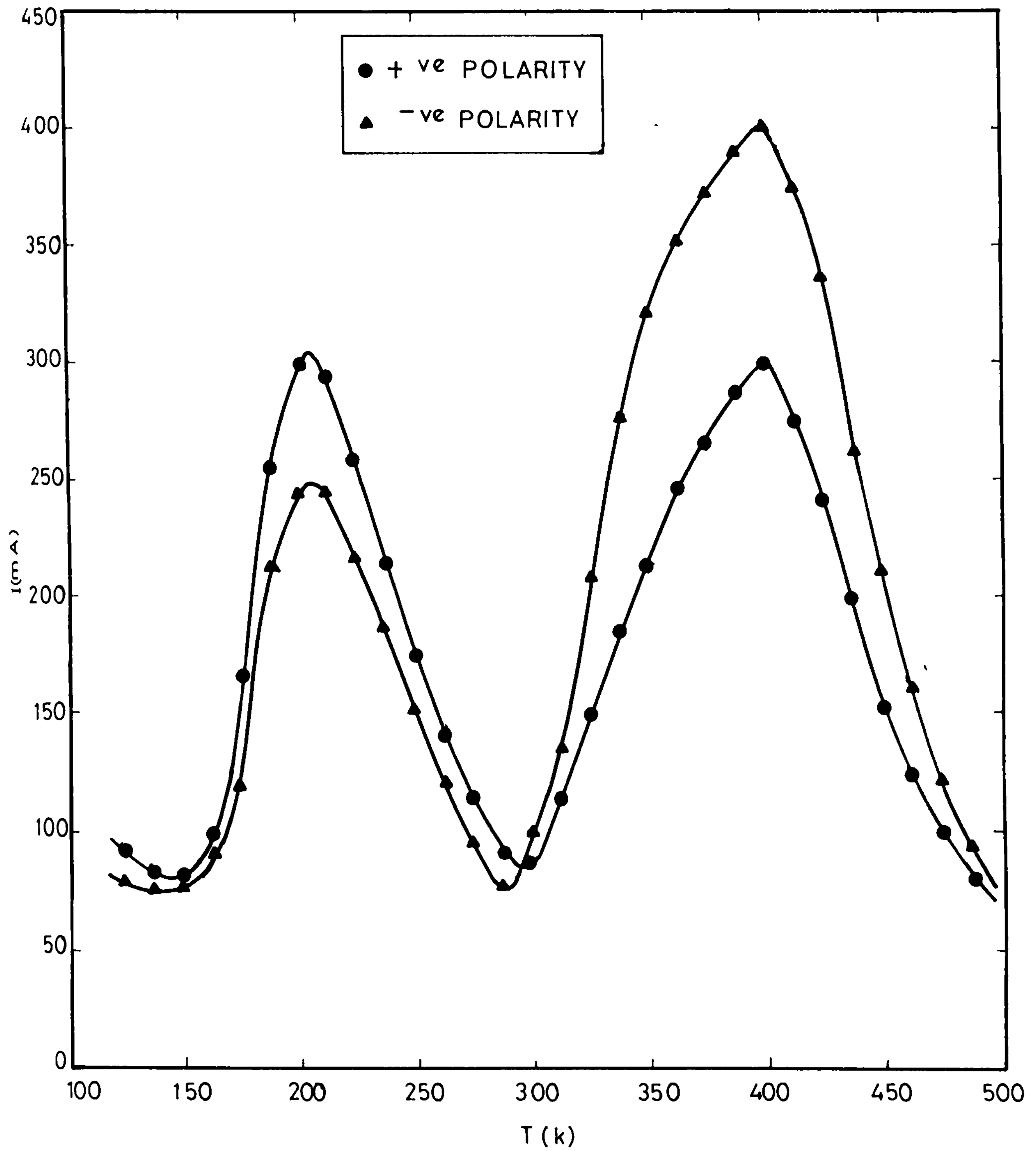

Figure 5.12. TSC spectra of CBD CIS film (annealed in air) with positive and negative polarity applied to the irradiating surface.

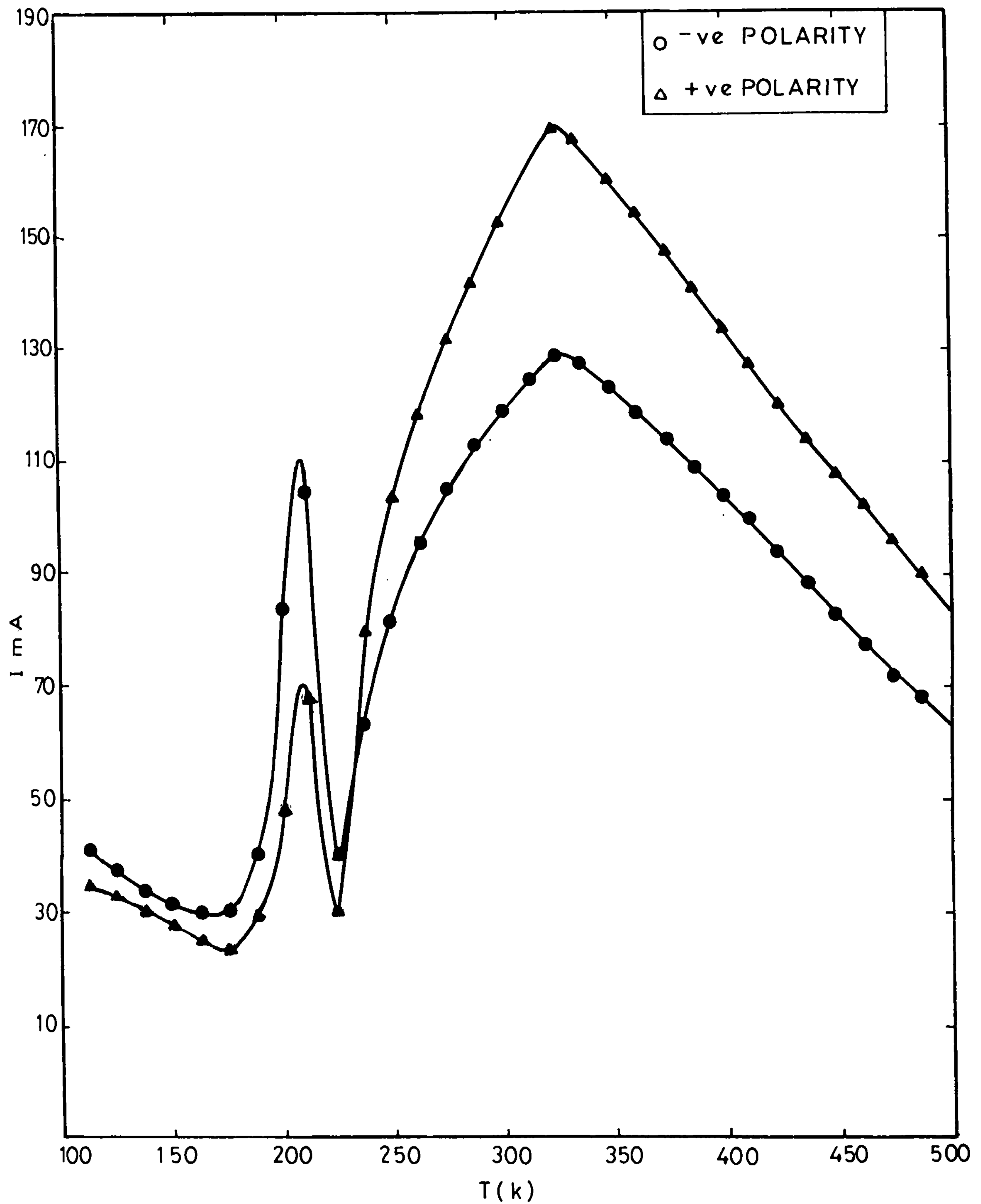

Figure 5.13. TSC spectra of CBD CIS film (annealed in vacuum) with positive and negative polarity applied to the irradiating surface.

5.4.2. Dark Conductivity Measurements

Figure 5.14 shows the Arrhenius plot of conductivity of as-deposited and vacuum annealed (200°C) samples. Similar plot for air annealed (220°C) samples is shown in figure 5.15. These two sets of graphs indicated two distinct slopes, from which activation energies were calculated (Table 4). As-deposited sample had trap levels of activation energies 70.72 meV and 40.5 meV indicating the presence of Se vacancy and Cu vacancy. Again vacuum annealed sample had levels of activation energy values 70.29 meV and 414 meV that supported the existence of Se vacancy and Fe impurity. In the case of air annealed samples, the plot indicated two activation energy values at 40.5 meV and 103 meV, which are attributed to Cu vacancy as obtained by Sridevi et al [28]. From this it is clear that the results of dark conductivity measurements very well corroborate the TSC measurements.

Table 4. Values of activation energy obtained from dark conductivity measurements on $CuInSe_2$ thin film samples.

Sample type	Activation energy (meV)	
As-prepared	1) 70.72	2) 40.5
Air annealed at 200°C for 1hour	1) 103	2) 40.5
Vacuum annealed at 200°C for 1hour	1)70.29	2) 414.5

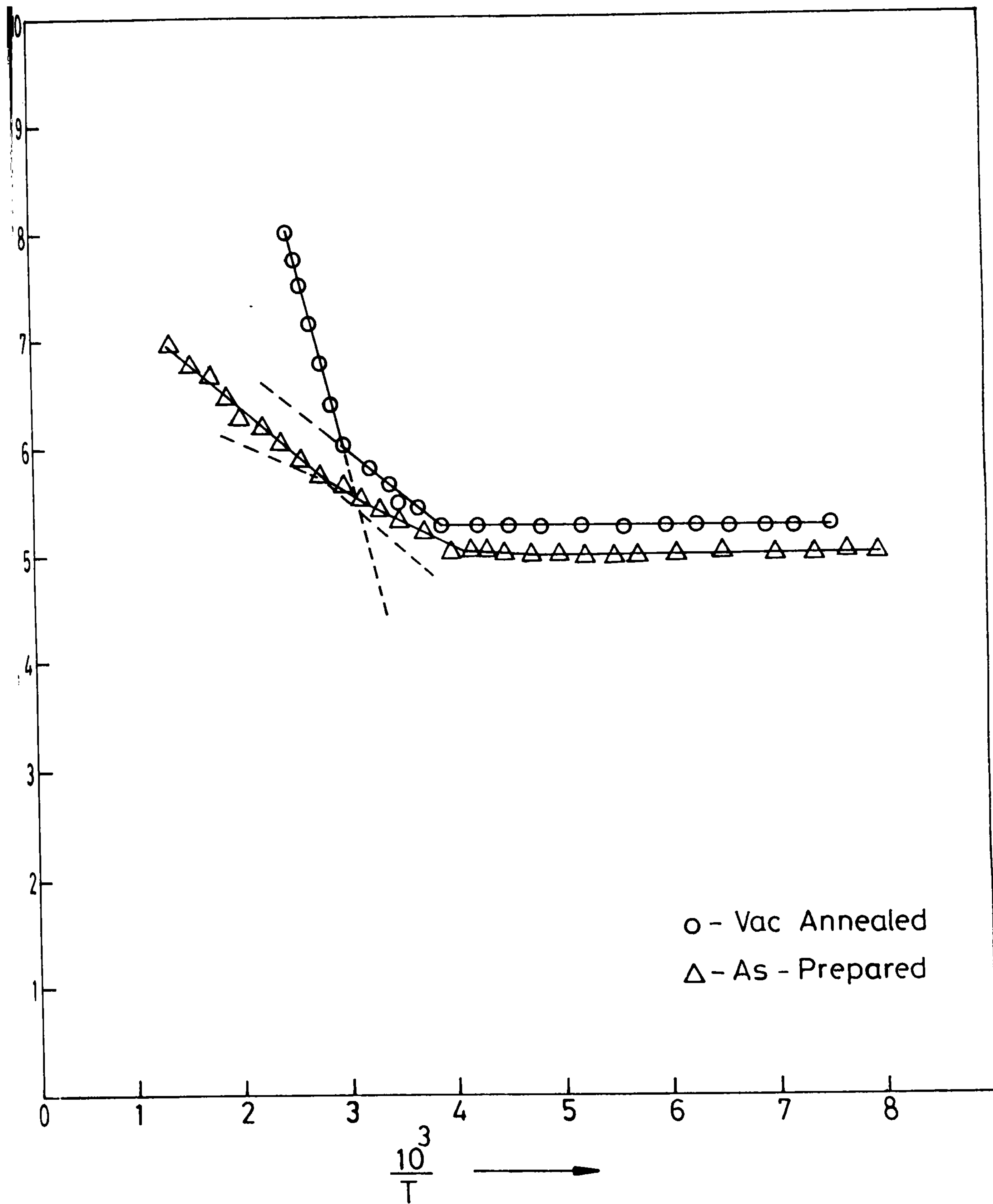

Figure 5.14. Arrhenius plot of conductivity of as-deposited and vacuum annealed CBD CIS films at 200°C

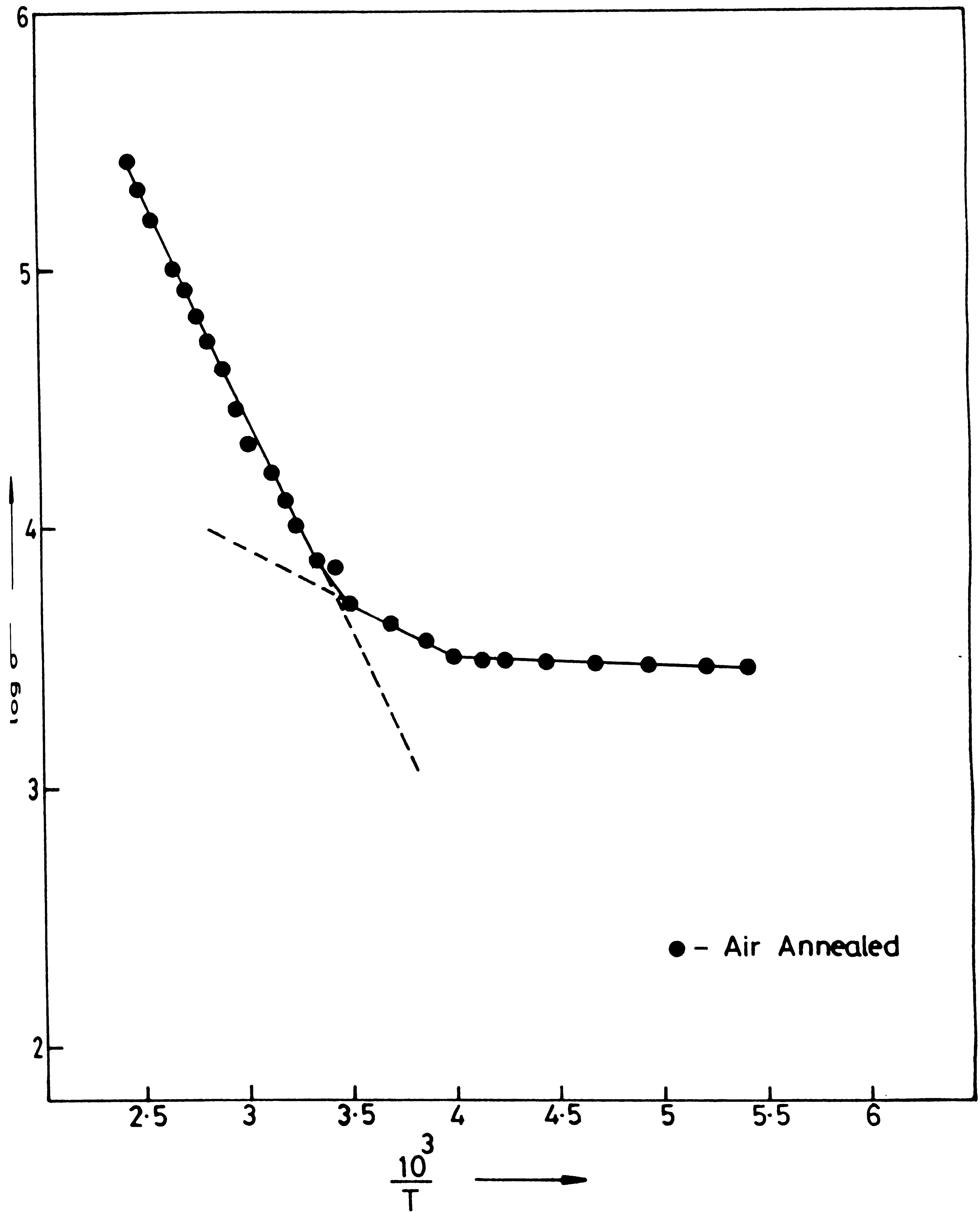

Figure 5.15. Arrhenius plot of conductivity of CBD CIS films annealed in air at 200°C

5.5 Conclusion

Trap level detection of CIS films prepared using CBD technique was performed by TSC measurement technique of as-prepared and annealed samples. The former type had Se vacancy as a prominent trap and Cu vacancy of smaller capture cross section. But when these samples were annealed in air, the Se vacancy of the as-deposited sample disappeared, and another donor level supposed to be due to the adsorption of oxygen came into existence. Cu vacancies continued to exist in air annealed sample. Vacuum annealing did not affect the presence of prominent Se vacancy , since oxygen adsorption is quite difficult under this condition. Interestingly, these samples also showed the presence of Fe impurity. A possible explanation for the presence of Fe impurity in the case of vacuum annealed CBD CIS samples is also discussed in this chapter. Nature of different trap levels observed in TSC measurements is also determined. Dark conductivity measurements on these CBD CIS samples were found to be in good agreement with the results obtained from TSC measurement.

References

1. J.L.Shay and J.H. Wernick, Ternary Chalcopyrite Semiconductors:Growth, Electronic properties and Applications, (Pergamon, New York, 1975)
2. S.Wagner, J.L.Shay, P.Migliorato and H.M.Kasper, *Appl.Phys.Lett.*, **25**(1974)434
3. H.Hahn, G.Frank, W.Klinger, A.D.Meyer and G.Storger, Z.Anorg, *Allg.Chem.*, **271**(1953)153
4. J.Parker, R.D. TomlinSon and M.J.Hampshire., *J.Appl.Crystallogr.*, **6**(1973)414
5. J.L.Shay, B.Tell, H.M.Kasper and L.M.Schiavone, *Phys.Rev.B.*, **7**(1973)4485
6. W.Horig, H.Neuman, H.J.Hobler and G.Kuhn, *Phys.Status Solidi (b)*, **80**(1977)K21
7. P.Migliorato, J.L.Shay, H.M.Kasper and S.Wagner, *J.Appl.Phys.*, **46**(1975)1777
8. S.Wagner and P.M.Brindenbaugh, *J.Crys.growth*, **39**(1977)151
9. J.L.Shay and S.Wagner, *Appl.Phys.Lett.*, **27**(1975)89
10. Kenneth Zwibel, Harin S Ullal and Bolko G Von Roedoern, 25th IEEE Photovoltaic Specialist Conf., Washington DC (1996) p 159
11. P.K.Vidyadharan Pillai, K.P.Vijayakumar, P.S.Mukherji, *J.Mater.Sci.Lett.*, **13**(1994)1725
12. P.K.Vidyadharan Pillai and K.P.Vijayakumar, *Solar energy materials and Solar cells*, **51**(1998)47
13. Phil Won Yu, *J.App.Phys.*, **47**(2)(1976)677
14. W.Horig, H.Neumann and H.Sobotta, *Thin Solid Films*, **48**(1978)67
15. B.Schumann, C.Georgi, A.Tempel, G.Khun, Nguyen Van Nam, H.Neumann and W.Horig, *Thin Solid Films*, **52**(1978)45
16. A.F.Fray and P.Lloyd, *Thin Solid Films*, **58**(1979)29
17. S.P.Grindle, A.H. Clark, S.Rezaie-Serej, E.Falconer and J.McNeily and L.L.Kazmerski, *J.Appl.Phys.*, **51**(10)(1980)5464
18. Clayton W Bates, J.R., Kim F Nelson, S.Aliq Raza, John B Moorney, Jutta M.Recktenwald, Loren Macinlosh and Robert Lamoreaux, *Thin Solid Films*, **88**(1982)279
19. R.A.Mickelson and W.S.Chen, Proc. of 16th IEEE Photovoltaic Specialist Conf. San Diego (1982)781

20. C.Rincon, J.Gonzalez and G.Sanchez Perez., *J.Appl.Phys.*, **54**(11)(1983)6634
21. M.Varela, J.L.Morenza, J.Esteva and J.M. Codia, *J.Phys.D.Appl.Phys.*, **17**(1984)2423
22. M.Varela, E.Bertran, J.Esteva and J.L. Morenza, *Solar Cells*, **14**(1985)155
23. Polla Raja Ram, R.Thangaraj, A.K. Sharma and O.P. Agnihotri, *Solar Cells*, **14**(1985)123
24. P.Lange, H.Neff, M.Fearheiley and K.J. Bachmann, *Phys.Rev.B*, **31**(6)(1985)4074
25. S.M.Wasim, *Solar Cells*, **16**(1986)289
26. Gary Hodes and David Cahen, *Solar Cells*, **16**(1986)245
27. S.Isomura, A.Nagamatsu and K.Shinohara and T.Aona, *Solar Cells*, **16**(1986)143
28. D.Sridevi and K.V.Reddy, *Indian J.of Pure and Appl.Phys.*, **24**(1986)392
29. R.Trykozko, R.Bacewicz and J.Filipowicz, *Solar Cells*, **16**(1986)351
30. R.W.Birkmire, L.C.Dinetta, P.G.Lasswell, J.D.Meakin and J.E. Phillips, *Solar Cells*, **16**(1986)419
31. R.Noufi, R.J.Matson, R.C. Powell and C.Herrington, *Solar Cells*, **16**(1986)479
32. J.D.Meakin, R.W.Birkmire, L.C.Dinetta, P.G.Lasswell and J.E. Phillips, *Solar Cells*, **16**(1986)447
33. T.Datta, R.Noufi and S.K.Das, *J.Appl.Phys.*, **59**(5)(1986)1548
34. I.Martil, J.Santamaria, E.Iborra, G.Gonazalez-Diaz and F.Sanchez-Quesada, *J.Appl.Phys.*, **62**(10)(1987)4163
35. R.J.Matson, R.Noufi, K.J.Bachmann and D.Cahen, *Appl.Phys.Lett.*, **50**(3)(1987)158
36. J.M.Stewart, *Solar Cells*, **19**(1986-1987)237
37. J.C.Garg, R.P.Sharma and K.C.Sharma, *Thin Solid Films*, **164**(1988)269
38. N.Christoforou, J.D. Leslie and S.Damaskinos, *Solar Cells*, **26**(1989)197
39. K.W.Mitchell, C.Eberspacher, J.Ermer, D.Pier and P.Milla., Proc.8th EC Photovoltaic Solar Energy Conf. Florence Itali (1988) p 1578
40. R.P.Sharma, Pankaj Garg and J.C. Garg, *Pramana J.Phys.*, **34**(1)(1990)67
41. D.S.Albin, G.D.Mooney, A.Duda, J.Tuttle, R.Matson and R.Noufi, *Solar Cells*, **30**(1991)47
42. C.Guillen and J.Herrero, *Solar Energy Materials*, **23**(1991)31
43. J.W.Chu and D.Haneman, *Appl.Phys.Lett.*, **58**(4)(1991)373
44. R.A.Sasala and J.R.Sites, *Solar Cells*, **30**(1991)101

45. K.W.Mitchell, W.Chesarek, D.R. Willett, C.Eberspacher, J.H.Ermer and R.R.Gay *Solar Cells*, **30**(1991)131

46. S.J.Kim and H.B.Im, *Thin Solid Films*, **214**(1992)194

47. Masayuki Tanda, Susumu Manaka, Jorge R Encinas Martin, Katsumi kushiya, Hideki Sano, Akira Yamada, Makoto Konagai and Kiyoshi Takahashi, *Jpn.J.Appl.Phys.*, **31**(1992)L753

48. Manorlal, Navdeep Goyal and Anil, Vohra, *Thin Solid Films*, **227**(1993)177

49. Bulent M Basol, Vijay K Kapur, Arvind Halani and Craig Leidholm, *Solar Energy Materials and Solar Cells*, **29**(1993)163

50. Shigemi Kohiki, Mikihiko nishitani, Takayuki Negami and Takahiro Wada, *Thin Solid Films*, **238**(1994)195

51. G.Masse and K.Djessas, K.Guenoun, *Thin Solid Films*, **237**(1994)129

52. Takayuki Negami, Mikihiko Nishitani, Mitsuske Ikeda, TakahiroWada, *Solar Energy Mat. & Solar Cells*, **35**(1994)215

53. F.O.Adurodija, M.J.Carter and R.Hill, *Solar Energy Mat. and Solar Cells*, **37**(1995)203

54. P.J.Sebastian, A.M.Fernandez and A.Sanchez, *Solar Energy Mat. and Solar Cells*, **39**(1995)55

55. G.Masse, K.Djessas, K.Guenoun and A.Smith, *Thin Solid Films*, **278**(1996)82

56. Bulent M Basol, Vijay K Kapur, Craig R. Leidholm, Arvind Halani and Kristen Gledhill, *Solar Energy Materials and Solar Cells*, **43**(1996)93

57. Miguel A. Contreras, John Tuttle, Andrew Gabor, Andrew Tennant, Kannan ramanathan, Sally Asher, Amy Franz, James Keane, L.Wang and Rommel Noufi, *Solar Energy Mat. & Solar Cells*, **41**(1996)231

58. H.Sakata and N.Nakao, *Phys.Stat.Solidi. (a)* **161**(1997)379

59. S.Niki, I.Kim, P.J.Fons, H.Shibata, A.Yamada, H.Oyanagi, T.Kurafuji, S.Chichibu and H.Nakanishi, *Solar Energy Mat. and Solar Cells*, **49**(1997)319

60. N.Stratieva, E.Tzvetkova, M.Ganchev, K.Kochev and I.Tomov, *Solar Energy Mat. & Solar Cells*, **45**(1997)87

61. Naoki Kohara, Takayuki Negami, Mikihiko Nishitani, Yasuhiro Hashimoto and Takahiro Wada, *Appl.Phys.Letts.*, **71**(6)(1997)835

62. Tokio Nakada, Hiroki Ohbo, Takayuki Watanabc, Hidenobu Nakazawa, Masahiro Matsui and Akn Kunioka, *Solar Energy Mat. and Solar Cells*, **49**(1997)261
63. Yasutoshi Ohtake, Tamotsu okamoto Akira Yamada, Makoto konagai and Koki Saito *Solar Energy Mat. & Solar Cells*, **49**(1997)269
64. Katsumi Kushiya, Muneyori Tachiyuki, Takahisa Kase, Ichiro Sugiyama,Yoshinori Nogoya, Daisuke Okumura, Masao Sato, Osamu Yamase, Hiroshi Takeshita, *Solar Energy Mat. & Solar Cells*, **49**(1997)277
65. Tokio Nakada, Hiroki Ohbo, Takayuki Watanabe, Hidenobu Nakazawa, Masahiro Matsui and Akn Kunioka, *Solar Energy Mat. and Solar Cells*, **49**(1997)285
66. M.Topic, F.smole, J.Furlan, *Solar Energy Mat.and Solar Cells*, **49**(1997)311
67. Sho Shirakata, Hotoshi Kubo, Chihiro Hamaguchi and Shigehiro Isomura, *Jpn.J.Appl.Phys.*, **36**(1997)L1394
68. Masakatsu Suzuki, Takeshi Uenoyama Takahiro Wada, Takeshi Hanada and Yoshio Nakamura, *Jpn.J.Appl.Phys.*, **36**(1997)L1139
69. P.Lange, H.Neff, M.Fearheiley and K.J.Backmann, *Phys.Rev.B.*, **31**(1985)4074
70. B.Tell, J.L.Shay and H.M.Kasper, *J.Appl.Phys.*, **43**(1972)2469
71. H.Neumann, Nguyen Van Nam, H.J.Hobler and G.kuhn, *Solid State Commn.*, **25**(1978)899
72. H.Sobotta, H.Neumann, V.Riede, G.Kuhn, J.Seltmann and Oppermann., *Phys. Stat. Solidi (a)*, **60**(1980)531
73. H.Neumann, E.Nowak and G.Kuhn, *Cryst.Res.Technol.*, **16**(1981)1369
74. H.J.Von Bardeleben and R.D.Tomlinson, *J.Phys.C.*, **13**(1980)L1097
75. J.M.Tchapkui-Niat, A.Goltzene and C.Schwab, *J.Phys.C.*, **15**(1982)4671

Chapter 6

Preparation and characterisation of PbS thin films

6.1. Introduction

Lead sulphide (PbS) is a narrow band gap semiconductor belonging to IV - VI family and possesses rock salt structure. It was one of the first semiconductors to find wide application as the material for point contact diodes in so-called "crystal set" radios. Present applications are limited to infrared detectors, while the IV-VI materials are generally candidates for long wavelength infrared lasers. Thin films of PbS are used as IR detectors [1-4], IR photographic plates [5-7] and selective coatings for the photothermal conversion of solar energy [8-11]. It has recently been proposed that a solar thermal photovoltaic system employing PbS photocells would be able to achieve 14 % efficiency for conversion of solar energy to electrical energy [12].

The thin films of PbS are prepared by the techniques of vacuum evaporation [2-4], solution growth (CBD) [1,13,14], spray pyrolysis [10] and electrochemical deposition [15]. The solution growth and spray pyrolysis are useful for large scale production. Use of chemically deposited PbS layers as infrared photodetectors has stimulated a more or less continuous investigation of the properties of the film over the last 50 years [16-19]. The most important property of PbS films prepared using CBD technique is the photosensitivity and study of this property in PbS films is of great importance [20-24].

This chapter describes the preparation of PbS thin films using CBD technique and characterisation. Here the photosensitive property of these films is studied mainly using TSC analysis and dark conductivity measurements. Before going into the details of the preparation and characterisation, we shall have a quick glance over the research works on PbS thin films in recent years.

6.2. Review of works on PbS

It was Lange who reported [25] a photovoltaic cell with galena (PbS) in 1930. Later W.D. Lawson developed a method of forming oxygen free single crystals of PbS [26]. A method of vapour phase growth was used to grow PbS crystal to have samples without any nonvolatile impurities [27]. Determination of mobility of electrons and holes in PbS crystals using Hall effect and resistivity analysis was reported by Richard et al [28]. The band structure of PbS crystals was investigated [29] using angle-resolved photoemission with synchrotron radiation as the excitation in 1992. It is found that many spectral features originate from direct transitions, while others are due to "density of states" features, i.e., they arise from electrons scattered into the observed direction. The study of surface structure of PbS (100) in the form of the mineral galena using X-ray standing wave technique was reported in 1998 [30]. Galena oxidation on potentiostaticaly treated specimens in acetate buffer was investigated in the same year [31]. Elemental sulphur was detected in these samples as an oxidation product by XPS analysis and it showed that sulphur is present on the galena surface as local accumulation rather than as a uniform layer.

Vacuum evaporation technique was developed to prepare PbS detectors [32]. Microstructure of vacuum deposited PbS layers was reported by Biryulev et al [33]. PbS layers sensitized in air were compared with those sensitized at low partial pressure of O_2. George et al prepared [34] polycrystalline films of PbS using reactive evaporation. Kovalev et al [35] explained the mechanism of photoconductivity in vacuum evaporated PbS films. They proposed a model of a photosensitive physical layer that account for the formation of a longitudinal technological surface p-layer and also of isotropic barriers at crystallite boundaries. The longitudinal p-n junction and the high isotopic barriers in the lower n layer effectively separate the light generated non equilibrium charge carriers, and give rise to high photosensitivity. The same group reported [36] formation of photosensitive PbS layers using thermal evaporation of different initial materials also. Z. Sell Mandouh employed [37] TEM and diffraction techniques to investigate growth and orientation of PbS films condensed from vapour phase. They also investigated effect of irradiation of electron beam on these films.

Quasi-static growth of PbS epitaxial films was reported in 1972 [38]. Later observation of deep impurity levels in epitaxial films was reported by Lopez et al [39]. Comparison of S-vacancies in these films produces material with low carrier concentration and at these lower concentrations, an impurity center is found. This center is identified with Si impurity and this produces a deep electron trap and an acceptor level of 0.079 eV above the VB. Photosensitivity in epitaxial PbS films was observed by Riedl et al [40]. Here epitaxial films were senstitized by heat treatmcnts in air or sulphur vapour.

Spray pyrolysed PbS films were reported by Tyagi et al [41] and electrical and optical properties of these films exhibit photosensitivity when they contain interparticle barriers and oxygen complexes of lead.

Later Martin et al produced spectrally selective PbS films using ion beam sputtering [42] and Fawcett reported [43] the production of electrodeposited PbS films. Electrodeposition of PbS films in acidic medium was also reported in 1997 by Sharon et al [44]. They produced polycrystalline thin films of PbS on titanium, aluminium and stainless steel substrate. Deposition on aluminium gave a crystalline phase of PbS with very prominent (200) and (111) planes, while growth on stainless steel substrate showed (200) plane only. Although the deposition on titanium was good, it showed (111) and (200) planes of lower intensity compared to that on aluminium.

Extensive study was made by Mahlman [45] on the preparation of PbS films using solution growth technique and their characterisation. In that work, chemically oxidized PbS films were prepared for a reaction mixture containing chemical oxidizing agents. These films were sometimes partially photosensitive and hence were baked in vacuum at a relatively low temperature to make it more photosensitive. Almost all of the basic research data had been taken on chemically oxidized films because these films are most uniform in their response to light and the amount of oxidation received by the films is under control for this method of preparation. The process of oxidation taking place in the film determines its physical properties to a very great extend. The variation of dark and photoconductivity with

temperature, the transient response of films as a function of temperature and illumination and photocurrent response at constant temperature as a function of illumination were presented in that work.

Effect of thickness of chemically deposited PbS on spectral response of photoconductivity was reported by H.E. Spencer [46] and influence of layer thickness and grain size on long wavelength limit of photoconductivity was reported by Simic et al [47]. Variation of the properties of chemically deposited PbS films with the use of oxidant was again reported [48]. The structural, chemical and photoelectric properties are compared for three types of PbS films, differing in the use of oxidant during deposition. Films are grainy and showed a decrease in grain compactness as concentration of oxidant is increased. Photosensitive films were described in terms of sensitizing centers that are present only when an oxidant is used, but which are not dependent solely on the presence of oxygen. Physical identification of sensitizing centers was not given.

A detailed study of photoconductivity was made by Svein Espevik et al [20] on both oxidized PbS layers and layers without any oxidant. They observed a sensitizing center at 0.13 eV below the CB in films without oxidant and a center at 0.22 eV in oxidised films. Semiconducting PbS films with high solar absorptivity [49], highly photoconducting films with dielectric over coating [21], and effect of morphological structure on photosensitivity of chemically deposited films [50] were also reported by different groups.

In 1981, Reddy et al reported [51] solution grown PbS/CdS multilayer stacks as selective absorber and a mathematical model was formulated using matrix multiplication method to calculate reflectance of these layers. They again reported [52] more studies on PbS/CdS composite films as selective surface and developed a spectrally selective PbS/CdS composite coating for photothermal conversion application. AES spectra of the specimen heated to 250°C did not show any interdiffusion of lead and cadmium and thus established the thermal stability of the composite. AES also indicated that concentration of both Cd and lead remains constant throughout the thickness of the film. The dependence of spectral selectivity on deposition parameters like pH, temperature of the bath and ratio of Pb^{2+} to

Cd^{2+} ions in the solution was also studied. A dip-dry process for preparing photosensitive PbS films for thermophotovoltaic applications was developed by Chaudhuri et al [53]. These films were photosensitive to IR radiation and films prepared by baking at 100°C have maximum response and are found to be p-type. Photovoltaic cell made of these films showed open circuit voltage of 140 mV and short circuit density of 1.7 mA/cm^2. Later Reddy et al [54] again reported chemically deposited PbS antireflection layer selective absorber and solution grown $(PbS)_{1-x}$ -$(CdS)_x$ composite selective surfaces.

Sharma et al reported [55] transport properties of chemically deposited PbS films in which copper doped PbS films were used and variation of electrical conductivity and carrier mobility with doping was presented. It was found that Cu doping affects the grain size and structure of PbS films, indicating the formation of copper-lead alloy. Electrical and photoelectric properties of solution deposited PbS films with low concentration of oxidant on Silicon substrate [56], local irregularities in photosensitivity of chemically deposited PbS thin layers [57], noise characteristics produced between electrode and chemically deposited PbS photoconductor surface [58] and experimental investigation of the photo-Hall effect in solution deposited photosensitive polycrystalline PbS films [59] were also reported by different groups.

Structural and optical properties of PbS thin films obtained by chemical deposition were reported in 1997 [24]. Here PbS films were obtained from alkaline baths containing lead nitrate, thiourea and different additions like hydroxylamine hydrochloride, triethanolamine or hydrogen peroxide. Films were photosensitive and are influenced by film thickness, grain and crystallite size, fault probability, number of layers, thermal treatment and the presence of impurities. During the same period, chemically deposited PbS film composition was reported by Marcu et al [60] and they prepared films from alkaline baths containing lead salts, thiourea and hydroxylamine hydrochloride.

Formation of pn junction in PbS using ion implantation was reported [61] where authors used Zn ion implantation to get doping effect. The forward I-V characteristics and photosensitivity of the junction were presented in that paper. A solar thermophotovoltaic

converter using PbS photovoltaic cell was proposed by Chaudhuri et al [62]. The converter was in the form of a flat plate consisting of a heat mirror, a black absorber, a cell filter and PbS photovoltaic cells. Theoretical efficiency was calculated as 30 %. Deposition of semiconducting PbS films by the action of laser radiation on a deposition bath was reported [63]. The growth rate, in which the growth is initiated by laser radiation is double the growth rate under normal condition. A reduction in resistivity and increase in temperature coefficient of resistance of PbS grown by laser radiation was observed. Use of PbS in IR detectors for military and civilian applications [64] and an assessment of safety, cost and the optimization of chemically deposited PbS thin films for solar control application were also reported [65].

6.3. Sample Preparation

For the preparation of PbS samples, 0.2M solutions of lead acetate [$Pb(CH_3COO)_2$], thiourea [$SC(NH_2)_2$] and ethylene diamine tetra acetic acid (EDTA disodium salt) were prepared. 20 ml of lead acetate was mixed with 15 ml of EDTA solution and this was followed by the addition of 25% ammonia solution and 20 ml of thiourea solution. The volume of ammonia was so adjusted that pH of the solution was around 10. Ultrasonically cleaned glass plates served as the substrate for deposition and were placed in the deposition bath kept at 70°C. The expected chemical reaction is as follows

$$Pb(CH_3COO)_2 + Na_2(EDTA) \rightarrow 2CH_3 - COONa + Pb(EDTA)$$

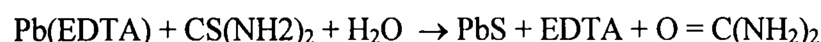

$$Pb(EDTA) + CS(NH2)_2 + H_2O \rightarrow PbS + EDTA + O = C(NH_2)_2$$

Different samples were prepared by varying the time of deposition as 3, 6, 9 and 12 hours. The thickness of the sample was measured using gravimetric method. It was found that thickness increases with time of deposition till the formation of PbS is complete i.e., till the terminal thickness was obtained. After several trial preparations, time of deposition was fixed as 3.5 hours for getting a thickness of 1 μm. Film deposition was repeated for different bath temperature from 40-80°C. It was observed that the rate of deposition

increases with temperature and then it comes to a steady state. Quality of the films were good (in appearance) for bath temperature of 70°C.

Deposition was attempted for different volumes of solutions of lead acetate and thiourea. This was done by keeping the volume of lead acetate solution constant while the volume of thiourea solution was varied as 20:20, 20:17.5, 20:15,20:12.5 and 20:10. Then this was repeated keeping the volume of thiourea at 20 ml while the volume of lead acetate solution was varied in the same manner. In all the cases the concentration was kept at 0.2 M. It was found that films obtained from bath containing solution in the ratio 20:20 were good. Films of thickness 1.2 μm could be obtained from this deposition bath at 70°C for a deposition time of 3.5 hours and were used for further characterisation.

6.4. Film Characterisation

The conductivity type of these PbS films was determined using hot probe analysis and was found to be p-type. Resistivity of these samples was found to be 10^7 Ω cm. Films were also prepared from deposition bath formed without EDTA. Time of deposition and temperature of the bath was fixed as 3.5 hours and 70°C respectively as in the previous case. Here also good films were obtained from reaction bath containing lead acetate and thiourea in the ratio 1:1 and were p-type. We found that resistivity of these PbS films prepared without EDTA was decreased to 10^5 Ω cm.

Crystalline nature of the films was revealed from X-ray diffraction studies [66]. Figure 6.1-6.3 show the X-ray diffraction spectra of PbS films prepared with EDTA in the as-prepared, air annealed and in vacuum annealed (10^{-2} Torr) condition after Mathew. C. Mathew [66]. From the diffraction pattern, it is observed that (200) plane becomes predominant in the microcrystals present in the film after an annealing in air at 200°C for 1 hour. However, annealing in vacuum does not bring any appreciable change in the crystal orientation. The d values and hkl planes of various diffraction lines observed in PbS films annealed in air (200°C) are shown in table 1.

Table 1. d-values and hkl planes observed in PbS thin film (annealed in air at 200°C) from XRD spectra

Observed 2θ (deg.)	Calculated d (nm)	Standard d (nm)	Identification
25.9	0.3435	0.3429	PbS (111)
30.0	0.2975	0.2969	PbS (200)
43.0	0.2100	0.2099	PbS (220)
50.9	0.1792	0.1790	PbS (311)
53.3	0.1714	0.1714	PbS (222)

6.4.1. TSC measurements

We conducted TSC measurements of PbS films prepared with and without the complexing agent EDTA. The experimental set up described in chapter 3 was used here. The duration of optical irradiation time was fixed as 5 minutes. Samples were annealed in air and vacuum (10^{-2} Torr) at 200°C for 1 hour.

TSC spectra of as-prepared PbS films prepared with EDTA is shown in figure 6.4. Various TSC curves are obtained for samples with different amount of EDTA. Irrespective of the amount of EDTA present, spectra for different samples show one peak at 375K and this corresponds to an activation energy of 0.21 eV. But it is noted that, as the quantity of EDTA increases, the peak height of TSC spectra decreases. This indicates that PbS sample with less amount of EDTA is capable of releasing more trapped carriers during the relaxation process. Even though the PbS films prepared using solution growth technique are photosensitive, it is reported [20] that films prepared from reaction bath containing some oxidant are more photosensitive. They could detect a sensitizing center in these oxidised films at an activation energy of 0.22 eV which was responsible for high photosensitivity.

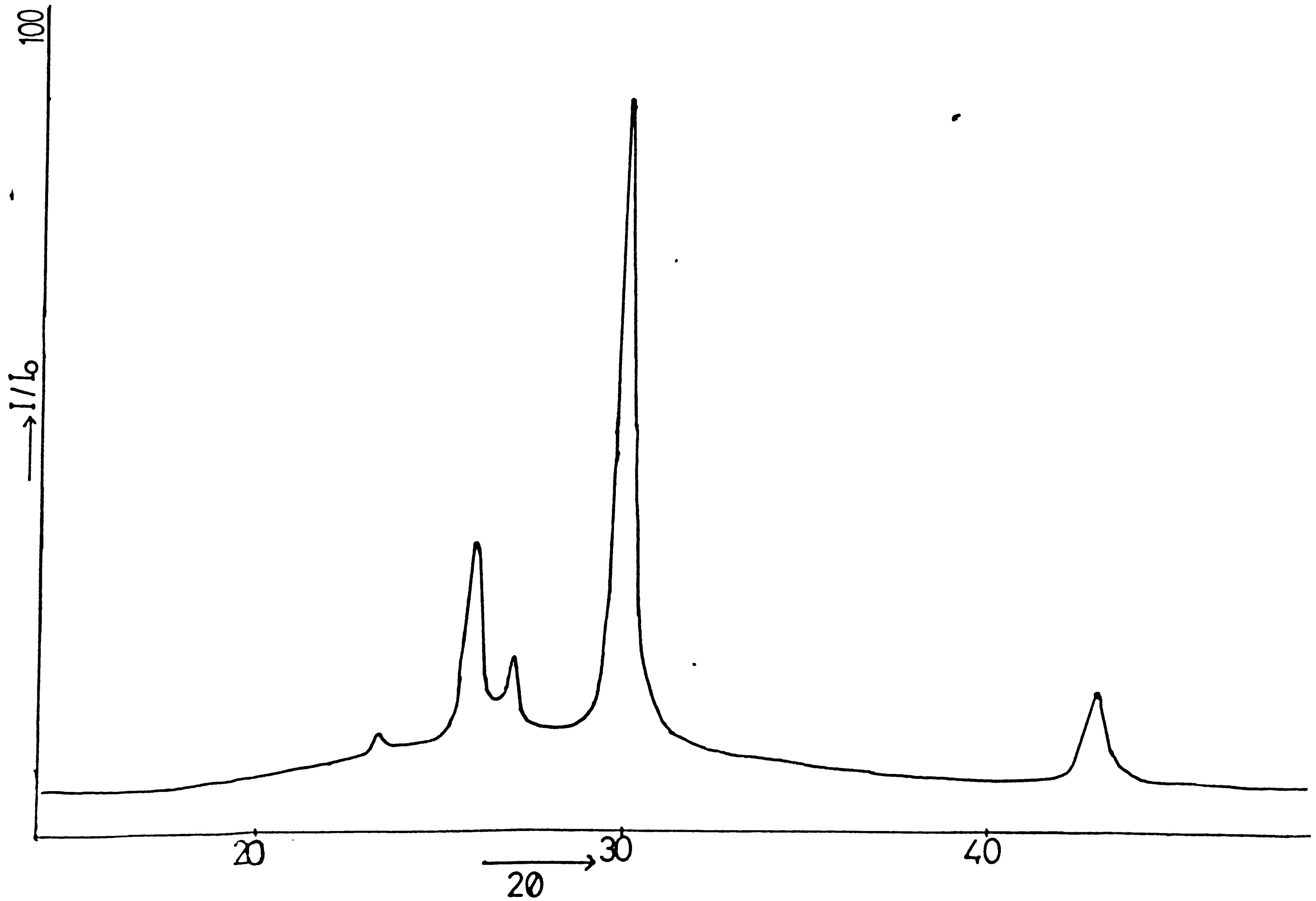

Figure 6.1. XRD spectrum of as-prepared PbS thin film

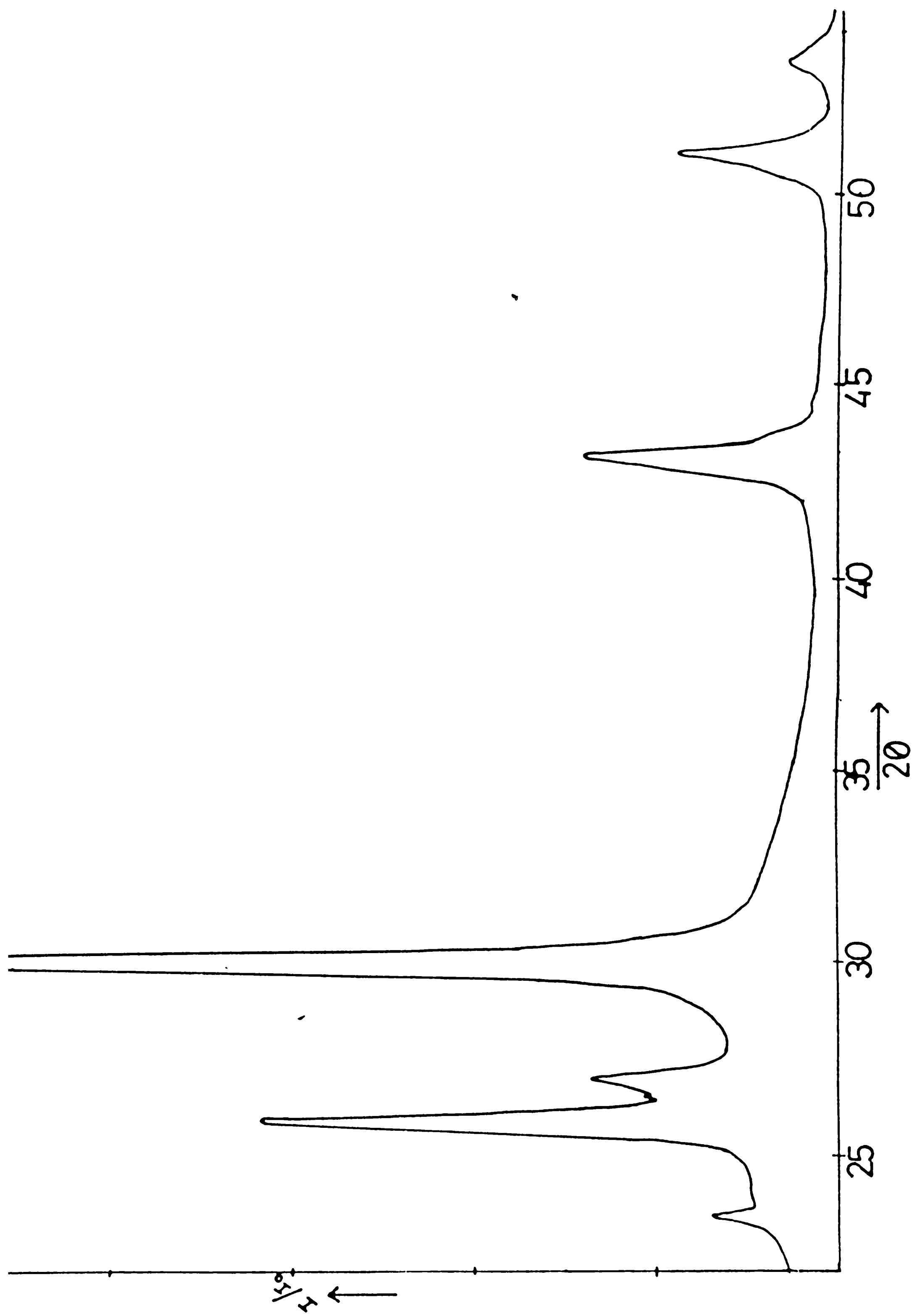

Figure 6.2. XRD spectrum of PbS thin films annealed in air (200°C)

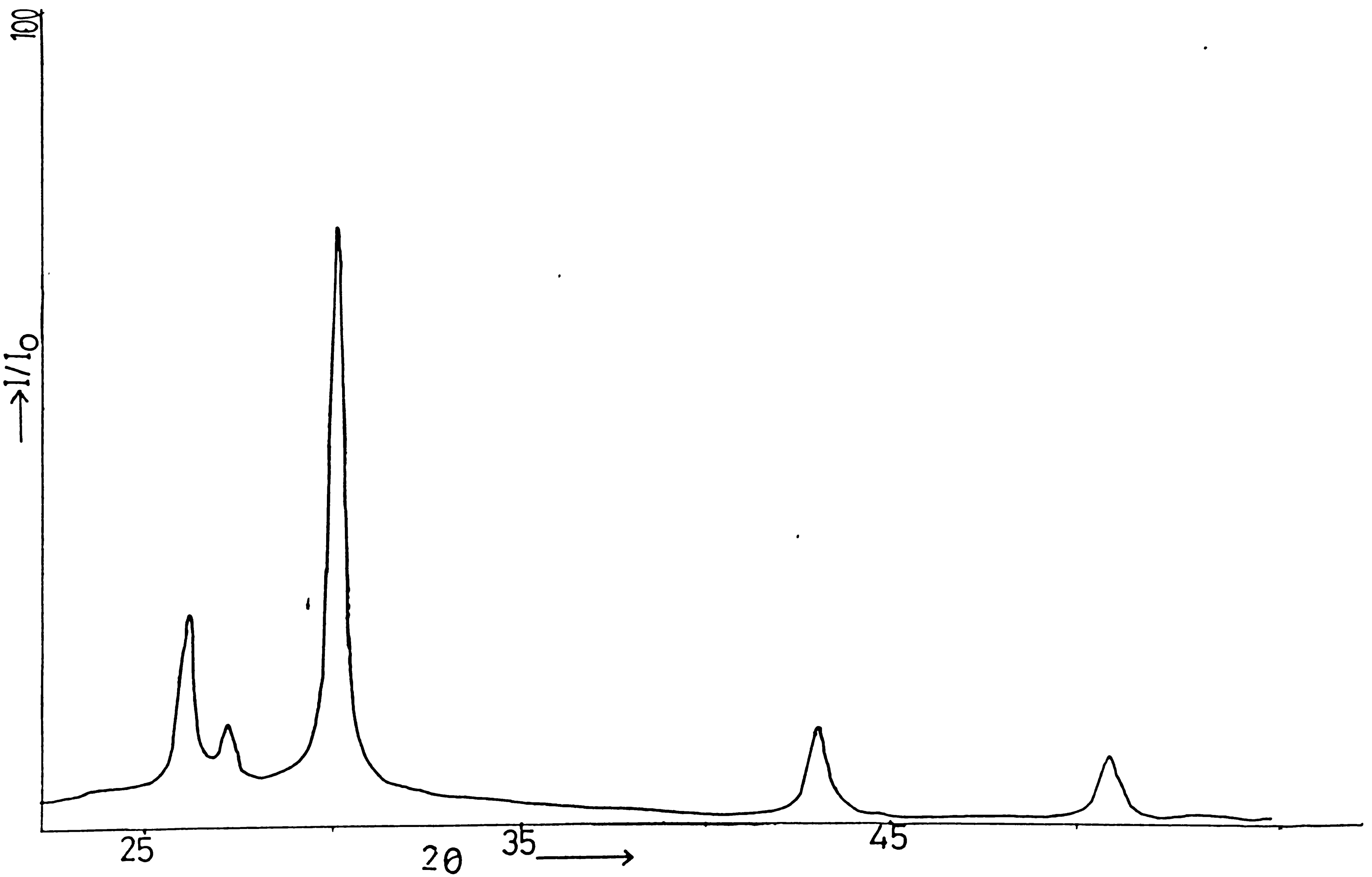

Figure 6.3. XRD spectrum of PbS thin films annealed in vacuum (200°C)

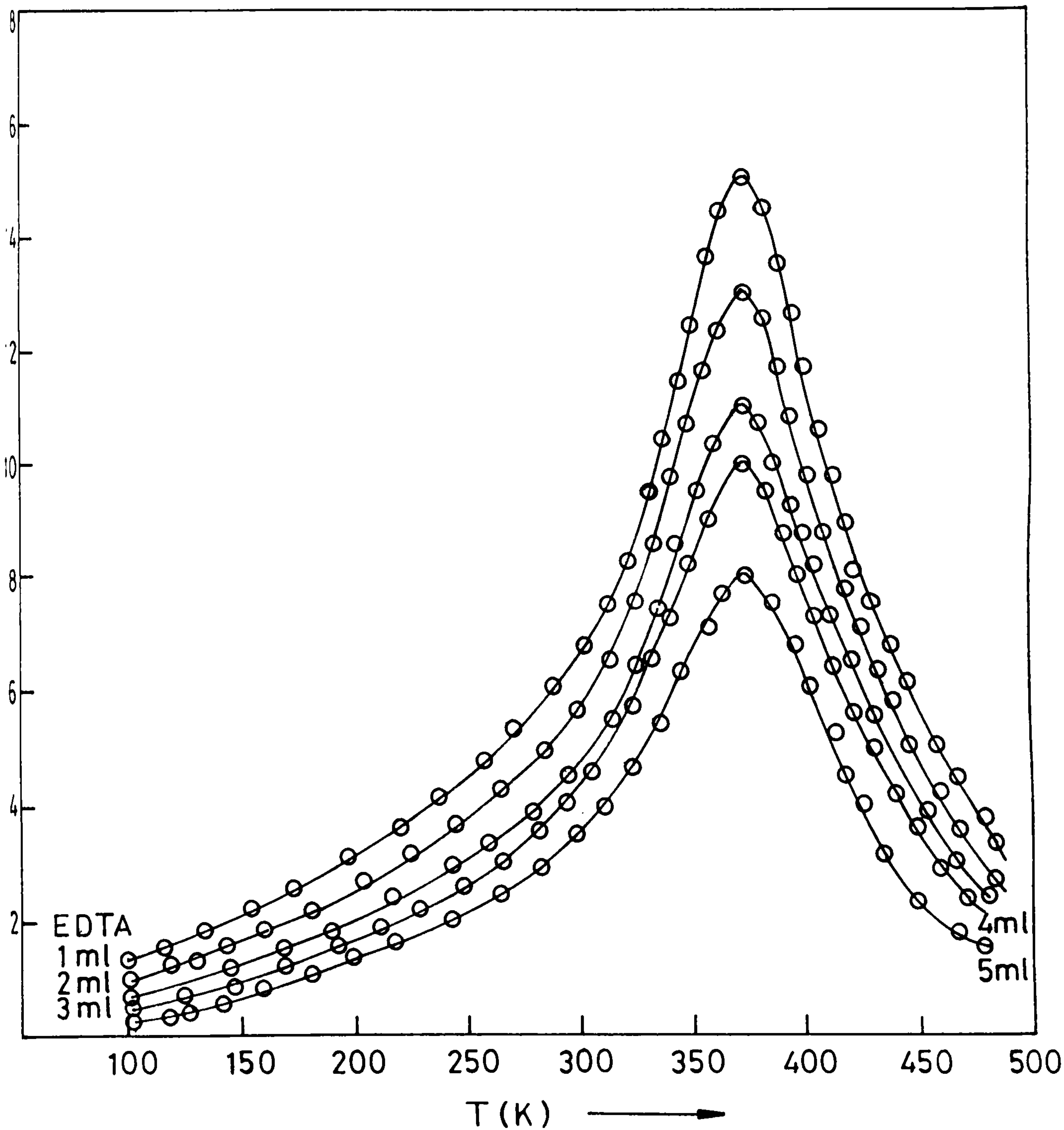

Figure 6.4. TSC spectra of as-prepared PbS thin films with different amounts of EDTA

In the present work, PbS films were prepared using solution growth technique without employing any oxidant. But from the TSC analysis of these, we could detect a sensitizing center at 0.21 eV which is very close to 0.22 eV of sensitizing center for high photosensitivity. The observed sensitizing center at 0.21 eV in the present work is a good evidence for the photoconductivity of PbS films prepared even without oxidant.

Figure 6.5 and 6.6 depict TSC spectra of PbS films with EDTA annealed in air and vacuum. As in the case of as-prepared samples, these spectra show only one peak of same activation energy (0.21 eV) at 375 K. Here also the amount of EDTA has the same effect on TSC spectra i.e., peak height decreases as the volume of EDTA increases.

We conducted TSC measurements on PbS films prepared without EDTA but with different amount of ammonia solution and spectra are shown in figures 6.7. Instead of one peak, here spectra depict two peaks of activation energy 0.21 eV (375 K) and 0.03 eV (150 K). The additional peak at 0.05 eV, may be the cause for the lower resistivity of PbS films prepared without EDTA. It is interesting to note that whether the sample is prepared with or without EDTA, the trap level (senstizing center) at 0.21 eV remains unchanged, which again indicate the high photosensitive character of the PbS films. Volume of NH_3 solution added in the reaction mixture (i.e pH) has got considerable effect on the TSC spectra. From the figure it is very clear that as the volume of NH_3 solution increases, peak height in the TSC spectra decreases.

TSC spectra of PbS films without EDTA annealed in air are shown in figure 6.8. and of films annealed in vacuum are shown in figure 6.9. As in the case of as-prepared samples, here also we could see two distinct peaks at 375 K and 150 K corresponding to the activation energies 0.21 eV and 0.05 eV respectively. Here samples with different amounts of NH_3 solution in the deposition bath were investigated and it is seen that as the amount of NH_3 solution increases, peak height is decreasing.

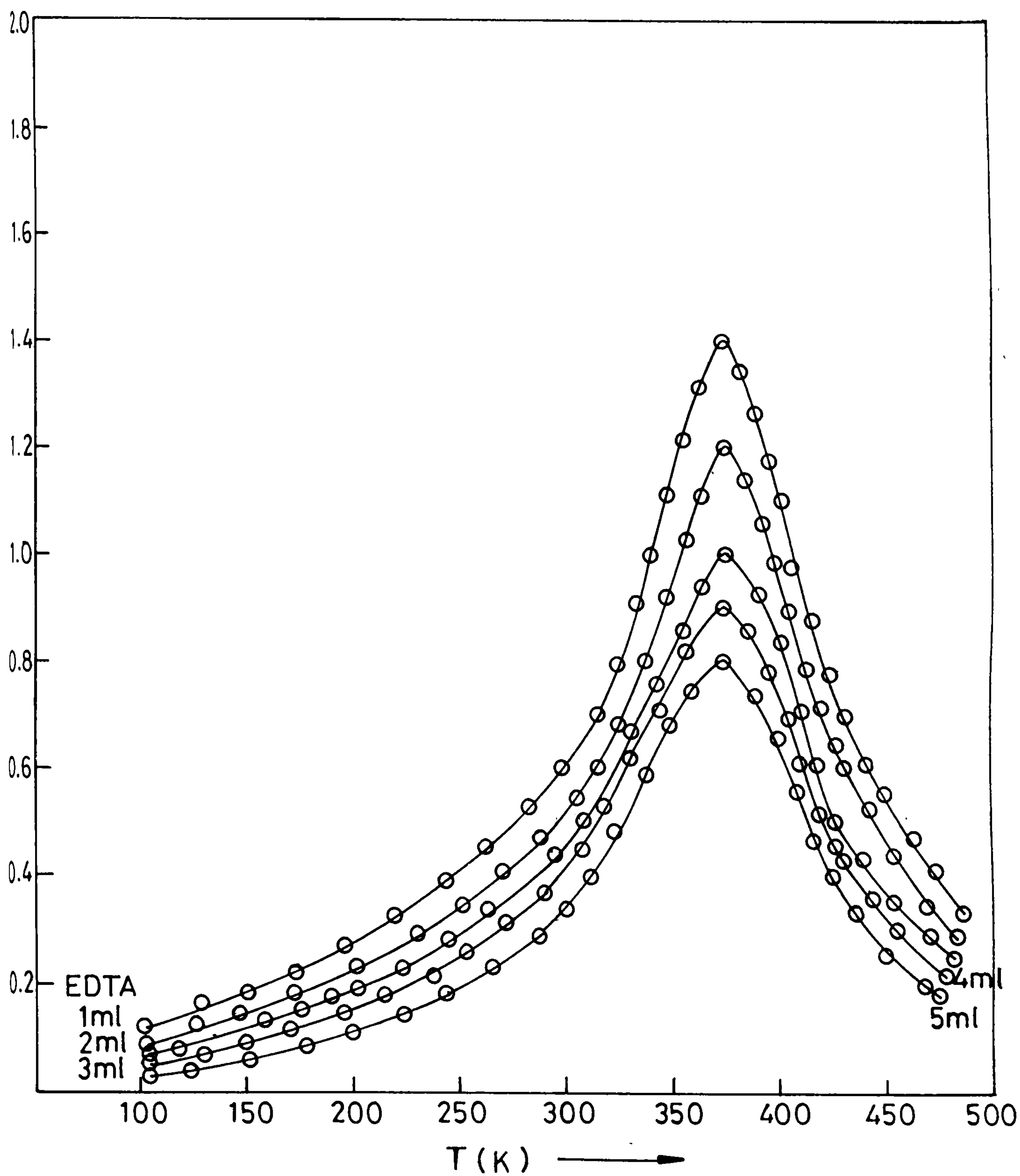

Figure 6.5. TSC spectra of PbS thin films annealed in air(200°C) with different amounts of EDTA

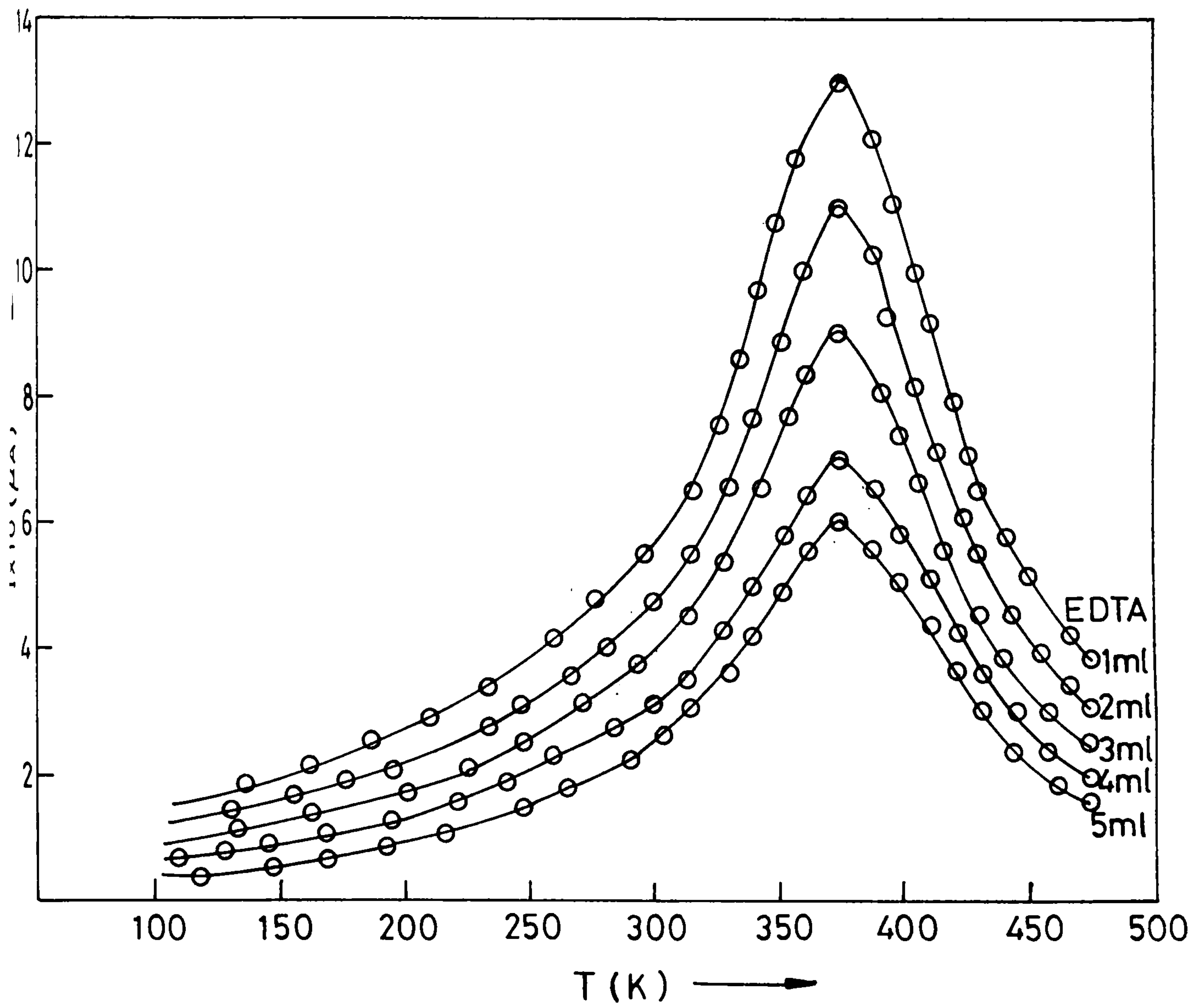

Figure 6.6. TSC spectra of PbS thin films annealed in vacuum (200°C) with different amounts of EDTA

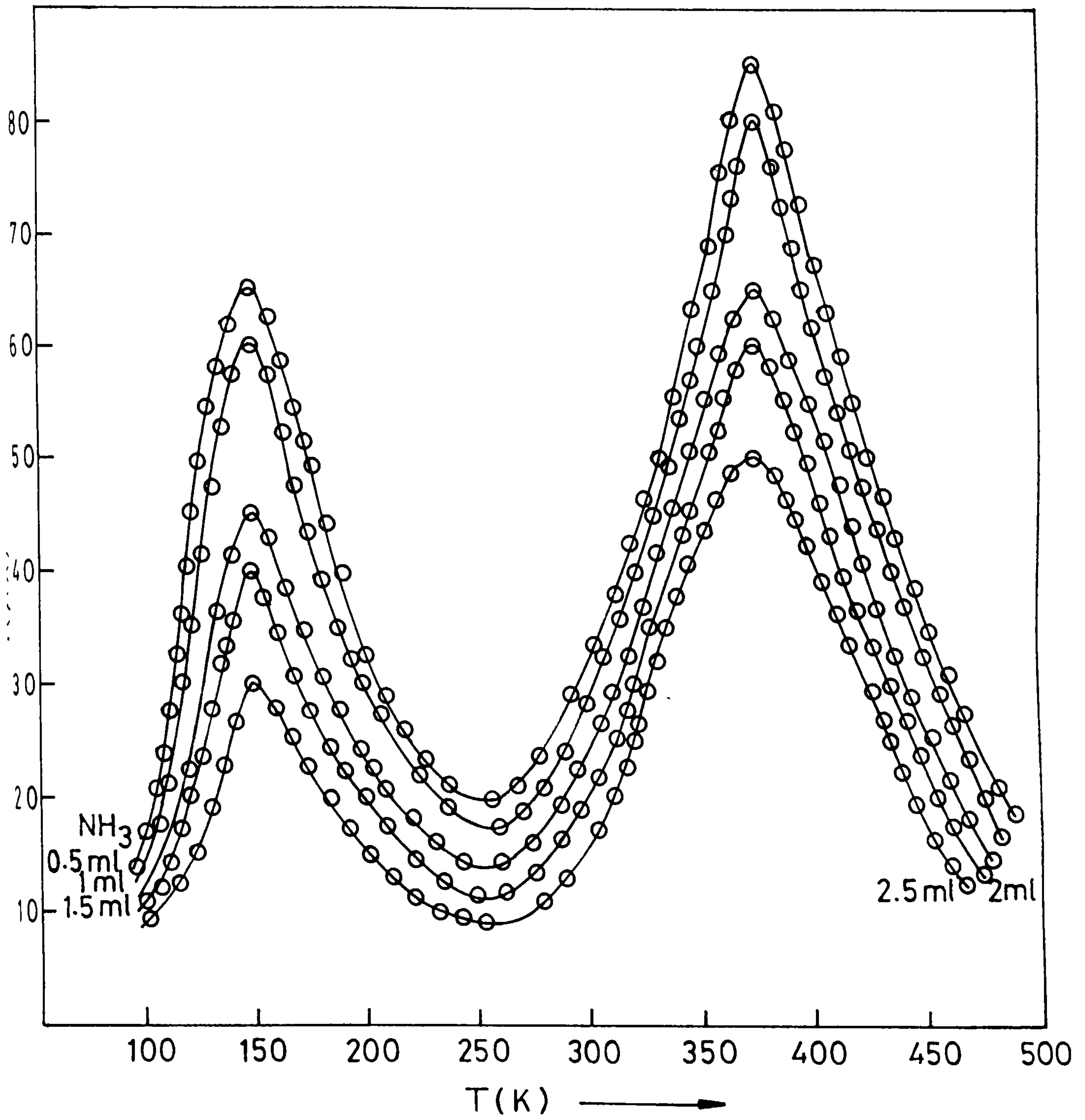

Figure 6.7. TSC spectra of PbS thin films without EDTA.

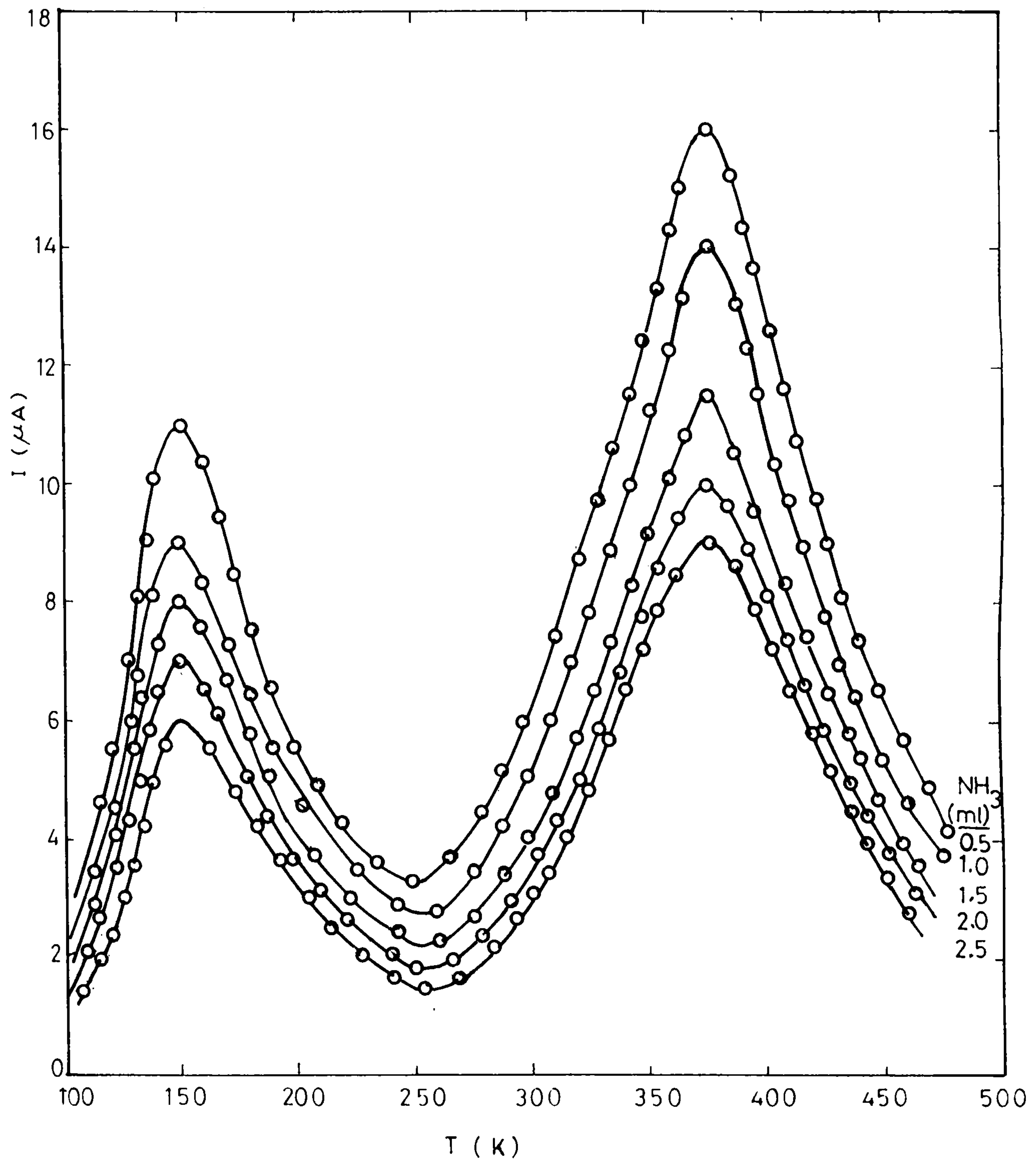

Figure 6.8. TSC spectra of PbS thin films annealed in air (200°C) without EDTA

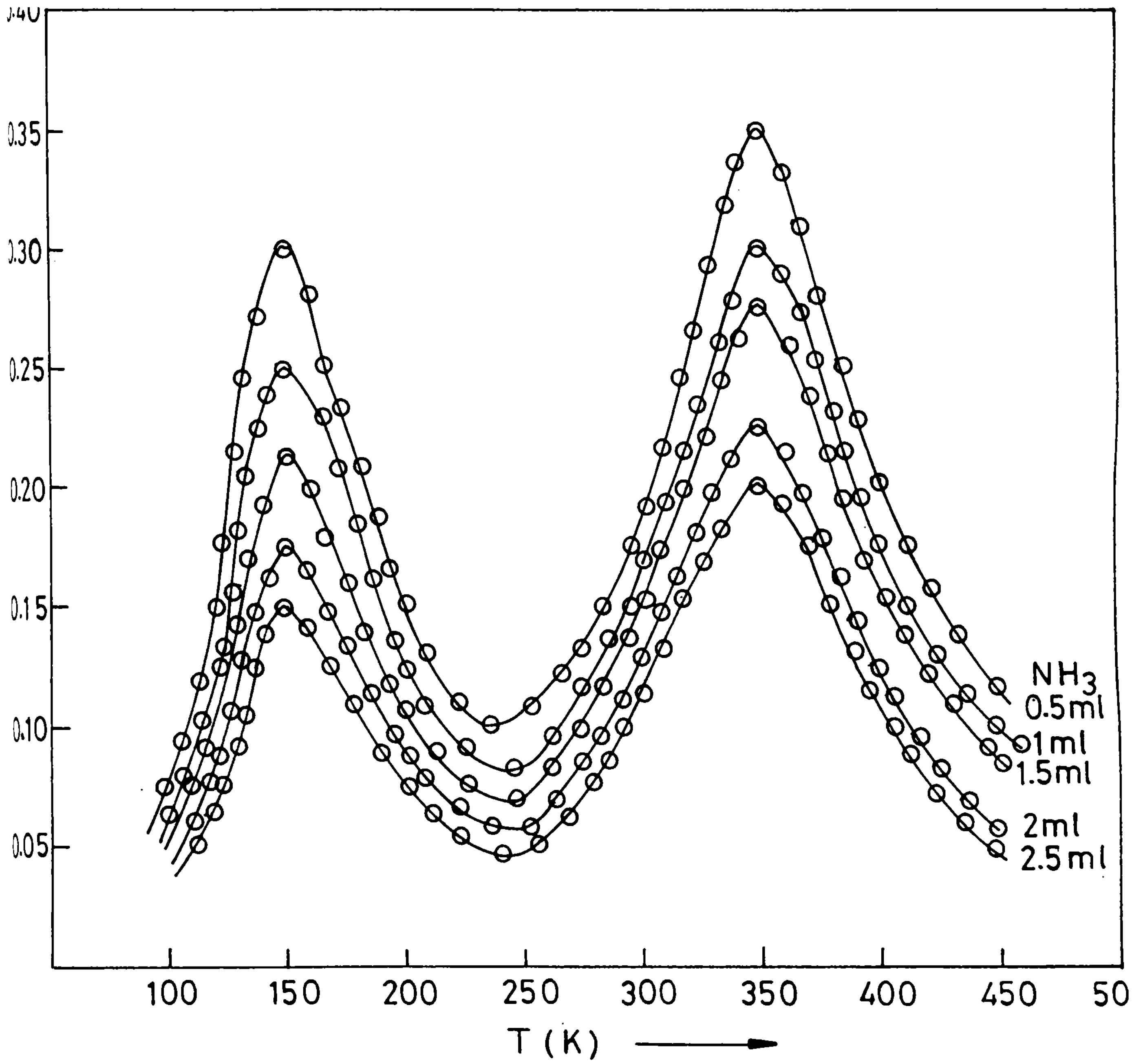

Figure 6.9. TSC spectra of PbS thin films annealed in vacuum (200°C) without EDTA

To determine the type of traps formed in PbS films, TSC measurements were performed by changing the polarity of bias voltage applied to the irradiating surface. Figure 6.10 shows the TSC curves for PbS films prepared with EDTA by applying positive and negative bias to the irradiating surface. From the spectra it is clear that I_{max} is higher for the case of negative bias voltage and hence the electron carrier is dominant here in the sensitizing center at 0.21 eV. Similar experiment was done with PbS film prepared without EDTA and the spectra are shown in figure 6.11 Here also the first trap at 0.21 eV shows higher value of I_{max} under negative bias, but for the second trap at 0.05 eV, the I_{max} is higher for the case of positive bias. Hence holes are the dominant carrier in the second trap. Results of TSC measurements including the capture cross section of the observed traps are summarised in the table 2. It is seen that the capture cross section of the second trap (0.05 eV) is somewhat smaller than the other at 0.21 eV, and is observed only in the case of sample without EDTA.

Table 2. Results of TSC measurements on PbS thin films

PbS sample type	Trap levels		
	Activation energy (eV)	Nature	Capture cross section (cm^2)
with EDTA	0.21	electron trap	0.532×10^{-26}
without EDTA	0.21	electron trap	0.532×10^{-26}
	0.05	hole trap	0.061×10^{-26}

6.4.2. Dark conductivity measurements

We made dark conductivity measurements on PbS films prepared with EDTA and also on films prepared without EDTA. Samples of thickness 1.2 μm was used for these measurements. The conductivity of the films was measured from 100 K to 500 K using the experimental set up described in chapter 3.

Figure 6.12 shows the Arrhenius plot of PbS film prepared from a deposition bath containing EDTA. From the slope of the graph, the activation energy was calculated to be 0.215 eV, which was very close to the value of activation energy calculated from the TSC

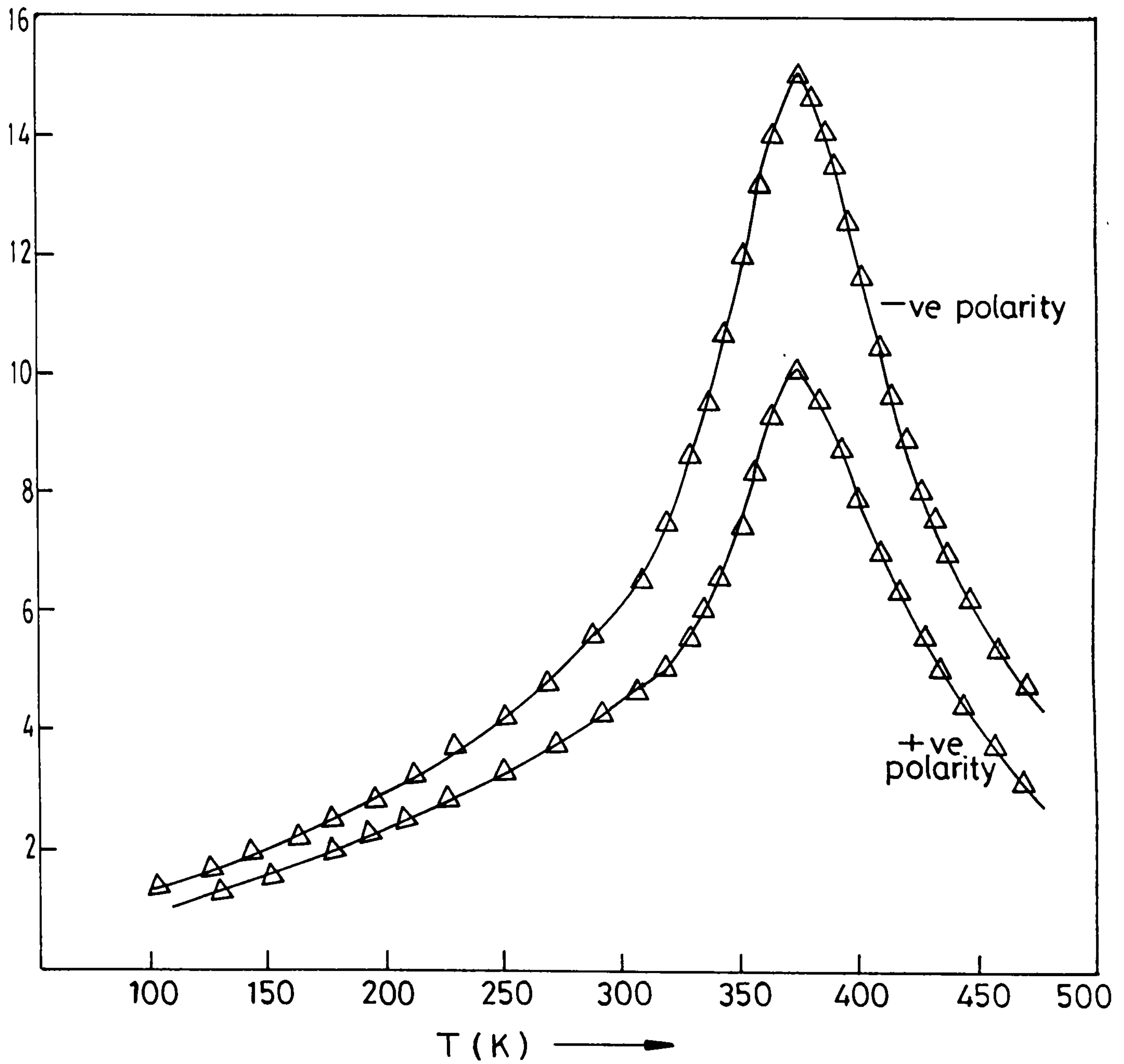

Figure 6.10 TSC spectra of PbS thin film (with EDTA) with positive and negative bias applied to the irradiating surface

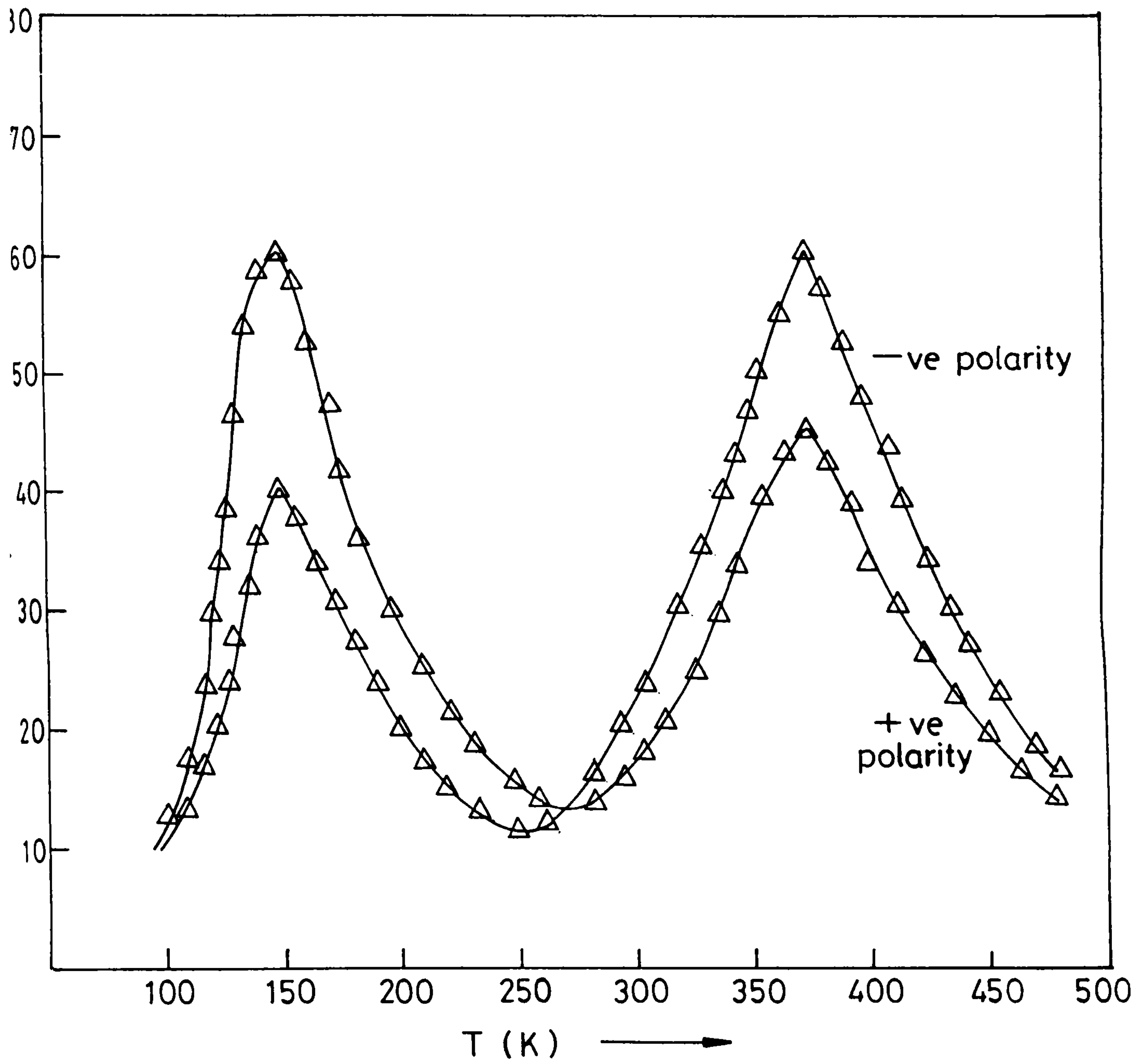

Figure 6.11. TSC spectra of PbS thin film (without EDTA) with positive and negative bias applied to the irradiating surface

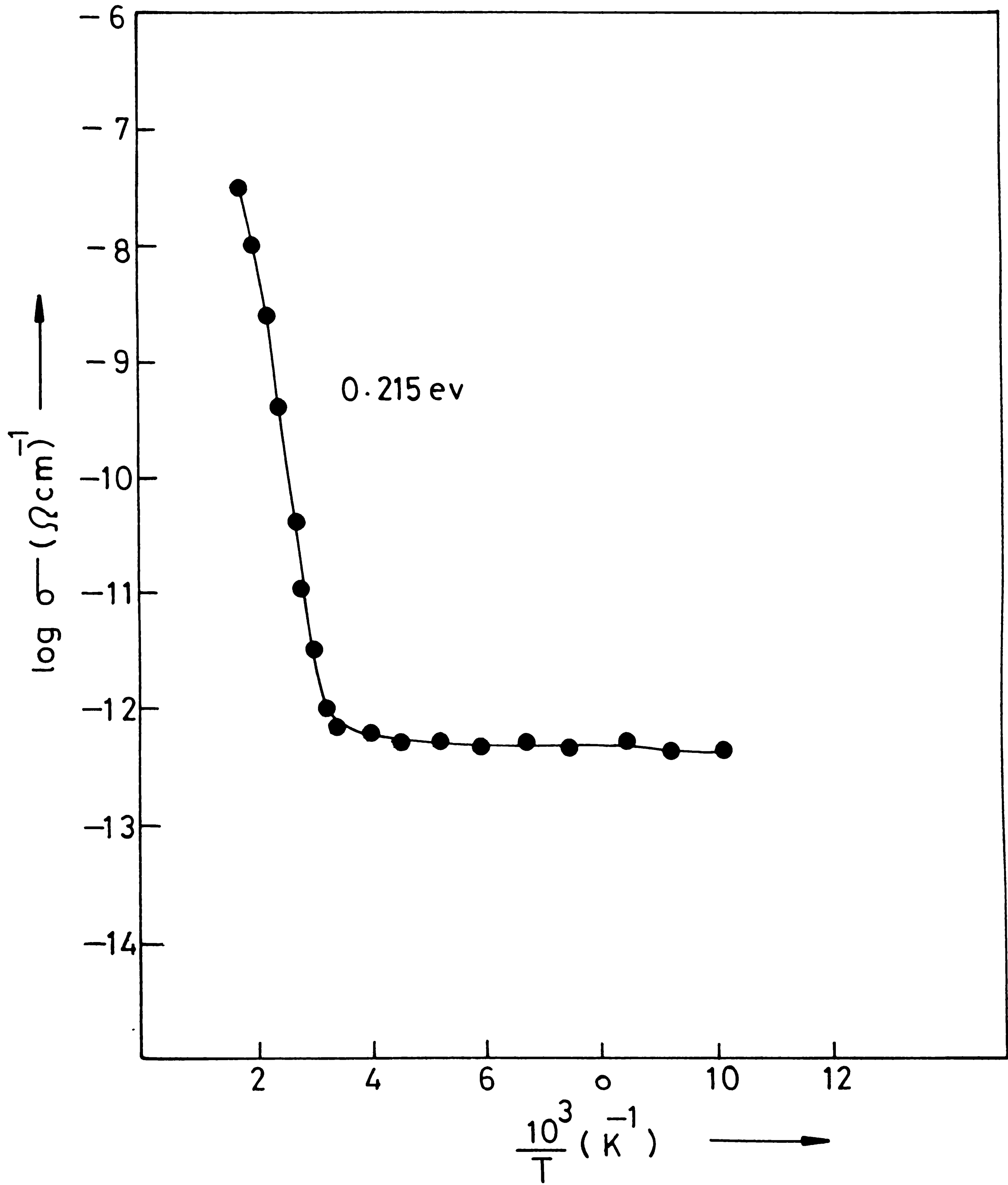

Figure 6.12. Arrhenius plot of PbS thin film with EDTA

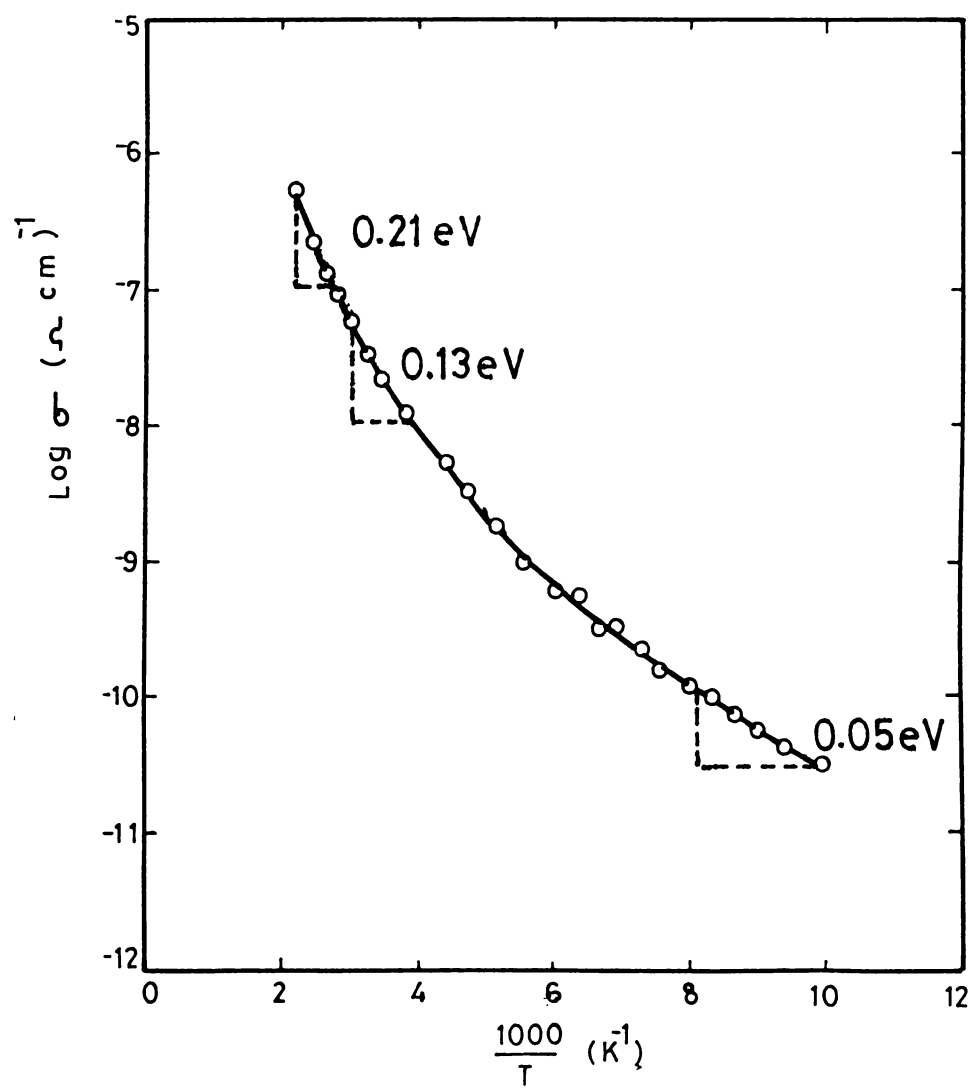

Figure 6.13 Arrhenius plot of PbS thin film without EDTA

spectra of these samples. So dark conductivity measurements also support the existence of a sensitizing center for photoconductivity in these samples.

Figure 6.13 shows Arrhenius plot of PbS film prepared without EDTA. From the slope of the plot different activation energies were calculated and are equal to 0.21 eV, 0.13 eV and 0.05 eV. The activation energy 0.21 eV corresponds to the presence of sensitizing center that was already obtained in TSC spectra. The 0.05 eV level is also detected in TSC spectra. The additional level 0.13 eV is attributed to a less effective sensitizing center that was reported earlier [20] in the chemical bath deposited films without any oxidant.

6.5. Conclusion

Thin films of PbS were prepared using a solution growth technique in which deposition bath was-prepared in two ways: one with the addition of complexing agent EDTA and the other without EDTA. Time of deposition and temperature of the bath in both cases were fixed as 3.5 hours and 70°C respectively. Resistivity of these two types of PbS films showed considerable difference. PbS films prepared with EDTA had resistivity of 10^7 Ω cm, while those prepared without EDTA had 10^5 Ω cm.

In order to get a clear picture of the trap levels present in these films, we conducted TSC measurements on both types of samples. We could detect a trap level at 0.21 eV in PbS films prepared with EDTA, while films prepared without EDTA showed two traps at 0.21 eV and 0.05 eV. It is observed that the common trap in these two types of PbS films is a very active sensitizing center for photoconductivity, which was reported earlier only in the case of films prepared with oxidants. The additional trap level at 0.05 eV in the PbS films without EDTA is an acceptor level and may contribute to its low resistivity. The sensitizing center at 0.21 eV was observed in the two types of samples from dark conductivity measurements also. This again supports the formation of highly photosensitive films useful for photovoltaic applications. Dark conductivity measurements also revealed the existence of additional levels at 0.13 eV and 0.05 eV in PbS films prepared without EDTA. The level at 0.13 eV is less effective sensitizing center and those at 0.05 eV are acceptor levels.

References

1. T.S.Moss, Proc.IRE, **43**(1955)1869
2. R.J.Cashman, Proc. IRE, **47**(1959)1471
3. D.E.Bode, *Phys. Thin Films*, **3**(1966)275
4. J.N.Zemel , *Solid Surface Physics*, **Vol 1** (Dekker, New York, 1969)p 291
5. D.N.Goryachev, L.G.Paritskii and S.M.Ryvkin, *Sov.Phys.Semicond.*, **4**(1971)1354
6. T.K.Chaudhuri, H.N.Acharya and H.N.Bose, Proc.Symp.on Luminescence and Allied phenomena, Kharagput, India, 1978
7. H.N.Acharya, T.K.Chaudhuri and H.N.Bose, 8th Annu.convention of the Optical Society of India, New Delhi, 1980
8. T.J.MeMohan and S.N.Jasperson, *Appl.Pot.*, **13**(1974)2750
9. R.Marchini and R.Gandi, *J.Appl.Phys.*, **49**(1978)390
10. B.K.Gupta, P.Thangaraj and O.P.Agnihotri, *Solar Energy Mater.*, **1**(1979)481
11. Chauduri, H.N.Acharya, H.N.Bose, Seminar or Solar Energy Rural & Industrial Applications, Kharagpur, India, 1981
12. A.J.Sievers, *Top.Appl.Phys.*,**31**(1979)107
13. H.N.Acharya and H.N.Bose, *Phys.Status Soilidi (a)*, **6**(1971)k3
14. J.Bloem, *Appl.Sci.Res.Sect.*, **B 6**(1956)92
15. A.S.Baranski and W.R.Fawcett, *J.Electrochem.Soc.*, **127**(1980)766
16. G.Brukmann, *Kolloid Z.*, **65**(1933)148
17. R.A.Smith, *Advan.Phys.*, **2**(1953)321
18. R.A.Smith, *Semiconductors* (Cambridge, England, 1959)p 414
19. R.H.Bube, *Photoconductivity of Solids* (Wiley, New York, 1960) p 356
20. Svein Espevik, Chen-hoWu and R.H.Bube, *J.Appl.Phys.*, **42**(9)(1971)3515
21. G.H.Blount, M.K.Preis, R.T.Yamada and R.H.Bube, *J.Appl.Phys.*, **46**(1975)3489
22. G.H.Blount, P.T.Schreiber, D.K.Smith, R.T.Yamada, *J.App.Phys.*, **44**(3)(1973)978
23. Sh.B.Atakulov and K.E.Onarkulov, *Sov.Phys.Semicond.*, **19**(7)(1985)811
24. I.Pop, C.Nascu, V.Ionescu, E.Indrea, I,Bratu, *Thin Solid Films*, **307** (1-2)(1997)240
25. Lange, *Physik*, **31**(1930)964
26. W.D.Lawson, *J.Appl.Phys.*, **23**(4)(1952)495

27. Frank Pizzarello, *J.Appl.Phys.*, **25**(6)(1954)804
28. Richard L Petriz and Wayne W Scanlon, *Phys.Rev.*, **97**(6)(1995)1620
29. A.Santoni, G.Paolucci, G.Santoro, K.C. Prince and N.E. Christensen, *J.Phys.Condens.Matter.*, **4**(1992)6759
30. T.Kendelewicz, P.Liu,G.E.Brown, and E.J. Nelson, *Surface Science*, **395**(2-3)(1998)229
31. I.Karto, G.Wittstock, K.Laajalehto, D.Hirsch, J.Simola, T.Laiho, R.Szargan, E.Suoninen, *International J. of mineral processing*, **51**(1-4)(1997)293
32. Hass and Rudoff E Theen, *Physics of thin films* 3 Ed.(Academic Press, New york, 1966)
33. V.I.Biryulev, G.P.Tokhomirov, *Sov.J.Opt.Techno.*, **41**(1974)352
34. J.George, T.I. Palson, K.S.Joseph, *Solid State Commun.*, **58**(9)(1986)605
35. A.N.Kovalev, F.I.Manyakhin, *Phys.Chem.and Mech.Surf.*, **5**(2)(1989)396
36. A.N.Kovalev, V.I.Paramanov, *Phys.Chem.and Mech.Surf.*, **4**(8)(1987)2437
37. Z.Sel Mandouh, *Fizika*, **21**(3)(1989)243
38. M.Paic, V.Paic, K.Duh, J.N.Zamel, *Thin Solid Films*, **12**(2)(1972)419
39. A.Lopez, D.Duh, J.N.Zamel, *Mater.Sci and Eng.*, **17**(1975)63
40. H.R.Riedl, R.B.Scholar, Report NOLR - 68-83 USA (1968)38
41. R.C.Tyagi, S.K.Agarwal, V.C.Sethi, *Indian J. Pure and Appl.Phys.*, **15**(9)(1977)670
42. P.J.Martin, R.P.Netterfield, W.G.Sainty, *Thin Solid Films*, **87**(3)(1982)203
43. W.R.Fawcett, *J.Electrochem.Soc.*, **127**(3)(1980)766
44. M.Sharon, K.S.Ramaiah, M.Kumar, M.Neumannspallart, C.Leryclement, *J. Electro analytical Chem.*, **436**(1-2)(1997)49
45. G.W.Mahlman. *Phys.Rev.*, **103**(6)(1956)1619
46. H.E.Spencer, *Phys.Rev.*, **113**(1959)1417
47. V.M.Simic and Z.B.Marin Kovic, *Phys.Status.Solidi*, **9**(1)(1965)k1
48. G.H.Blount, P.J.Schreiber, D.K.Smith, R.T.Yamada, *J.Appl.Phys.*,**44**(3)(1973)978
49. D.M.Mattox, G.J.Kominiak, *J.Vac.Sci and Technol.*, **12**(1975)182
50. G.P.Kothiyal, B.Ghosh, R.Y.Deshpande, *J.Phys.D.*, **13**(5)(1980)869
51. G.B.Reddy, V.Dutta, D.K.Pandya and K.L.Chopra, *Solar Energy Mater.*, **5**(2)(1981)187
52. G.B.Reddy, D.K.Pandya and K.L.Chopra, *Thin Solid Films*, **90**(4)(1982)410
53. T.K.Chaudhuri, H.N.Acharya and B.B.Nayak, *Thin Solid Films*, **83**(1981)L169

54. G.B.Reddy, D.K.Pandya and K.L.Chopra, *Solar Energy Mater.*, **15**(5)(1987)383

55. T.P.Sharma, R.Kumar, and G.Jain, *Indian J.Pure and Appl.Phys.*, **29**(8)(1991)583

56. A.V.burlak, V.V.Zotov, A.V.Ignatov, A.V.Tyurin and V.G.Tsukerman, *Sov.Phys.Semicond.*, **26**(3)(1992)311

57. O.A.Gudeav, E.E.Paul, Optoelectron Instrum.Data Process (USA) 117(1989)

58. M.Ohtsaka, *Acad.Rep.Fac.Eng.*, **11**(1990)26

59. Sh.B.Atakulov,K.E.Onarkulov, *Sov.Phys.Semicond.*, **24**(10)(1990)1173

60. G.Marcu and V.Ionescu, *Revista de Chimic*, **48**(10-11)(1997)872

61. M.P.Belyanskii, A.M.Gas'kov, Z.M.Dashevskii, K.V.Rozhkova and M.P.Rulenko, *Sov.Phys.Semicond.*, **24**(1990)1271

62. T.K.Chaudhuri, *Int.J.Energy.Res.*, **16**(1992)481

63. L.L.Derofeeva, A.N.Komov, I.V.Lenivkina, S.G.Losevskaya, *Phys.Chem. and Mech.Surf.*, **6**(3)(1990)723

64. M.J.Resso and R.E.Harris, *Photonics Spectra*, **24**(4)(1990)111

65. P.K.Nair and M.T.S.Nair, *J.Phys.D.Appl.Phys.*, **23**(2)(1990)150

66. Mathew C Mathew, M.Phil Thesis, Cochin University of Science and Technology, 1994

Chapter 7

Preparation and characterisation of FeS_2 thin films

7.1. Introduction

The high production cost of conventional solar cells at present makes it necessary to search for alternate low cost and simple production methods and better materials. Semiconductors with high absorption coefficient are favourite candidate because of the possibility of using a thin film as the active layer. One of such materials is pyrite (FeS_2). For more than fifteen years this material has been investigated as an alternate solar cell material due to its extraordinary optical absorption ($\alpha \geq 6 \times 10^5$ cm^{-1} for $h\nu > 1.3$ eV) [1] and suitable band gap, $E_g = 0.9$-1 eV [2]. A pyrite film of 0.1μm thickness absorbs more than 99% of the sun light (AM 1.5) [3]. Moreover, FeS_2 is composed of very abundant and cheap components that are non toxic. These reasons make it a promising material for low cost large scale production of thin film solar cells. However, the large scale preparation of pyrite thin films is still a problem.

First part of this chapter presents a review of work done in pyrite, both crystals and thin films. In the second part, details of the attempts made in our laboratory to prepare FeS_2 thin films using spray pyrolysis and CBD are discussed. The results of characterisation of these samples are also included in this section.

7.2. Pyrite Crystals

In 1968, single crystals of Iron pyrite had been prepared by R.J. Bouchard using chlorine transport in various temperature gradients [4]. It was reported in 1974 that natural single crystals of pyrite from Spanish mines appear to be 'n' type semiconductors. In that work, the resistivity, Hall coefficient and Hall mobility had been studied as a function of temperature and chemical decomposition of the samples at temperature $\geq 200^{\circ}C$ was

considered as a factor influencing the determination of intrinsic properties of pyrite. Magnetic susceptibility studies of $Fe_{(1-x)}$ S single crystals were performed by J.L. Horwood et al in 1976 [5]. Optical properties, phonons and electronic structure of FeS_2 were studied by A. Schlegel et al [6]. Optical absorption studies in this natural single crystals of iron pyrite were reported in 1978 [7]. Accordingly, in low resistivity samples, there is a pronounced absorption varying nearly as λ^2 (λ is the wavelength) for energies below the absorption edge (may be due to the absorption of free carriers) and in high resistivity samples the absorption band results from phonons assisted indirect transition between the valence band and conduction band. Later temperature dependence of the band gap in a 150 μm thick natural single crystal of FeS_2 had been reported by M. S. Seehra et al [8]. They proposed a variation of the form $E_g(T) = E_g(0) + aT + bT^2$, with the parameter $E_g(0) = 0.835$ eV, $a = 4 \times 10^{-5}$ eV/K, b = -7.4 ×10-7 eV/K^2. The reflectivity spectra of FeS_2 single crystals had been measured for photon energies between 0.2 and 4.4 eV by Katsuaki Sato in 1984 [9].

The pyrite has a structure that can be considered as an NaCl-like grouping of iron atoms and S_2 pairs [10]. The crystals are cubic with four molecules in a cell of dimension a_o = 5.40667 A^0 [11]. In the pyrite structure each iron atom is surrounded by six sulphur atoms at the corners of a nearly regular octahedron with the Fe-S distance of 2.26^0A, while each sulphur atom is bond to one other sulphur atom and to three iron atoms. The bonding throughout the structure is wholly covalent. The pyrite FeS_2 is the d^6 low-spin semiconductor with the configuration $t^6_{2g}\ e^0_g$ [10]. The main features of local coordination are common to both NiAs type FeS and the pyrite type FeS_2. But Fe-S distance for FeS (2.5 A^0) is somewhat larger than that of FeS_2 (2.26A^0). The results of a rigorous energy-band calculation for the series of 3d transition metal disulfides including FeS_2 had been reported by Bullet[12].

The segregation studies of pyrite crystals had been reported in 1984 by G. Panzner et al [13]. In that study the surfaces of iron crystals covered by segregated sulphur and of iron sulphide layer were analysed in a combined electron spectroscopic study by means of XPS, AES and Electron Energy Loss Spectroscopy (EELS). The binding energies of iron and

sulphur core levels reveal a strong electron transfer from the iron surface atoms to the segregated sulphur atoms. Auger spectra indicated a distinct interaction between sulphur and iron surface atoms, which is most pronounced for sulphur segregated on the iron surface and decreases to FeS and to FeS_2.

Later in 1985, polycrystalline layers of As-doped pyrite have been produced in bromine atmosphere with the aim of developing these sulfide materials for solar energy application [14]. Its photoelectrochemical behaviour in contact with an aqueous electrolyte was investigated. It was operated as a photoelectrochemical solar cell and showed reasonably stable behaviour under illumination. Optical measurements performed on FeS_2 showed that the visible light is absorbed in an extremely thin layer of 160 A^o in spite of the apparently indirect band gap of this semiconductor. SEM of the samples revealed well developed crystallites of about 5-10 μm with distinct boundaries. Scanning laser spot analysis over macroscopic areas (5mm) showed homogeneous as well as inhomogeneous regions. The photoelectric properties of the polycrystalline pyrite samples were found to be poor.

A study of chemical vapour transport of pyrite with halogen had been reported in 1986 by S. Fiechter et al [15]. In the same year characterisation of the photoactive FeS_2/electrolyte interface was performed by A. Ennaoui et al [16]. In that work, the electronic properties of synthetic pyrite single crystal of (100) orientation were investigated. The spectral response of the photoconductivity was determined by the four point probe technique. The carrier concentration (N_D -N_A ~ 1×10^{18} cm^{-3}) was calculated from capacitance measurements and the minority carrier diffusion length (0.13μm) was determined by photocurrent and capacitance vs voltage measurements [16]. These calculations allowed the construction of an energy band diagram for FeS_2/electrolyte contact and the parameters determined could explain the high quantum efficiency (~90%) obtained with FeS_2/I^-, I_3^- photoelectrochemical cells. Photoelectrochemistry of highly quantum efficient single crystalline n-FeS_2 was reported in 1986 itself [17]. In that work, monocrystalline n-FeS_2 photoelectrodes with high quantum efficiency (>90%) had been obtained by improvement of the solid-state and interfacial chemistry. The influence of

etching treatments, various redox systems and organic-electrolytes on the photochemistry of FeS_2 was investigated. The formation and the dynamics of a thin oxidised layer deposited at the surface of the electrode in the presence of an acid electrolyte were studied using light reflection techniques and ESCA. A low effective carrier density ($n= 0.7 \times 10^{1}$ cm^{-3}) was measured, resulting in an extended space-charge layer, which has to be compared with the high absorption coefficient [17].

The influence of molecular as well as atomic hydrogen on the interfacial properties of pyrite had been investigated [18]. It is reported that molecular hydrogen selectively converts FeS_2 surfaces other than the (100) to FeS. Interestingly atomic hydrogen generated by electrochemical and chemical treatment does not lead to this type of selective attack of the pyrite surface, but significantly improves the photocurrent to dark current ratio. Atomic hydrogen is supposed to be associated with sulphur atoms adjacent to sulphur vacancies. It thereby attracts negative charges from iron and transforms the electronically unfavourable FeS states that produce defect levels in the band gap into more favaourable FeSH centers [18].

It was reported that [19] a temporary photoelectrochemical oxidation of chloride on a pyrite electrode surface can lead to a considerable enhancement of photocurrent response and a decrease of the dark current. The improvement of the interface is caused by a photocorrosive transformation of the interface that reduces the concentration of surface recombination centers and leads to a change in the concentration and redistribution of energy levels in the forbidden energy region. XPS studies identify the surface states in the pyrite interface that are responsible for its poor photoelectrochemical behaviour and which can be removed during chloride oxidation as FeSH group.

The bandgap nature of FeS_2 determined from optical and photoelectrochemical measurements were reported in 1990 by I.J. Ferrer et al [20]. In that work experimental values of Eg show a considerable dispersion from 0.7 eV to 2.6eV, but a clear nature of transition responsible for the energy gap is not given.

In order to produce a good solar cell with pyrite, several problems have to be overcome that were uncovered in photoelectrochemical cells. Open circuit voltage (V_{oc}) of n-type crystals were found only in the range of 0.15-0.2 V [16,17,21] and never reached a value of half the band gap or more, as usual for semiconductor in electrochemical cell [22]. The consistency with which low open-circuit voltages were measured raised the question whether it would be due to an intrinsic defect (i.e. an electronic defect coupled to the material). This hypothesis gained importance as investigations using Inductively Coupled Plasma with AES (ICPAES) revealed that natural and synthetic crystals were found to be exclusively sulphur deficient. So pyrite would more appropriately be expressed as FeS_{2-x} rather than FeS_2, with x ranging between 0.05 and 0.25 [23,24].

Ideal pyrite had an atomic ratio S:Fe = 2:1 and a density of ρ = 5.01 gm/cm^3. Deviation from this ideality had been reported [23,25-29]. It is also suggested that natural crystals with S:Fe ratios less than 2 have iron atoms residing on sulphur position due to densities greater than the theoretical value of 5.01gm/cm^3. The possibility of missing S atoms in the lattice is also suggested.

If pyrite occurs with variable chalcogen-content and this leads to a contraction of the unit cell, powders with different sulphur to iron ratios should have different unit cell edges [30]. Therefore it should be possible to distinguish between samples having different S:Fe ratios by careful measurement of the lattice constant. Large differences in unit cell lengths were not expected, since the crystallographic hardness for pyrite is quite large[31], which would indicate a low flexibility of chemical bonds. The nature of sulphur deficit in pyrite had been investigated by powder X-ray diffraction [30] in which it was suggested that the most important thing for optimising pyrite as a solar cell material would be to reduce S vacancy concentration and to produce material having S:Fe ratio very close to 2:1. In 1992, metal/n-pyrite (metal=Pt,Au,Nb) Schottky barrier type diodes were fabricated on electrochemically reduced (either synthetic or natural (100) and (111)) surfaces of single crystalline n-FeS_2 by K.Buker et al [32]. In that work the temperature dependence of I-V curves in darkness was analysed in the range of 200-350 K on the basis of thermionic emission and recombination models. Photovoltaic parameters like open circuit

photovoltage and short circuit photocurrent were studied down to a temperature of 200 K. It was also suggested that the critical limitation of the open-circuit photovoltage of the pyrite/metal junctions was due to a defect level probably prominent from a sulphur deficiency. Regarding the type of conduction in pyrite crystals, natural crystals exhibit both n and p-type conduction [33]. It had been suggested that natural pyrite formed at lower temperature tends to be p-type whereas high temperature pyrite tends to be n-type due to an iron or sulphur deficiency respectively [34]. It is also suggested that Co and Ni acts as donors, whereas As acts as an acceptor in pyrite [35]. In another work by the Fiechter group [15] small pyrite crystals prepared using iodine as transport agent in a CVT experiment, were found to be p-type, from thermoprobe measurements. In the work of Blenk [34] also, p-type pyrite single crystals could be prepared in a high sulphur pressure and was confirmed with Hall measurements.

7.3. Pyrite thin films

The first pyrite thin film was prepared thermally by Seehra et al in 1979 [36]. After that different techniques had been employed by different groups. It was reported in 1980 that pyrite is decomposed even before it melts [37] and therefore it is relatively difficult to prepare a pyrite thin film by thermal evaporation. But in 1986, these films had been prepared by two groups [38,39] using thermal evaporation technique itself with some modification in the method suggested by Seehra [36]. In the work of Karaguppikar et al [38] the resistivity of the films were measured in the thickness range 10-150 nm. Semiconducting nature of the films were confirmed using Hall effect and TCR techniques. The films of thickness higher than 50 nm yields the saturated value for resistivity. In the second work by Gupta et al [39] amorphous nature of as-deposited films was reported. On annealing ordering was produced in those films. Again Mossbauer spectrum of the films was fitted with two doublets. The two doublets had been attributed to the presence of non-stoichiometry in the films. Following these two works, pyrite films were chemically deposited on quartz plates using spray pyrolysis by Abass et al [40] in 1986 itself. Absorption coefficient data in the fundamental absorption region were analysed and interpreted in terms of interband transition. Later the same group reported the absorption

edge measurement in these films [41]. Optical absorption data for photon energies between 1 and 3.8 eV were analysed and interpreted in terms of electronic transitions and assisting phonons. A direct forbidden band gap of 1.12 ± 0.003 eV and assisting phonons of 0.0065 eV were detected in that work. In the same year thin film iron pyrite was also prepared using chemical vapour deposition of ironpentacarbonyl and sulphur or H_2S by Chatsitheodorou et al [42]. Pyrite thin films were also prepared by the reaction of ironpentacarbonyl with sulphur source in an organic solvent in 1988 [43].

Condition for the production of thin pyrite layers using spray pyrolysis had been investigated for potential use as a solar cell material by G.Smestad et al in 1989 [44]. In that work, best results were obtained from an aqueous molar ferric chloride to thiourea ratio of 0.03M : 0.072M. The films were deposited on glass substrate at 350°C in presence of gaseous sulphur and were sprayed with nitrogen as carrier gas. A simple hydrolysis reaction mechanism was proposed where thiourea, iron chloride and sulphur react on the hot substrate to form CO_2, NH_3, HCl and FeS_2. The crystallinity and phase of the films were confirmed as pyrite by X-ray diffractometry. Steady state conductivity measurements showed the films to be extrinsic semiconductors with an activation energy of 0.03 eV. Optical transmission measurements indicated a soft band gap due to grain boundaries. Lifetime of photo-excited carriers were studied and only at high excitation intensities reasonable carrier lifetime was detected [44]. The film-substrate interface on the films showed a much higher recombination rate than the film-air interface and this was explained by strain at the substrate-film interface. The film on the glass substrates exhibited cracking pinholes also.

Preparation of pyrite thin films by plasma-assisted sulphurization of thin iron films were reported by S. Bausch et al in 1990 [45]. In that work, pyrite films were prepared using the pure elements as source materials, thin iron films were evaporated on quartz substrates and exposed to a sulphur plasma. The thermoprobe measurements of the samples indicated p-type conductivity. X-ray spectroscopy was used to characterise the films and preliminary optical and electrical measurements were carried out. Later, photoactive thin film semiconducting iron pyrite was prepared using sulphurisation of iron oxides by

G. Smestad et al [46]. The process involved the reaction of Fe_3O_4 or Fe_2O_3 with elemental sulphur. The oxide layers were exposed to the gaseous sulphur in open or closed ampoules at 350°C for 0.5-2 hour. The morphology, composition and photoactivity of the films produced were checked using XRD, XPS, optical absorption and steady state and transient photoconductivity. Photoelectrochemical measurements revealed p-type conductivity of the samples. Major result of this work is that oxygen and sulphur treatment of the films can yield conversion to nearly 100% pyrite. After this work, optical properties of chemically deposited (spray pyrolysed) pyrite FeS_2 coatings on quartz plates were reported by A.K. Abass et al [47].

In 1991, FeS_2 thin films were prepared by thermal sulphuration of two flash evaporated iron layers and characterised by I. J. Ferrer et al [48]. Morphological, compositional, crystallographic, optical and electrical properties of the films produced and their relation with the parameters involved in the sulphurisation process were presented in that paper. It was also concluded that FeS_2 starts to be formed at sulphurisation temperature about 200°C. X-ray pattern showed that crystallinity and grain size of the films improve with the sulphuration temperature with a "critical value" that varies with the sulphur pressure. But the film resistivity and optical absorption coefficient change abruptly at temperature higher than 350°C. Above 500°C polycrystalline aggregates (known a "framboidal pyrite") were observed.

In 1992 vapour phase epitaxial growth of and evaluation of the carrier collection in liquid-junction solar cells had been reported by A.Ennaoui et al [49]. In that work photoactive epitaxial layers of FeS_2 were grown using bromine as a transport agent in a simple closed ampoule technique. The substrate used were (100) oriented slices of natural pyrite 1mm thick. Localized photovoltaic response for the evaluation of carrier collection using a scanning laser spot system had been used to effectively locate and characterize non-uniformities present in the epitaxial thin films. Later iron pyrite thin films for flexible solar cell were reported by B. Rezig et al [50]. In that work vacuum thermal evaporation technique was used to grow iron thin films on heated glass substrate. Thick fresh iron layers

(1000-3000A^{0}) sulphurised under nitrogen flux were converted into iron pyrite FeS_2 phase that was identified by X-ray study. These FeS_2 layers showed p-type conductivity and this work confirmed the highly absorbing character of FeS_2. It also revealed the presence of an indirect gap at 1.31 eV and a direct gap at 1.45eV. In another work by A.Ennaoui et al [51] ultra thin (10^{-20}nm) polycrystalline films of FeS_2 were grown on TiO_2 using chemical vapour deposition. Photoelectrochemical solar cells using these pyrite films generated high open circuit photovoltage up to 600 mV, compared to a single crystal of pyrite electrode (200mV). Strong dependence of photovoltage and photocurrent on pH of the solution was also suggested in this paper. Following this work infrared spectroscopic and X-ray diffraction characterisation of FeS_2 thin films prepared by MOCVD were reported by Ennaoui et al [52].

Later in 1992, thin pyrite films prepared using magnetron sputtering were reported by G.Willeke et al [53]. In that work, thin films had been prepared by sulphur assisted magnetron sputtering at deposition temperature between 88°C and 390°C. The films were microcrystalline with an average grain size 400A^{0} and preferential orientation changing from (200) to (111) on going to higher deposition temperature. The electrical conductivity was degenerate with $\sigma_{RT} = 4\Omega^{-1}$ cm^{-1} and $\mu_{HRT} = 5$ cm^{2} v^{-1}S^{-1} and indicated holes to be the predominant current carrier. Argon and reactive ion beam sputtering of thin pyrite FeS_2 and other iron sulfide films had been reported by M.Birkholz et al [54]. In that work films were characterised using XRD, RBS, Optical spectroscopy and by the measurements of temperature dependent conductivity.

In 1993, optical, electrical and structural properties of polycrystalline FeS_2 layers deposited by reactive DC magnetron sputtering were reported by D. Lichtenberger et al [55]. Optical and electrical properties of the films were found to be strongly depended on the deposition conditions. Later improvements in optical and electrical properties of flash evaporated pyrite thin films, by annealing at different temperature in a sulphur atmosphere were reported by C de las Heras et al [56]. In that work sulphuration temperature had a clear influence on the optical absorption and electrical resistivity of the films, with some

differences in their behaviour depending on the film thickness . Again electrical resistivity seemed to be influenced by both the film grain size and point defect density.

The growth process of polycrystalline pyrite thin films employing low pressure MOCVD (LP-MOCVD) in a vertical cold wall reactor had been investigated by C.Hopfner et al in 1995 [57]. Study of the growth rate as a function of temperature revealed a kinetically controlled growth process with an activation energy of 73 kJ/mol over the temperature range 250-400°C. Decomposition of the films into pyrrhotite ($Fe_{1-x}S$) occurs at higher growth temperature. The S/Fe ratio in the films had been controlled from 1.23 upto 2.03 by changing tributyldisulphide (TBDS) partial pressure. In the case of films deposited over amorphous substrates the crystallites show a tendency to grow in (100) orientation with increasing deposition temperature. The growth rate is found to be 2.5A°/ sec.

7.4. Pyrite as a solar energy material - A comparative study

First report on FeS_2 solar cells came in 1984 [58]. In that study synthetic pyrite was-prepared in the form of an electrode and was used in photoeletrochemical solar cells. As a result of the poor value of the fill factor, the low photovoltage and relatively high resistance of pyrite electrode, the energy conversion efficiency was insignificant for practical application (of the order of 1% and lower). But they obtained an average quantum efficiency of 33% for photocurrent generation. Later the same group has obtained a high quantum efficiency (90%) [17] and high photocurrent without evidence of any corrosion in electrochemical pyrite solar cells.

For an analysis of energy conversion in addition to suitable energy band gap and high absorption coefficient, the diffusion length and carrier mobility are also important. The diffusion length (L) is in the range of 0.12-1 μm and Hall mobility of this material (μ) is 350 cm^2/Vs [42,44,59,60]. In comparison with the well known solar energy material Silicon (1.1 eV) the preparation of FeS_2 consumes less energy and in contrast with amorphous Silicon, FeS_2 is inherently stable. Unlike most intensively studied photoactive materials such GaAs, CdS CdTe and $CuInSe_2$, FeS_2 is a non-toxic material and the production of pyrite solar cells would never be limited by the nonavailability of the

constituent elements. A comparative data related to the most commonly used materials for photovoltaic cell is given in Table 1.

Table 1 - Comparative data related to the most known absorbers

PV materials	C:Si	a.Si:H	$CuInSe_2$	FeS_2
Energy gap (eV)	1.1	!.5-1.8	0.95-1.05	0.9-1.1
Absorption Coefficient (cm^{-1})	5×10^3	3×10^4	2×10^5	6×10^5
Absorption length (A^o)	2×10^4	3.3×10^3	5×10^2	1.7×10^2
Quantum efficiency (%)	25	10-12	25-30	80-90

7.5. Preparation and Characterisation of Spray pyrolysed samples

At first attempts were made to prepared pyrite thin films using spray pyrolysis technique.

7.5.1. Sample preparation

Samples were prepared by spraying an aqueous solution of $FeCl_3$ (0.1N) and thiourea (0.4N) on a glass substrate kept at 300°C. The ratio of thiourea to $FeCl_3$ was 2:1 in all experiments. Detailed description of the experimental set up used for spray pyrolysis is given in chapter 2. The atomization of the chemical solution into a spray of fine droplets is effected by the spray nozzle with the help of compressed air as the carrier gas. The spray rate was kept at 12 cm^3/minute and the high scanning rate (100/minute) ensures a uniform film thickness. Films of thickness 0.5 μm were obtained (measured using gravimetric method) for a spray time 30 minutes.

7.5.2. Characterisation

The conductivity type of the samples was found to be p-type from hot probe analysis. Thin films prepared by many other techniques had also shown this behaviour [61].

X-ray diffraction studies of these spray pyrolysed samples were made. Figure 7.1 shows the XRD spectra of as-deposited samples. Spectra reveal peaks corresponding to $Fe_{1-x}S$, Fe_2O_3 and FeS phases. XRD spectra of the sample vacuum annealed (10^{-2} Torr) at 200°C for 1 hour is shown in figure 7.2 and spectra show an increase in peak height. Table 2 shows the values of grain size, d values and hkl planes observed in XRD spectra. Grain size is found to be increased in the case of annealed samples and this shows that crystallinity of the sample is also increased after annealing. Thus from XRD analysis of the sample it is clear that the spray pyrolysis results in sulphur deficient sample with more oxygen content and stoichiometric FeS_2 phase is not formed.

Table 2. Values of hkl plane of various phases with d values and grain size obtained from XRD spectra of spray pyrolysed sample

Sample type	observed 2θ (deg.)	hkl	Phase	Grain size (A°)	d-value (A°)
As-prepared	51.30	-	$Fe_{1-x}S$	0.6690	1.78
	43.95	[202]	Fe_2O_3	0.4336	2.06
	26.50	-	FeS	0.3540	3.36
Vacuum annealed	51.5	-	FeS	0.7305	1.77
	44.4	[400]	Fe_2O_4	0.558	2.040
	32.05	[200]	FeS	-	2.792
	31.0	-	FeS	-	2.884
	30.6	[220]	Fe_3O_4	-	2.921
	26.6	-	FeS	0.572	3.351

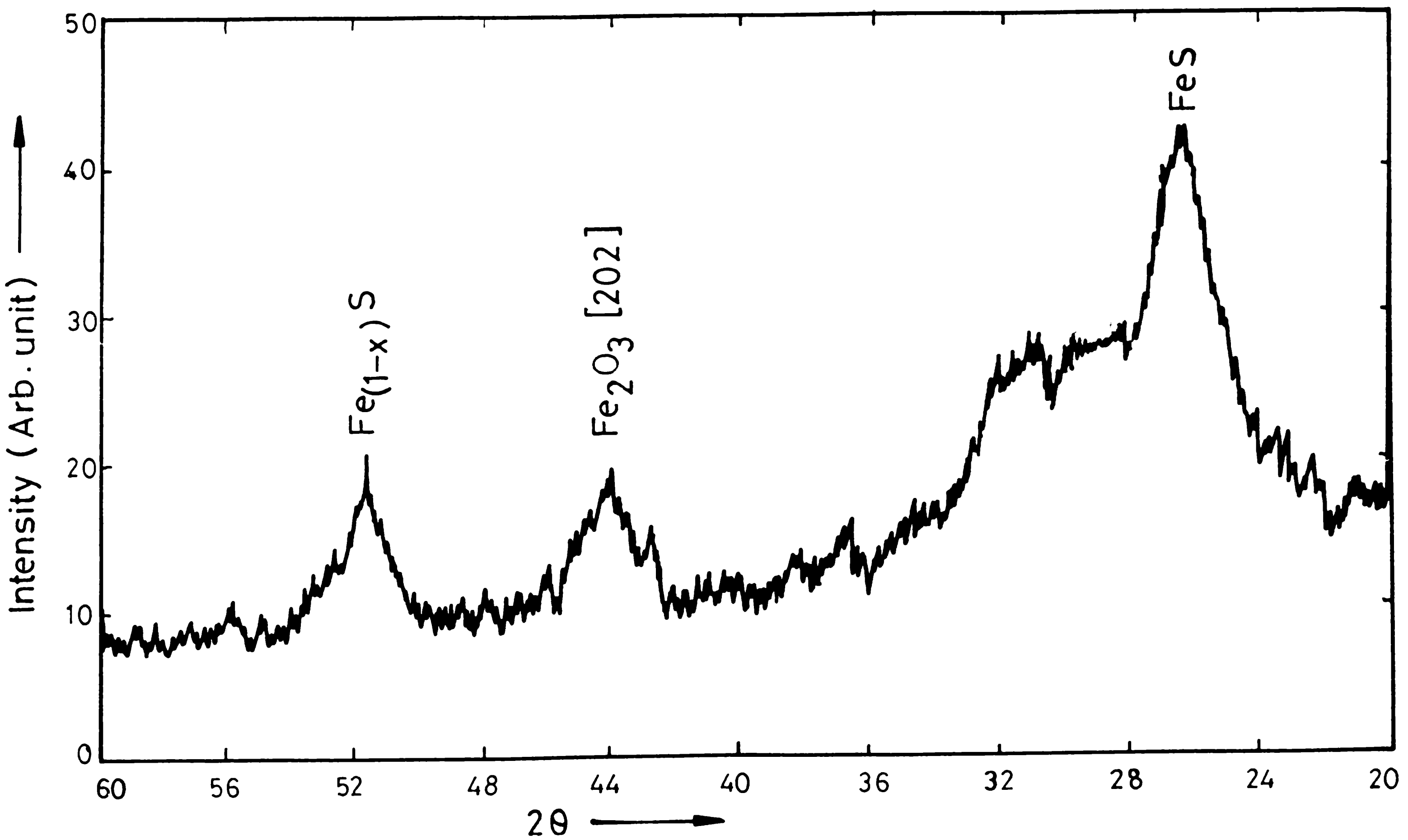

Figure 7.1. XRD spectra of as-prepared spray pyrolysed sample

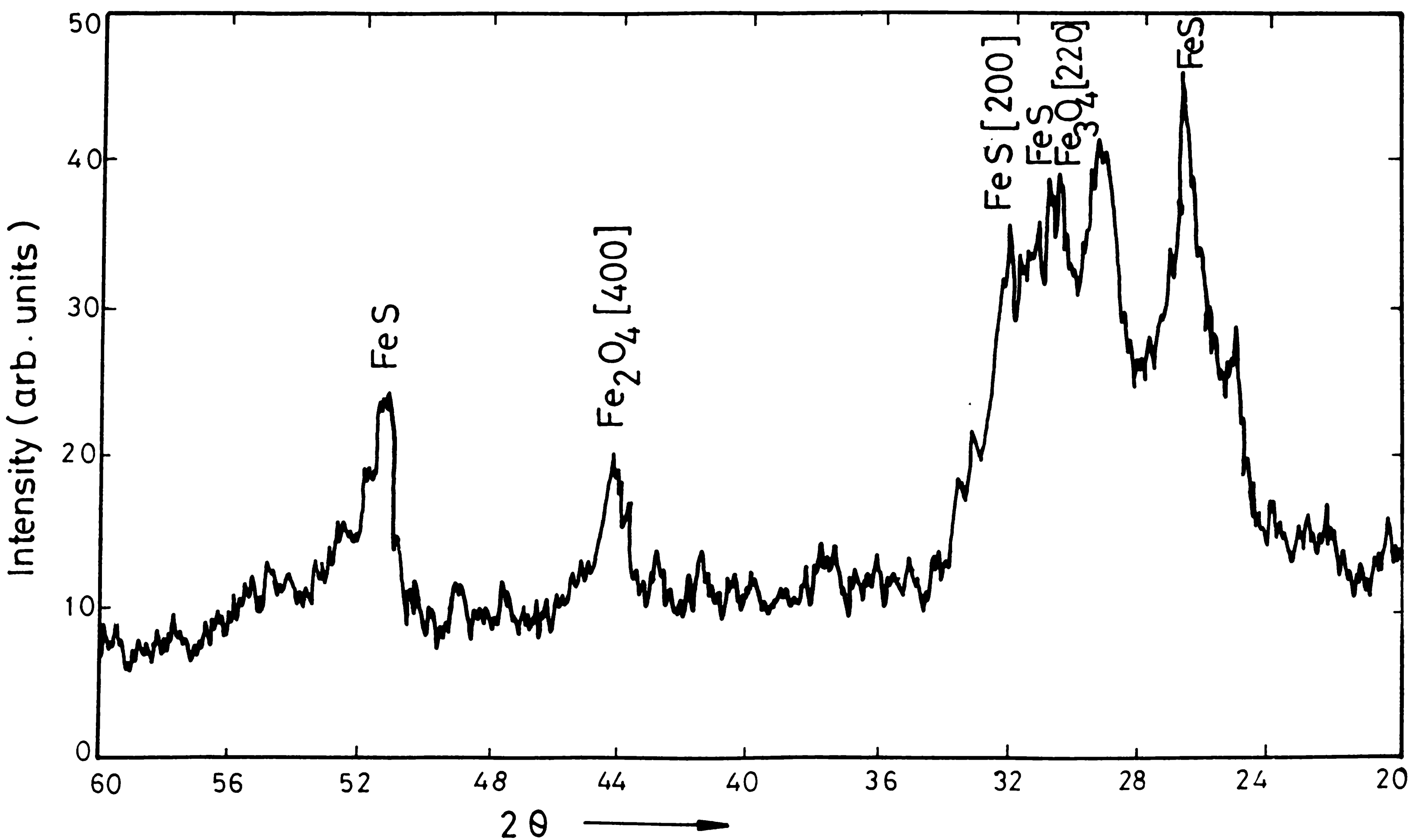

Figure 7.2. XRD spectra of spray pyrolysed sample annealed in vacuum

7.6. Preparation and characterisation of CBD samples

Even though numerous techniques had been employed for the preparation of pyrite films, to the best of our knowledge there is no report on the preparation of this compound using CBD technique. So attempts were made to prepare pyrite thin film using CBD technique.

7.6.1. Sample Preparation

Samples were prepared from a reaction mixture containing $FeCl_3$ (1N) and thiourea (1N). TEA was used as the complexing agent. Ultrasonically cleaned glass slides were used as the substrate and pH of the solution was kept above 10. Several trial preparations were made in order to establish the deposition temperature to make adhesive thin films on glass substrate, by varying bath temperature from room temperature to 80°C. The temperature of the bath was selected as 70°C and dipping the substrate for 2 hours in the bath yielded films of thickness 0.5 μm. Films with more thickness could be obtained with multiple dipping. The present work is based on TEA complex method, the chemical equation for this is

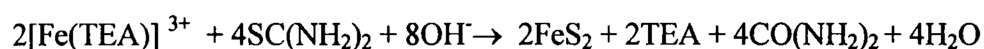

$$2[Fe(TEA)]^{3+} + 4SC(NH_2)_2 + 8OH^- \rightarrow 2FeS_2 + 2TEA + 4CO(NH_2)_2 + 4H_2O$$

Reaction mixture was-prepared with different volumes of $FeCl_3$ and thiourea in order to make pyrite films with different Fe:S ratio. Results of deposition and quality of films obtained for various Fe:S ratios is shown in table 3.

7.6.2. Characterisation of CBD samples

The conductivity type of the samples was found to be n-type from hot probe analysis. It is well established that pyrite films exist in n-type and as well as p-type material [38]. Resistivity of the samples was found to be 10^{13} Ω cm which is very high for any photovoltaic application.

Table 3. Nature of CBD samples obtained for different ratio between Fe and S

Ratio of Fe:S	Film Quality
0.25:1	Discontinuous
0.5:1	Discontinuous
0.75:1	Discontinuous
1:1	Slightly improved
1.25:1	Much Improved
1.5:1	Very poor deposition
1.75:1	No deposition
2:1	No deposition
Ratio of S:Fe	Film Quality
0.25:1	Discontinuous
0.5:1	Discontinuous
0.75:1	Discontinuous
1:1	Slightly improved
1.25:1	Much Improved
1.5:1	Very poor deposition
1.75:1	No deposition
2:1	No deposition

Optical absorption studies of the various films were done and a typical absorption spectrum is shown is figure 7.3. Band gap values were calculated from the spectra and variation of band gap with bath temperature is shown in table 4. In the present study films with Fe and S in the ratio 1.25:1 and 1:1 prepared at 70°C has band gap of 0.9 e V and is in agreement with the values reported earlier [44]. In addition to this, different values of band gap from 0.79 eV to 2.25 eV were obtained for different samples, the cause of which is not clear. Similar type of dispersion of Eg values from 0.7 eV-2.6 eV had been reported in pyrite crystals by I.J. Ferrer et al [20]. The nature of transition responsible for this energy gap was not given by them.

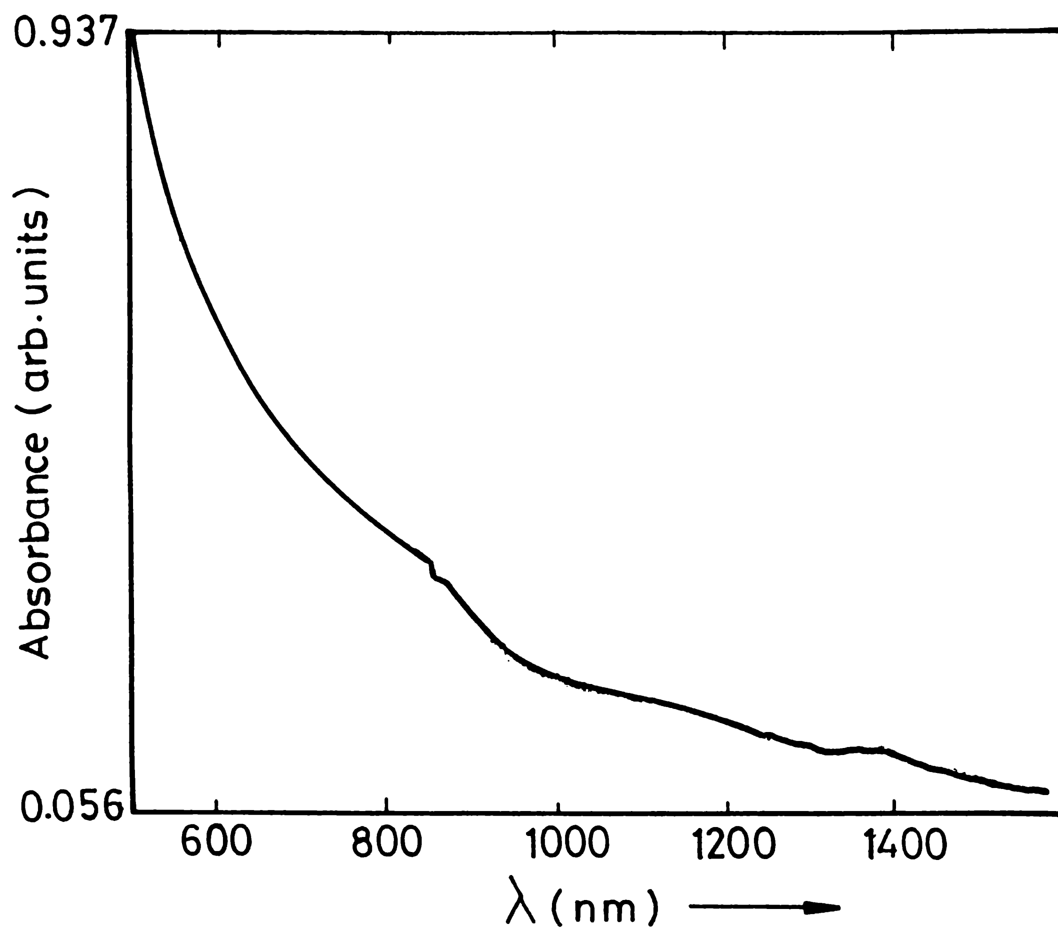

Figure7.3. Absorption spectra of CBD sample

The absorption spectra were taken for samples annealed at different temperature from 100-300°C for 1 hour. Band gaps determined from the absorption spectra of annealed films are shown in table 5. Interestingly it is observed that when the film was annealed at 300°C, the band gaps obtained were 0.8 eV and 1.04 eV which is very near to the 0.9 eV and 1.1eV that had been reported earlier [15,44,62].

Table 4. Band gap values of CBD samples with different Fe:S ratio at different deposition bath temperature

Ratio of Fe:S	Bath temperature	Band gap (eV)
1.25:1	Room temperature 70°C	0.79, 2.07 0.9, 2.12
1:1	Room temperature 70°C	1.9, 2.2 0.9, 2.25

Table 5. Variation of band gap of CBD sample (Fe:S = 1.25:1) prepared at 70°C with annealing temperature

Sample type	Band gap (eV)
As-deposited	0.77, 1.02
Vacuum annealed at 100°C 200°C 300°C	 0.79, 1.05 0.79, 1.05 0.80, 1.04

We conducted PIXE measurement of the sample and figure 7.4 shows PIXE spectra (proton 3 MeV) of the sample vacuum annealed at 300°C for 1 hour. Spectrum indicates number of peaks and three of them are identified. One is due to Fe and other is due to Ca. Source of Ca in the sample could not be identified. Most probably it could be from the glass used as the substrate. One peak could be identified due to the presence of S.

XRD studies were made on as-deposited as well as annealed samples. Figure 7.5 shows the XRD spectra of the sample vacuum annealed at 300°C for 1 hour. Here we could not identify any phase from XRD spectrum and this may be due to the amorphous nature of the sample. The high resistivity of the sample is suspected to be due to the presence of this amorphous phase of the pyrite. It is reported that absorption of sulphur and crystallinity of the film increases with an increase in grain size and thickness of the films [52]. The film preparation has to be further modified for obtaining better crystalline films with lower resistance and higher thickness.

In order to analyse the defect levels present in the CBD films, we carried out TSC measurement of these samples. Figure 7.6. shows the TSC spectra of a CBD sample. The spectra show no peaks at all and from this it is clear that this CBD sample does not provide any defect level detectable in TSC measurement. Spectra show only a semiconducting behaviour.

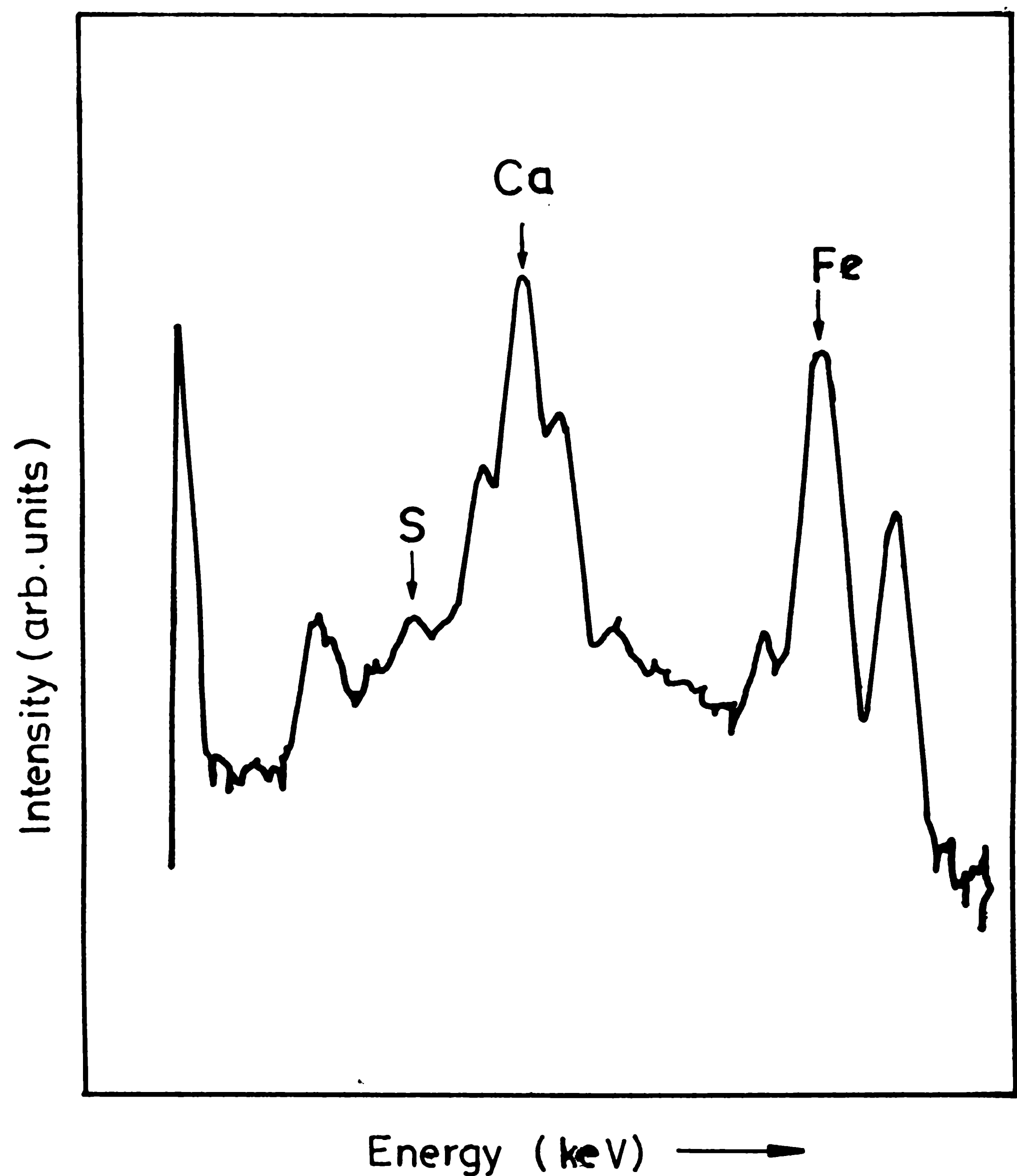

Figure 7.4. PIXE spectra of vacuum annealed CBD sample

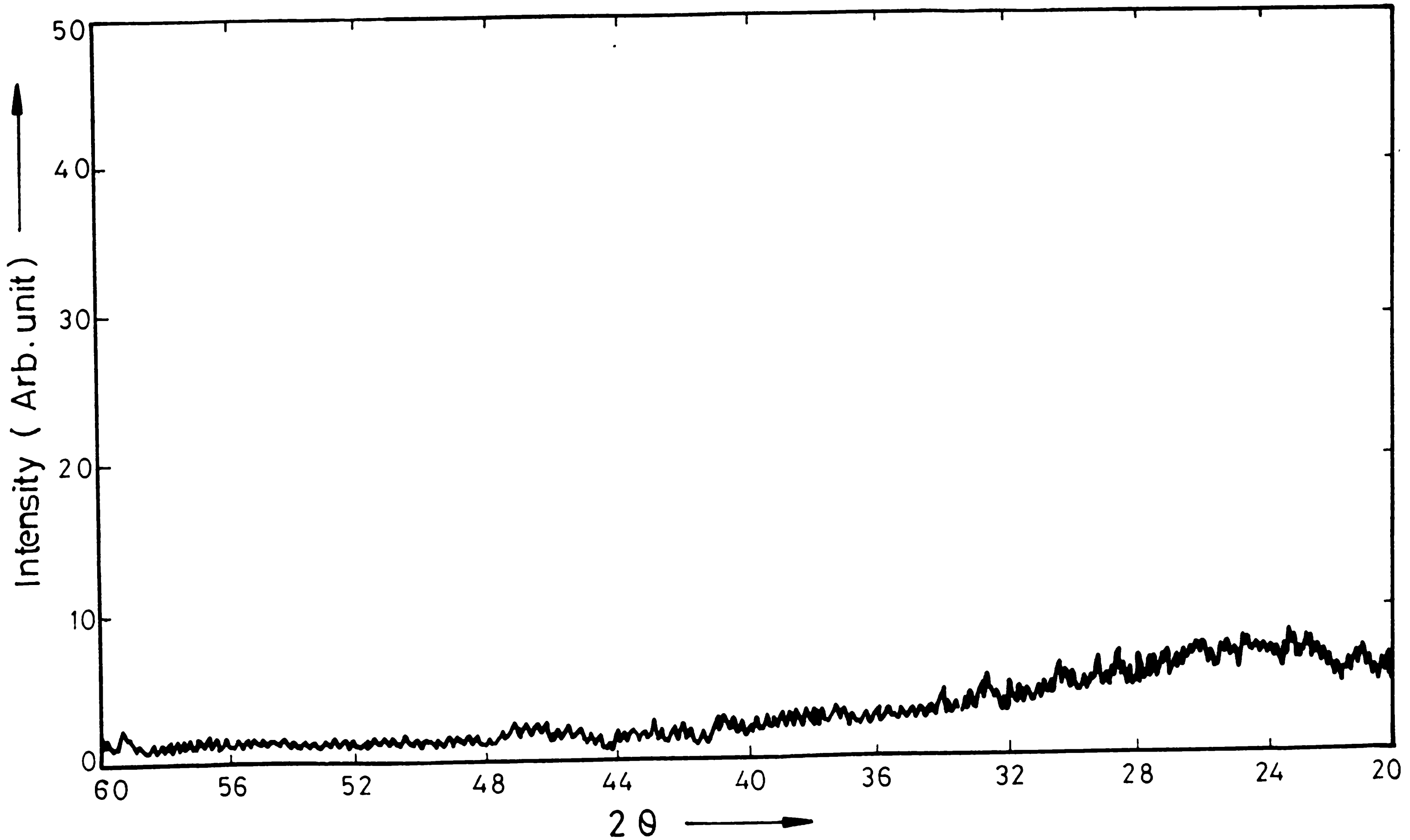

Figure 7.5. XRD spectra of vacuum annealed CBD sample

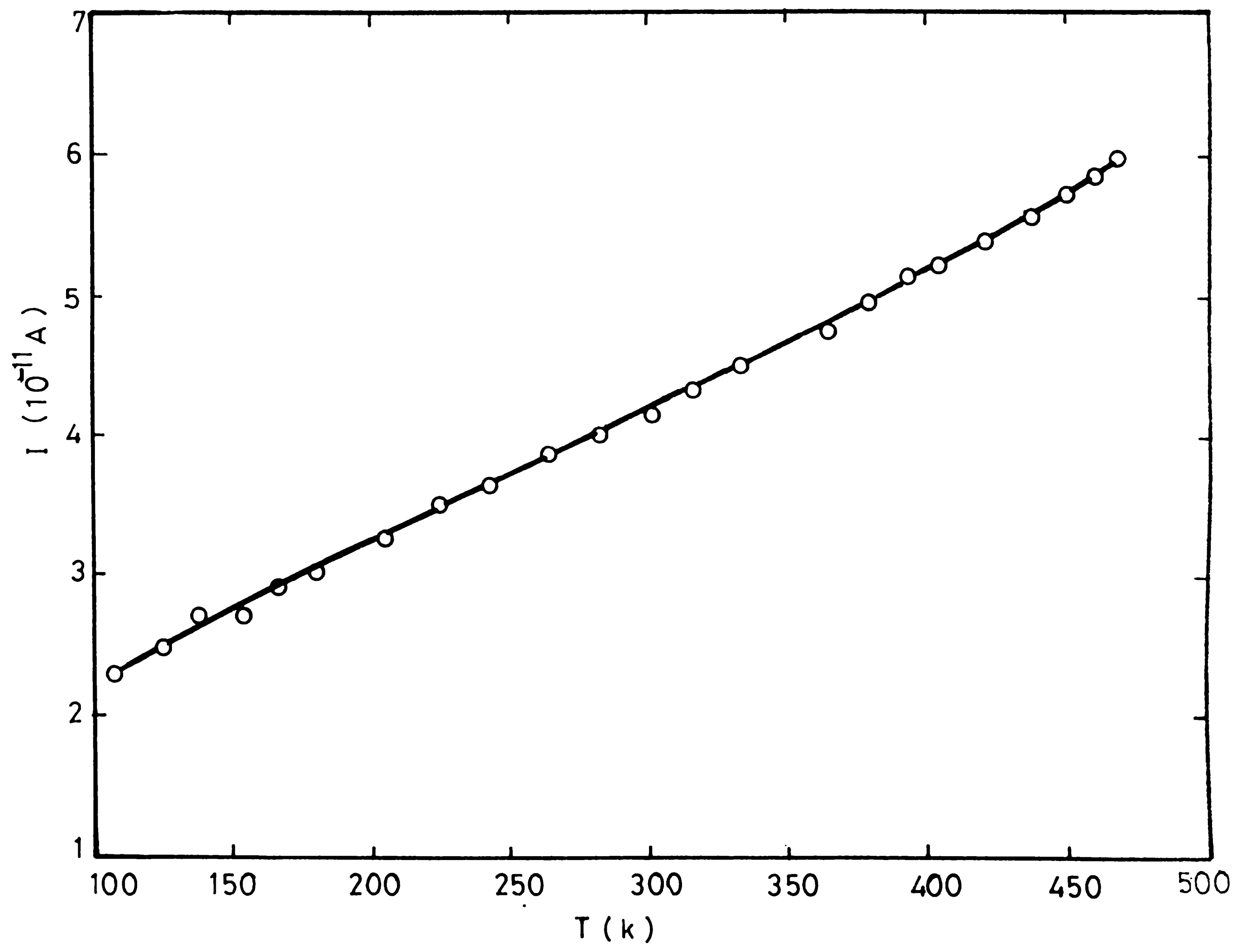

Figure 7.6. TSC spectra of CBD sample

7.7. Conclusion

Attempts were made to prepare pyrite thin films using simple chemical methods like Spray pyrolysis and Chemical Bath Deposition techniques. XRD analysis of spray pyrolysed samples indicates that films are sulphur deficient, probably in FeS phase and it also reveals the presence of iron oxide phase in these samples. In the process of spray pyrolysis, we used compressed air as the carrier gas and probably this may be the reason for the presence of the oxygen in the sample. Analysis of the spray pyrolysed samples revealed that it is quite difficult to prepare pyrite films on glass substrate in the presence of oxygen / air.

Samples were also prepared using CBD technique. From PIXE analysis we could detect the presence of iron and sulphur in these CBD samples. Presence of Ca from unidentified source could also be detected from this analysis. Optical absorption studies of these CBD samples gave band gap values almost similar to the previously reported values. Variation of the band gap with deposition temperature and annealing temperature is also presented in this work. XRD analysis of these CBD samples could not reveal any crystalline phase and this may be due to the amorphous nature of the samples. We carried out TSC measurements these samples, but could not detect any defect levels. It merely shows a semiconducting behaviour. This also may be due to the amorphous character of the sample prepared using CBD. The defect levels may be distributed almost continuously in the band gap.

References

1. A.Ennaoui, S.Fiechter, H.Goslowsky and H. Tributsch, *J.Electrochem Soc.*, **132** (1985) 1579; A. Ennaoui, S. Fiechter, W. Jaegermann and H. Tributsch, *J. Electrochem.Soc.*, **133**(1986)97.
2. I.J.Ferrer, D.M. Nevskaia, C.de Las Heras and C. Sanchez, *Solid State Commun.*, **74**(1990)913
3. M.Birkholz, D. Lichtenberger, C. Hopfner and S. Fiechter, *Solar Energy Materials and Solar cells*, **27**(1992)243
4. R.J.Bouchard, *J. Crystal Growth*, **2**(1968)40
5. J.L.Horwood, M.G. Townsted and A.H. Webster., *J.Solidstate Chemicstry*, **17**(1976)35
6. A.Schlegel and P.Wachter., *J.Phys.C. Solid State Physics.*, **9**(1976)3363
7. Willliam W. Kou and Mohindar S. Seehra, *Phys. Rev.B*, **18**(1978)7062
8. M.S.Seehra and S.S. Seehra, *Phys.Rev. B*, **19**(1979)6620
9. Katsuaki Sato, *J. Physical Society of Japan*, **53**(1984)1617
10. Chikara Sugiura, *J.Chem.Phys.* **80**,(3)(1984)1047
11. R.W.G.Wyckoff, Crystal structure 2nd ed. (Interscience, New York 1965) **vol. 1**. p 346
12. D.W.Bullet, *J.Phys.C.*, **15**(1982)6163
13. G.Panzner and B.Egert, *Surface Science*, **144**(1984)651
14. A.Ennaoui,S.Fiechter, H.Goslowsky and H.Tributscg, *J.Electrochem Soc.*,**132**(7) (1985)1579
15. S.Fiechter, J.Maio and A.Ennaoui., *J.Crystal Growth*, **78**(1986)438
16. A.Ennaoui and H.Tributsch, *Solar Energy Materials*, **14**(1986)461
17. A.Ennaoui, S.Fiechter, W.Jaegermann and H.Tributsch, *J. Electrochem. Soc.*, **133**(1)(1986)97
18. N.Alonso-Vante, G.Cchatzithcodorou, S.Fiechter, N.Mgoduka, I.Poulios and H. Tributsch, *Solar Energy materials*, **18**(1986)9
19. LIU Chongyang,C.Petterkofer and H.Tributsch,*Surface Science*, **204**(1986)537
20. I.J.Ferrer, D.M. Nevskaia, C.de las Heras and C.Sanchez, *Solid state Commun.*, **74**(9)(1990)913
21. A.Ennaoui and H.Tributsch, *Solar cells*, **13**(1984)197

22. R.Memming, *Photochemistry and photophysics* edited by J.F. Rabek (Chemical Rubber Cleveland 1990) p157
23. A.Hartmann, PhD thesis, Technische Universitat, Berlin,1990.
24. J.Luck, a.Hartmann and S.Fiechter, *Z.Anal.Chem.*,**334**(1989)441
25. E.H.Kraus and I.D. Scott,*Z.Kristallogr*, **44**(1908)153
26. R.Juza,W.Biltz and K.Meisel,*Z.Anorg.Allg.Chem.*, **205**(1932)273
27. C.T.Anderson, *J.Am.Chem.Soc.*, **59**(1937)486
28. F.G.Smith, *Am.MinerAL*,**27**(1942)1
29. J.Bittner, Jenaer Zeiss-Jahresberi cht (Zeiss,Jena,1950) p177
30. M.Birkholz, S. Fiechter, A.Hartmann and H.Tributsch, *Phys.Rev.B.* **43** (14) (1991) 11926
31. R.Kretz in Handbook of chemistry and Physics edited by R.C.Weast (Chemical Rubber, Boca Raton 1986)p B-186
32. K.Buker,N.Alonso-Vante and H.Tributsch., *J.Appl.Phys.*, **72**(12)(1992)5721
33. Vaughan and J.R. Craig, Mineral Chemistry of Metal sulfides (Cambridge University Press,Cambridge,1978) p36
34. O.Blenk, E. Bucher and G.Willeke., *Appl.Phys.Lett.*, **62**(17)(1993)2093
35. R.T.Shuey,Semiconducting Ore Minerals, (Elsevier,Amserdam, 1975) p304
36. S.S.Seehra,P.A. Montano and M.S. Seehra.,*J.Mater.Sci.*, **14**(1979)2761
37. H.Horita and T.Suzuki, *Jpn.J.Appl.Phys.*, **19**(1980)391
38. A.M.Karaguppikar and A.G.Vedeshwar., *Phys.stat.sol.(a)* **95**(1986)717
39. V.P.Guptha,K.Chandra,V.K.Srivastava., *J.Mat.Science.Letters.*, **5**(1986)165
40. A.K.Abass, Z.A. Ahmed and R.E.Tahir., *Phys.Stat.Sol.(a)*, **97**(1986)243
41. A.K.Abass,Z.A. Ahmed and R.E. Tahir., *J.Appl.Phys.*,**61**(6)(1987)2339
42. G.Chatzitheodorou, S.Fiechter, R.Konekamp, M.Kunst, W.Jaegermann and H.Tributsch, *Mat.Res.Bull.*, **23** (1988)1261
43. G.Chatzitheodorou, S.Fiechter, M.Kunst, J.Luck and H.Tributsch, *Mater.Res.Bull.*, **23**(1988)1261
44. G.Smestad,A. Da Silva, H.Tributsch, S.Fiechter,M.Kunst,N.Mesiani and M.Birkholz, *Solar Energy materials*, **18**(1989)299

45. S.Bausch, B.Sailer ,H.Keppner, G.Willeke, E.Bucher and G.Frommeyer., *Appl.Phys.Letters*, **57**(1)(1990)25
46. G.Smestad, A. Ennaoui, S. Fiechter, H. Tributsch, W.K. Hofmann, M. Birkholz and W. Kantek., *Solar Energy Materials*, **20**(1990)149
47. A.K.Abass,Z.A. Ahmed and R.H.Sammuel, *Phys.Stat.Sol(a)*, **120**(1990)247
48. I.J.Ferrer and C.Sanchez., *J.Appl.Phys.*, **70**(5)(1991)2641
49. A.Ennaoui,G.Schlichthori,S.Fiechter and H.Tributsch, *Solar Energy Materials and Solar cells* , **25**(1992)169
50. B.Rezig, H.Dahman and M.Kensari, *Renewable Energy*, **2**(2)(1992)125
51. A.Ennaoui,S.Fiechter and H.Tributsch, m.Giersig and R.Vogel and H.Weller., *J.Electrochem.Soc.* **139**(9)(1992)2514
52. A.Ennaoui,S.Schroetter,S.Fiechter,H.Tributsch, *J. .Mat. Sci.Letts.*, **11**(1992)1131
53. G.Willeke,R.Dasbach,B.Sailer and E.Bucher, *Thin Solid Films*, **213**(1992)271
54. M.Birkolz, D.Lichtenberger,C.hopfner and S.Fiechter., *Solar Energy Material and Solar cells.*, **27**(1992)243
55. D.Lichtenberger, k.Ellmer,R.Schieck and S.Fiechter, *Appl.Surf.Sci.*, **70/71**(1993)583
56. C de las Heras, I.J. Ferrer and C.Sanchez., *J.Appl.Phys.*,**74**(7)(1993)4551
57. C.Hopfner,K.Ellmer,A.Ennaoui,C.Pettenkofer, S.Fiechter and H.Tributsch, *J. Crys.Growth*, **151**(1995)325
58. A.Ennaoui and H.Tributsch,*Solar Cells*, **13**(1984)197
59. G.Kullerud,Carneggie.Inst.Washigton Annu.Rep.Dir.Geophys.Lab, **56**(1957)198
60. E.R.Cohen and B.N. Taylor. *Phys.Today*,BG (1989)88
61. G.Willeke, R.Dasbach, B.Sailer and E.Bucher, *Thin Solid Films*, **213**(1992)271
62. B.Rezig, H.Dahman, and M.Kensari,*Renewable Energy*, **2**(2)(1992)125

Chapter 8

Summary and Conclusion

The present work mainly concentrates on the Thermally Stimulated Current studies of some compound semiconductor thin films used for photovoltaic applications. We selected this technique because of its simplicity and sensitivity. Thin films of compound semiconductor materials like CdS, $CuInSe_2$, PbS and FeS_2 were investigated in this work. We also conducted dark conductivity measurements. Results of the analysis of different samples are summarised in the following sections.

CdS thin films

TSC measurements were conducted on n-type and p-type spray pyrolysed CdS thin films in order to get a picture of the activation energies of different trap levels present in the samples. From this study we found that the mobility of sulphur vacancy is a prominent cause of electrical conductivity in as-prepared and annealed (both in air and vacuum) n-type CdS samples. But in addition to the mobility of sulphur vacancy, as-prepared and vacuum annealed n-CdS samples showed a level of Cd and S vacancy complexes of smaller cross section which could be detected only under an excitation time of 10 minutes. In the case of air-annealed n-CdS, even under 10 minutes excitation, we could not find the presence of Cd and S vacancy complexes. Instead we obtained a trap level of chemisorbed oxygen. TSC studies on p-type CdS gave two distinct trap levels, viz. sulphur vacancy and copper impurity having the same cross section. A possible explanation is also discussed and we found that it is the Cu impurity on Cd-S complex vacancy sites that gives the p-type conductivity to this sample. Nature of different trap levels observed in n and p-type CdS films were also determined. We made a study on existing trap levels in these samples by dark conductivity measurements and the results are found to be in agreement with the results obtained from TSC studies.

As-prepared CBD CdS films are highly resistive (10^7 Ω cm) and the variation of sheet resistance with aging and annealing was also included in this study. It was found that CBD CdS films of resistivity 10^5 Ω cm could be obtained after annealing in air at 250°C for 3 hours. The present work also discuss a simple technique for producing low resistivity CdS films in which high resistive films were chemically treated with halides of Cd, In and Sn. It was found that samples treated with $InCl_3$ had the least resistivity (5 Ω cm). The effect of annealing on resistivity of these samples were also studied. While air annealing slightly increased the resistivity, vacuum annealing converted the film into highly resistive form.

TSC measurements of high resistive CBD CdS films revealed that the samples contain no defect levels detectable by this measurement. But the low resistivity CBD CdS samples indicate the presence of Cd-S vacancy complexes, independent S vacancies and chloride ions. Annealing in air removes the Cd-S vacancy complexes and chloride ions, but these samples posses S-vacancies and chemisorbed oxygen. TSC measurements of vacuum annealed CBD CdS films indicate no defect levels and this explains the high resistive nature of these samples.

$CuInSe_2$ thin films

Trap level detection of CIS films prepared using CBD was performed by TSC measurement technique. As-prepared samples had Se vacancy as a prominent trap and Cu vacancy of smaller cross section. But when annealed in air, the Se vacancy of the as-prepared samples disappeared and another donor level, supposed to be due to the adsorption of oxygen, came into existence. Cu vacancies continued to exist in the air annealed samples. Vacuum annealing did not affect the presence of Se vacancy, since oxygen adsorption is quite difficult under this condition. Interestingly these samples also showed the presence of Fe impurity. Fe impurity can come from the copper salt used in the preparation. When Fe is present in the reaction mixture at a pH ~ 7, Fe $(OH)_3$ may be formed which decomposes and deposits as γ-FeO along with CIS. When such film is annealed in air, Fe_2O_3 may be formed and hence it may not give rise to any TSC peak. But when the sample is annealed in vacuum, FeO may be transformed to FeSe and SeO_2. FeSe

is unstable and will be associated with other molecule or defects and may give rise to a TSC peak.

Nature of the different trap levels observed in TSC measurements were also determined. Dark conductivity measurements on these CBD CIS samples were found to be in good agreement with the results obtained from TSC measurements. As far as the fabrication of CIS/CdS solar cells by CBD technique is concerned, these investigations are quite relevant.

PbS thin films

Thin films of PbS were prepared using CBD technique, without the addition of any oxidants. Two types of samples were prepared from deposition bath, one with the complexing agent EDTA and the other without EDTA. Resistivity of PbS films prepared from deposition bath without EDTA was found to be $10^5\ \Omega$ cm, where as that with EDTA was $10^7\ \Omega$ cm . TSC measurements on PbS film with EDTA revealed the existence of a sensitizing center for photoconductivity at an activation energy of 0.21 eV. Those films without EDTA showed two traps, one at 0.21 eV (observed in the previous case) and the other at 0.05 eV. This second trap is an acceptor level and this may contribute to the decrease in resistivity of these films. We conducted dark conductivity measurements on these two types of PbS films. From the Arrhenius plot, an activation energy of 0.215 eV was calculated in the case of PbS film with EDTA. The similar plot for the second type of sample without EDTA revealed various slopes and the calculated activation energies were 0.215 eV (sensitizing center), 0.13 eV and 0.05 eV (acceptor level). The level at 0.13 eV is a less effective sensitizing center. So it is very clear that the dark conductivity measurements also support the existence of sensitizing center responsible for high photosensitivity of PbS films. Earlier this type of films were prepared using solution growth technique with the addition of oxidants only. Works are in progress in our laboratory to produce PbS films, with lower resistivity and improved characteristics in order to try the fabrication of p-n junctions.

FeS_2 (Pyrite)

In the present work, attempts were made to prepare pyrite thin films using simple chemical methods like spray pyrolysis and CBD technique. XRD analysis of spray pyrolysed samples indicated sulphur deficiency and presence of iron oxide. In the process of spray pyrolysis, we used compressed air as the carrier gas and probably this may be the reason for the presence of oxygen in the samples. Analysis of spray pyrolysed samples revealed that it is quite difficult to prepare pyrite films on glass substrate in the presence of oxygen/air.

Samples were also prepared using CBD technique. From PIXE analysis, we could detect the presence of iron and sulphur in these samples. Presence of Ca from unidentified source could also be detected from this analysis. Optical absorption studies of these CBD samples gave band gap values almost similar to the previously reported values. Variation of band gap with deposition temperature and annealing temperature is also presented. XRD analysis of these samples could not reveal any crystalline phase and this may be due to the amorphous nature. We carried out TSC measurements on these samples, but could not detect any defect levels. It merely showed a semiconducting behaviour. This also may be due to the amorphous character of the CBD sample and continuous distribution of defect levels in the band gap.

Various defect levels observed in semiconducting samples of CdS, PbS and FeS_2 are summarised in table 1. It gives the activation energies, the probable reason and nature of the observed defects.

Sample type	Observed defect level activation energy(eV)	Reason	Nature or typeness
Sprayed CdS			
n-type as-prepared	1.2	Mobility of V_S	electron trap
	0.4	V_{Cd-S} complex	hole trap
n-type air annealed	1.2	Mobility of V_S	electron trap
	0.9	Chemisorbed O_2	hole trap
n-type vac.annealed	1.2	Mobility of V_S	electron trap
	0.4	V_{Cd-S} complex	hole trap
p-type as-prepared	1.2	Mobility of V_S	electron trap
	0.73	Cu impurity	hole trap
CBD CdS			
High resistive	No defect levels	-	-
Low resistive			
as-prepared	0.4	V_{Cd-S} complex	hole trap
	0.12	V_S	hole trap
	0.03	Chloride ions	electron trap
air-annealed	0.1	V_S	hole trap
	0.92	Chemisorbed O_2	-
Vacuum annealed	No defect levels	-	-
PbS			
With EDTA	0.21	Donor level	electron trap
Without EDTA	0.21	Donor level	electron trap
	0.05	Acceptor level	hole trap
FeS_2			
As-prepared	No defect levels	-	-